

ADD42P32

NASA CR-135085

IITRI D6073-II

DEPARTMENT OF DEFENSE
PLASTICS TECHNICAL EVALUATION CENTER
PICATINNY ARSENAL, DOVER, N. J.

DECLASSIFICATION STATEMENT A

Approved for public release;
Distribution Unlimited

LAMINATION RESIDUAL STRESSES IN HYBRID COMPOSITES

Final Report - Part I

by I.M. Daniel and T. Liber
IIT RESEARCH INSTITUTE

PLASTICS TECHNICAL EVALUATION CENTER
PICATINNY ARSENAL, DOVER, N. J.

DTIC QUALITY INSPECTED

Prepared for

NATIONAL AERONAUTICS AND SPACE ADMINISTRATION

NASA - Lewis Research Center
Contract NAS3-16766

19960313 136

REF ID: A624233

1. Report No. NASA CR-135085		2. Government Accession No.		3. Recipient's Catalog No.	
4. Title and Subtitle Lamination Residual Stresses in Hybrid Composites				5. Report Date June 1976	
				6. Performing Organization Code	
7. Author(s) I. M. Daniel and T. Liber				8. Performing Organization Report No. D6073-II	
				10. Work Unit No.	
9. Performing Organization Name and Address IIT Research Institute 10 W. 35 Street Chicago, IL 60616				11. Contract or Grant No. NAS3-16766	
				13. Type of Report and Period Covered Final - Part I	
12. Sponsoring Agency Name and Address National Aeronautics & Space Administration Washington, DC 20546				14. Sponsoring Agency Code	
15. Supplementary Notes Project Manager, C. C. Chamis Materials & Structures Division NASA Lewis Research Center Cleveland, OH 44135					
16. Abstract An experimental investigation was conducted to study lamination residual stresses for various material and loading parameters. The effects of hybridization on residual stresses and residual properties after thermal cycling under load were determined in angle-ply graphite/Kevlar/epoxy and graphite/S-glass/epoxy laminates. Residual strains in the graphite plies are not appreciably affected by the type and number of hybridizing plies. Computed residual stresses at room temperature in the S-glass plies reach values up to seventy-five percent of the transverse strength of the material. Computed residual stresses in the graphite plies exceed the static strength by approximately ten percent. In the case of Kevlar plies, computed residual stresses far exceed the static strength indicating possible early failure of these plies. Static testing of the hybrids above indicates that failure is governed by the ultimate strain of the graphite plies. In thermally cycled hybrids, in general, residual moduli were somewhat lower and residual strengths were higher than initial values.					
17. Key Words (Suggested by Author(s)) Hybrid composites, angleplied laminates, residual stresses, thermal load cycling, residual strength, residual stiffness, mechanical properties, thermal properties, static load characterization				18. Distribution Statement Unclassified, Unlimited	
19. Security Classif. (of this report) Unclassified		20. Security Classif. (of this page) Unclassified		22. Price* 6.25	
		21. No. of Pages 168			

* For sale by the National Technical Information Service, Springfield, Virginia 22161

FOREWORD

This is the Final Report on IIT Research Institute Project No. D6073-II, "Lamination Residual Stresses in Hybrid Composites," prepared by IITRI for NASA-Lewis Research Center, under Contract No. NAS3-16766. The work described in this report was conducted in the period July 1, 1974 to February 29, 1976. The work performed in the preceding period August 1, 1972 to June 30, 1974 was reported in the First Interim Report, NASA CR-134826 dated March 1975. Dr. C.C. Chamis was the NASA-Lewis Project Manager. Dr. I.M. Daniel of IITRI was the principal investigator. Additional contributions to the work reported herein were made by Dr. T. Liber and Messrs. M. Iyengar, and T. Niuro.

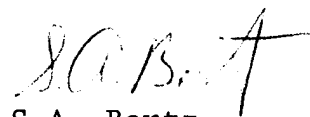
Respectfully submitted,

IIT RESEARCH INSTITUTE



I.M. Daniel
Science Advisor
Mechanics of Materials Division

APPROVED:



S.A. Bortz
Assistant Director
Mechanics of Materials Division

IIT RESEARCH INSTITUTE

LAMINATION RESIDUAL STRESSES IN HYBRID COMPOSITES

ABSTRACT

An experimental investigation was conducted to study lamination residual stresses for various material and loading parameters. The effects of hybridization on residual stresses and residual properties after thermal cycling under load were determined in angle-ply graphite/Kevlar/epoxy and graphite/S-glass/epoxy laminates. Residual strains in the graphite plies are not appreciably affected by the type and number of hybridizing plies. Computed residual stresses at room temperature in the S-glass plies reach values up to seventy-five percent of the transverse strength of the material. Computed residual stresses in the graphite plies exceed the static strength by approximately ten percent. In the case of Kevlar plies computed residual stresses far exceed the static strength indicating possible early failure of these plies. Static testing of the hybrids above indicates that failure is governed by the ultimate strain of the graphite plies. In thermally cycled hybrids, in general, residual moduli were somewhat lower and residual strengths were higher than initial values.

TABLE OF CONTENTS

<u>SECTION</u>		<u>PAGE</u>
1.0	INTRODUCTION	1
2.0	MATERIAL QUALIFICATION AND CHARACTERIZATION	4
2.1	Material Qualification	4
2.2	Laminate Fabrication	4
2.3	Characterization of Unidirectional Laminates	8
3.0	RESIDUAL STRAINS	15
3.1	Experimental Procedure	15
3.2	Residual Strains	16
3.3	Residual Stresses	22
4.0	STATIC STRENGTH	25
5.0	TENSILE LOAD WITH THERMAL CYCLING	28
5.1	Residual Properties After Thermal Cycling Between Room Temperature and 411 degK (280°F) Under Tensile Load	28
5.2	Residual Properties After Thermal Cycling Between Room Temperature and 200 degK (-100°F) Under Tensile Load	31
6.0	SUMMARY, CONCLUSIONS AND RECOMMENDATIONS FOR FUTURE WORK	33
	REFERENCES	140
	DISTRIBUTION LIST	141

LIST OF TABLES

<u>TABLE</u>		<u>PAGE</u>
1	QUALIFICATION FLEXURE TESTS ON HM-S GRAPHITE/ERLA 4617	5
2	QUALIFICATION INTERLAMINAR SHEAR TESTS ON HM-S GRAPHITE/ERLA 4617	5
3	QUALIFICATION FLEXURE TESTS ON KEVLAR 49/ERLA 4617	6
4	QUALIFICATION INTERLAMINAR SHEAR TESTS ON KEVLAR 49/ERLA 4617	6
5	QUALIFICATION FLEXURE TESTS ON S-GLASS/ERLA 4617	7
6	QUALIFICATION INTERLAMINAR SHEAR TESTS ON S-GLASS/ERLA 4617	7
7	PROPERTIES OF UNIDIRECTIONAL GRAPHITE/HIGH MODULUS EPOXY (HM-S/ERLA 4617)	11
8	PROPERTIES OF UNIDIRECTIONAL KEVLAR/HIGH MODULUS EPOXY (Kevlar 49/ERLA 4617)	12
9	PROPERTIES OF UNIDIRECTIONAL S-GLASS/HIGH MODULUS EPOXY (S-Glass/ERLA 4617)	13
10	PROPERTIES OF UNIDIRECTIONAL KEVLAR 49/EPOXY (DuPont Published Data)	14
11	RESIDUAL STRAINS AT ROOM TEMPERATURE IN ANGLE-PLY GRAPHITE AND HYBRID LAMINATES	21
12	RESIDUAL STRESSES AT ROOM TEMPERATURE IN ANGLE-PLY GRAPHITE AND HYBRID LAMINATES	24
13	STATIC TENSILE PROPERTIES OF HYBRID ANGLE-PLY LAMINATES	26
14	RESIDUAL PROPERTIES OF HYBRID ANGLE-PLY LAMINATES AFTER 100 THERMAL CYCLES BETWEEN ROOM TEMPERATURE AND 411 degK (280°F) UNDER TENSILE PRELOAD	29

LIST OF TABLES (Cont'd)

<u>TABLE</u>		<u>PAGE</u>
15	RESIDUAL PROPERTIES OF HYBRID ANGLE-PLY LAMINATES AFTER 100 THERMAL CYCLES BETWEEN ROOM TEMPERATURE AND 200 degK (-100°F) UNDER TENSILE PRELOAD	32

LIST OF FIGURES

<u>FIGURE</u>		<u>PAGE</u>
1	STRAINS IN 0-DEGREE UNIDIRECTIONAL GRAPHITE/ HIGH MODULUS EPOXY SPECIMEN UNDER UNIAXIAL TENSION	37
2	STRAINS IN 0-DEGREE UNIDIRECTIONAL GRAPHITE/ HIGH MODULUS EPOXY SPECIMEN UNDER UNIAXIAL TENSION	38
3	STRAINS IN 0-DEGREE UNIDIRECTIONAL KEVLAR 49/ HIGH MODULUS EPOXY SPECIMEN UNDER UNIAXIAL TENSION	39
4	STRAINS IN 0-DEGREE UNIDIRECTIONAL KEVLAR 49/ HIGH MODULUS EPOXY SPECIMEN UNDER UNIAXIAL TENSION	40
5	STRAINS IN 0-DEGREE UNIDIRECTIONAL S-GLASS/ HIGH MODULUS EPOXY SPECIMEN UNDER UNIAXIAL TENSION	41
6	STRAINS IN 0-DEGREE UNIDIRECTIONAL S-GLASS/ HIGH MODULUS EPOXY SPECIMEN UNDER UNIAXIAL TENSION	42
7	STRAINS IN 90-DEGREE UNIDIRECTIONAL GRAPHITE/ HIGH MODULUS EPOXY SPECIMEN UNDER UNIAXIAL TENSION	43
8	STRAINS IN 90-DEGREE UNIDIRECTIONAL GRAPHITE/ HIGH MODULUS EPOXY SPECIMEN UNDER UNIAXIAL TENSION	44
9	STRAINS IN 90-DEGREE UNIDIRECTIONAL KEVLAR 49/ HIGH MODULUS EPOXY SPECIMEN UNDER UNIAXIAL TENSION	45
10	STRAINS IN 90-DEGREE UNIDIRECTIONAL KEVLAR 49/ HIGH MODULUS EPOXY SPECIMEN UNDER UNIAXIAL TENSION	46
11	STRAINS IN 90-DEGREE UNIDIRECTIONAL S-GLASS/ HIGH MODULUS EPOXY SPECIMEN UNDER UNIAXIAL TENSION	47

LIST OF FIGURES (Cont'd)

<u>FIGURE</u>		<u>PAGE</u>
12	STRAINS IN 90-DEGREE UNIDIRECTIONAL S-GLASS/ HIGH MODULUS EPOXY SPECIMEN UNDER UNIAXIAL TENSION	48
13	STRAINS IN 90-DEGREE UNIDIRECTIONAL S-GLASS/ HIGH MODULUS EPOXY SPECIMEN UNDER UNIAXIAL TENSION	49
14	STRESS-STRAIN CURVE FOR 0-DEGREE UNI- DIRECTIONAL GRAPHITE/HIGH MODULUS EPOXY SPECIMEN UNDER UNIAXIAL COMPRESSION	50
15	STRESS-STRAIN CURVE FOR 0-DEGREE UNI- DIRECTIONAL GRAPHITE/HIGH MODULUS EPOXY SPECIMEN UNDER UNIAXIAL COMPRESSION	51
16	STRESS-STRAIN CURVE FOR 0-DEGREE UNI- DIRECTIONAL KEVLAR 49/HIGH MODULUS EPOXY SPECIMEN UNDER UNIAXIAL COMPRESSION	52
17	STRESS-STRAIN CURVE FOR 0-DEGREE UNI- DIRECTIONAL KEVLAR 49/HIGH MODULUS EPOXY SPECIMEN UNDER UNIAXIAL COMPRESSION	53
18	STRESS-STRAIN CURVE FOR 0-DEGREE UNI- DIRECTIONAL S-GLASS/HIGH MODULUS EPOXY SPECIMEN UNDER UNIAXIAL COMPRESSION	49
19	STRESS-STRAIN CURVE FOR 0-DEGREE UNI- DIRECTIONAL S-GLASS/HIGH MODULUS EPOXY SPECIMEN UNDER UNIAXIAL COMPRESSION	55
20	STRESS-STRAIN CURVE FOR 90-DEGREE UNI- DIRECTIONAL GRAPHITE/HIGH MODULUS EPOXY SPECIMEN UNDER UNIAXIAL COMPRESSION	56
21	STRESS-STRAIN CURVE FOR 90-DEGREE UNI- DIRECTIONAL S-GLASS/HIGH MODULUS EPOXY SPECIMEN UNDER UNIAXIAL COMPRESSION	57
22	STRESS-STRAIN CURVE FOR 90-DEGREE UNI- DIRECTIONAL S-GLASS/HIGH MODULUS EPOXY SPECIMEN UNDER UNIAXIAL COMPRESSION	58

LIST OF FIGURES (Cont'd)

<u>FIGURE</u>		<u>PAGE</u>
23	SHEAR STRESS VERSUS SHEAR STRAIN FOR 10-DEGREE OFF-AXIS UNIDIRECTIONAL GRAPHITE/HIGH MODULUS EPOXY	59
24	SHEAR STRESS VERSUS SHEAR STRAIN FOR 10-DEGREE OFF-AXIS UNIDIRECTIONAL GRAPHITE/HIGH MODULUS EPOXY	60
25	SHEAR STRESS VERSUS SHEAR STRAIN FOR 10-DEGREE OFF-AXIS UNIDIRECTIONAL KEVLAR 49/HIGH MODULUS EPOXY	61
26	SHEAR STRESS VERSUS SHEAR STRAIN FOR 10-DEGREE OFF-AXIS UNIDIRECTIONAL KEVLAR 49/HIGH MODULUS EPOXY	62
27	SHEAR STRESS VERSUS SHEAR STRAIN IN 10-DEGREE OFF-AXIS UNIDIRECTIONAL S-GLASS/HIGH MODULUS EPOXY SPECIMEN	63
28	APPARENT STRAIN AS A FUNCTION OF TEMPERATURE OF WK-00-125TM-350 GAGE BONDED ON TITANIUM SILICATE	64
29	STRAINS IN [08] UNIDIRECTIONAL GRAPHITE/HIGH MODULUS EPOXY SPECIMEN AS A FUNCTION OF TEMPERATURE	65
30	STRAINS IN [08] UNIDIRECTIONAL KEVLAR 49/HIGH MODULUS EPOXY SPECIMEN AS A FUNCTION OF TEMPERATURE	66
31	STRAINS IN [08] UNIDIRECTIONAL S-GLASS/HIGH MODULUS EPOXY SPECIMEN AS A FUNCTION OF TEMPERATURE	67
32	STRAINS IN $[0^K/+45^C/0^C]_S$ GRAPHITE/KEVLAR 49/HIGH MODULUS EPOXY SPECIMEN	68
33	STRAINS IN $[+45^C/0^K/0^C]_S$ GRAPHITE/KEVLAR 49/HIGH MODULUS EPOXY SPECIMEN	69
34	STRAINS IN $[0^K/+45^C/0^K]_S$ GRAPHITE/KEVLAR 49/HIGH MODULUS EPOXY SPECIMEN	70

LIST OF FIGURES (Cont'd)

<u>FIGURE</u>		<u>PAGE</u>
35	STRAINS IN $[+45^{\text{C}}/0_2^{\text{K}}]_{\text{s}}$ GRAPHITE/KEVLAR 49/ HIGH MODULUS EPOXY SPECIMEN	71
36	STRAINS IN $[0^{\text{G}}/+45^{\text{C}}/0^{\text{C}}]_{\text{s}}$ GRAPHITE/S-GLASS/ HIGH MODULUS EPOXY SPECIMEN	72
37	STRAINS IN $[+45^{\text{C}}/0^{\text{G}}/0^{\text{C}}]_{\text{s}}$ GRAPHITE/S-GLASS/ HIGH MODULUS EPOXY SPECIMEN	73
38	STRAINS IN $[0^{\text{G}}/+45^{\text{C}}/0^{\text{C}}]_{\text{s}}$ GRAPHITE/S-GLASS/ HIGH MODULUS EPOXY SPECIMEN	74
39	STRAINS IN $[+45^{\text{C}}/0_2^{\text{G}}]_{\text{s}}$ GRAPHITE/S-GLASS/ HIGH MODULUS EPOXY SPECIMEN	75
40	RESTRAINT STRAINS IN 0-DEG. KEVLAR 49 PLIES OF $[0^{\text{K}}/+45^{\text{C}}/0^{\text{K}}]_{\text{s}}$ GRAPHITE/KEVLAR 49/HIGH MODULUS EPOXY SPECIMEN	76
41	RESTRAINT STRAINS IN 0-DEG. GRAPHITE PLIES OF $[0^{\text{K}}/+45^{\text{C}}/0^{\text{C}}]_{\text{s}}$ GRAPHITE/KEVLAR 49/HIGH MODULUS EPOXY SPECIMEN	77
42	RESTRAINT STRAINS IN 45-DEG. GRAPHITE PLIES OF $[0^{\text{K}}/+45^{\text{C}}/0^{\text{C}}]_{\text{s}}$ GRAPHITE/KEVLAR 49/HIGH MODULUS EPOXY SPECIMEN	78
43	RESTRAINT STRAINS IN 0-DEG. KEVLAR 49 PLIES OF $[+45^{\text{C}}/0^{\text{K}}/0^{\text{C}}]_{\text{s}}$ GRAPHITE/KEVLAR 49/HIGH MODULUS EPOXY SPECIMEN	79
44	RESTRAINT STRAINS IN 0-DEG. GRAPHITE PLIES OF $[+45^{\text{C}}/0^{\text{K}}/0^{\text{C}}]_{\text{s}}$ GRAPHITE/KEVLAR 49/HIGH MODULUS EPOXY SPECIMEN	80
45	RESTRAINT STRAINS IN 45-DEG. GRAPHITE PLIES OF $[+45^{\text{C}}/0^{\text{K}}/0^{\text{C}}]_{\text{s}}$ GRAPHITE/KEVLAR 49/HIGH MODULUS EPOXY SPECIMEN	81
46	RESTRAINT STRAINS IN 0-DEG. KEVLAR 49 PLIES OF $[0^{\text{K}}/+45^{\text{C}}/0^{\text{K}}]_{\text{s}}$ GRAPHITE/KEVLAR 49/HIGH MODULUS EPOXY SPECIMEN	82

LIST OF FIGURES (Cont'd)

<u>FIGURE</u>		<u>PAGE</u>
47	RESTRAINT STRAINS IN 45-DEG. GRAPHITE PLIES OF $[0^K/+45C/0^K]_S$ GRAPHITE/KEVLAR 49/HIGH MODULUS EPOXY SPECIMEN	83
48	RESTRAINT STRAINS IN 0-DEG. KEVLAR 49 PLIES OF $[+45C/0_2^K]_S$ GRAPHITE/KEVLAR 49/HIGH MODULUS EPOXY SPECIMEN	84
49	RESTRAINT STRAINS IN 45-DEG. GRAPHITE PLIES OF $[+45C/0_2^K]_S$ GRAPHITE/KEVLAR 49/HIGH MODULUS EPOXY SPECIMEN	85
50	RESTRAINT STRAINS IN 0-DEG. S-GLASS PLIES OF $[0G/+45C/0C]_S$ GRAPHITE/S-GLASS/HIGH MODULUS EPOXY SPECIMEN	86
51	RESTRAINT STRAINS IN 0-DEG. GRAPHITE PLIES OF $[0G/+45C/0C]_S$ GRAPHITE/S-GLASS/HIGH MODULUS EPOXY SPECIMEN	87
52	RESTRAINT STRAINS IN 45-DEG. GRAPHITE PLIES OF $[0G/+45C/0C]_S$ GRAPHITE/S-GLASS/HIGH MODULUS EPOXY SPECIMEN	88
53	RESTRAINT STRAINS IN 0-DEG. S-GLASS PLIES OF $[+45C/0G/0C]_S$ GRAPHITE/S-GLASS/HIGH MODULUS EPOXY SPECIMEN	
54	RESTRAINT STRAINS IN 0-DEG. GRAPHITE PLIES OF $[+45C/0G/0C]_S$ GRAPHITE/S-GLASS/HIGH MODULUS EPOXY SPECIMEN	90
55	RESTRAINT STRAINS IN 45-DEG. GRAPHITE PLIES OF $[+45C/0G/0C]_S$ GRAPHITE/S-GLASS/HIGH MODULUS EPOXY SPECIMEN	91
56	RESTRAINT STRAINS IN 0-DEG. S-GLASS PLIES OF $[0G/+45C/0G]_S$ GRAPHITE/S-GLASS/HIGH MODULUS EPOXY SPECIMEN	92
57	RESTRAINT STRAINS IN 45-DEG. GRAPHITE PLIES OF $[0G/+45C/0G]_S$ GRAPHITE/S-GLASS/HIGH MODULUS EPOXY SPECIMEN	93

LIST OF FIGURES (Cont'd)

<u>FIGURE</u>		<u>PAGE</u>
58	RESTRAINT STRAINS IN 0-DEG. S-GLASS PLIES OF $[+45^C/0_2^G]_s$ GRAPHITE/S-GLASS/HIGH MODULUS EPOXY SPECIMEN	94
59	RESTRAINT STRAINS IN 45-DEG. GRAPHITE PLIES OF $[+45^C/0_2^G]_s$ GRAPHITE/S-GLASS/HIGH MODULUS EPOXY SPECIMEN	95
60	STRAINS IN $[0^K/+45^C/0^C]_s$ GRAPHITE/KEVLAR 49/HIGH MODULUS EPOXY SPECIMEN UNDER UNIAXIAL TENSILE LOADING	96
61	STRAINS IN $[0^K/+45^C/0^C]_s$ GRAPHITE/KEVLAR 49/HIGH MODULUS EPOXY SPECIMEN UNDER UNIAXIAL TENSILE LOADING	97
62	STRAINS IN $[+45^C/0^K/0^C]_s$ GRAPHITE/KEVLAR 49/HIGH MODULUS EPOXY SPECIMEN UNDER UNIAXIAL TENSILE LOADING	98
63	STRAINS IN $[+45^C/0^K/0^C]_s$ GRAPHITE/KEVLAR 49/HIGH MODULUS EPOXY SPECIMEN UNDER UNIAXIAL TENSILE LOADING	99
64	STRAINS IN $[0^K/+45^C/0^K]_s$ GRAPHITE/KEVLAR 49/HIGH MODULUS EPOXY SPECIMEN UNDER UNIAXIAL TENSILE LOADING	100
65	STRAINS IN $[0^K/+45^C/0^K]_s$ GRAPHITE/KEVLAR 49/HIGH MODULUS EPOXY SPECIMEN UNDER UNIAXIAL TENSILE LOADING	101
66	STRAINS IN $[+45^C/0_2^K]_s$ GRAPHITE/KEVLAR 49/HIGH MODULUS EPOXY SPECIMEN UNDER UNIAXIAL TENSILE LOADING	102
67	STRAINS IN $[+45^C/0_2^K]_s$ GRAPHITE/KEVLAR 49/HIGH MODULUS EPOXY SPECIMEN UNDER UNIAXIAL TENSILE LOADING	103
68	STRAINS IN $[0^G/+45^C/0^C]_s$ GRAPHITE/S-GLASS/HIGH MODULUS EPOXY SPECIMEN UNDER UNIAXIAL TENSILE LOADING	104

LIST OF FIGURES

FIGURE		PAGE
69	STRAINS IN $[0^G/+45^C/0^C]_s$ GRAPHITE/S-GLASS/ HIGH MODULUS EPOXY SPECIMEN UNDER UNIAXIAL TENSILE LOADING	105
70	STRAINS IN $[+45^C/0^G/0^C]_s$ GRAPHITE/S-GLASS/ HIGH MODULUS EPOXY SPECIMEN UNDER UNIAXIAL TENSILE LOADING	106
71	STRAINS IN $[+45^C/0^G/0^C]_s$ GRAPHITE/S-GLASS/ HIGH MODULUS EPOXY SPECIMEN UNDER UNIAXIAL TENSILE LOADING	107
72	STRAINS IN $[0^G/+45^C/0^G]_s$ GRAPHITE/S-GLASS/ HIGH MODULUS EPOXY SPECIMEN UNDER UNIAXIAL TENSILE LOADING	108
73	STRAINS IN $[0^G/+45^C/0^G]_s$ GRAPHITE/S-GLASS/ HIGH MODULUS EPOXY SPECIMEN UNDER UNIAXIAL TENSILE LOADING	109
74	STRAINS IN $[+45^C/0_2^G]_s$ GRAPHITE/S-GLASS/ HIGH MODULUS EPOXY SPECIMEN UNDER UNIAXIAL TENSILE LOADING	110
75	STRAINS IN $[+45^C/0_2^G]_s$ GRAPHITE/S-GLASS/ HIGH MODULUS EPOXY SPECIMEN UNDER UNIAXIAL TENSILE LOADING	111
76	STRAINS IN $[0^K/+45^C/0^C]_s$ GRAPHITE/KEVLAR 49/ HIGH MODULUS EPOXY SPECIMEN UNDER UNIAXIAL TENSILE LOADING AFTER 100 THERMAL CYCLES BETWEEN ROOM TEMPERATURE AND 411 degK (280°F) WITH 244 MPa (35 ksi) TENSILE PRELOAD	112
77	STRAINS IN $[0^K/+45^C/0^C]_s$ GRAPHITE/KEVLAR 49/ HIGH MODULUS EPOXY SPECIMEN UNDER UNIAXIAL TENSILE LOADING AFTER 100 THERMAL CYCLES BETWEEN ROOM TEMPERATURE AND 411 degK (280°F) WITH 244 MPa (35 ksi) TENSILE PRELOAD	113
78	STRAINS IN $[+45^C/0_2^K]_s$ GRAPHITE/KEVLAR 49/ HIGH MODULUS EPOXY SPECIMEN UNDER UNIAXIAL TENSILE LOADING AFTER 100 THERMAL CYCLES BETWEEN ROOM TEMPERATURE AND 411 degK (280°F) WITH 369 MPa (54 ksi) TENSILE PRELOAD	114

LIST OF FIGURES (Cont'd)

<u>FIGURE</u>		<u>PAGE</u>
79	STRAINS IN $[+45^{\text{C}}/0_2^{\text{K}}]_s$ GRAPHITE/KEVLAR 49/ HIGH MODULUS EPOXY SPECIMEN UNDER UNIAXIAL TENSILE LOADING AFTER 100 THERMAL CYCLES BETWEEN ROOM TEMPERATURE AND 411 degK (280°F) WITH 369 MPa (54 ksi) TENSILE PRELOAD	115
80	STRAINS IN $[0^{\text{G}}/+45^{\text{C}}/0^{\text{C}}]_s$ GRAPHITE/S-GLASS/ HIGH MODULUS EPOXY SPECIMEN UNDER UNIAXIAL TENSILE LOADING AFTER 100 THERMAL CYCLES BETWEEN ROOM TEMPERATURE AND 411 degK (280°F) WITH 219 MPa (32 ksi) TENSILE PRELOAD	116
81	STRAINS IN $[0^{\text{G}}/+45^{\text{C}}/0^{\text{C}}]_s$ GRAPHITE/S-GLASS/ HIGH MODULUS EPOXY SPECIMEN UNDER UNIAXIAL TENSILE LOADING AFTER 100 THERMAL CYCLES BETWEEN ROOM TEMPERATURE AND 411 degK (280°F) WITH 219 MPa (32 ksi) TENSILE PRELOAD	117
82	STRAINS IN $[+45^{\text{C}}/0^{\text{G}}/0^{\text{C}}]_s$ GRAPHITE/S-GLASS/ HIGH MODULUS EPOXY SPECIMEN UNDER UNIAXIAL TENSILE LOADING AFTER 100 THERMAL CYCLES BETWEEN ROOM TEMPERATURE AND 411 degK (280°F) WITH 201 MPa (29 ksi) TENSILE PRELOAD (0-DEG. GRAPHITE PLYS FAILED)	118
83	STRAINS IN $[+45^{\text{C}}/0^{\text{G}}/0^{\text{C}}]_s$ GRAPHITE/S-GLASS/ HIGH MODULUS EPOXY SPECIMEN UNDER UNIAXIAL TENSILE LOADING AFTER 100 THERMAL CYCLES BETWEEN ROOM TEMPERATURE AND 411 degK (280°F) WITH 201 MPa (29 ksi) TENSILE PRELOAD	119
84	STRAINS IN $[0^{\text{G}}/+45^{\text{C}}/0^{\text{G}}]_s$ GRAPHITE/S-GLASS/ HIGH MODULUS EPOXY SPECIMEN UNDER UNIAXIAL TENSILE LOADING AFTER 100 THERMAL CYCLES BETWEEN ROOM TEMPERATURE AND 411 degK (280°F) WITH 422 MPa (61 ksi) TENSILE PRELOAD	120
85	STRAINS IN $[0^{\text{G}}/+45^{\text{C}}/0^{\text{G}}]_s$ GRAPHITE/S-GLASS/ HIGH MODULUS EPOXY SPECIMEN UNDER UNIAXIAL TENSILE LOADING AFTER 100 THERMAL CYCLES BETWEEN ROOM TEMPERATURE AND 400 degK (280°F) WITH 422 MPa (61 ksi) TENSILE PRELOAD	121

LIST OF FIGURES (Cont'd)

<u>FIGURE</u>		<u>PAGE</u>
86	STRAINS IN $[+45^{\circ}/0^{\circ}]_s$ GRAPHITE/S-GLASS/ HIGH MODULUS EPOXY SPECIMEN UNDER UNIAXIAL TENSILE LOADING AFTER 100 THERMAL CYCLES BETWEEN ROOM TEMPERATURE and 411 degK (280°F) WITH 422 MPa (61 ksi) TENSILE PRELOAD	122
87	STRAINS IN $[+45^{\circ}/0^{\circ}]_s$ GRAPHITE/S-GLASS/ HIGH MODULUS EPOXY SPECIMEN UNDER UNIAXIAL TENSILE LOADING AFTER 100 THERMAL CYCLES BETWEEN ROOM TEMPERATURE AND 411 degK (280°F) WITH 422 MPa (61 ksi) TENSILE PRELOAD	123
88	CHARACTERISTIC FAILURE PATTERNS OF THREE GRAPHITE/S-GLASS/HIGH MODULUS EPOXY SPECIMENS UNDER UNIAXIAL TENSILE LOADING AFTER 100 THERMAL CYCLES BETWEEN ROOM TEMPERATURE AND 411 degK (280°F) UNDER TENSILE PRELOAD	124
89	STRAINS IN $[0^{\circ}/+45^{\circ}/0^{\circ}]_s$ GRAPHITE/KEVLAR 49/ HIGH MODULUS EPOXY SPECIMEN UNDER UNIAXIAL TENSILE LOADING AFTER 100 THERMAL CYCLES BETWEEN ROOM TEMPERATURE AND 200 degK (-100°F) WITH 244 MPa (35 ksi) TENSILE PRELOAD	125
90	STRAINS IN $[0^{\circ}/+45^{\circ}/0^{\circ}]_s$ GRAPHITE/KEVLAR 49/ HIGH MODULUS EPOXY SPECIMEN UNDER UNIAXIAL TENSILE LOADING AFTER 100 THERMAL CYCLES BETWEEN ROOM TEMPERATURE AND 200 degK (-100°F) WITH 244 MPa (35 ksi) TENSILE PRELOAD	126
91	STRAINS IN $[+45^{\circ}/0^{\circ}/0^{\circ}]_s$ GRAPHITE/KEVLAR 49/ HIGH MODULUS EPOXY SPECIMEN UNDER UNIAXIAL TENSILE LOADING AFTER 100 THERMAL CYCLES BETWEEN ROOM TEMPERATURE AND 200 degK (-100°F) WITH 258 MPa (37 ksi) TENSILE PRELOAD	127
92	STRAINS IN $[+45^{\circ}/0^{\circ}/0^{\circ}]_s$ GRAPHITE/KEVLAR 49/ HIGH MODULUS EPOXY SPECIMEN UNDER UNIAXIAL TENSILE LOADING AFTER 100 THERMAL CYCLES BETWEEN ROOM TEMPERATURE AND 200 degK (-100°F) WITH 258 MPa (37 ksi) TENSILE PRELOAD	128
93	STRAINS IN $[0^{\circ}/+45^{\circ}/0^{\circ}]_s$ GRAPHITE/KEVLAR 49/ HIGH MODULUS EPOXY SPECIMEN UNDER UNIAXIAL TENSILE LOADING AFTER 100 THERMAL CYCLES BETWEEN ROOM TEMPERATURE AND 200 degK (-100°F) WITH 560 MPa (81 ksi) TENSILE PRELOAD	129

IIT RESEARCH INSTITUTE

LIST OF FIGURES (Cont'd)

<u>FIGURE</u>		<u>PAGE</u>
94	STRAINS IN $[0^K/+45^C/0^K]_s$ GRAPHITE/KEVLAR 49/ HIGH MODULUS EPOXY SPECIMEN UNDER UNIAXIAL TENSILE LOADING AFTER 100 THERMAL CYCLES BETWEEN ROOM TEMPERATURE AND 200 degK (-100°F) WITH 560 MPa (81 ksi) TENSILE PRELOAD	130
95	STRAINS IN $[+45^C/0^K]_s$ GRAPHITE/KEVLAR 49/ HIGH MODULUS EPOXY SPECIMEN UNDER UNIAXIAL TENSILE LOADING AFTER 100 THERMAL CYCLES BETWEEN ROOM TEMPERATURE AND 200 degK (-100°F) WITH 516 MPa (75 ksi) TENSILE PRELOAD	131
96	STRAINS IN $[+45^C/0^K]_s$ GRAPHITE/KEVLAR 49/ HIGH MODULUS EPOXY SPECIMEN UNDER UNIAXIAL TENSILE LOADING AFTER 100 THERMAL CYCLES BETWEEN ROOM TEMPERATURE AND 200 degK (-100°F) WITH 516 MPa (75 ksi) TENSILE PRELOAD	132
97	STRAINS IN $[0^G/+45^C/0^C]_s$ GRAPHITE/S-GLASS/ HIGH MODULUS EPOXY SPECIMEN UNDER UNIAXIAL TENSILE LOADING AFTER 100 THERMAL CYCLES BETWEEN ROOM TEMPERATURE AND 200 degK (-100°F) WITH 256 MPa (37 ksi) TENSILE PRELOAD	133
98	STRAINS IN $[0^G/+45^C/0^C]_s$ GRAPHITE/S-GLASS/ HIGH MODULUS EPOXY SPECIMEN UNDER UNIAXIAL TENSILE LOADING AFTER 100 THERMAL CYCLES BETWEEN ROOM TEMPERATURE AND 200 degK (-100°F) WITH 256 MPa (37 ksi) TENSILE PRELOAD	134
99	STRAINS IN $[+45^C/0^G/0^C]_s$ GRAPHITE/S-GLASS/ HIGH MODULUS EPOXY SPECIMEN UNDER UNIAXIAL TENSILE LOADING AFTER 100 THERMAL CYCLES BETWEEN ROOM TEMPERATURE AND 200 degK (-100°F) WITH 234 MPa (34 ksi) TENSILE PRELOAD	135
100	STRAINS IN $[0^G/+45^C/0^G]_s$ GRAPHITE/S-GLASS/ HIGH MODULUS EPOXY SPECIMEN UNDER UNIAXIAL TENSILE LOADING AFTER 100 THERMAL CYCLES BETWEEN ROOM TEMPERATURE AND 200 degK (-100°F) WITH 591 MPa (86 ksi) TENSILE PRELOAD	136

LIST OF FIGURES (Cont'd)

<u>FIGURE</u>		<u>PAGE</u>
101	STRAINS IN $[0^G/+45^C/0^G]_s$ GRAPHITE/S-GLASS/ HIGH MODULUS EPOXY SPECIMEN UNDER UNIAXIAL TENSILE LOADING AFTER 100 THERMAL CYCLES BETWEEN ROOM TEMPERATURE AND 200 degK (-100°F) WITH 591 MPa (86 ksi) TENSILE PRELOAD	137
102	STRAINS IN $[+45^C/0_2^G]_s$ GRAPHITE/S-GLASS/ HIGH MODULUS EPOXY SPECIMEN UNDER UNIAXIAL TENSILE LOADING AFTER 100 THERMAL CYCLES BETWEEN ROOM TEMPERATURE AND 200 degK (-100°F) WITH 584 MPa (85 ksi) TENSILE PRELOAD	138
103	STRAINS IN $[+45^C/0_2^G]_s$ GRAPHITE/S-GLASS/ HIGH MODULUS EPOXY SPECIMEN UNDER UNIAXIAL TENSILE LOADING AFTER 100 THERMAL CYCLES BETWEEN ROOM TEMPERATURE AND 200 degK (-100°F) WITH 584 MPa (85 ksi) TENSILE PRELOAD	139

LAMINATION RESIDUAL STRESSES IN HYBRID COMPOSITES

1.0 INTRODUCTION

In the design and evaluation of composite structures one must take into account any preexisting residual stresses and superimpose them onto those stresses produced by subsequent mechanical and thermal loading. Lamination residual stresses in composite laminates are produced during curing as a result of the anisotropic thermal deformations of the various plies. The analysis of these stresses has been the subject of many recent analytical and experimental investigations.¹⁻⁶ Residual stresses are a function of many parameters, such as ply orientation and stacking sequence, fiber content, curing temperature and other variables.¹⁻² They can reach values comparable to the transverse strength of the ply and thus induce cracking of that ply within the laminate. Residual stresses in each ply are equilibrated with interlaminar shear stresses transmitted from adjacent plies and thus may result in ply separation.

Recognizing the need to verify the theory experimentally, the NASA-Lewis Research Center has sponsored a two-phase multi-task program with IIT Research Institute under Contract No. NAS3-16766. This was a systematic experimental program with the following objectives: (1) to measure directly the magnitude of lamination residual strains in a variety of angle-ply laminates of various materials and hybrids thereof and evaluate their dependence on composite design variables, (2) to evaluate their influence on the structural integrity, stiffness and strength of the composite, (3) to study their relationship with composite response to dynamic loading and (4) to provide experimental data for verification,

extension and application of existing residual stress theory.

The first phase of this program consisted of five tasks: (1) Literature survey and materials selection, (2) Residual strains and static strength, (3) Evaluation of stress relaxation, (4) Cyclic loading and residual strength, and (5) Effects of laminate configuration variables. Results of this phase of work have been described in the first interim report⁵ and various publications.^{3,7,8} Embedded strain gage techniques were developed and used for measuring residual strains during curing. It was shown that strains recorded in the first part (heating) of the curing cycle are not significant as they correspond to the fluid state of the matrix resin. Strains measured in the second part (cooling) of the curing cycle correspond to differential thermal expansion of the various plies. It was concluded also that the extent of relaxation of residual stresses is low. Tensile load cycling, thermal cycling and thermal cycling under tensile load did not have a measurable influence on residual strength and stiffness of the laminates. Stacking sequence variations of the same basic construction did not have an effect on residual stresses and residual properties after thermal cycling under load.

The objective of the second phase of this investigation described in this final report was to investigate the influence of hybridization on curing residual strains and residual properties after thermal cycling in angle-ply laminates. The laminates investigated were graphite/Kevlar 49/high modulus epoxy and graphite/S-glass/high modulus epoxy of $[0/\pm 45/0]_s$ and $[\pm 45/0_2]_s$ layups where half or all of the 0-degree plies were Kevlar 49 or S-glass. The same matrix, ERLA 4617, was used in all three material systems to insure uniform curing of the various plies and to produce more compatible hybrids. Residual strains during

curing were determined using previously developed techniques, described in the First Interim Report.⁵ Uniaxial tensile properties of these laminates under static loading to failure were determined and compared with similar properties after thermal cycling under load.

2.0 MATERIAL QUALIFICATION AND CHARACTERIZATION

2.1 Material Qualification

The three basic materials, HM-S graphite/ERLA 4617, Kevlar 49/ERLA 4617 and S-glass/ERLA 4617 were ordered and received in prepreg form, (Fothergill and Harvey, Ltd., Composite Materials Division, Summit Littleborough, Lancashire, England). Unidirectional 15-ply laminates were prepared and the standard qualification tests were conducted. Results of these tests for the three materials are tabulated in Tables 1 to 6.

It can be seen from these tables that the results for the graphite/high modulus epoxy are better than those obtained by the manufacturer. In the case of Kevlar 49/epoxy, however, the qualification results indicate strength values lower than those suggested by the manufacturer.

2.2 Laminate Fabrication

Laminate plates were fabricated from each material system to provide specimens for the qualification testing, characterization of unidirectional laminates and residual stress studies.

Each plate was layed up from prepreg sheets on a flat metal plate according to established procedures. The prepreg layup was vacuum-bagged to the autoclave table using a teflon film sealed by means of "Prestite" tape vacuum sealant. The curing schedule used for all three materials is as follows:

1. Apply full vacuum to bagged layup
2. Pressurize autoclave to 587 kPa (85 psi)
3. Heat to 444° degK (340°F) and hold for 7 hours
4. Allow to cool to room temperature

Table 1

QUALIFICATION FLEXURE TESTS ON HM-S GRAPHITE/ERLA 4617

Specimen Number	Thickness		Width		Flexural Strength	
	cm	(in)	cm	(in)	MPa	(ksi)
1	0.178	(0.070)	1.280	(0.504)	1110	(161)
2	0.175	(0.069)	1.273	(0.501)	1035	(150)
3	0.175	(0.069)	1.283	(0.505)	970	(141)
4	0.178	(0.070)	1.283	(0.505)	1130	(164)
5	0.170	(0.067)	1.288	(0.507)	1050	(152)

Average: 1060 (154)
 Manufacturer's Data: 1030 (149)

Table 2

QUALIFICATION INTERLAMINAR SHEAR TESTS ON HM-S GRAPHITE/ERLA 4617

Specimen Number	Thickness		Width		Shear Strength	
	cm	(in)	cm	(in)	MPa	(ksi)
1	0.163	(0.064)	0.635	(0.250)	55.6	(8.06)
2	0.160	(0.063)	0.653	(0.257)	58.4	(8.47)
3	0.160	(0.063)	0.650	(0.256)	61.3	(8.88)
4	0.160	(0.063)	0.635	(0.250)	55.2	(8.00)
5	0.160	(0.063)	0.658	(0.259)	61.6	(8.93)

Average: 58.4 (8.47)
 Manufacturer's Data: 54.5 (7.90)

Table 3
QUALIFICATION FLEXURE TESTS ON KEVLAR-49/ERLA 4617

Specimen Number	Thickness		Width		Flexural Strength	
	cm	(in)	cm	(in)	MPa	(ksi)
1	0.175	(0.069)	1.260	(0.496)	500	(72)
2	0.170	(0.067)	1.262	(0.497)	500	(73)
3	0.178	(0.070)	1.270	(0.500)	510	(74)
4	0.188	(0.074)	1.260	(0.496)	500	(73)
5	0.168	(0.066)	1.262	(0.497)	500	(73)
6	0.165	(0.065)	1.260	(0.496)	500	(72)
Average:					500	(73)
Manufacturer's Data:					610	(88)

Table 4
QUALIFICATION INTERLAMINAR SHEAR TESTS ON KEVLAR 49/ERLA 4617

Specimen Number	Thickness		Width		Shear Strength	
	cm	(in)	cm	(in)	MPa	(ksi)
1	0.163	(0.064)	0.645	(0.254)	27.4	(3.97)
2	0.160	(0.063)	0.648	(0.255)	27.4	(3.97)
3	0.168	(0.066)	0.648	(0.255)	28.3	(4.10)
4	0.168	(0.066)	0.650	(0.256)	27.9	(4.04)
5	0.165	(0.065)	0.645	(0.254)	28.2	(4.09)
6	0.160	(0.063)	0.648	(0.255)	28.4	(4.11)
Average:					27.9	(4.05)
Manufacturer's Data:					49.7	(7.20)

Table 5
QUALIFICATION FLEXURE TESTS ON S-GLASS/ERLA 4617

Specimen Number	Thickness		Width		Flexural Strength	
	cm	(in)	cm	(in)	MPa	(ksi)
1	0.180	(0.071)	1.265	(0.498)	1309	(190)
2	0.193	(0.076)	1.270	(0.500)	1245	(180)
3	0.185	(0.073)	1.262	(0.497)	1495	(217)
4	0.185	(0.073)	1.250	(0.492)	1313	(190)
5	0.180	(0.071)	1.262	(0.497)	1415	(205)
Average:					1355	(196)

Table 6
QUALIFICATION INTERLAMINAR SHEAR TESTS ON S-GLASS/ERLA 4617

Specimen Number	Thickness		Width		Shear Strength	
	cm	(in)	cm	(in)	MPa	(ksi)
1	0.170	(0.067)	0.630	(0.248)	95.6	(13.9)
2	0.168	(0.066)	0.632	(0.249)	96.0	(13.9)
3	0.173	(0.068)	0.630	(0.248)	89.0	(12.9)
4	0.178	(0.070)	0.638	(0.251)	90.4	(13.1)
5	0.168	(0.066)	0.630	(0.248)	93.3	(13.5)
Average:					92.9	(13.5)

This procedure is slightly different from that used previously for the graphite/high modulus epoxy, in that the recommended 6-hour postcuring was combined with the 1-hour curing.

2.3 Characterization of Unidirectional Laminates

Two unidirectional $[0_6]$ specimens 2.54 cm (1 in.) wide and 23 cm (9 in.) long of each material were tested to determine 0-degree tensile properties. Stress-strain curves obtained are shown in Figs. 1 to 6. For each specimen, the initial axial modulus, Poisson's ratio and strength were computed from the data. Results are indicated on the respective graphs and summarized later in Tables 7 to 12. Strains in the graphite/epoxy are linear to failure. In the Kevlar/epoxy they are linear up to a stress of approximately 965 MPa (140 ksi) thereafter, there seems to be a stiffening of the specimen. The strains in the S-glass/epoxy are linear up to approximately 1450 MPa (210 ksi), thereafter they increase at a faster rate. The graphite/epoxy has the lowest ultimate strain (0.0035) and the S-glass/epoxy has the highest (0.035), ten times that of graphite/epoxy.

Two unidirectional $[90_8]$ specimens 2.54 cm (1 in.) wide and 23 cm (9 in.) long of each material were tested to determine 90-degree tensile properties. Stress-strain curves are shown in Figs. 7 to 13. Results are indicated in the graphs and tabulated in Tables 7 to 12. Strains in the graphite/epoxy and Kevlar/epoxy are linear to failure. In the S-glass/epoxy they become nonlinear above a stress of 28 MPa (4 ksi). The Kevlar/epoxy exhibited unusually low strength (5.3 MPa; 765 psi), much lower than published values.

Compression tests were conducted with the IITRI fixture. The specimens were 13.5 cm (5.3 in.) long and 0.63 cm (0.25 in.) wide. The 0-degree graphite/epoxy and Kevlar/epoxy specimens were 8-ply thick with a gage section 0.63 cm (0.25 in.) long. The 90-degree graphite/epoxy and Kevlar/epoxy specimens were 15-ply thick and had a gage section 0.95 cm (0.375 in.) long. All S-glass/epoxy specimens, prepared and tested last, were 20-ply thick with a gage section 0.95 in. (0.375 in.) long. All compression specimens were instrumented with longitudinal strain gages on both sides. Strain gages were monitored throughout loading to failure. Stress-strain curves and the computed modulus and strength values are shown in Figs. 14 to 22. Figures 14 and 16 for the 0-degree tests on graphite/epoxy and Kevlar/epoxy show nonlinear behavior not associated with buckling. Figures 15 and 17 for similar specimens show linear response to failure. Initial modulus and strength in both cases seem to be within expected experimental variability. In the S-glass/epoxy the 0-degree specimens respond linearly up to approximately 890 MPa (130 ksi), but their strength is appreciably lower than the corresponding tensile strength. The measured compressive modulus also appears somewhat lower than the corresponding 0-degree tensile modulus. The response of the 90-degree compression specimens is nonlinear, apparently due to material response. The nonlinearity in the S-glass/epoxy specimens is highly pronounced above a stress of approximately 48 MPa (7 ksi). Strain data for the 90-degree Kevlar/epoxy specimens were erratic and inadequate due to their low strength. Most specimens displayed negligible bending in compression. In all cases the 0-degree compressive strength was lower than the corresponding tensile strength; it was relatively higher for the graphite/epoxy and lowest for the Kevlar/epoxy. The 90-degree compressive strength is always appreciably higher than the corresponding tensile strength.

In-plane shear properties were determined by testing two 10-degree off-axis unidirectional specimens of each material. The specimens were 1.25 cm (0.5 in.) wide, 6-ply thick, and 25.4 cm (10 in.) long. They were instrumented with a three-gage rosette on each side. Shear stress and shear strain computed from the measured data are plotted in Figs. 23 to 27. The in-plane shear modulus and shear strength are also shown in the figures. Of the two graphite/epoxy specimens the one described in Fig. 23 apparently failed prematurely at a low strength. The second specimen (Fig. 24) shows linear response up to a shear stress of 16 MPa (2.3 ksi). The behavior of the S-glass/epoxy becomes nonlinear at a small fraction of its shear strength (17 MPa; 2.5 ksi).

All of the characterization results obtained for the three materials tested are summarized in Tables 7, 8 and 9. Results for the graphite/epoxy are comparable to those obtained for the same material, but of lower fiber volume ratio, tested in Task II.⁵ Properties for Kevlar/epoxy were compared with similar data available from the manufacturer.⁹ The latter are summarized in Table 10. The longitudinal tensile properties measured are in good agreement, but in general the other properties measured are lower than those published.

Table 7
PROPERTIES OF UNIDIRECTIONAL GRAPHITE/HIGH MODULUS EPOXY
(HM-S/ERLA 4617)

Property	No. of Specimens	Value Range
Ply Thickness		0.114 mm (0.0045 in)
Fiber Volume Ratio, FVR		0.61
Longitudinal Modulus, E_{11}	2	218.7-220.8 GPa(31.7-32.0x10 ⁶ psi)
Transverse Modulus, E_{22}	2	7.04 GPa (1.02 x 10 ⁶ psi)
Shear Modulus, G_{12}	2	6.0-7.3 GPa(0.86-1.06 x 10 ⁶ psi)
Major Poisson's Ratio, ν_{12}	2	0.28-0.34
Minor Poisson's Ratio, ν_{21}	2	0.02
Longitudinal Tensile Strength, S_{11T}	2	631-1007 MPa (91.5-146 ksi)
Ultimate Longitudinal Tensile Strain, ϵ_{11T}^u	2	0.0029-0.0041
Longitudinal Compressive Strength, S_{11C}	2	642-690 MPa (93-100 ksi)
Ultimate Longitudinal Compressive Strain, ϵ_{11C}^u	2	0.0033-0.0045
Transverse Tensile Strength, S_{22T}	2	33-39 MPa (4800-5600 psi)
Ultimate Transverse Tensile Strain, ϵ_{22T}^u	2	0.0048-0.0054
Transverse Compressive Strength, S_{22C}	2	143-159 MPa (20.8-23 ksi)
Ultimate Transverse Compressive Strain, ϵ_{22C}^u	1	0.0277
Intralaminar Shear Strength, S_{12}	2	30-72 MPa (4200-10,400 psi)
Ultimate Intralaminar Shear Strain, ϵ_{12}^u	2	0.0025-0.0061

Table 8
PROPERTIES OF UNIDIRECTIONAL KEVLAR/HIGH MODULUS EPOXY
 (Kevlar 49/ERLA 4617)

Property	No. of Specimens	Value Range
Ply Thickness		0.114 mm (0.0045 in.)
Fiber Volume Ratio, FVR		0.65
Longitudinal Modulus, E_{11}	2	69.0 GPa (10.0×10^6 psi)
Transverse Modulus, E_{22}	2	4.35-4.67 GPa (630,000-680,000 psi)
Shear Modulus, G_{12}	2	2.37-2.60 GPa (340,000-380,000 psi)
Major Poisson's Ratio, ν_{12}	2	0.39-0.42
Minor Poisson's Ratio, ν_{21}	2	0.01-0.02
Longitudinal Tensile Strength, S_{11T}	2	1364-1481 MPa (198-215 ksi)
Ultimate Longitudinal Tensile Strain, ϵ_{11T}^u	2	0.0189-0.0198
Longitudinal Compressive Strength, S_{11C}	2	180-207 MPa (26-30 ksi)
Ultimate Longitudinal Compressive Strain, ϵ_{11C}^u	2	0.0034-0.0048
Transverse Tensile Strength, S_{22T}	2	4.8-5.8 MPa (700-830 psi)
Ultimate Transverse Tensile Strain, ϵ_{22T}^u	2	0.0011-0.0012
Transverse Compressive Strength, S_{22C}	1	64 MPa (9,200 psi)
Intralaminar Shear Strength, S_{12}	2	23.9-24.1 MPa (3460-3500 psi)
Ultimate Intralaminar Shear Strain, ϵ_{12}^u	2	0.0049-0.0054

Table 9
PROPERTIES OF UNIDIRECTIONAL S-GLASS/HIGH MODULUS EPOXY
(S-Glass/ERLA 4617)

Property	No. of Specimens	Value Range
Ply Thickness		0.119 mm (0.0047 in.)
Fiber Volume Ratio, FVR		0.58
Longitudinal Modulus, E_{11}	2	47.8-52.1 GPa (6.9-7.5 x 10 ⁶ psi)
Transverse Modulus, E_{22}	3	19.1-19.3 GPa (2.77-2.80 x 10 ⁶ psi)
Shear Modulus, G_{12}	1	7.2 GPa (1.04 x 10 ⁶ psi)
Major Poisson's Ratio, ν_{12}	2	0.29
Minor Poisson's Ratio, ν_{21}	3	0.10
Longitudinal Tensile Strength, S_{11T}	2	1587-1960 MPa (230-284 ksi)
Ultimate Longitudinal Tensile Strain, ϵ_{11T}^u	2	0.0325-0.0387
Longitudinal Compressive Strength, S_{11C}	2	942-1072 MPa (137-155 ksi)
Ultimate Longitudinal Compressive Strain, ϵ_{11C}^u	2	0.0187-0.0218
Transverse Tensile Strength, S_{22T}	3	72-85 MPa (10.5-12.4 ksi)
Ultimate Transverse Tensile Strain, ϵ_{22T}^u	3	0.0041-0.0052
Transverse Compressive Strength, S_{22C}	2	174-194 MPa (25-28 ksi)
Ultimate Transverse Compressive Strain, ϵ_{22C}^u	2	0.0142-0.0187
Intralaminar Shear Strength, S_{12}	2	69-72 MPa (10.0-10.4 ksi)
Ultimate Intralaminar Shear Strain, ϵ_{12}^u	1	0.0101

IIT RESEARCH INSTITUTE

Table 10
PROPERTIES OF UNIDIRECTIONAL KEVLAR-49/EPOXY
(DuPont Published Data)

Property	Value
Fiber Volume Ratio, FVR	0.60
Longitudinal Modulus, E_{11}	76 GPa (11.0×10^6 psi)
Transverse Modulus, E_{22}	5.5 GPa (800,000 psi)
Shear Modulus, G_{12}	2.07 GPa (300,000 psi)
Major Poisson's Ratio	0.34
Longitudinal Tensile Strength, S_{11T}	1379 MPa (200 ksi)
Ultimate Longitudinal Tensile Strain, ϵ_{11T}^u	0.018
Longitudinal Compressive Strength, S_{11C}	276 MPa (40 psi)
Transverse Tensile Strength, S_{22T}	30 MPa (4,300 psi)
Ultimate Transverse Tensile Strain, ϵ_{22T}^u	0.006
Transverse Compressive Strength, S_{22C}	138 MPa (20 ksi)
Intralaminar Shear Strength, S_{12}	60 MPa (8700 psi)

3.0 RESIDUAL STRAINS

3.1 Experimental Procedure

The specimens were 2.54 cm x 22.9 cm (1 in. x 9 in.) eight-ply graphite/Kevlar 49/epoxy (HM-S Graphite/Kevlar 49/ERLA 4617) and graphite/S-glass/epoxy (HM-S Graphite/S-Glass/ERLA 4617) laminates of the following constructions:

$$[0^K/\pm 45^C/0^C]_s, [0^K/\pm 45^C/0^K]_s, [\pm 45^C/0^K/0^C]_s, [\pm 45^C/0_2^K]_s$$

$$[0^G/\pm 45^C/0^C]_s, [0^G/\pm 45^C/0^G]_s, [\pm 45^C/0^G/0^C]_s, [\pm 45^C/0_2^G]_s$$

where superscripts C, K and G denote graphite, Kevlar and S-glass, respectively. The same matrix resin, ERLA 4617, was selected for all three basic materials to insure compatibility and uniform curing of the various plies. Three specimens of each of the laminate configurations above were prepared. Unidirectional $[0_8]$ specimens of graphite/epoxy, Kevlar 49/epoxy and S-glass/epoxy were also used for control purposes to determine the unrestrained thermal deformations of the three basic materials. The ply thicknesses for these materials are 0.114 mm (0.0045 in.), 0.114 mm (0.0045 in.) and 0.119 mm (0.0047 in.), respectively.

In order to facilitate data reduction from embedded gages recorded during curing and thermal cycling of the laminates, a "zero expansion coefficient" gage was evaluated. Samples of this type of gage were bonded on a quartz specimen and subjected to thermal cycling between room temperature and 450° degK (350°F). The maximum purely thermal output of these sample gages was approximately 150 $\mu\epsilon$. It was then decided to use this type of gage for embedment in the hybrid laminates.

The unidirectional specimens were prepared and instrumented with embedded two-gage rosettes (Micro-Measurements WK-00-125TM-350, Option B-157) between the second and third ply and between the fourth and fifth ply. The angle-ply hybrid specimens were

prepared with embedded three-gage rosettes (Micro-Measurements WK-00-125RA-350, Option B-157). One rosette was embedded in the middle of the laminate thickness and the other between the ± 45 -degree plies and the outer 0-degree ply. The gages used were fully encapsulated and had a minimal purely thermal output. The attached ribbon leads were sandwiched between thin (0.013 mm; 0.0005 in.) polyimide strips. In all cases above a thermocouple was also embedded in the middle surface of the specimen. To determine the purely thermal output of the gage, a Titanium Silicate specimen, which has a very low coefficient of thermal expansion ($\alpha = 0.03 \times 10^{-6} \text{K}^{-1} = 0.017 \times 10^{-6} \text{ in/in/}^\circ\text{F}$), was also instrumented with a two-gage rosette and a thermocouple.

The instrumented specimens, including the reference unidirectional and Titanium Silicate specimens, were subjected to the curing and postcuring cycles in the autoclave. Strain gage and thermocouple readings were taken throughout. Subsequently, the same specimens were subjected to a thermal cycle from room temperature to 444 degK (340°F) and down to room temperature. Strain gages and thermocouples were recorded at 5.5 degK (10°F) intervals. The true thermal strains were obtained by subtracting algebraically from the recorded apparent strains the small output of the gage on the Titanium Silicate specimen and adding the known thermal expansion of the latter.

3.2 Residual Strains

The purely thermal output of the gages used is shown by the apparent strains recorded on the Titanium Silicate specimen (Fig. 28). The maximum apparent strain is 75 $\mu\epsilon$. Thermal strains recorded in the three $[0_g]$ unidirectional specimens are plotted versus temperature in Figs. 29 to 31. Both Kevlar 49/epoxy and graphite/epoxy exhibit negative thermal strains in the longitudinal (fiber) direction. The Kevlar 49/epoxy exhibits the largest positive transverse and negative

longitudinal strains. The S-glass/epoxy undergoes the lowest thermal deformation in the transverse direction and the highest (positive) in the longitudinal direction.

Coefficients of thermal expansion computed from these data for the graphite/epoxy are:

At 297 degK (75°F)

$$\alpha_{11} = -1.26 \times 10^{-6} \text{K}^{-1} \quad (-0.7 \mu\epsilon/^{\circ}\text{F})$$

$$\alpha_{22} = 33.9 \times 10^{-6} \text{K}^{-1} \quad (18.8 \mu\epsilon/^{\circ}\text{F})$$

at 444 degK (340°F)

$$\alpha_{11} = -1.26 \times 10^{-6} \text{K}^{-1} \quad (-0.7 \mu\epsilon/^{\circ}\text{F})$$

$$\alpha_{22} = 83.7 \times 10^{-6} \text{K}^{-1} \quad (46.5 \mu\epsilon/^{\circ}\text{F})$$

Coefficients of thermal expansion computed for the Kevlar/epoxy are:

At 297 degK (75°F)

$$\alpha_{11} = -4.0 \times 10^{-6} \text{K}^{-1} \quad (-2.2 \mu\epsilon/^{\circ}\text{F})$$

$$\alpha_{22} = 57.6 \times 10^{-6} \text{K}^{-1} \quad (32.0 \mu\epsilon/^{\circ}\text{F})$$

at 444 degK (340°F)

$$\alpha_{11} = -5.7 \times 10^{-6} \text{K}^{-1} \quad (-3.2 \mu\epsilon/^{\circ}\text{F})$$

$$\alpha_{22} = 82.8 \times 10^{-6} \text{K}^{-1} \quad (46.0 \mu\epsilon/^{\circ}\text{F})$$

Coefficients of thermal expansion computed for the S-glass/epoxy are:

At 297 degK (75°F)

$$\alpha_{11} = 6.6 \times 10^{-6} \text{K}^{-1} \quad (3.7 \mu\epsilon/^{\circ}\text{F})$$

$$\alpha_{22} = 19.7 \times 10^{-6} \text{K}^{-1} \quad (10.9 \mu\epsilon/^{\circ}\text{F})$$

at 444 degK (340°F)

$$\alpha_{11} = 14.1 \times 10^{-6} \text{K}^{-1} \quad (7.9 \mu\epsilon/^{\circ}\text{F})$$

$$\alpha_{22} = 26.5 \times 10^{-6} \text{K}^{-1} \quad (14.7 \mu\epsilon/^{\circ}\text{F})$$

Thermal strains recorded during cool down were very close to and averaged with those obtained during subsequent thermal cycling. Thermal strains as a function of temperature obtained for the eight hybrid laminates described above are shown in Figs. 32 to 39. It can be seen from these results that the stacking sequence does not have an influence on the measured thermal strains for laminates composed of the same type and number of plies. The longitudinal strains in all graphite/Kevlar specimens are negative. The specimens with all 0-degree plies of Kevlar have higher transverse (positive) and longitudinal (negative) strains than the specimens with only half 0-degree Kevlar plies. This is a direct consequence of the relative magnitudes of unrestrained thermal strains in unidirectional Kevlar/epoxy and graphite/epoxy (Figs. 29 and 30). In the case of the graphite/glass specimens the substitution of the last two 0-degree graphite plies with glass plies changes the longitudinal strain from negative to positive (Figs. 36 to 39).

The residual stresses induced in each ply correspond to the so-called restraint strains, i.e., the difference between the unrestrained thermal expansion of that ply (unidirectional specimen) and the restrained expansion of the ply within the laminate (angle-ply specimen). Restraint or residual strains

obtained for the 0-degree Kevlar, 0-degree graphite and 45-degree graphite plies of the $[0^K/+45^C/0^C]_s$ and $[+45^C/0^K/0^C]_s$ graphite/Kevlar 49/epoxy specimens are plotted in Figs. 40 to 45. These strains are plotted as a function of temperature with room temperature shown as the stress-free level. The actual stress-free level is at 444 degK (340°F), the temperature at which the matrix solidifies. To refer these residual strains to this level, the curves of Figs. 40 to 45 must be shifted parallel to the strain axis until they intersect the temperature axis at 444 degK (340°F). The highest residual strain is the transverse (ϵ_{90}) strain in the 0-degree Kevlar plies exceeding $9 \times 10^{-3}\epsilon$ (Figs. 40 and 43). This is associated with the high transverse thermal expansion of the unidirectional Kevlar 49/epoxy (Fig. 30). The transverse strain in the 0-degree graphite plies is much lower reaching a peak value of $5.6 \times 10^{-3}\epsilon$. The maximum strain in the 45-degree graphite plies is $6.3 \times 10^{-3}\epsilon$.

Restraint strains were computed for the 0-degree Kevlar and 45-degree graphite plies of the $[0^K/+45^C/0^K]_s$ and $[+45^C/0_2^K]_s$ graphite/Kevlar 49/epoxy specimens. Results, shown graphically in Figs. 46 to 49, do not differ much from corresponding strains in the preceding group of specimens. In the 0-degree Kevlar plies the only noticeable difference is the small reduction in the longitudinal (ϵ_0) residual strain from $-0.4 \times 10^{-3}\epsilon$ to $-0.2 \times 10^{-3}\epsilon$. The strains in the 45-degree graphite plies show a small increase in the longitudinal direction and a slight reduction in the transverse direction.

Residual strains in the 0-degree S-glass, 0-degree graphite and 45-degree graphite plies of the $[0^G/+45^C/0^C]_s$ and $[+45^C/0^G/0^C]_s$ specimens were obtained as before and plotted in Figs. 50 to 55 with room temperature as the reference temperature. The transverse strains in the 0-degree S-glass plies are relatively low, compared to similar strains in the 0-degree graphite plies, because of the lower transverse thermal expansion of the unidirectional

S-glass/epoxy. All three strain components in the 0-degree S-glass plies are close to each other because the corresponding strain components are similarly related in the unidirectional material. Residual strains in the graphite plies are very close to those obtained for the graphite/Kevlar 49/epoxy specimens, since these strains are primarily dominated by the strains in the unidirectional graphite/epoxy.

Residual strains in the 0-degree S-glass and 45-degree graphite plies of the $[0^G/\pm 45^C/0^G]_s$ and $[\pm 45^C/0_2^G]_s$ graphite/S-glass/epoxy are not much different from the corresponding strains in the preceding group (Figs. 56 to 59). The main difference are a reduction in the peak longitudinal (ϵ_0) strain in the 0-degree S-glass ply from $1.75 \times 10^{-3}\epsilon$ to $1.45 \times 10^{-3}\epsilon$ and a reduction in the peak longitudinal (ϵ_0) strain in the 45-degree graphite plies from $3.5 \times 10^{-3}\epsilon$ to $3.1 \times 10^{-3}\epsilon$.

The peak residual strains occurring at room temperature are tabulated in Table 11 for all laminates tested including the all-graphite laminate tested under Task II.⁵ Several conclusions can be drawn from these results. For laminates of the same composition, stacking sequence variations have no influence on residual stresses. Hybridizing the basic $[0_2^C/\pm 45^C]_s$ graphite/epoxy laminate by substituting Kevlar or S-glass plies for 0-degree graphite plies has a relatively small influence, a small reduction, on residual strains in the remaining graphite plies. This is due in part to the fact that the thermal deformations in the angle-ply laminates are an order of magnitude lower than the unrestrained strains in the unidirectional material and in part to the relatively lower stiffness of Kevlar and S-glass. Increasing the number of Kevlar plies in the graphite/Kevlar group increases slightly the transverse (to the fibers) strains in the Kevlar and graphite plies. Replacing Kevlar with S-glass reduces slightly the transverse strains in the graphite plies. Increasing the number of S-glass plies in the graphite/S-glass group reduces the transverse strain in the graphite plies slightly more.

Table 11
RESIDUAL STRAINS AT ROOM TEMPERATURE IN ANGLE-PLY
GRAPHITE AND HYBRID LAMINATES

Laminate	Ply	Strain, $10^{-3}\epsilon$			
		ϵ_0	ϵ_{90}	ϵ_{45}	ϵ_{-45}
$[0_2^C/\pm 45^C]_s$	0^C	0	6.0	2.9	
	45^C	3.4	2.6	-0.4	6.5
$[0^K/\pm 45^C/0^C]_s$	0^K	-0.4	9.0	4.3	
	0^C	0	5.6	2.8	
	45^C	3.4	2.4	-0.5	6.3
$[\pm 45^C/0^K/0^C]_s$	0^K	-0.4	9.2	4.4	
	0^C	0	5.6	2.8	
	45^C	3.4	2.3	-0.5	6.2
$[0^K/\pm 45^C/0^K]_s$	0^K	-0.2	9.1	4.4	
	45^C	3.7	2.2	-0.5	6.3
	0^K	-0.2	9.3	4.6	
$[\pm 45^C/0_2^K]_s$	0^K	-0.2	9.3	4.6	
	45^C	3.6	2.2	-0.4	6.4
$[0^G/\pm 45^C/0^C]_s$	0^G	1.7	2.4	2.0	
	0^C	-0.1	5.5	2.7	
	45^C	3.5	2.2	-0.6	6.3
$[\pm 45^C/0^G/0^C]_s$	0^G	1.8	2.4	2.1	
	0^C	0	5.6	2.8	
	45^C	3.5	2.2	-0.6	6.2
$[0^G/\pm 45^C/0^G]_s$	0^G	1.4	2.4	1.9	
	45^C	3.1	2.1	-0.8	6.0
	0^G	1.5	2.5	2.0	
$[\pm 45^C/0_2^G]_s$	0^G	1.5	2.5	2.0	
	45^C	3.2	2.2	-0.7	6.1

Note: Superscripts K, C and G denote Kevlar, graphite and S-glass, respectively.

IIT RESEARCH INSTITUTE

3.3 Residual Stresses

Residual stresses in any given ply can be computed from the residual strains using the appropriate orthotropic constitutive relations. Assuming linear elastic behavior, these relations take the form

$$[\sigma_{ij}(T)] = [Q(T)] [\epsilon_{ij}(T)]$$

where $[Q]$, $[\sigma_{ij}]$ and $[\epsilon_{ij}]$ are the temperature-dependent stiffness, stress and strain matrices, respectively. In the case of unidirectional graphite/epoxy and Kevlar 49/epoxy the strain response in the longitudinal and transverse directions is linear to failure. In the case of unidirectional S-glass/epoxy the response in the longitudinal direction is linear up to at least a strain of $25 \times 10^{-3} \epsilon$, but in the transverse direction is linear only up to a strain of approximately $1.5 \times 10^{-3} \epsilon$.

In the linear range, the residual stress components in a given ply at a given temperature are given by the following stress-strain relations:

$$\sigma_{11} = \frac{E_{11}}{1 - \nu_{12}\nu_{21}} [\epsilon_{11} + \nu_{21}\epsilon_{22}]$$

$$\sigma_{22} = \frac{E_{22}}{1 - \nu_{12}\nu_{21}} [\nu_{12}\epsilon_{11} + \epsilon_{22}]$$

$$\sigma_{12} = 2G_{12}\epsilon_{12}$$

where the subscripts 1 and 2 refer to the fiber and the transverse to the fiber directions and all quantities above correspond to one temperature.

Residual stresses at room temperature were computed for the various plies of the laminates studied assuming linear elastic behavior. Results are tabulated in Table 12. The maximum transverse tensile stress for the graphite plies is 45.0 MPa (6.5 ksi) in the all-graphite laminate and 41.0 MPa (5.9 ksi) in the hybrid laminates. Both of these values exceed the static transverse tensile strength of the material which is 36 MPa (5.2 ksi). This means that these plies are most likely damaged in the transverse direction upon completion of curing. In the case of Kevlar plies the computed transverse stresses far exceed the measured static strength, which means that these plies must be damaged transversely in the early stages of cool down. Residual stresses in the S-glass plies reach values up to seventy-five percent of the static strength.

Table 12

RESIDUAL STRESSES AT ROOM TEMPERATURE IN ANGLE-PLY
GRAPHITE AND HYBRID LAMINATES

Laminate	Ply	Stress, MPa (ksi)		
		σ_{11}	σ_{22}	σ_{12}
$[0_2^C/\pm 45^C]_s$	0^C	13.1(1.9)	42.5(6.2)	0
	45^C	-73.5(-10.6)	45.0(6.5)	5.4(0.8)
$[0^K/\pm 45^C/0^C]_s$ or $[\pm 45^C/0^K/0^C]_s$	0^K	-11.2(-1.6)	40.8(5.9)	0
	0^C	12.3(1.8)	39.6(5.7)	0
	45^C	-97.0(-14.0)	43.2(6.3)	6.9(1.0)
$[0^K/\pm 45^C/0^K]_s$ or $[\pm 45^C/0_2^K]_s$	0^K	2.8(0.4)	39.4(5.7)	0
	45^C	-85.5(-12.4)	44.0(6.4)	9.3(1.4)
$[0^G/\pm 45^C/0^C]_s$ or $[\pm 45^C/0^G/0^C]_s$	0^G	103.5(15.0)	58.0(8.4)	0
	0^C	6.9(1.0)	39.2(5.7)	0
	45^C	-117.8(-17.1)	42.8(6.2)	9.0(1.3)
$[0^G/\pm 45^C/0^G]_s$ or $[\pm 45^C/0_2^G]_s$	0^G	88.3(12.8)	57.2(8.3)	0
	45^C	-151.3(-22.1)	41.0(5.9)	6.9(1.0)

Note: Superscripts K, C and G denote Kevlar, graphite and S-glass, respectively.

4.0 STATIC STRENGTH

In addition to the specimens containing embedded gages, three additional specimens of each laminate construction were prepared without embedded instrumentation. Two specimens, one with embedded gages and one instrumented with surface gages, of each of the eight hybrid laminates described before were tested statically in tension to failure. Stress-strain curves to failure for these specimens are shown in Figs. 60 to 75. The axial modulus, Poisson's ratio and strength for each specimen are indicated in these graphs as well as tabulated in Table 13. Measured values are compared with theoretically predicted ones.¹⁰ Predicted values for moduli and Poisson's ratios are based on linear lamination theory using measured values of the constituent properties. The predicted ultimate strains are based on the predicted moduli and measured strengths of the hybrid laminates assuming linear behavior to failure.

Specimens containing only two 0-degree Kevlar plies behave linearly to failure. Measured moduli range between 90 and 96 GPa (13.0 and 13.9×10^6 psi), the average Poisson's ratio is 0.79, and the measured ultimate strain is 3.9×10^{-3} . These values are compared with corresponding predicted values of 85 GPa (12.3×10^6 psi), 0.76 and 4.2×10^{-3} . The measured and predicted ultimate strains are comparable to the highest measured ultimate strain of 4.1×10^{-3} in the unidirectional graphite/epoxy material (Table 7). Specimens containing four 0-degree Kevlar plies display a characteristic nonlinearity starting in most cases at a strain of approximately 4×10^{-3} . The measured modulus, Poisson's ratio and ultimate strain are 47 GPa (6.8×10^6 psi), 0.83 and 17.4×10^{-3} , respectively. The corresponding predicted values are 47 GPa (6.8×10^6 psi), 0.77 and 16.4×10^{-3} , respectively. The reason for the lower predicted ultimate strain is the underlying

Table 13
STATIC TENSILE PROPERTIES OF HYBRID ANGLE-PLY LAMINATES

Laminate	Modulus, E_{xx} GPa (10^6 psi)		Poisson's Ratio, ν		Strength, S_{xxT} MPa (ksi)	Ultimate Longitudinal Strain, ϵ_{xxT}^u , ($10^3\epsilon$)	
	Measured	Predicted	Measured	Predicted		Measured	Predicted
$[0^K/+45^C/0^C]_s$	96(13.9) 94(13.6)	85(12.3)	0.78 0.72	0.76	384 (56) 311 (45)	3.9 3.3	4.1
$[+45^C/0^K/0^C]_s$	90(13.0) 92(13.3)	85(12.3)	0.73 0.87	0.76	373 (54) 366 (53)	4.2 4.0	4.3
$[0^K/+45^C/0^K]_s$	50(7.3) 46(6.7)	47(6.8)	0.78 0.85	0.76	776(112) 828(120)	17.0 17.8	17.0
$[+45^C/0_2^K]_s$	46(6.7) 46(6.6)	47(6.8)	0.82 0.86	0.77	725(105) 752(109)	17.7 17.2	15.8
$[0^G/+45^C/0^C]_s$	93 (13.5) 86 (12.4)	81(11.7)	0.74 0.73	0.71	345 (50) 386 (56)	3.7 4.5	4.5
$[+45^C/0^G/0^C]_s$	86 (12.4) 81 (11.8)	81(11.7)	0.75 0.73	0.71	324 (47) 345 (50)	3.8 4.2	4.1
$[0^G/+45^C/0^G]_s$	38 (5.5) 37 (5.3)	39(5.6)	0.74 0.85	0.68	876(127) 814(118)	29.2 24.8	22.0
$[+45^C/0_2^G]_s$	37 (5.3) 38 (5.5)	39(5.6)	0.75 0.73	0.68	982(142) 690(100)	35.8 20.0	21.4

Note: Superscripts C, K and G refer to graphite, Kevlar and S-glass, respectively.

assumption of linearity made for the prediction. The ultimate strain measured is still lower than the ultimate strain (19.3×10^{-3}) of unidirectional Kevlar (Table 2-8), which indicates that failure may still be governed by the ± 45 graphite/epoxy plies.

In the graphite/glass group specimens containing only two 0-degree S-glass plies behave linearly to failure (Figs. 68 to 71). The average measured modulus, Poisson's ratio and ultimate strain are 86 GPa (12.5×10^6 psi), 0.74 and 4.1×10^{-3} , compared to predicted values of 81 GPa (11.7×10^6 psi), 0.71 and 4.3×10^{-3} . The ultimate strain is comparable to that of 0-degree unidirectional graphite/epoxy, indicating that hybrid failure is governed by the 0-degree graphite/epoxy plies. Specimens containing four 0-degree S-glass plies display a characteristic nonlinearity starting at a strain of approximately 8×10^{-3} . The average measured modulus, Poisson's ratio and ultimate strain are 37 GPa (5.4×10^6 psi), 0.77 and 27.5×10^{-3} compared to predicted values of 39 GPa (5.6×10^6 psi), 0.68, and 21.7×10^{-3} . The ultimate strain in the hybrid is lower than the measured unidirectional ultimate strain 35.6×10^{-3} in the S-glass/epoxy (Table 9), indicating that failure may be influenced by a lower ultimate strain of the ± 45 -degree graphite/epoxy plies.

5.0 TENSILE LOAD WITH THERMAL CYCLING

5.1 Residual Properties After Thermal Cycling Between Room Temperature and 411 degK (280°F) Under Tensile Load

Two specimens, including one with embedded gages, of each of the eight hybrid configurations discussed were subjected to a static tensile load and to 100 thermal cycles between room temperature and 411 degK (280°F). The first group of specimens tested, laminates $[0^K/+45^C/0^C]_s$, $[+45^C/0^K/0^C]_s$ and $[0^K/+45^C/0^K]_s$, were subjected to a tensile load equal to 70 percent of the static strength. Of these, the two $[0^K/+45^C/0^C]_s$ specimens survived the thermal cycling. The $[+45^C/0^K/0^C]_s$ specimens failed on the 90th and 97th thermal cycles, and the $[0^K/+45^C/0^K]_s$ specimens failed on the third and sixth thermal cycles. These failures are attributed to the higher strength reduction with temperature of the Kevlar 49 component. In subsequent batches the tensile preload was reduced to 60 percent of the ultimate in those specimens containing two Kevlar 49 or two S-glass plies and to 50 percent of ultimate in those specimens containing four plies of Kevlar 49 or S-glass. All these specimens survived the elevated temperature thermal cycling.

All specimens that survived the thermal cycling above were tested statically to failure to determine residual elastic properties and strength. Stress-strain curves obtained are shown in Figs. 76 to 87. The modulus, Poisson's ratio and strength for each specimen are indicated in these graphs as well as tabulated in Table 14.

All specimens containing two Kevlar 49 or S-glass plies behaved linearly to failure, with the exception of one of the $[+45^C/0^G/0^C]_s$ specimens where the 0-deg. graphite plies had failed. The residual moduli in these specimens are somewhat lower than initially measured values, probably because of some damage in the 0-deg. plies. Ultimate strains vary between 3.9×10^{-3} and

Table 14

RESIDUAL PROPERTIES OF HYBRID ANGLE-PLY LAMINATES
AFTER 100 THERMAL CYCLES BETWEEN ROOM TEMPERATURE
AND 411 degK (280°F) UNDER TENSILE PRELOAD

Laminate	Preload During Cycling MPa (ksi)	Modulus E_{xx} GPa (10^6 psi)	Poisson's Ratio ν_{xy}	Strength S_{xxT} MPa (ksi)	Ultimate Longi- tudinal Strain, $(\epsilon_{xx})_{max}$ $10^3\epsilon$
$[0^K/+45^C/0^C]_s$	244 (35) 244 (35)	86 (12.5) 87 (12.6)	0.74 0.85	421 (61) 338 (49)	4.8 3.9
$[+45^C/0_2^K]_s$	369 (54) 369 (54)	52 (7.6) 51 (7.4)	0.85 0.90	852 (123) 760 (110)	16.6 13.7
$[0^G/+45^C/0^C]_s$	219 (32) 219 (32)	86 (12.5) 86 (12.5)	0.75 0.75	370 (54) 400 (58)	4.3 4.7
$[+45^C/0^G/0^C]_s$	201 (29) 201 (29)	25 (3.6)* 76 (11.0)	1.01* 0.75	483 (70)* 363 (53)	27.8* 4.7
$[0^G/+45^C/0^G]_s$	422 (61) 422 (61)	38 (5.5) 37 (5.3)	0.70 0.70	884 (128) 713 (103)	24.8 20.0
$[+45^C/0_2^G]_s$	422 (61) 422 (61)	32 (4.6) 33 (4.8)	0.89 1.06	1023 (148) 738 (107)	>30 26.7

*0-deg. Graphite Plies Failed

Note: Superscripts C, K and G refer to graphite, Kevlar 49 and S-glass, respectively.

4.8×10^{-3} , which are slightly higher than those measured initially. Residual strength values are also somewhat higher than initial strengths, even in the specimen with the damaged 0-deg. graphite plies. A possible explanation for this trend is some possible relief of deleterious residual stresses by thermal cycling under load.

Specimens containing four Kevlar 49 or S-glass plies show some nonlinear behavior. The residual modulus of the $[\pm 45^C/0_2^K]_s$ specimens was higher and that of the $[\pm 45^C/0_2]_s$ specimens was lower than initial values. Residual ultimate strains were, with the exception of the $[\pm 45^C/0_2^G]_s$ specimens, lower than those measured initially. The residual strengths in this group were, in five out of six specimens, somewhat higher than initial strengths.

The modes of failure in some of the specimens above are of special interest. One $[\pm 45^C/0^G/0^G]_s$ specimen failed in a "brooming" fashion (Fig. 2-88). Upon loading, the 0-degree graphite plies failed first and isolated the outer layers consisting of the ± 45 -degree graphite and 0-degree S-glass plies. The residual tensile stresses in the S-glass ply made the layer curve with the convex side outward. Specimens $[0^G/\pm 45^C/0^G]_s$ failed in a different fashion illustrating the relief of lamination residual stresses. The outer layers consisting of one 0-degree S-glass ply and the ± 45 -degree graphite plies curled up after the graphite plies probably delaminated from the middle 0-degree S-glass plies. This again illustrates the presence of tensile residual stresses in the 0-degree S-glass plies.

5.2 Residual Properties After Thermal Cycling Between Room Temperature and 200 degK (-100°F) Under Tensile Load

Two specimens, including one with embedded gages, of each of the eight hybrid configurations discussed before were subjected to a static tensile load equal to 70 percent of the static strength and to 100 thermal cycles between room temperature and 200 degK (-100°F). One of the $[\pm 45^{\text{C}}/0^{\text{G}}/0^{\text{C}}]_{\text{s}}$ specimens failed during static preloading prior to thermal cycling. The rest of the specimens survived the thermal cycling above and subsequently were tested statically to failure. Stress-strain curves are shown in Figs. 89 to 103. The modulus, Poisson's ratio and strength for each specimen are indicated in these graphs as well as tabulated in Table 15.

All specimens containing two Kevlar 49 or S-glass plies behaved linearly to failure, with the exception of a $[\pm 45^{\text{C}}/0^{\text{K}}/0^{\text{C}}]_{\text{s}}$ specimen in which a rapid increase in strain was noticed prior to failure (Fig. 91). The residual moduli of these specimens are consistently lower than initially measured values. Ultimate strains are higher than initial values. Residual strength values are also, with one exception, somewhat higher than initial values. The results above may indicate some damage during thermal cycling but sufficient relief of deleterious residual stresses to increase the residual strength.

Specimens containing four Kevlar 49 or S-glass plies showed some nonlinear behavior but less pronounced than in initial static testing. Residual moduli, with one exception, are all lower than initial moduli. No significant differences were noticed in residual strength of this group of specimens.

Table 15

RESIDUAL PROPERTIES OF HYBRID ANGLE-PLY LAMINATES AFTER 100
THERMAL CYCLES BETWEEN ROOM TEMPERATURE AND 200 degK (-100°F)

UNDER TENSILE PRELOAD

Laminate	Preload During Cycling MPa (ksi)	Modulus E_{xx} GPa (10^6 psi)	Poisson's Ratio ν_{xy}	Strength S_{xxT} MPa (ksi)	Ultimate Longi- tudinal Strain, $(\epsilon_{xx})_{max}$, $10^{-3}\epsilon$
$[0^K/+45^C/0^C]_s$	244 (35) 244 (35)	75 (10.8) 92 (13.3)	0.75 0.80	407 (59) 355 (51)	5.5 3.9
$[+45^C/0^K/0^C]_s$	258 (37) 258 (37)	76 (11.0) 81 (11.7)	0.70 0.86	366 (53) 366 (53)	19.6 4.5
$[0^K/+45^C/0^K]_s$	560 (81) 560 (81)	41 (6.0) 46 (6.7)	0.75 0.80	725 (105) 752 (109)	18.5 16.2
$[+45^C/0_2^K]_s$	516 (75) 516 (75)	41 (6.0) 43 (6.3)	0.77 0.86	759 (110) 797 (115)	18.6 18.3
$[0^G/+45^C/0^C]_s$	256 (37) 256 (37)	77 (11.2) 78 (11.3)	0.74 0.68	373 (54) 331 (48)	4.9 4.3
$[+45^C/0^G/0^C]_s$	234 (34) 234 (34)	72 (10.5)	0.74 -	462 (67) -	>6 -
$[0^G/+45^C/0^G]_s$	591 (86) 591 (86)	39 (5.7) 36 (5.2)	0.73 0.68	925 (134) 759 (110)	29.5 22.3
$[+45^C/0_2^G]_s$	584 (85) 584 (85)	35 (5.1) 30 (4.3)	0.70 0.63	959 (139) 745 (108)	32.5 29.2

6.0 SUMMARY, CONCLUSIONS AND RECOMMENDATIONS FOR FUTURE WORK

Residual strains were determined experimentally in the various plies of angle-ply hybrid graphite/Kevlar 49/epoxy and graphite/S-glass/epoxy laminates.

The unidirectional Kevlar 49/epoxy material exhibits the highest positive transverse and negative longitudinal thermal expansion. The unidirectional S-glass/epoxy undergoes the lowest thermal deformation in the transverse direction and the highest (positive) in the longitudinal direction.

For laminates of the same composition, the ply stacking sequence did not have an influence on measured thermal strains.

Residual strains in each ply were obtained as the difference between the unrestrained thermal expansion of that ply (unidirectional specimen) and the restrained expansion of the ply within the laminate (angle-ply specimen).

Hybridizing seems to reduce residual strains and stresses in the graphite plies, however, these strains are not affected much by the type and degree of hybridization. The maximum residual strain at room temperature in the 45-degree graphite plies is 6.5×10^{-3} for the all-graphite laminate and decreases to 6.3×10^{-3} for the graphite/Kevlar hybrids and to 6.2×10^{-3} for the graphite/S-glass hybrids.

In the hybrid laminates the 0-degree Kevlar plies have the highest residual strain, reaching a value of 9.2×10^{-3} in the transverse direction. The 0-degree S-glass plies have the lowest (2.4×10^{-3}) transverse strain.

Residual stresses at room temperature were computed for all the plies assuming linear elastic behavior. Computed transverse to the fiber residual stresses in the S-glass plies are approximately seventy-five percent of the static transverse strength of the unidirectional material. Computed residual stresses in the graphite plies exceed the static strength of these plies by approximately ten percent, indicating that these plies may have already failed transversely. In the case of Kevlar the computed stresses indicate that these plies must have failed in the early stages of cool down before reaching room temperature.

Specimens of all eight hybrid laminates were tested statically to failure. Results were summarized in Table 2-13 and compared with predicted values based on linear lamination theory. Specimens containing only two Kevlar 49 or S-glass 0-degree plies behave linearly to failure, which is governed by the ultimate strain in the 0-degree graphite plies. Specimens consisting of ± 45 -degree graphite plies and 0-degree Kevlar or S-glass plies display a characteristic nonlinearity. The ultimate strains of the hybrid laminates are lower than the 0-degree ultimate strains of unidirectional Kevlar or S-glass, indicating that failure in this group is governed by a lower ultimate strain of the ± 45 -degree graphite/epoxy plies. Specimens containing four 0-degree S-glass plies are only slightly stronger than those containing 0-degree Kevlar plies although the ultimate strains in the latter are much lower. This is another indication that failure in this case is governed by the ± 45 -degree graphite plies. Poisson's ratios, influenced primarily by the ± 45 -degree graphite plies, vary between 0.73 and 0.86. No significant correlations can be seen between measured values and laminate construction.

Another group of hybrid specimens was subjected to a tensile preload and 100 thermal cycles between room temperature and 411 degK (280°F). Subsequently they were tested statically to failure to determine residual properties. Specimens containing two 0-degree Kevlar or S-glass plies behaved linearly to failure. They exhibited somewhat higher than initial ultimate strains and strength, possibly due to some relief of deleterious residual stresses by thermal cycling. Residual moduli were somewhat lower than initial values, possibly because of some damage in the 0-degree graphite plies. Specimens containing four 0-degree Kevlar or S-glass plies displayed the same characteristic non-linearity as the initially tested specimens. Their residual strengths were, in general, somewhat higher than initial values. The presence of tensile residual stresses in the S-glass plies was clearly illustrated by the failure modes of some of these specimens (Fig. 2-88).

A similar group of hybrid specimens was subjected to a tensile preload and 100 thermal cycles between room temperature and 200 degK (-100°F). Subsequently they were tested statically to failure. Specimens containing only two 0-degree Kevlar or S-glass plies had consistently lower than initial residual moduli and higher residual ultimate strains and strengths. These results may indicate some damage during thermal cycling which, however, is accompanied by sufficient relief of deleterious residual stresses to increase residual strength. Specimens with four Kevlar or S-glass plies had residual moduli lower than initial ones but unchanged residual strength.

In all the tasks conducted to date the effects of residual stresses are measured in an indirect manner, because there is no comparison with similar residual-stress-free specimens. The independent influence of residual stresses should be studied by comparing conventionally fabricated angle-ply laminates with similar stress-free laminates produced by bonding together precured plies at room temperature. The effect of residual stresses on laminates with defects and damaged areas would be of importance. Specimens with cutouts, cracks or other defects with different laminate configurations should be prepared and tested. The interaction of residual stresses and interlaminar stresses near edges or cutout boundaries should be investigated.

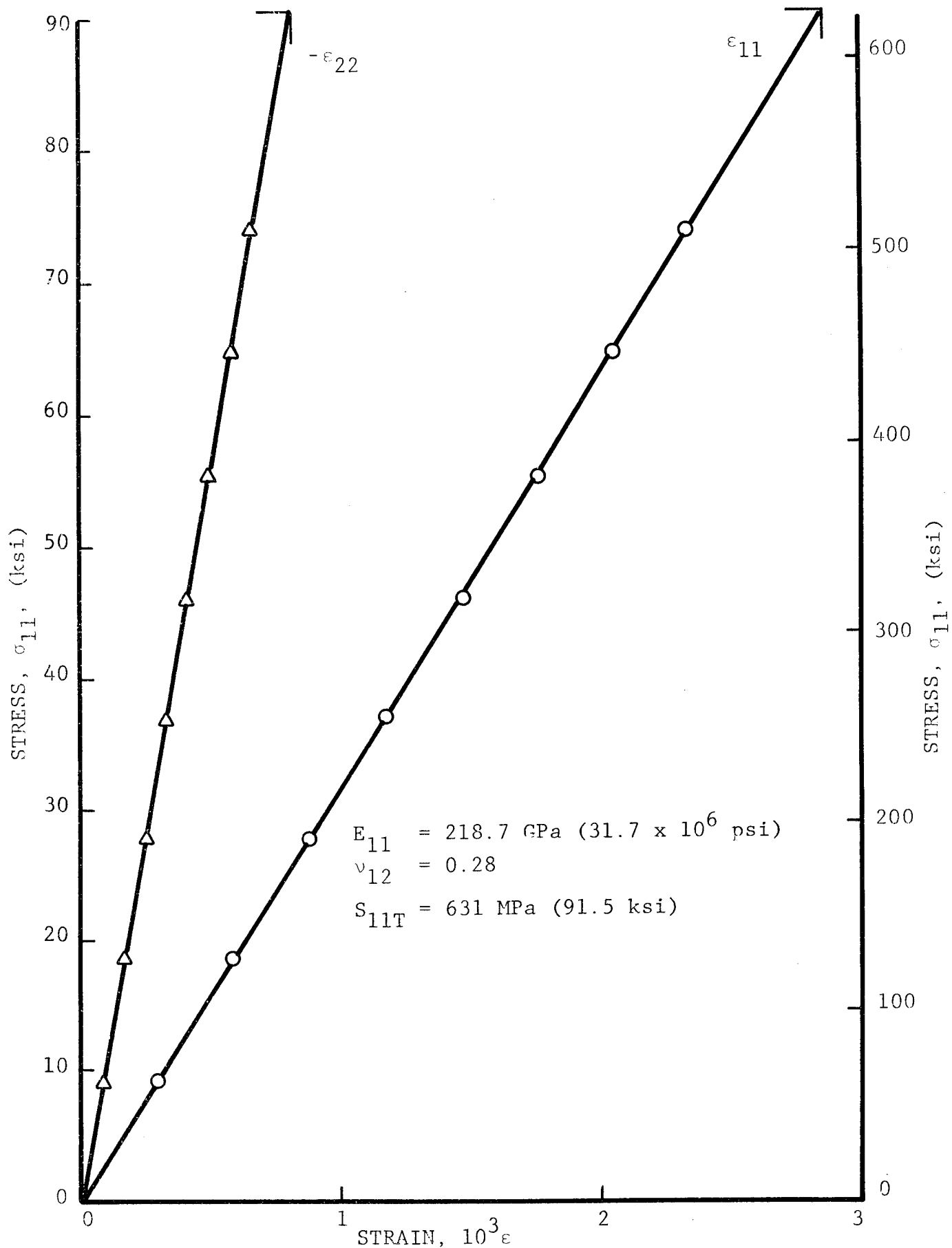


Fig. 1 STRAINS IN 0-DEGREE UNIDIRECTIONAL GRAPHITE/HIGH MODULUS EPOXY SPECIMEN UNDER UNIAXIAL TENSION

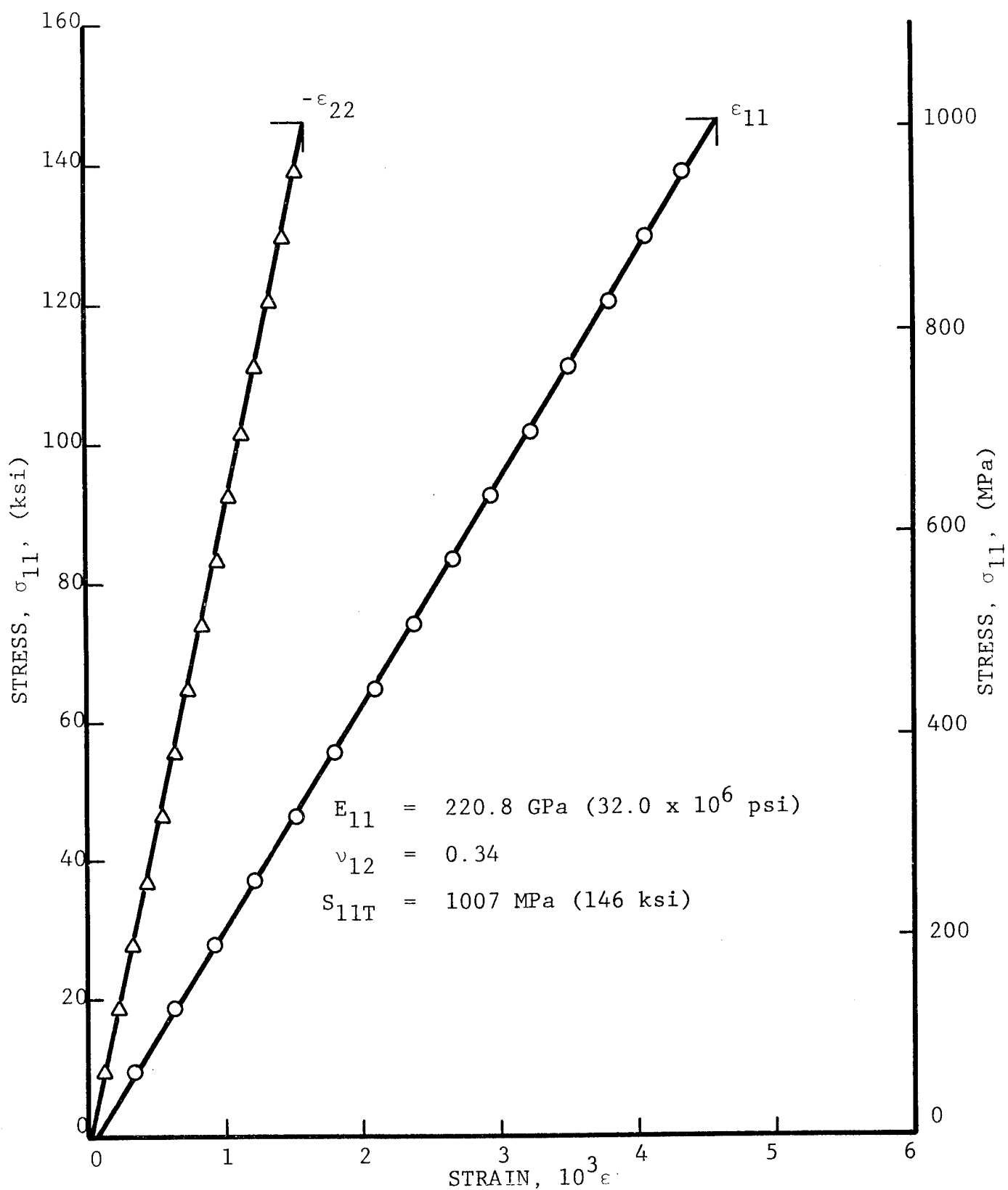


Fig. 2 STRAINS IN 0-DEGREE UNIDIRECTIONAL GRAPHITE/HIGH MODULUS EPOXY SPECIMEN UNDER UNIAXIAL TENSION

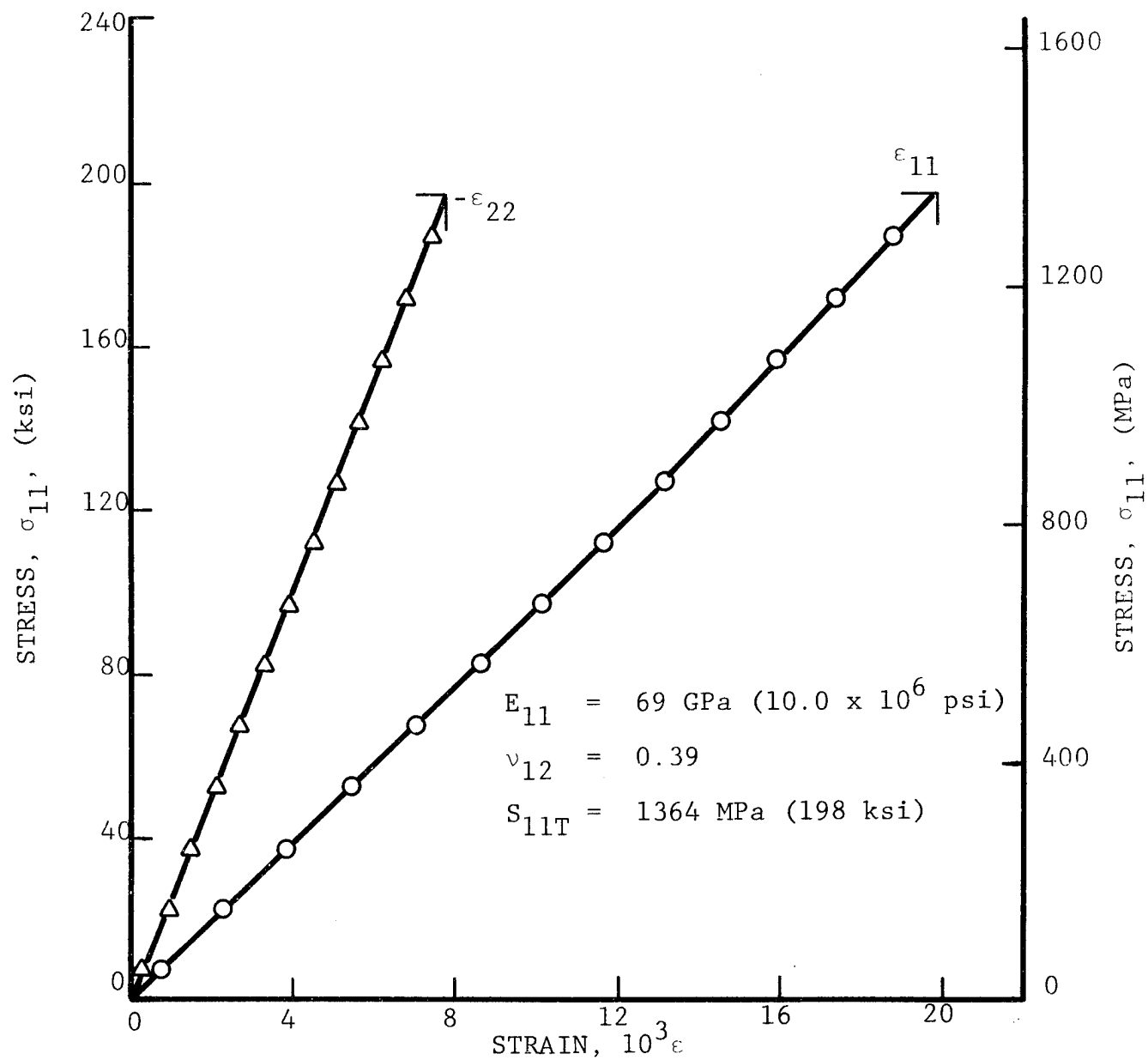


Fig. 3 STRAINS IN 0-DEGREE UNIDIRECTIONAL KEVLAR 49/
HIGH MODULUS EPOXY SPECIMEN UNDER UNIAXIAL
TENSION

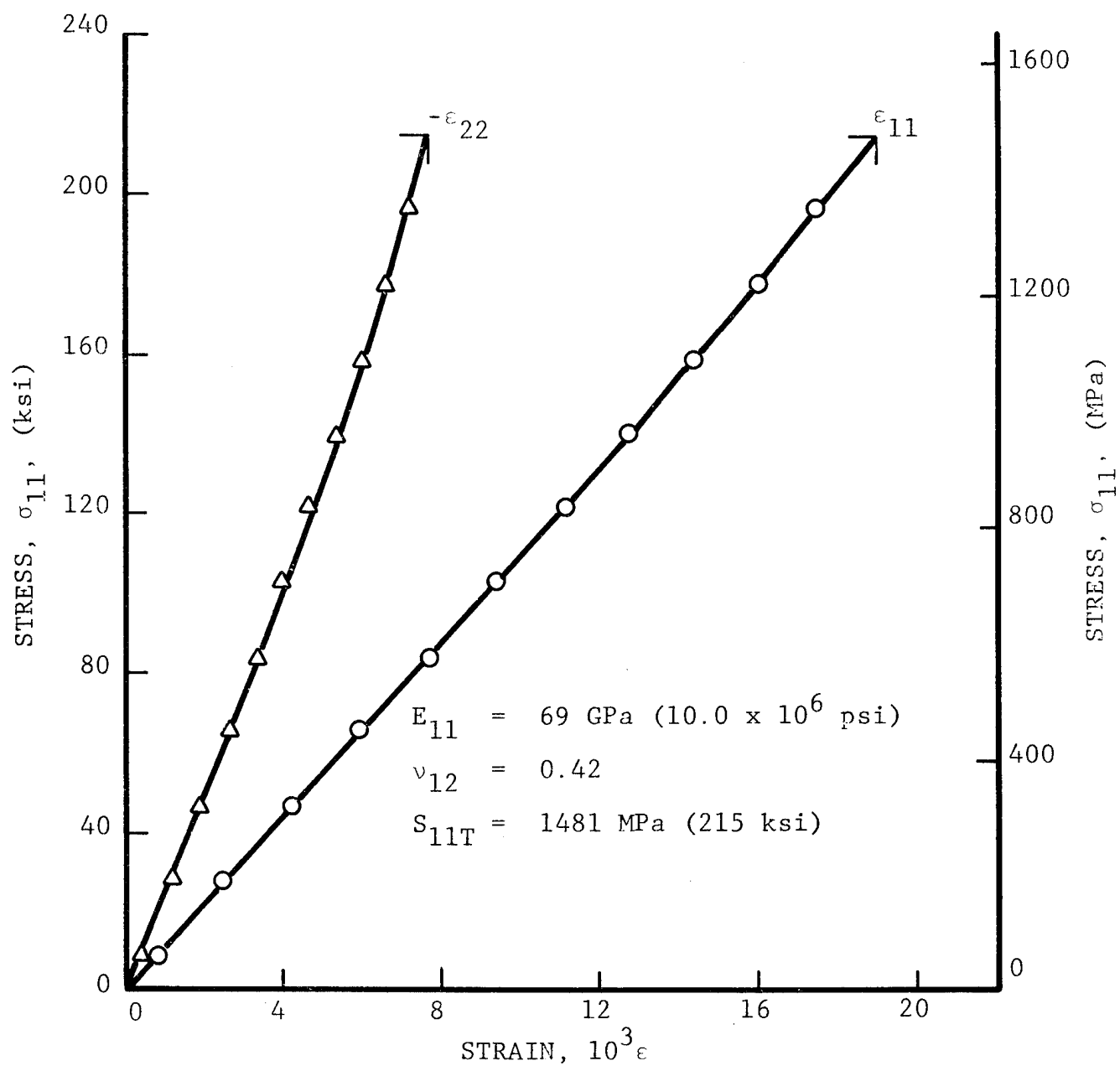


Fig. 4 STRAINS IN 0-DEGREE UNIDIRECTIONAL KEVLAR 49/
HIGH MODULUS EPOXY SPECIMEN UNDER UNIAXIAL
TENSION

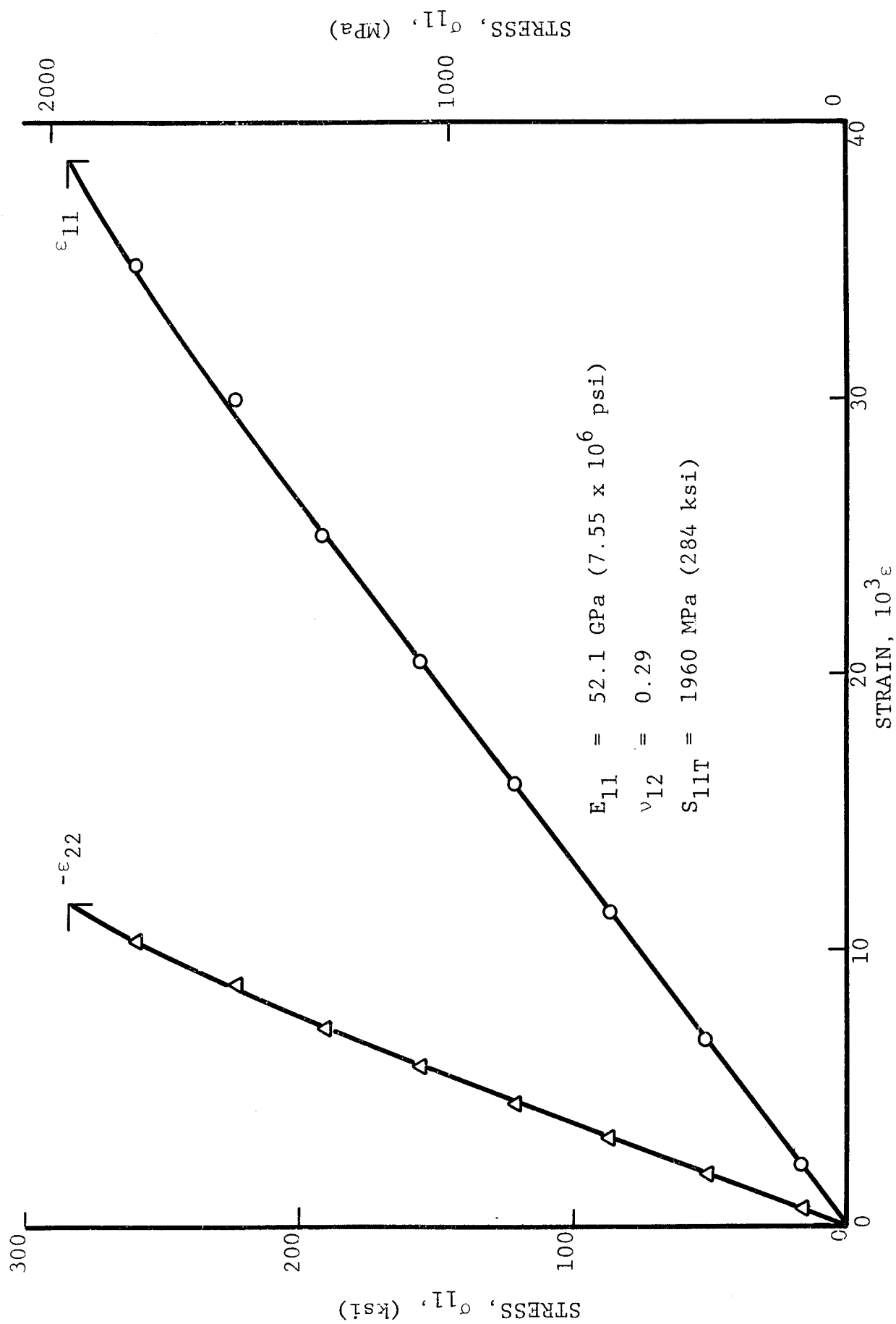


Fig. 5 STRAINS IN 0-DEGREE UNIDIRECTIONAL S-GLASS/HIGH MODULUS EPOXY SPECIMEN UNDER UNIAXIAL TENSION

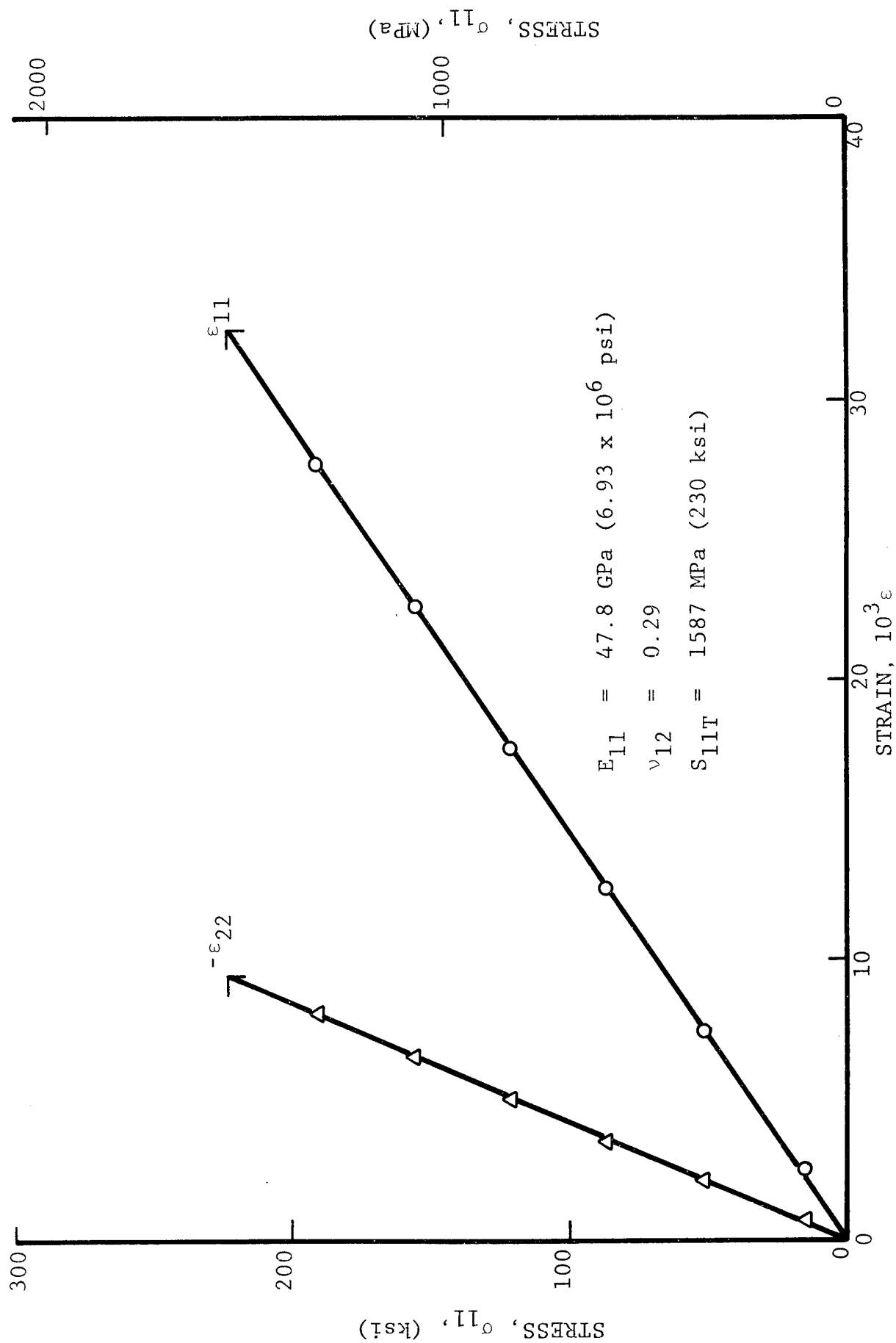


Fig. 6 STRAINS IN 0-DEGREE UNIDIRECTIONAL S-GLASS/HIGH MODULUS EPOXY SPECIMEN UNDER UNIAXIAL TENSION

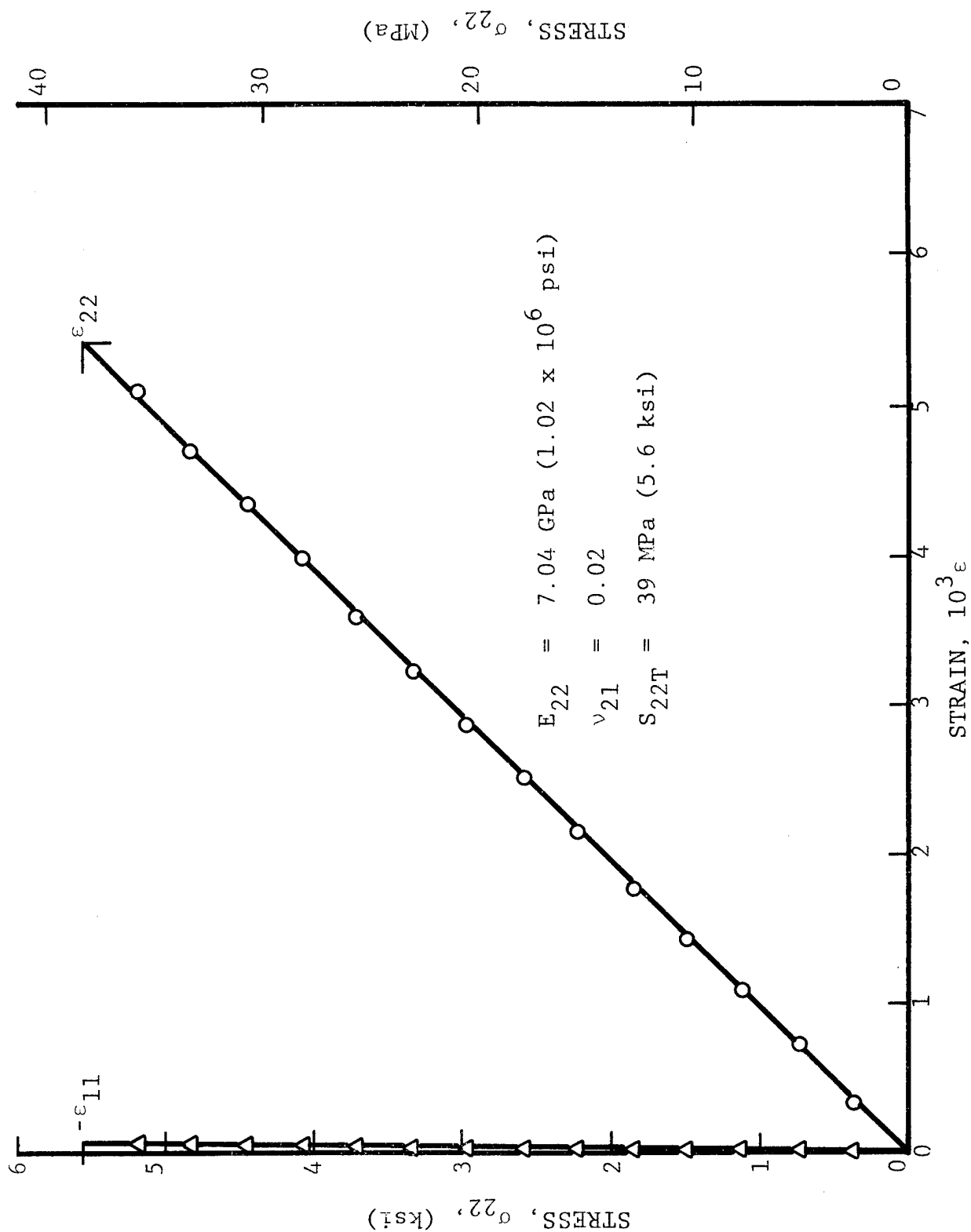


Fig. 7 STRAINS IN 90-DEGREE UNIDIRECTIONAL GRAPHITE/HIGH MODULUS EPOXY SPECIMEN UNDER UNIAXIAL TENSION

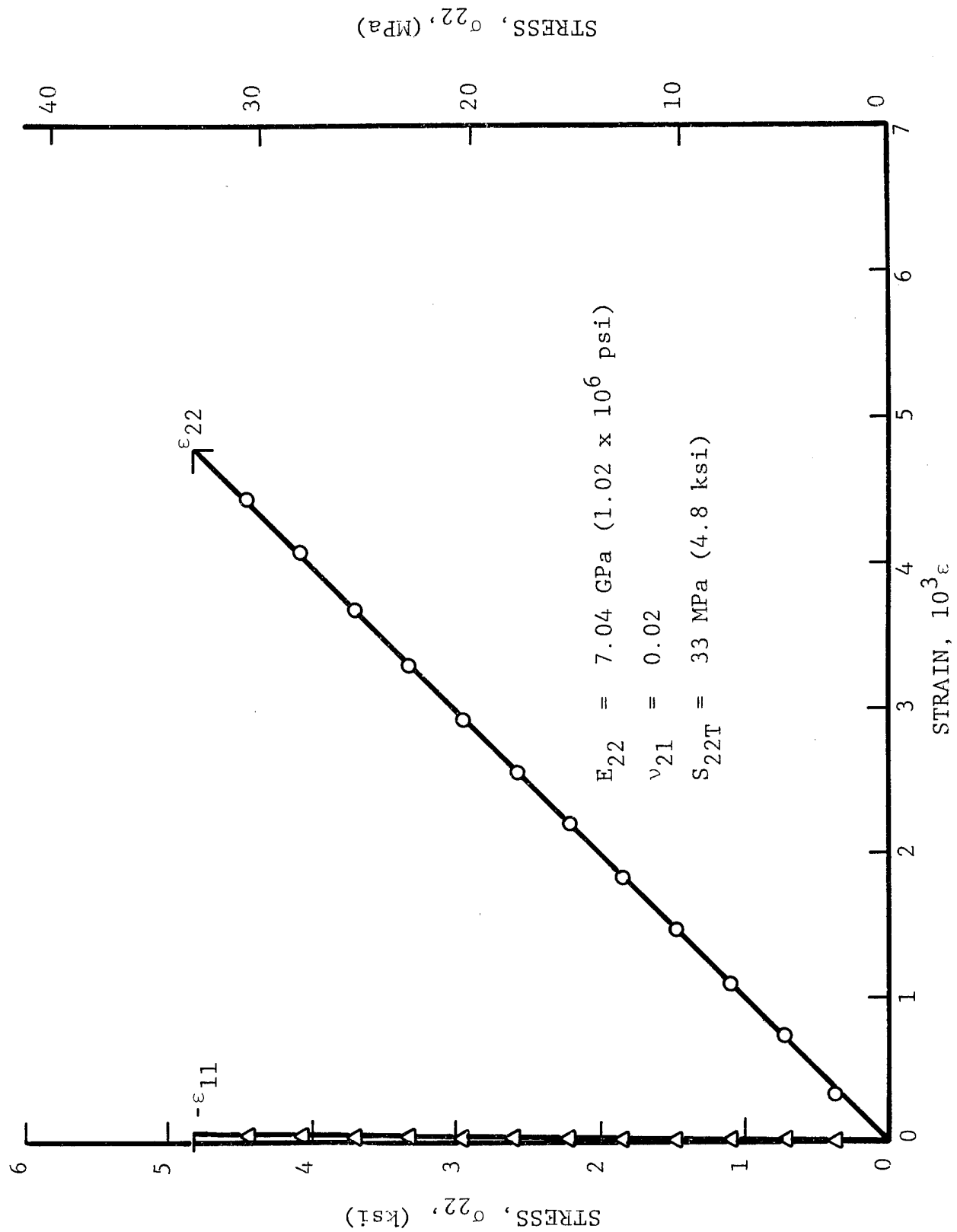


Fig. 8 STRAINS IN 90-DEGREE UNIDIRECTIONAL GRAPHITE/HIGH MODULUS EPOXY SPECIMEN UNDER UNIAXIAL TENSION

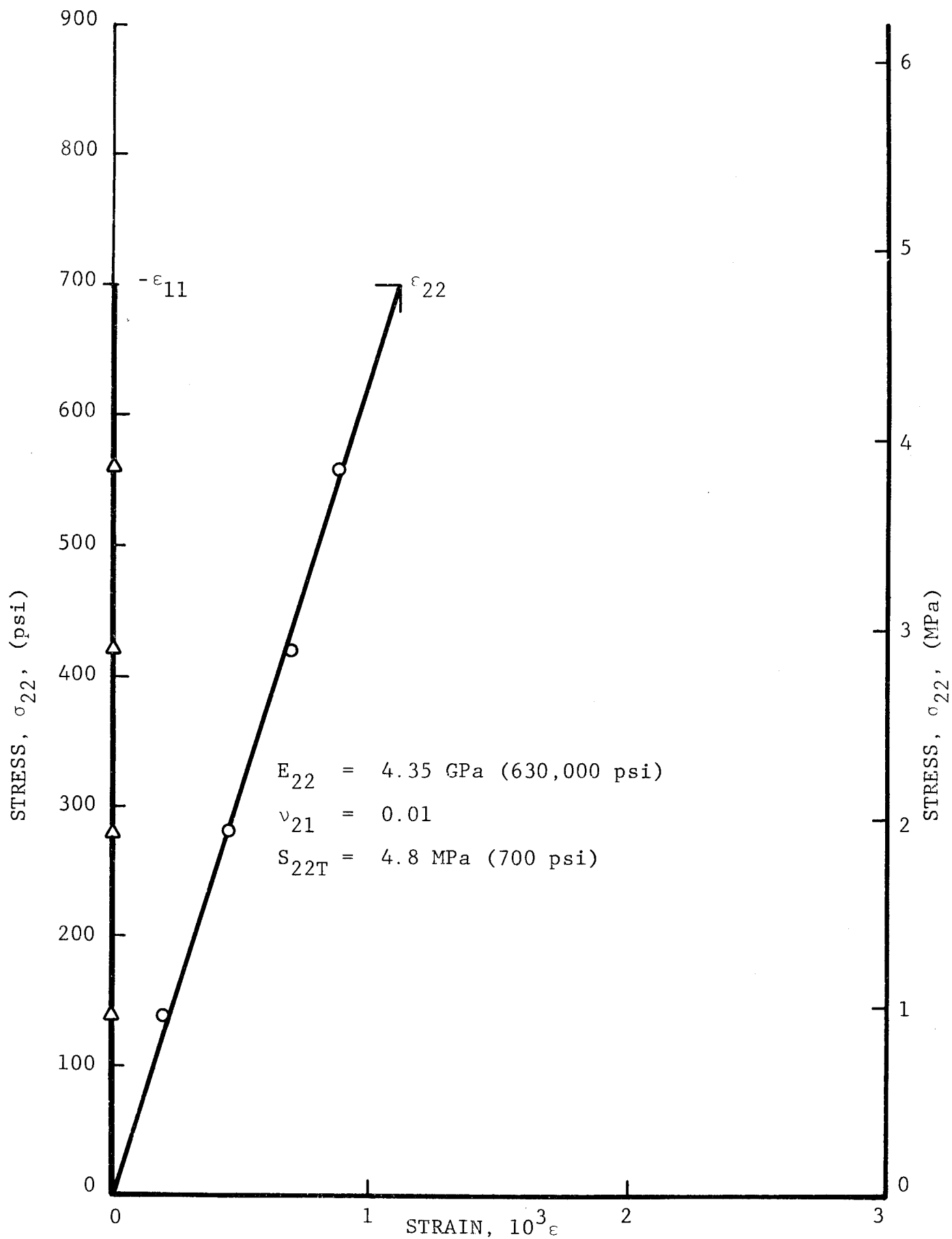


Fig. 9 STRAINS IN 90-DEGREE UNIDIRECTIONAL KEVLAR 49/HIGH MODULUS EPOXY SPECIMEN UNDER UNIAXIAL TENSION

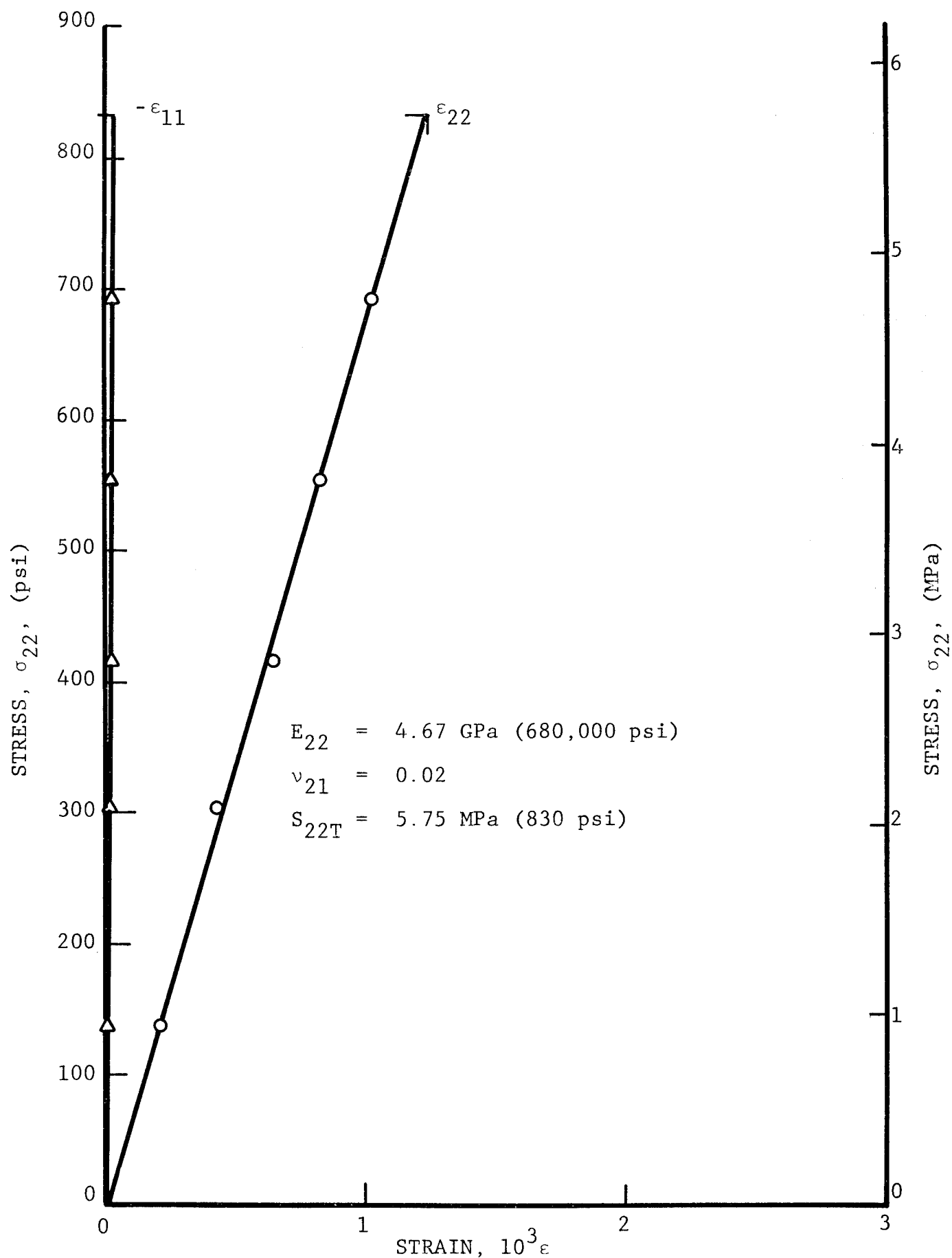


Fig. 10 STRAINS IN 90-DEGREE UNIDIRECTIONAL KEVLAR 49/
HIGH MODULUS EPOXY SPECIMEN UNDER UNIAXIAL TENSION

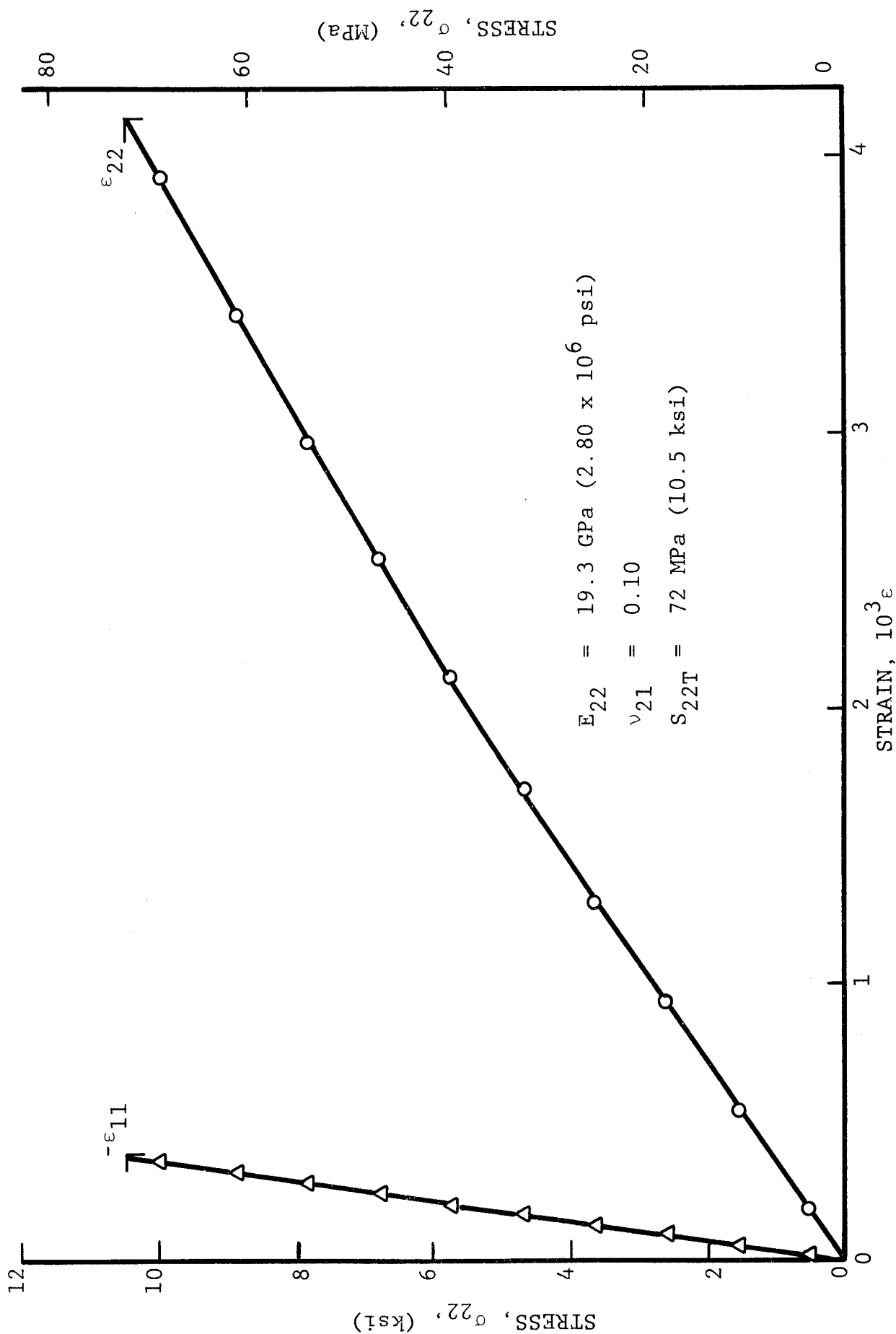


Fig. 11 STRAINS IN 90-DEGREE UNIDIRECTIONAL S-GLASS/HIGH MODULUS EPOXY SPECIMEN UNDER UNIAXIAL TENSION

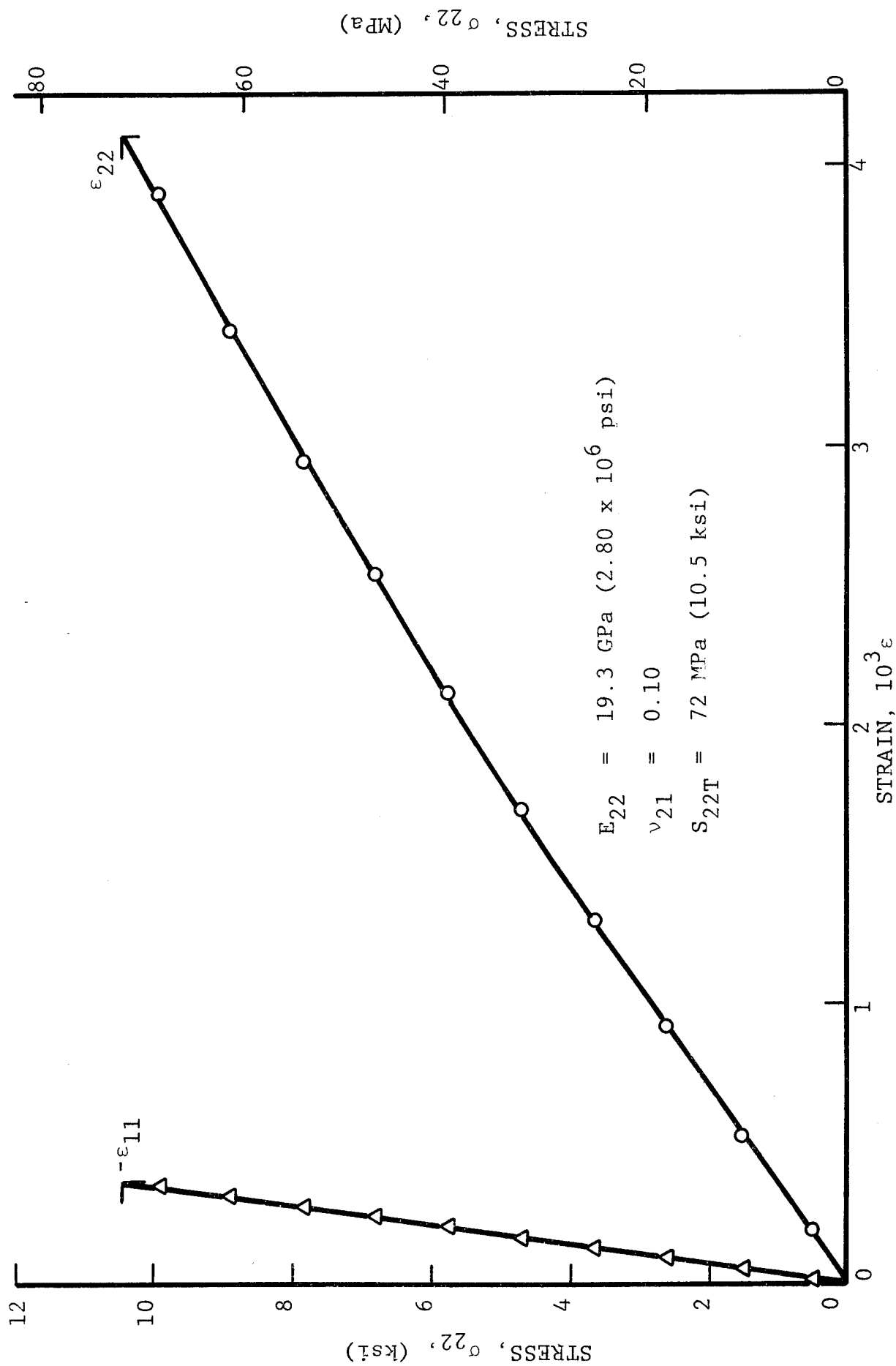


Fig. 12 STRAINS IN 90-DEGREE UNIDIRECTIONAL S-GLASS/HIGH MODULUS EPOXY SPECIMEN UNDER UNIAXIAL TENSION

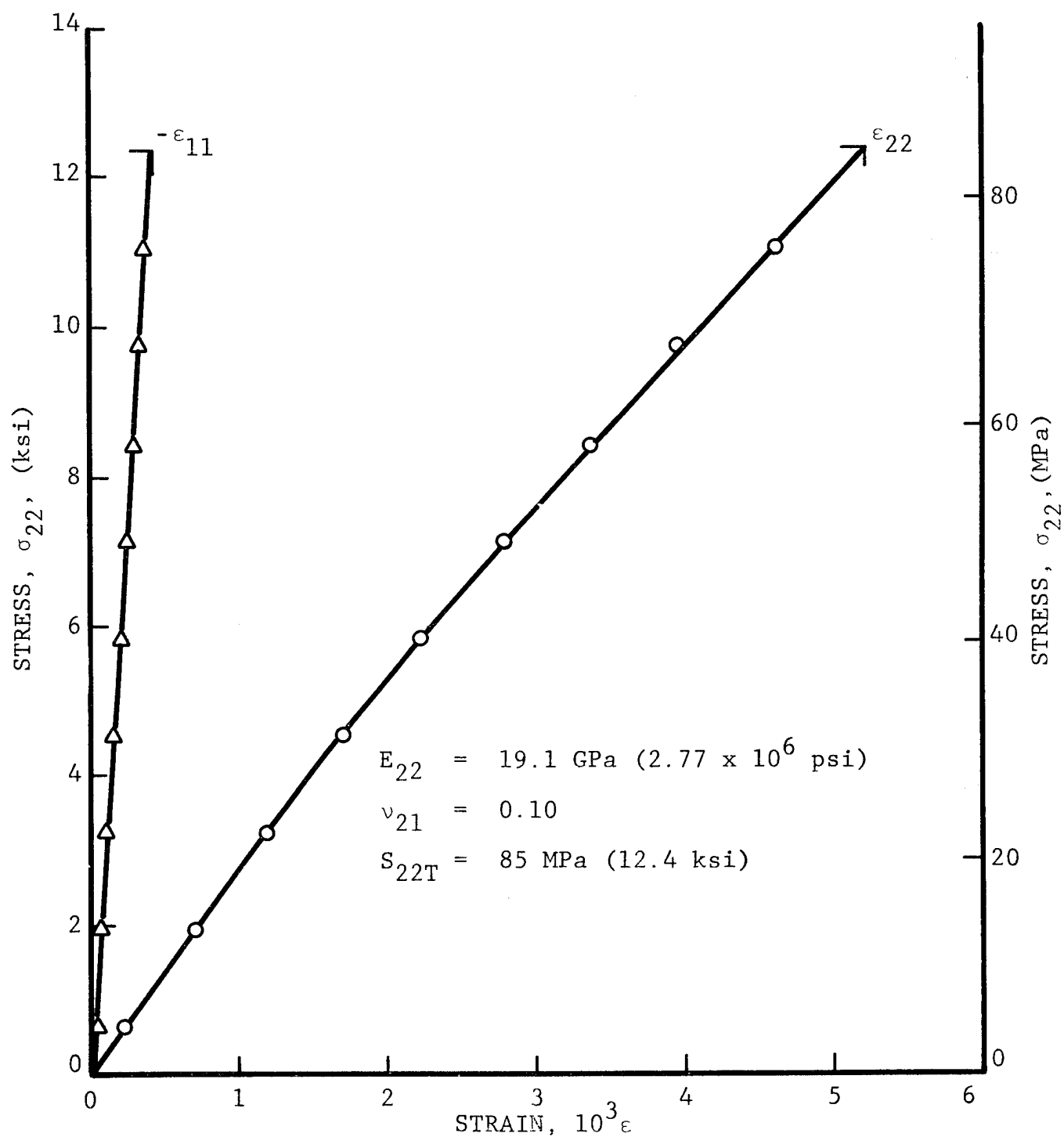


Fig. 13 STRAINS IN 90-DEGREE UNIDIRECTIONAL S-GLASS/HIGH MODULUS EPOXY SPECIMEN UNDER UNIAXIAL TENSION

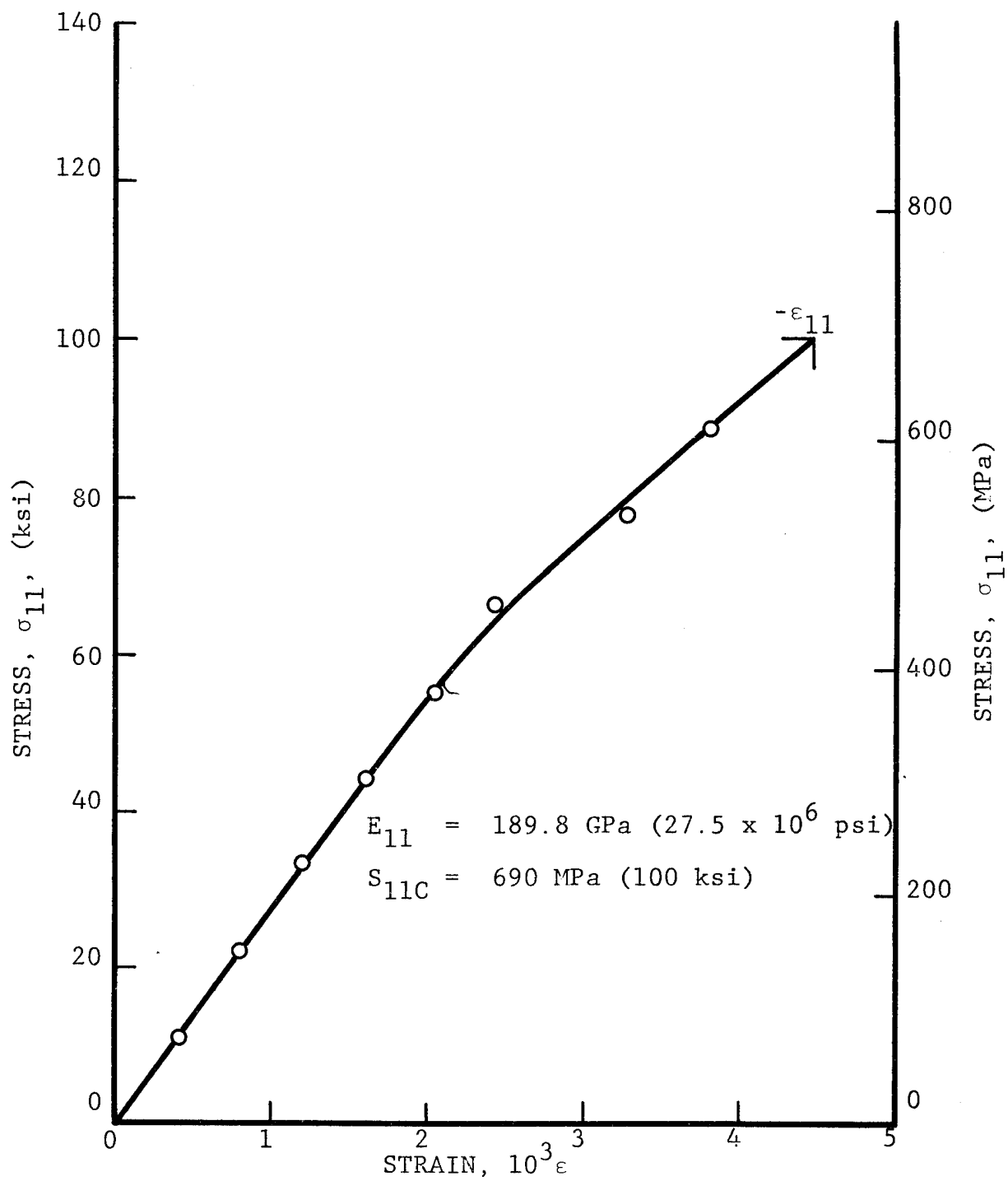


Fig. 14 STRESS-STRAIN CURVE FOR 0-DEGREE UNIDIRECTIONAL GRAPHITE/HIGH MODULUS EPOXY SPECIMEN UNDER UNIAXIAL COMPRESSION

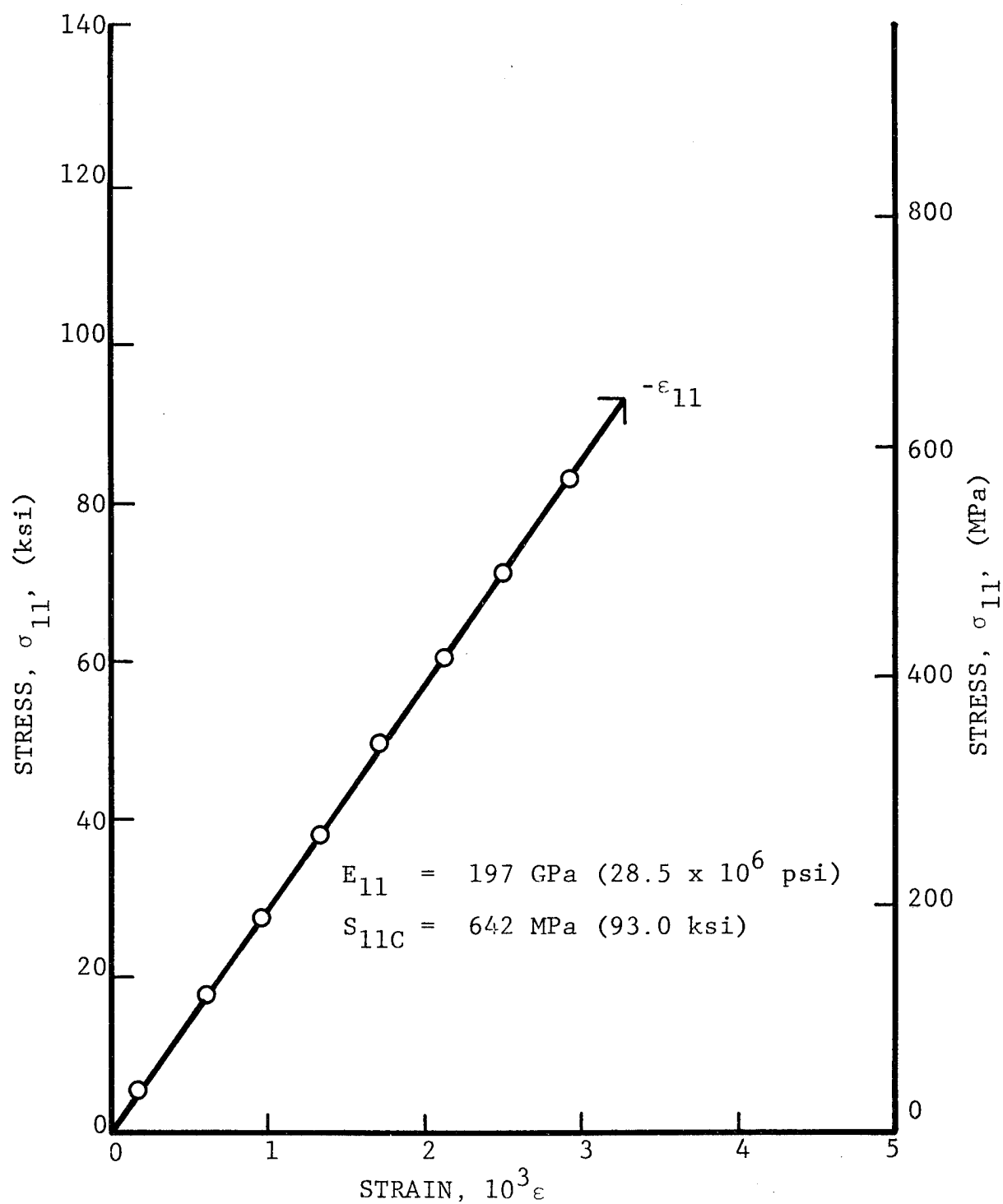


Fig. 15 STRESS-STRAIN CURVE FOR 0-DEGREE UNIDIRECTIONAL GRAPHITE/HIGH MODULUS EPOXY SPECIMEN UNDER UNIAXIAL COMPRESSION

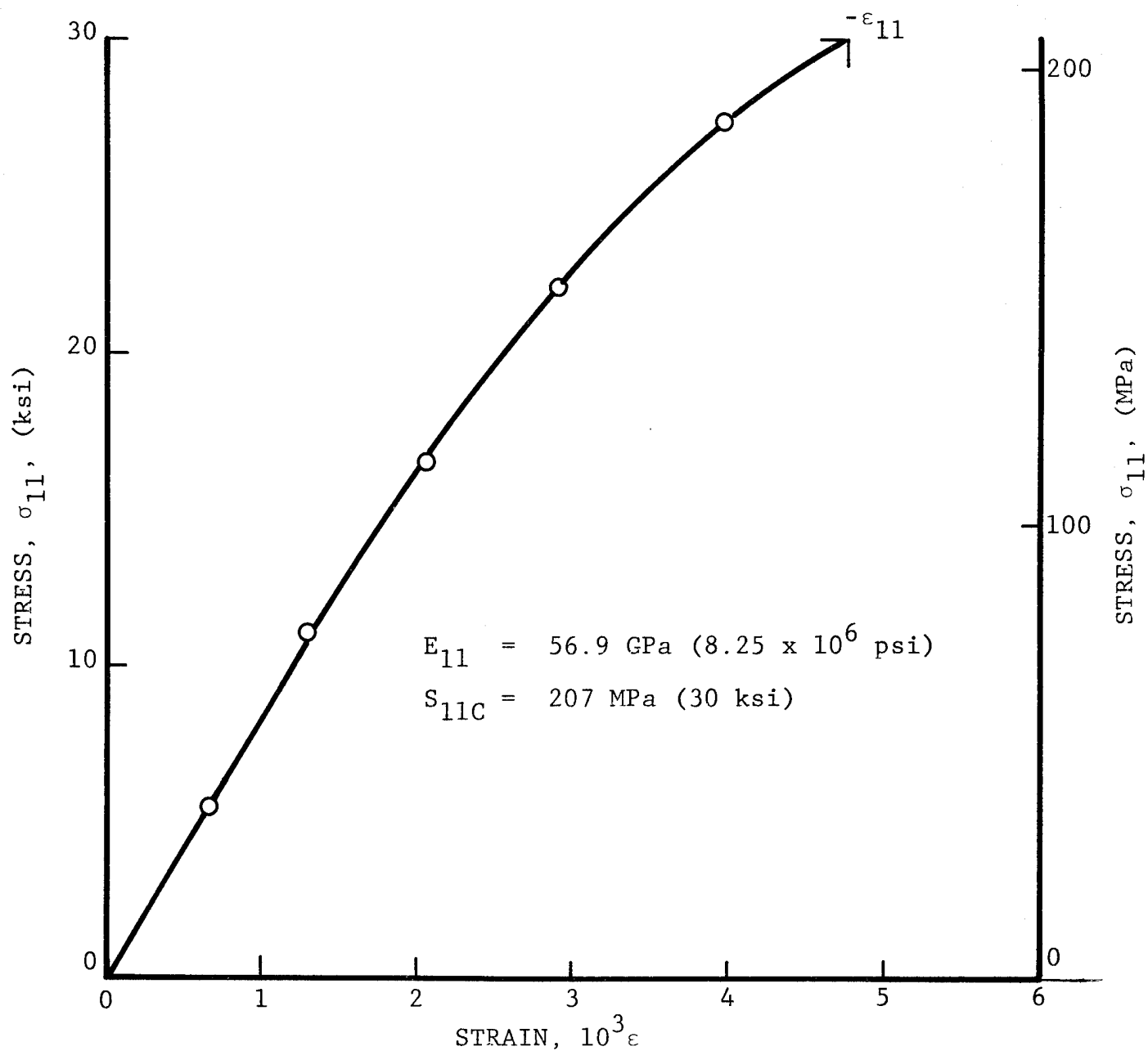


Fig. 16 STRESS-STRAIN CURVE FOR 0-DEGREE UNIDIRECTIONAL KEVLAR 49/HIGH MODULUS EPOXY SPECIMEN UNDER UNIAXIAL COMPRESSION

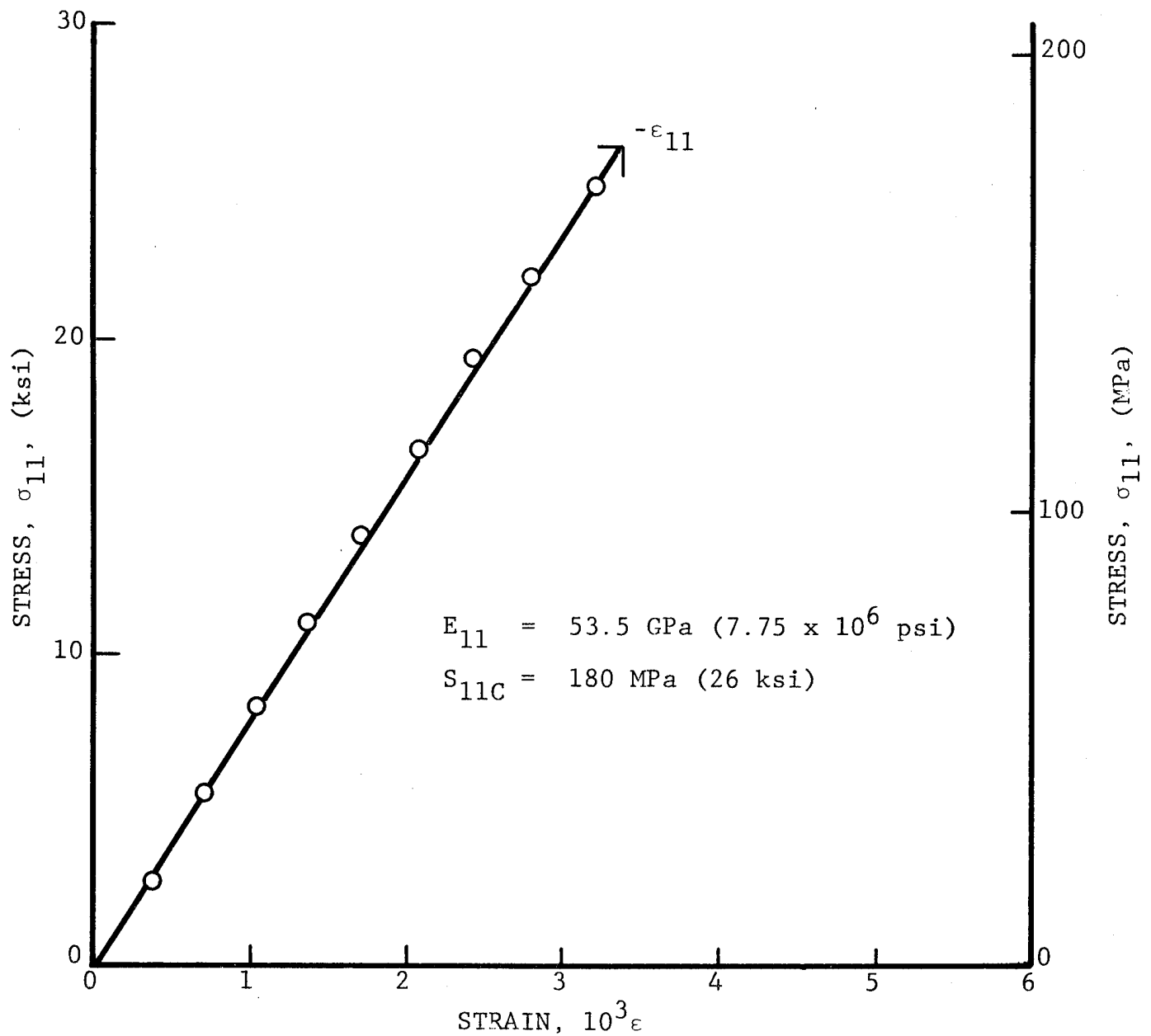


Fig. 17 STRESS-STRAIN CURVE FOR 0-DEGREE UNIDIRECTIONAL KEVLAR 49/HIGH MODULUS EPOXY SPECIMEN UNDER UNIAXIAL COMPRESSION

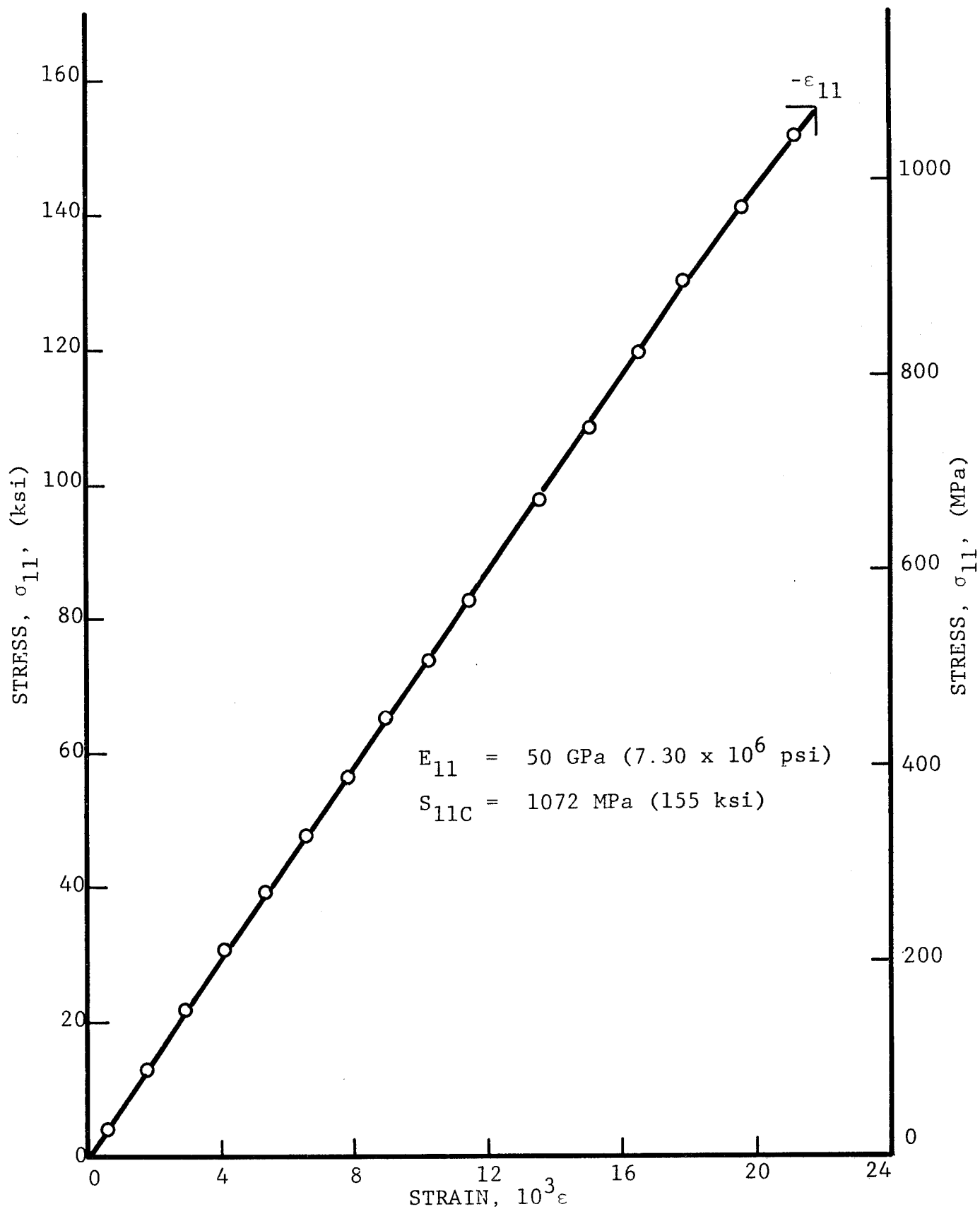


Fig. 18 STRESS-STRAIN CURVE FOR 0-DEGREE UNIDIRECTIONAL S-GLASS/HIGH MODULUS EPOXY SPECIMEN UNDER UNIAXIAL COMPRESSION

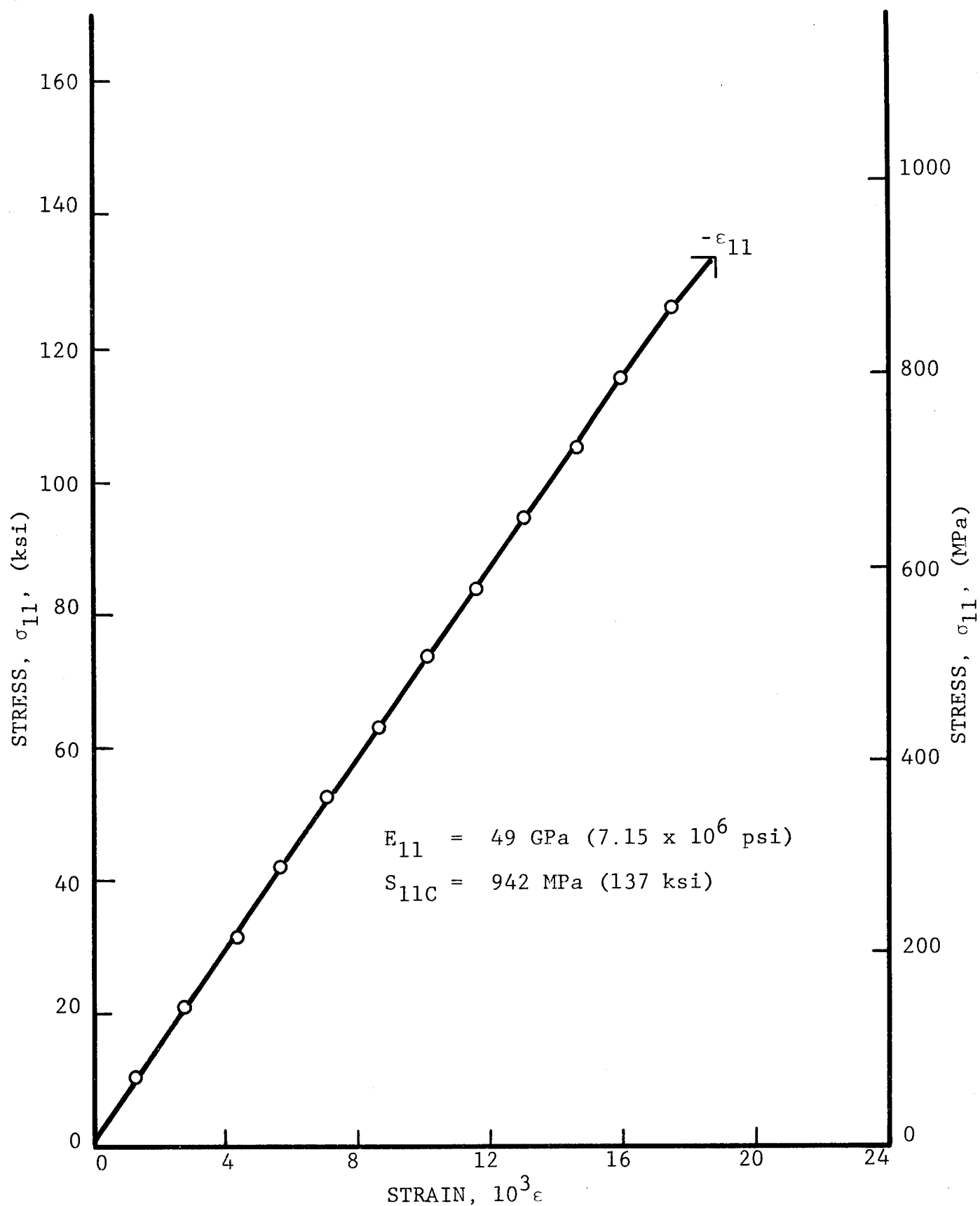


Fig. 19 STRESS-STRAIN CURVE FOR 0-DEGREE UNIDIRECTIONAL S-GLASS/HIGH MODULUS EPOXY SPECIMEN UNDER UNIAXIAL COMPRESSION

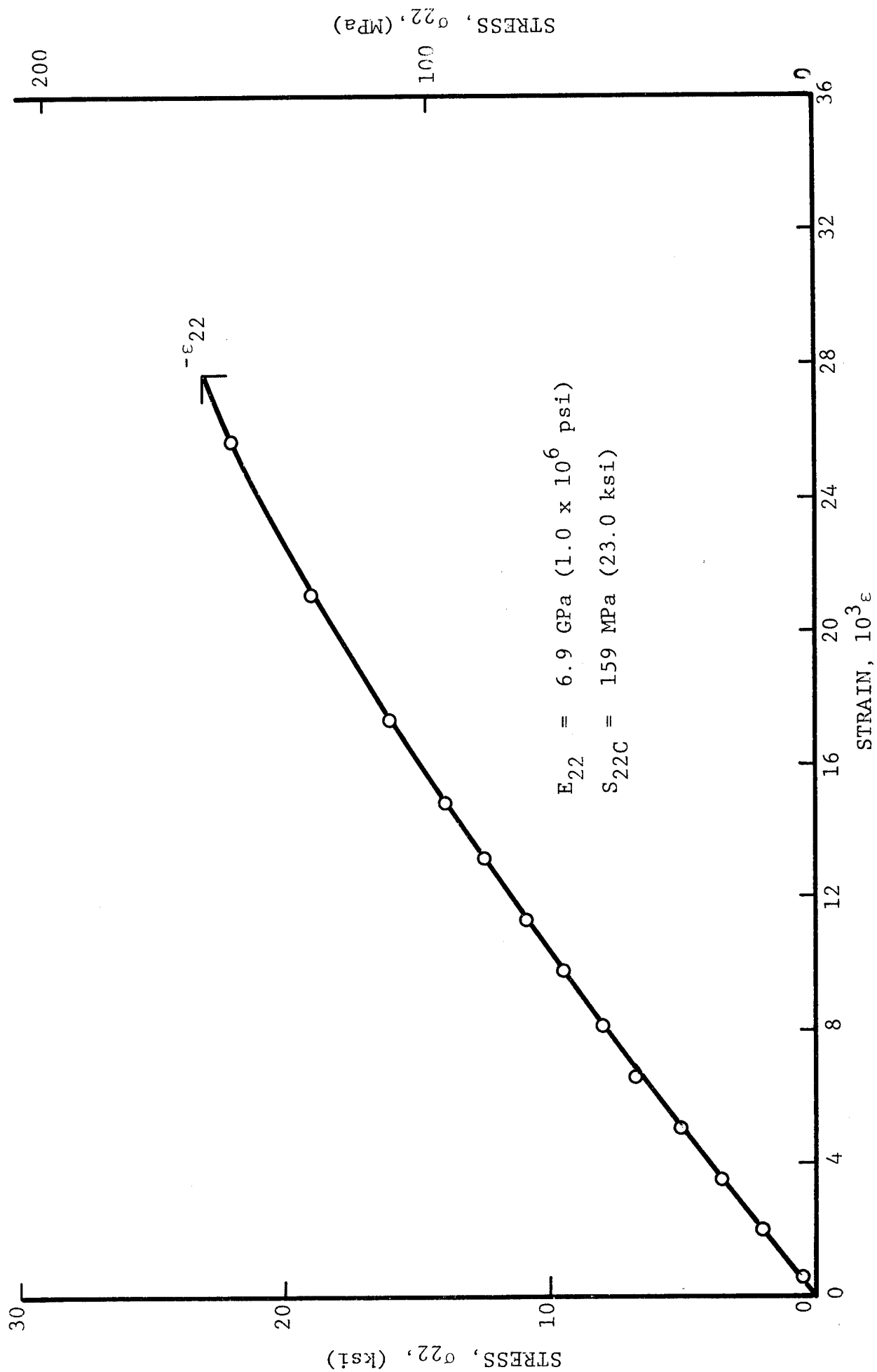


Fig. 20 STRESS-STRAIN CURVE FOR 90-DEGREE UNIDIRECTIONAL GRAPHITE/HIGH MODULUS EPOXY SPECIMEN UNDER UNIAXIAL COMPRESSION

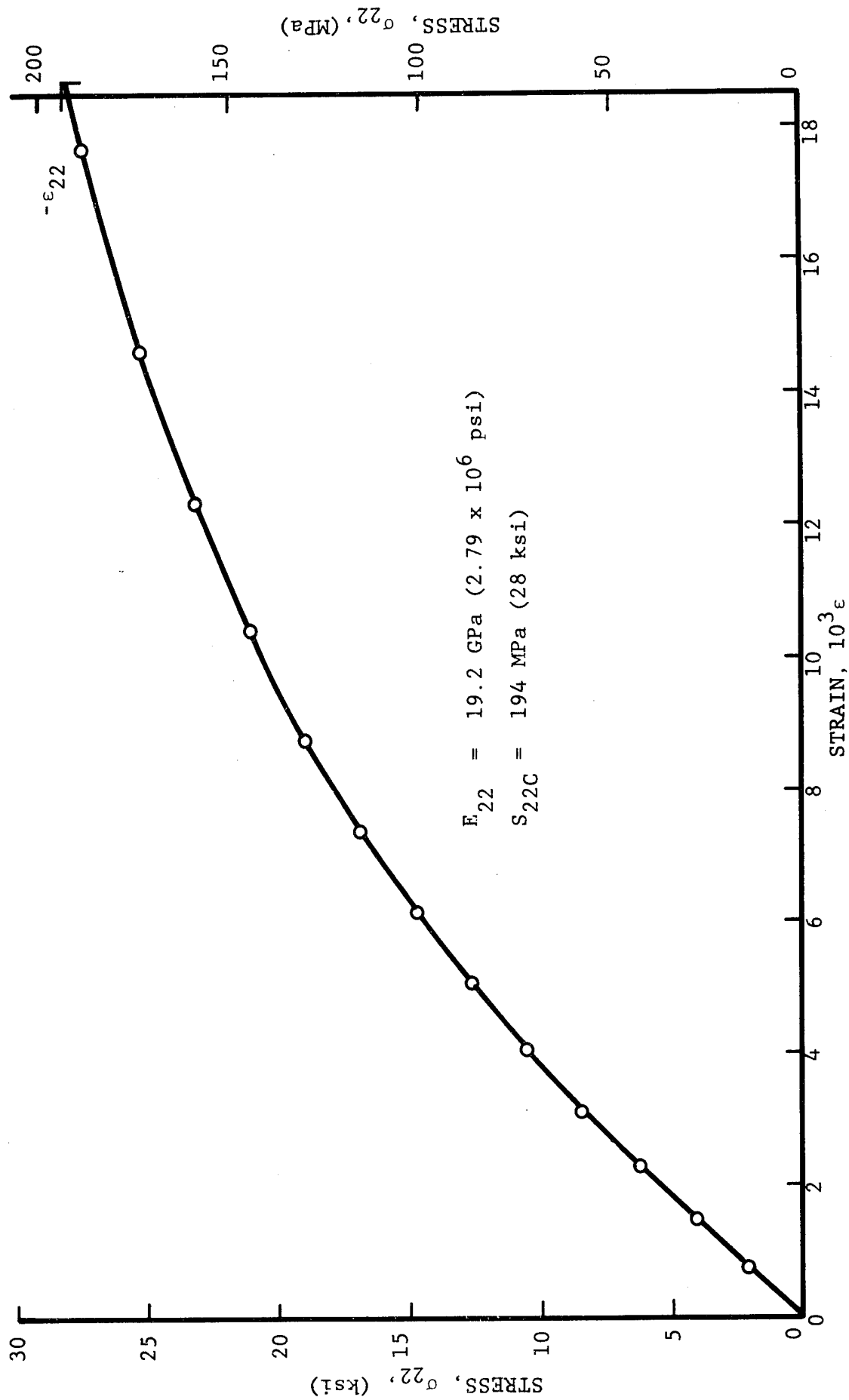


Fig. 21 STRESS-STRAIN CURVE FOR 90-DEGREE UNIDIRECTIONAL S-GLASS/HIGH MODULUS EPOXY SPECIMEN UNDER UNIAXIAL COMPRESSION

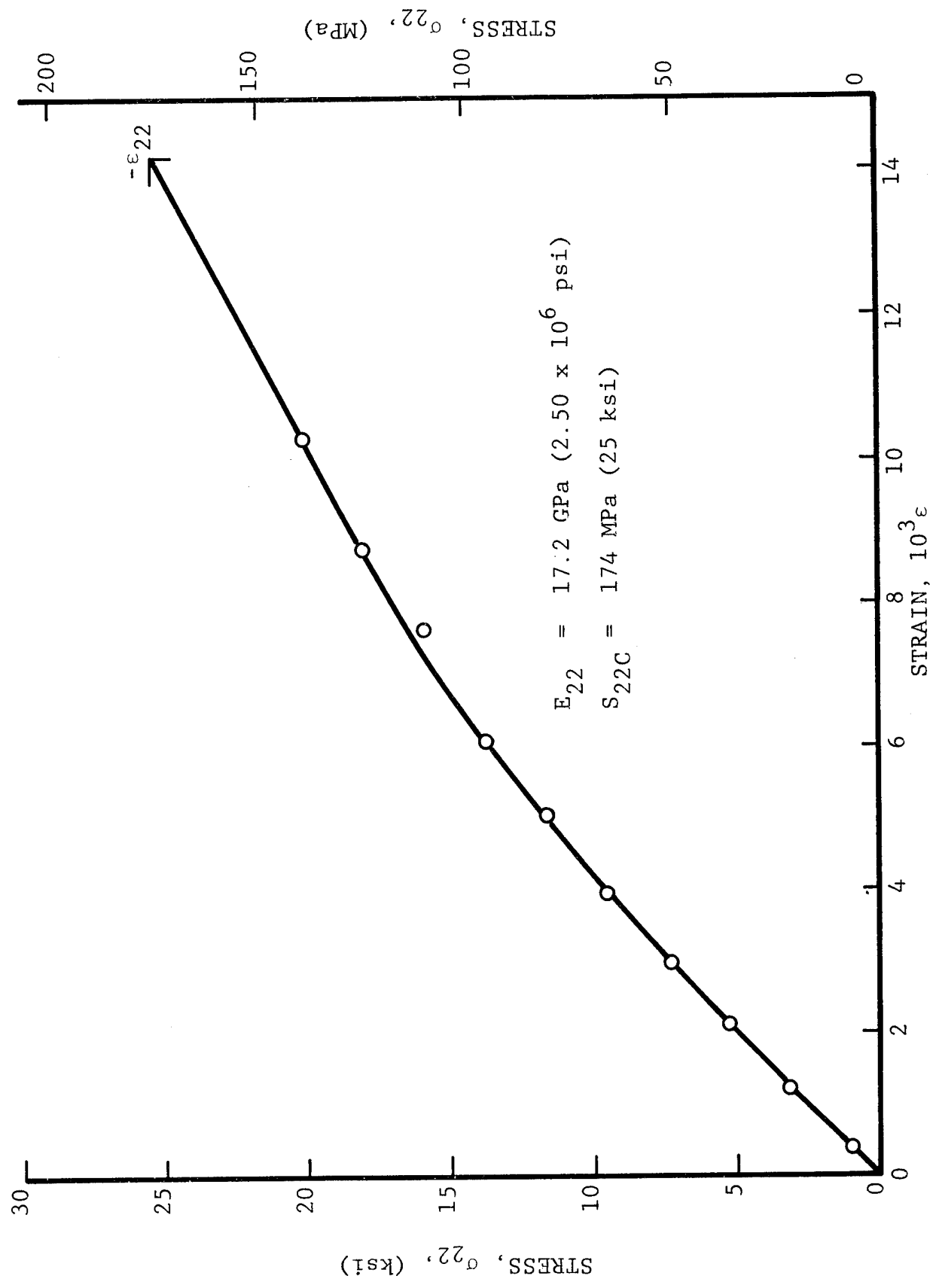


Fig. 22 STRESS-STRAIN CURVE FOR 90-DEGREE UNIDIRECTIONAL S-GLASS/HIGH MODULUS EPOXY SPECIMEN UNDER UNIAXIAL COMPRESSION

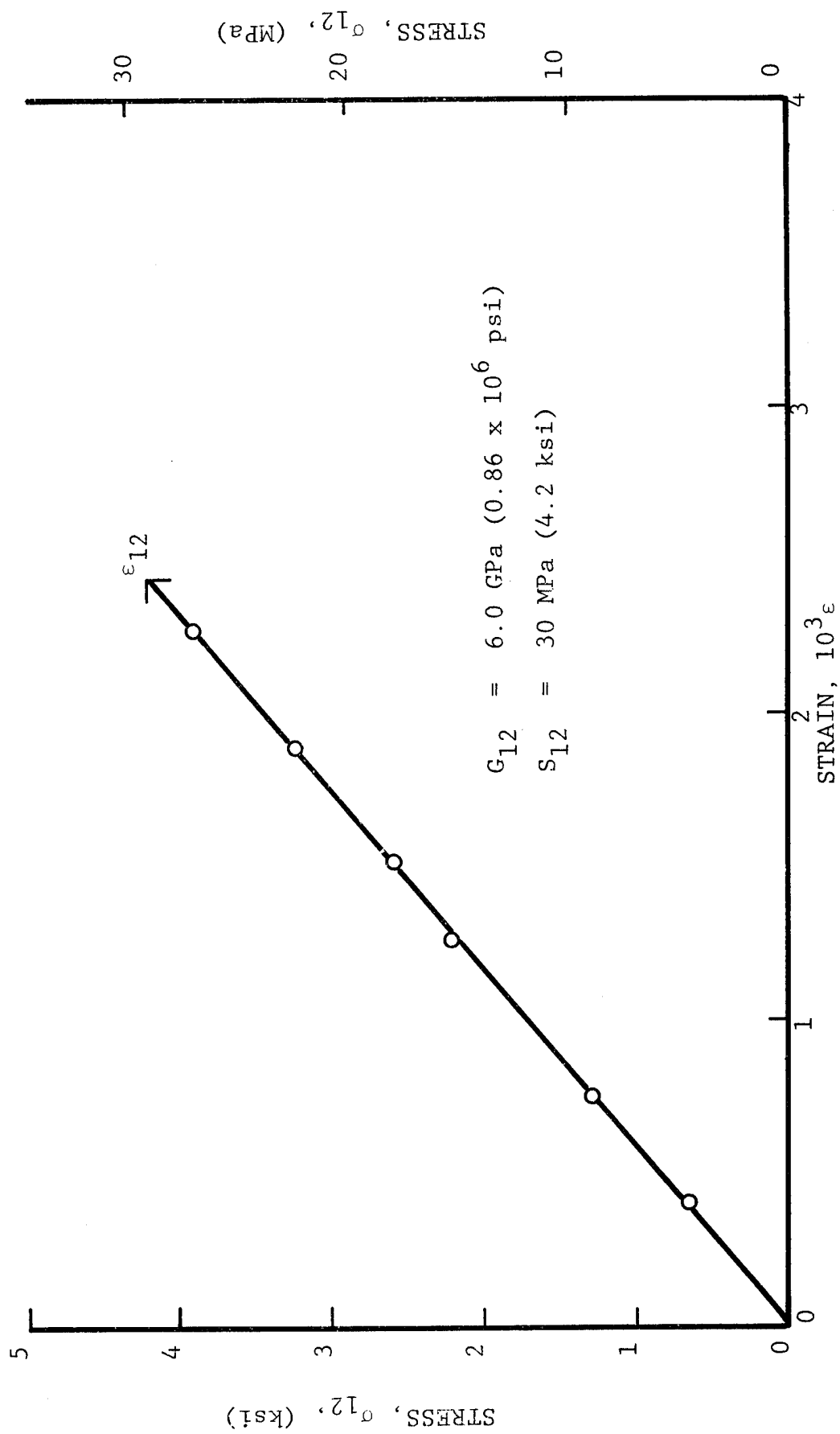


Fig. 23 SHEAR STRESS VERSUS SHEAR STRAIN FOR 10-DEGREE OFF-AXIS UNIDIRECTIONAL GRAPHITE/HIGH MODULUS EPOXY

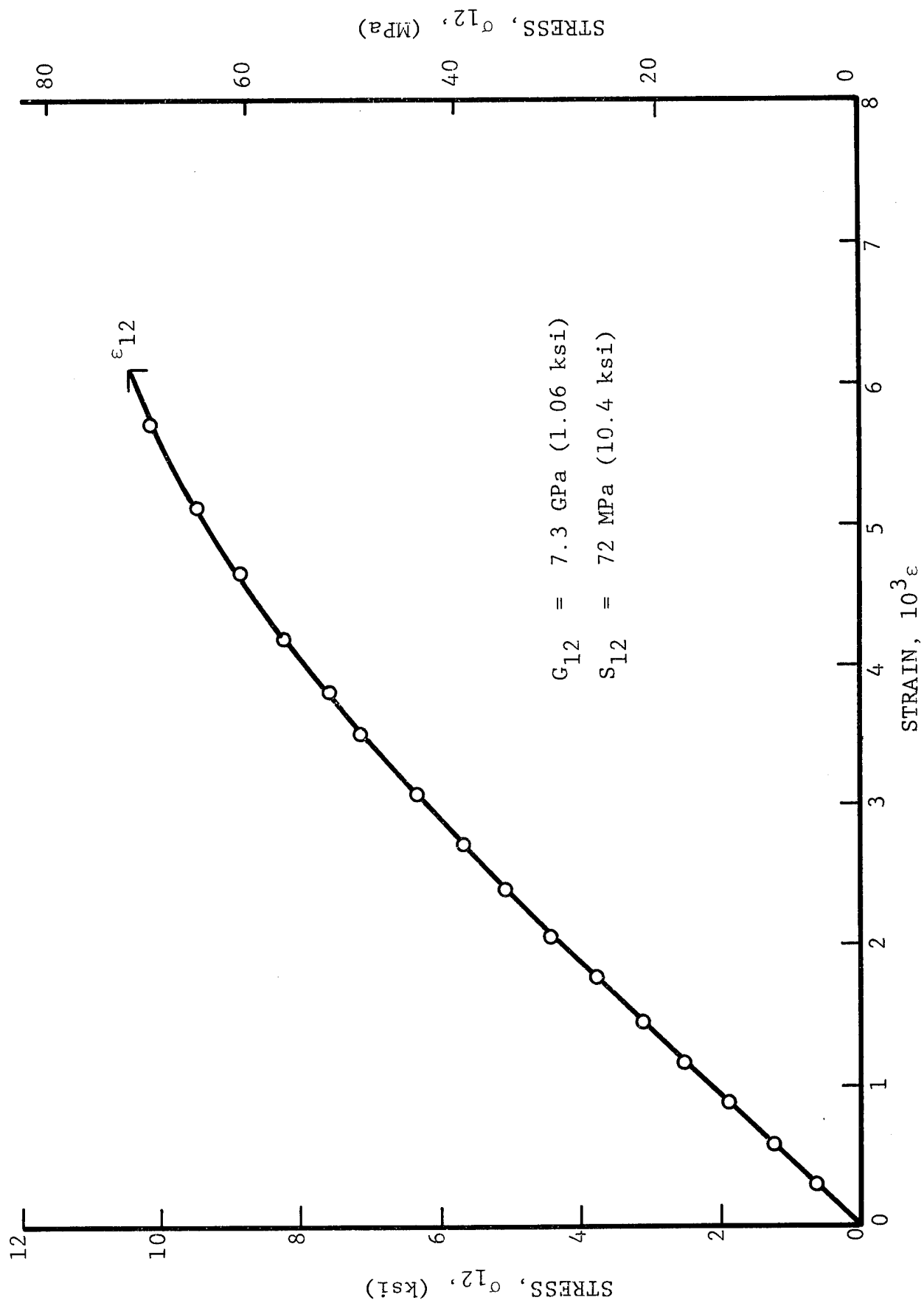


Fig. 24 SHEAR STRESS VERSUS SHEAR STRAIN FOR 10-DEGREE OFF-AXIS UNIDIRECTIONAL GRAPHITE/HIGH MODULUS EPOXY

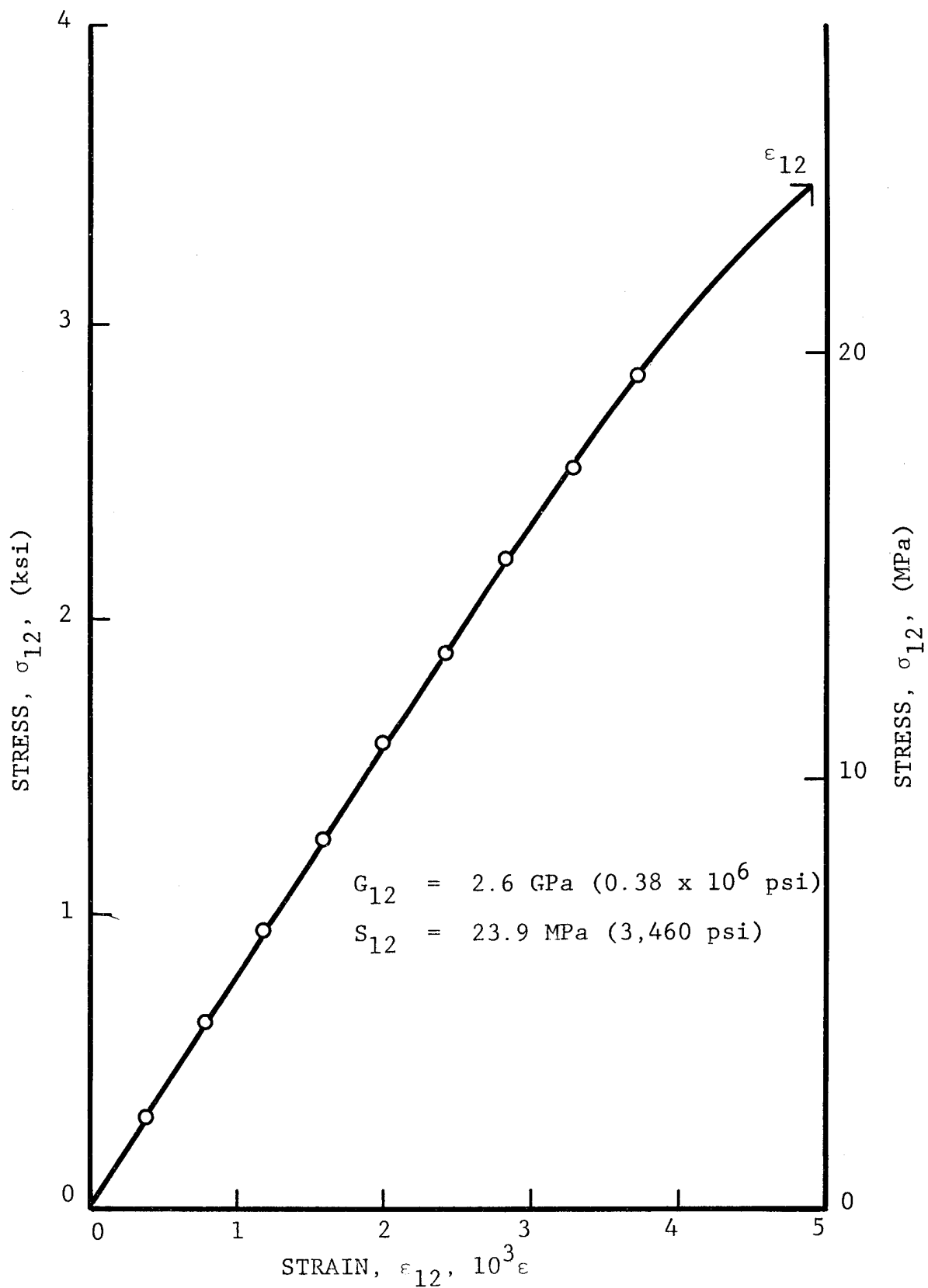


Fig. 25 SHEAR STRESS VERSUS SHEAR STRAIN FOR 10-DEGREE OFF-AXIS UNIDIRECTIONAL KEVLAR 49/HIGH MODULUS EPOXY

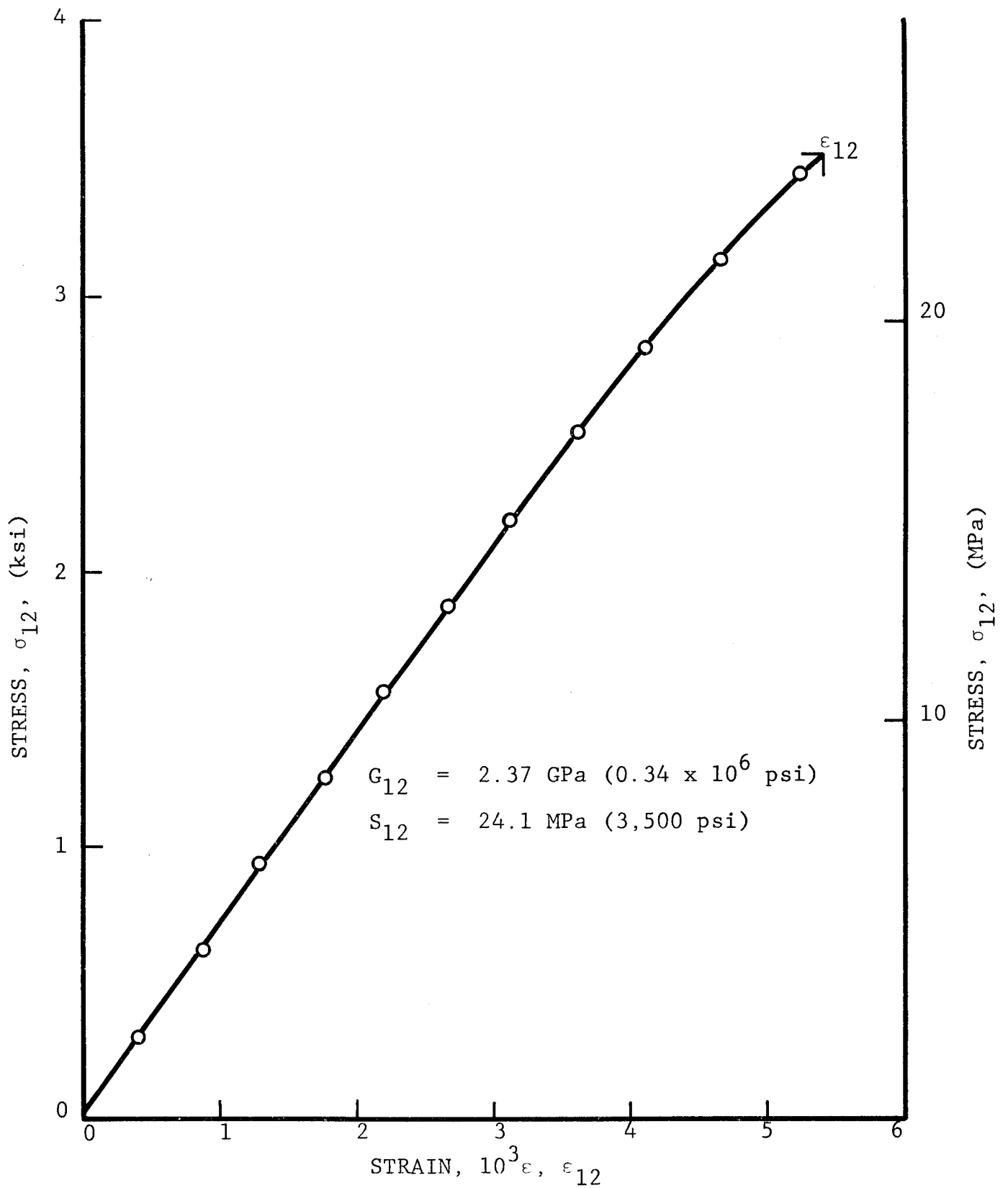


Fig. 26 SHEAR STRESS VERSUS SHEAR STRAIN FOR 10-DEGREE OFF-AXIS UNIDIRECTIONAL KEVLAR 49/HIGH MODULUS EPOXY

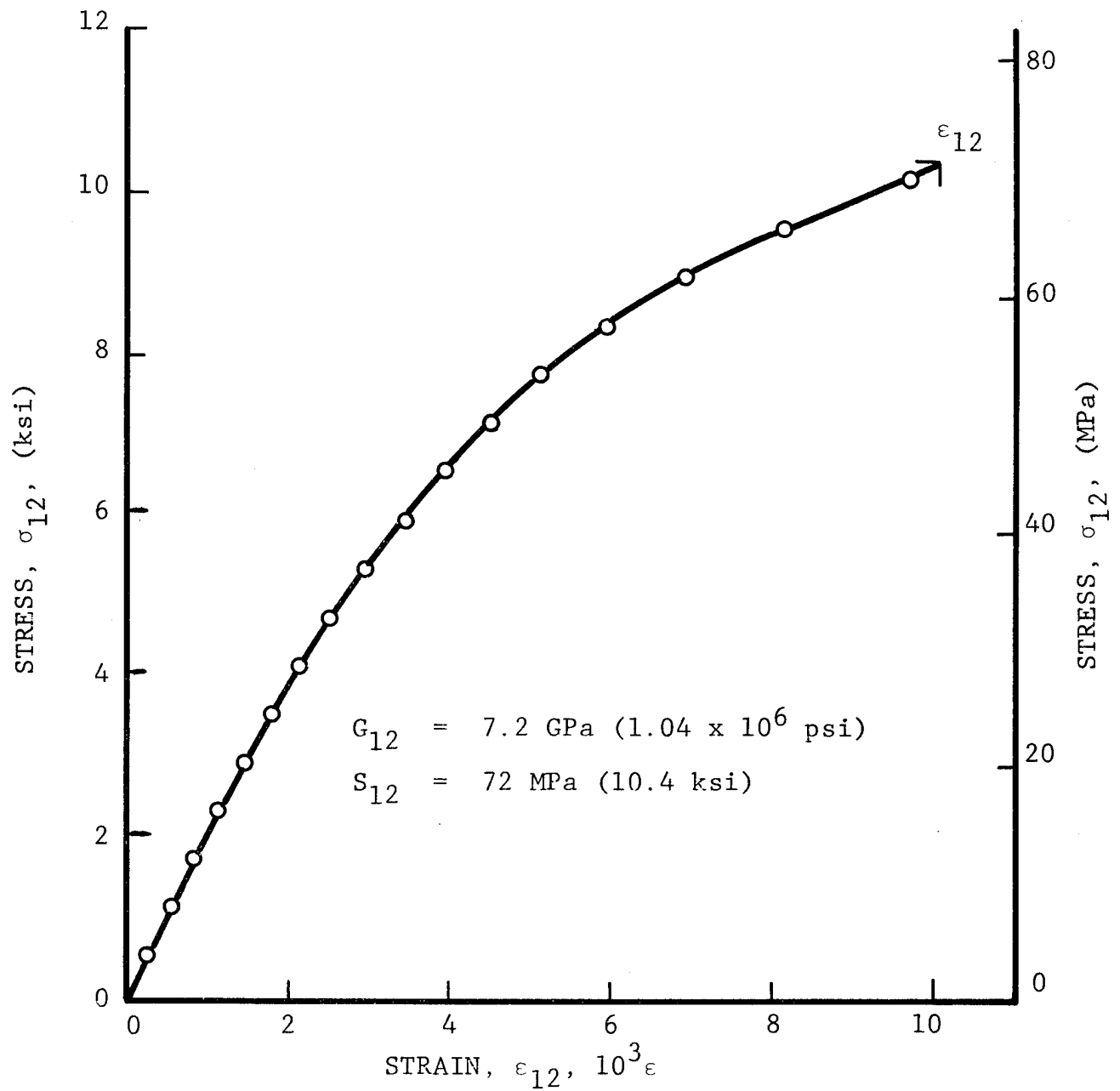


Fig. 27 SHEAR STRESS VERSUS SHEAR STRAIN IN 10-DEGREE OFF-AXIS UNIDIRECTIONAL S-GLASS/HIGH MODULUS EPOXY SPECIMEN

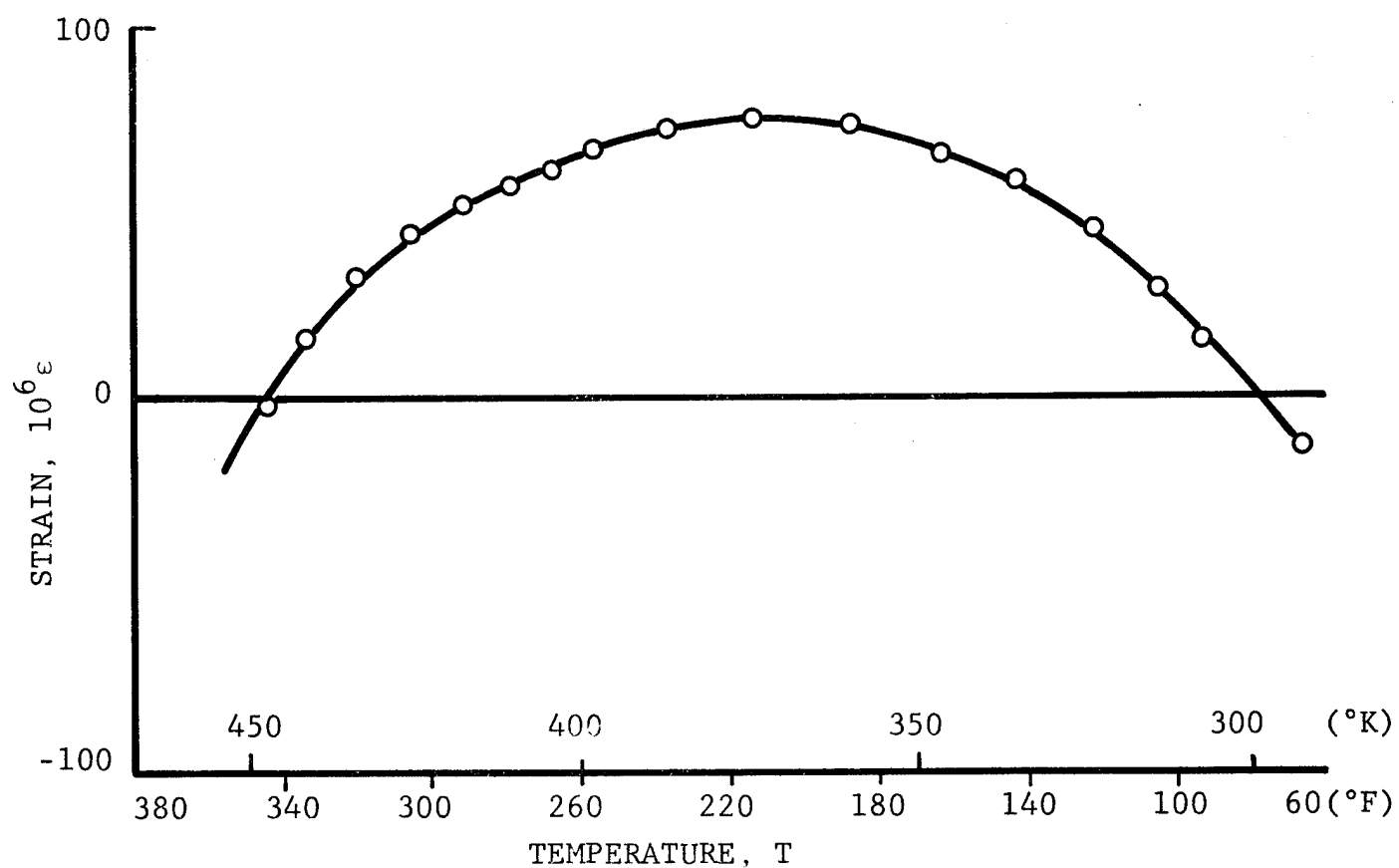


Fig. 28 APPARENT STRAIN AS A FUNCTION OF TEMPERATURE OF WK-00-125TM-350 GAGE BONDED ON TITANIUM SILICATE

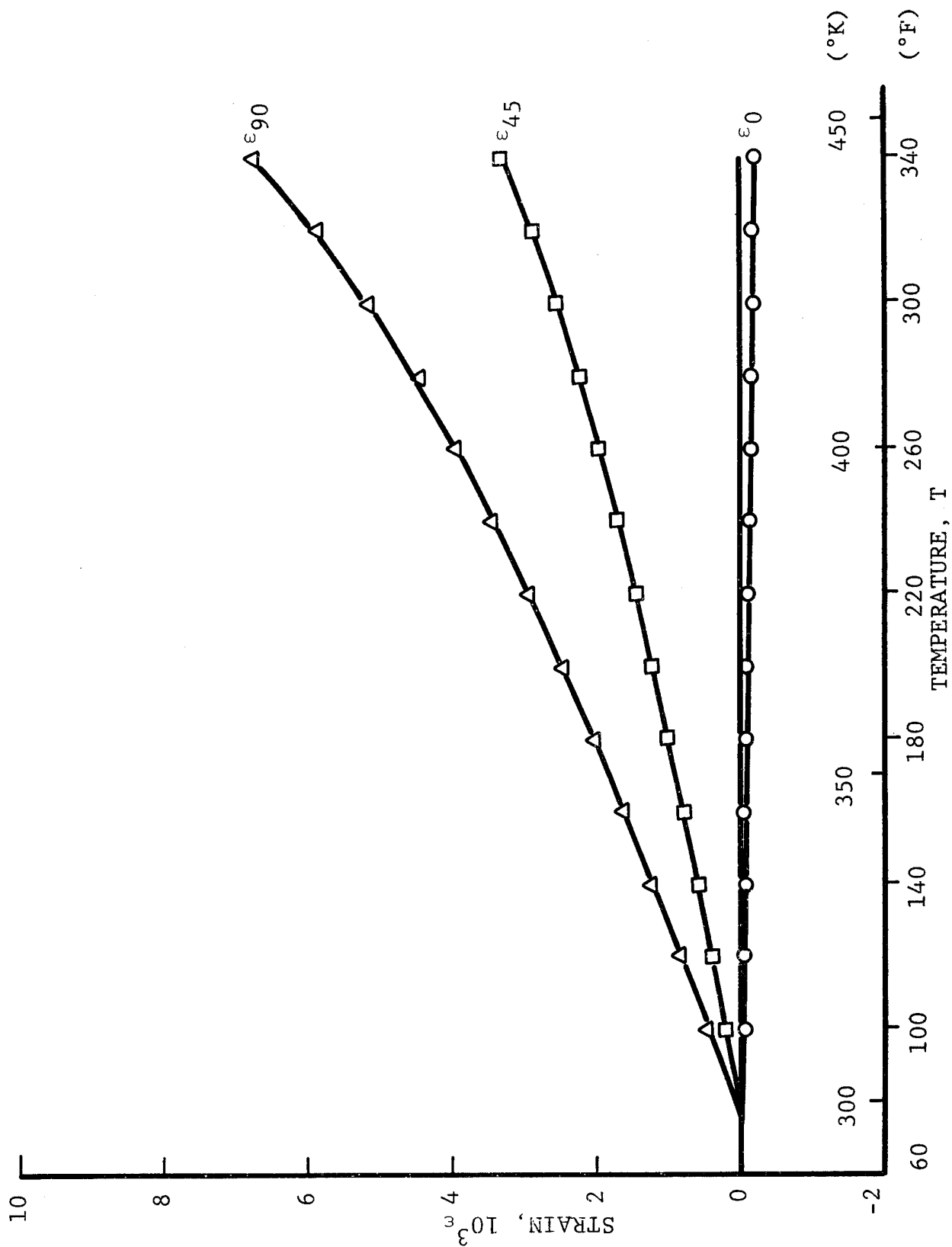


Fig. 29 STRAINS IN $[0_8]$ UNIDIRECTIONAL GRAPHITE/HIGH MODULUS EPOXY SPECIMEN AS A FUNCTION OF TEMPERATURE

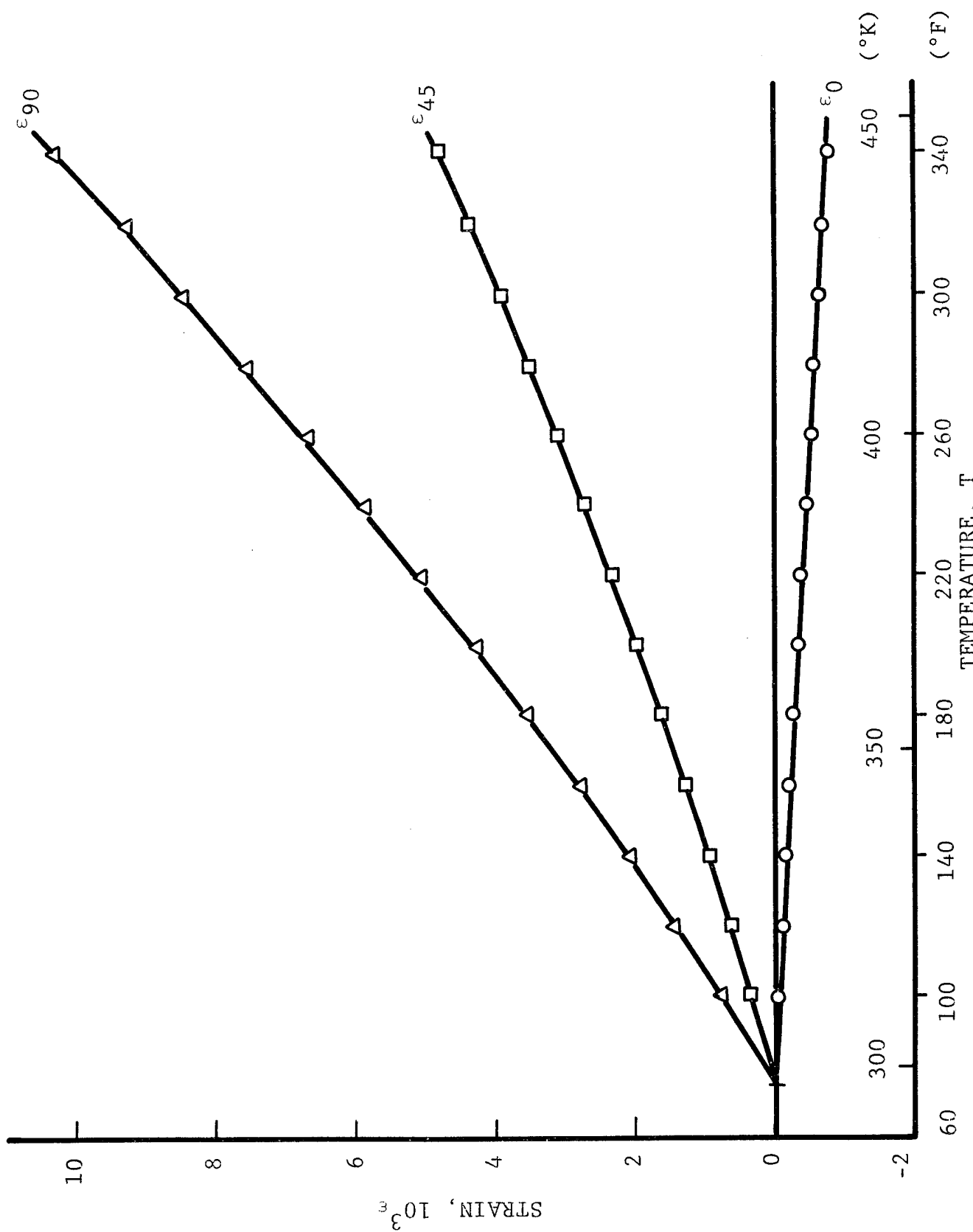


Fig. 30 STRAINS IN $[0_8]$ UNIDIRECTIONAL KEVLAR 49/HIGH MODULUS EPOXY SPECIMEN AS A FUNCTION OF TEMPERATURE

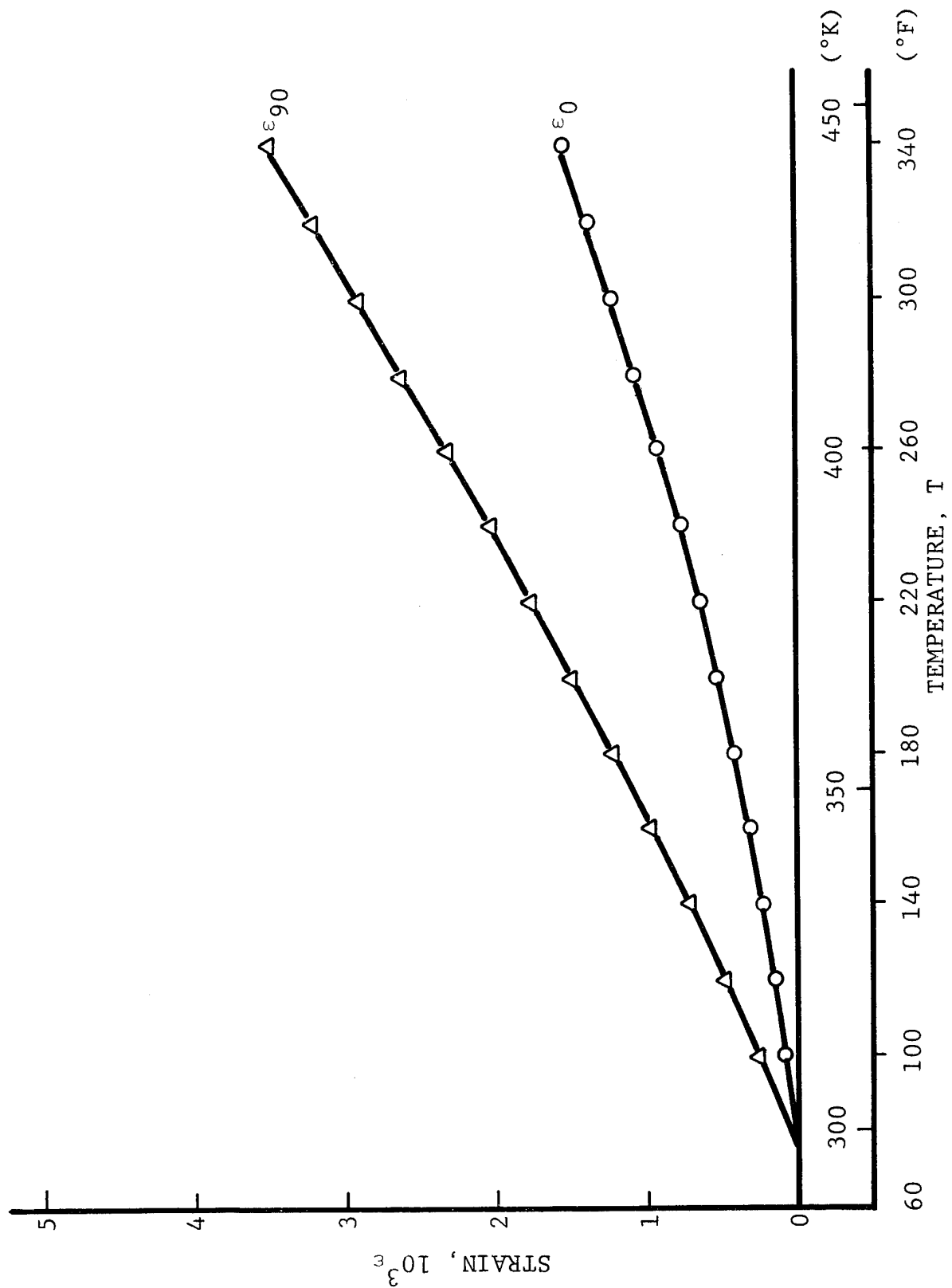


Fig. 31 STRAINS IN $[0_8]$ UNIDIRECTIONAL S-GLASS/HIGH MODULUS EPOXY SPECIMEN AS A FUNCTION OF TEMPERATURE

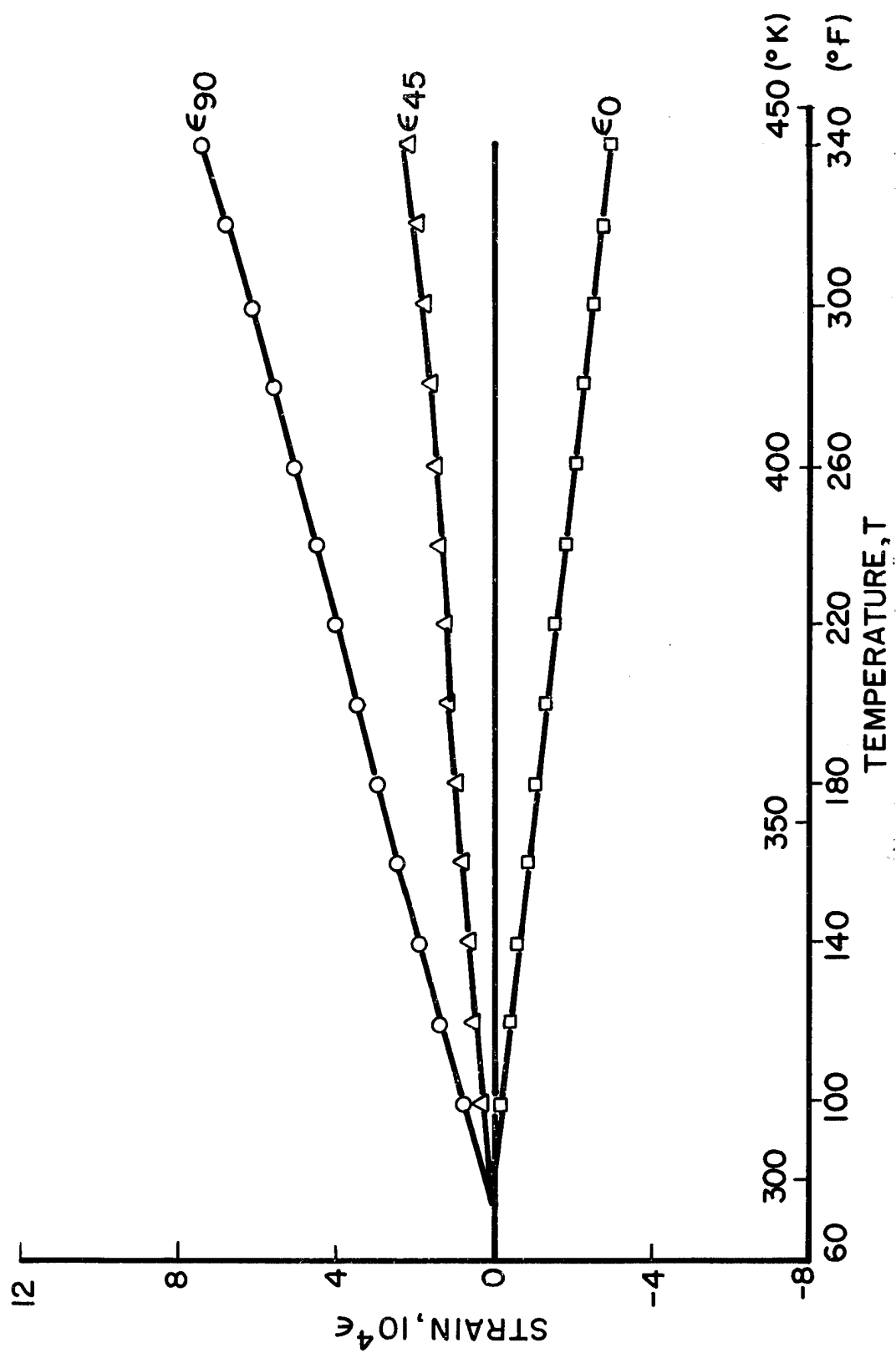


Fig. 32 STRAINS IN $[0^K/+45^C/0^C]_s$ GRAPHITE/KEVLAR 49/HIGH MODULUS EPOXY SPECIMEN

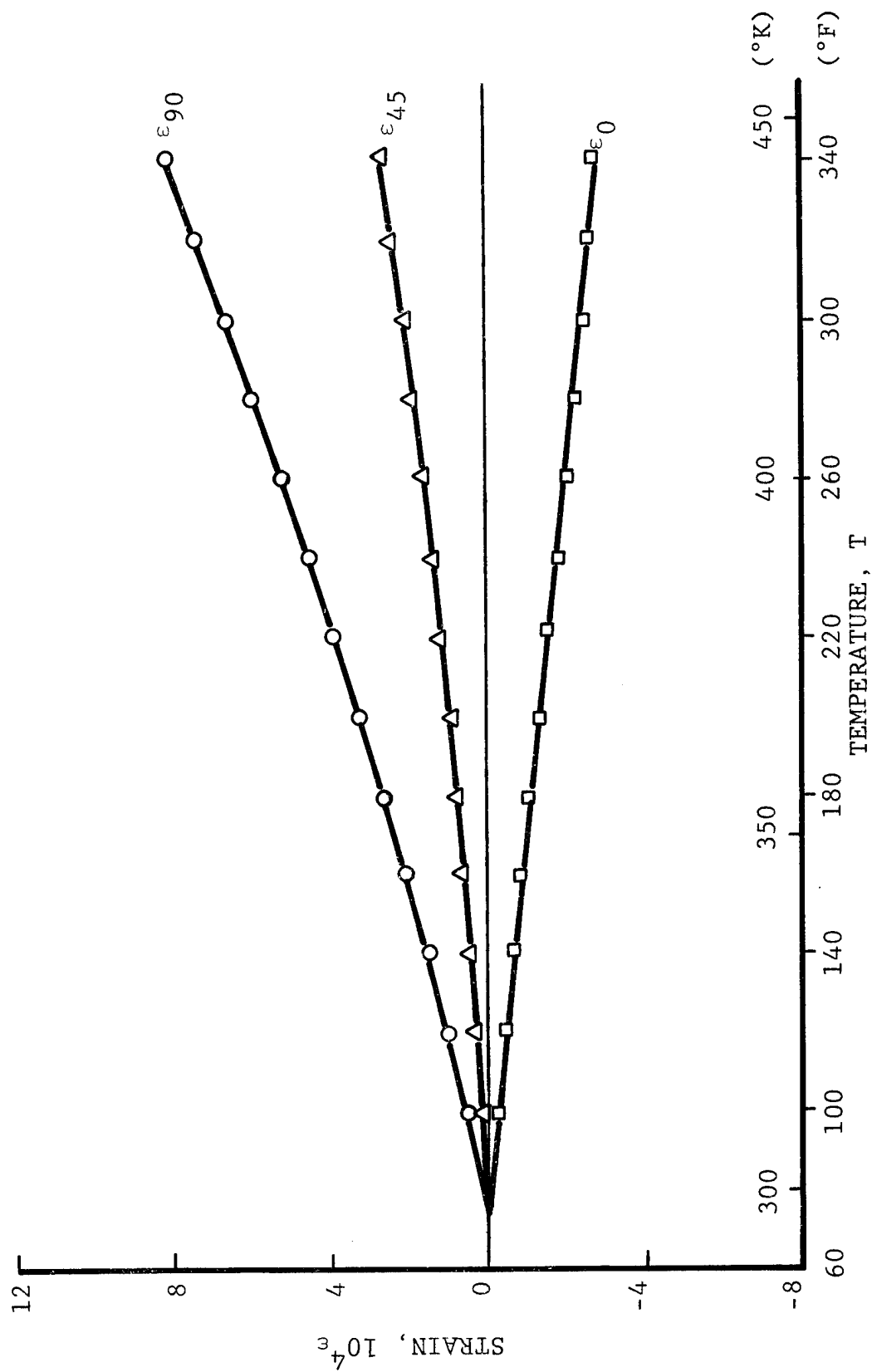


Fig. 33 STRAINS IN $[+45^{\circ}/0^{\circ}/0^{\circ}]_s$ GRAPHITE/KEVLAR 49/HIGH MODULUS EPOXY SPECIMEN

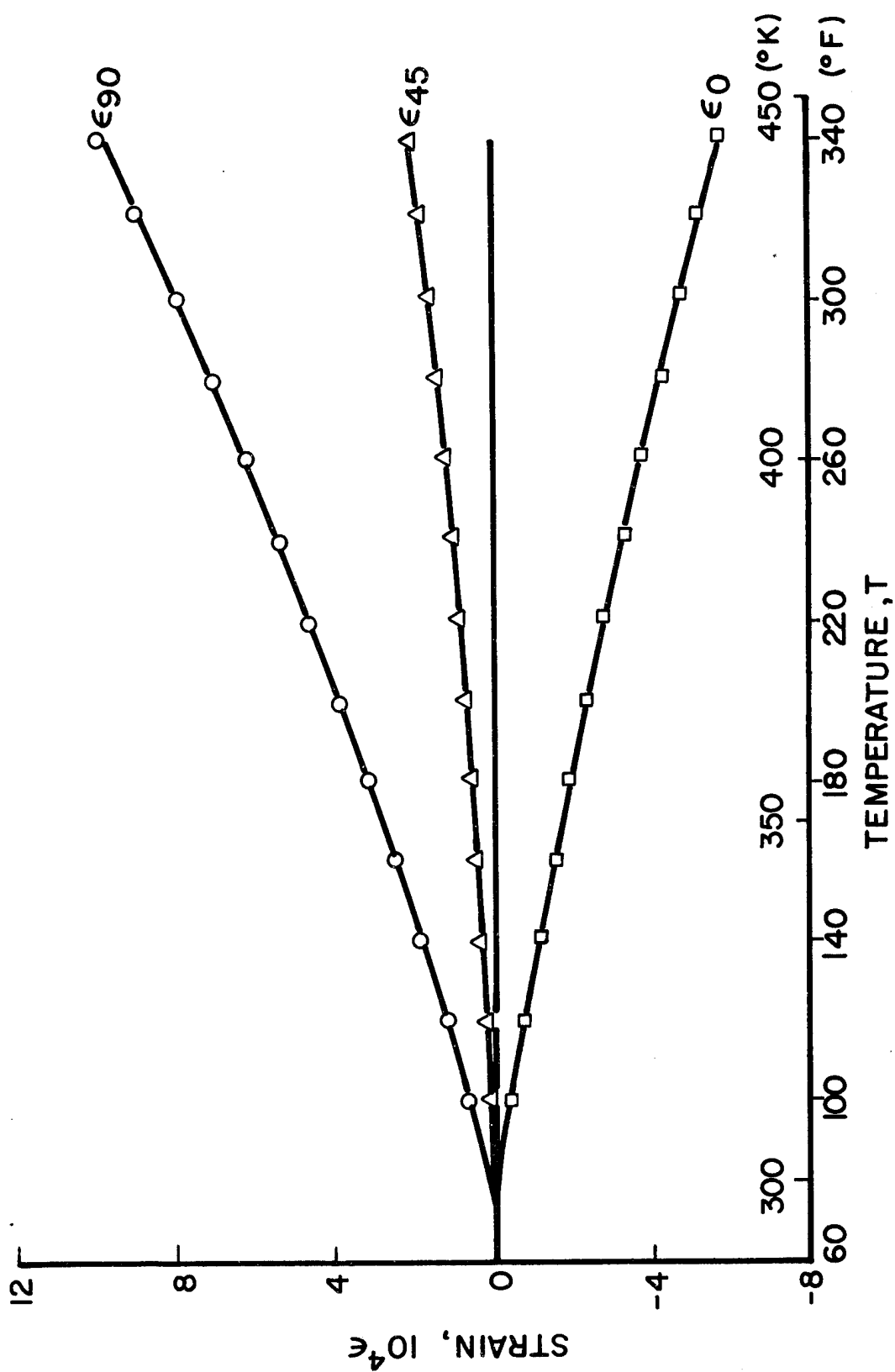


Fig. 34 STRAINS IN $[0^K/+45^C/0^K]_s$ GRAPHITE/KEVLAR 49/HIGH MODULUS EPOXY SPECIMEN

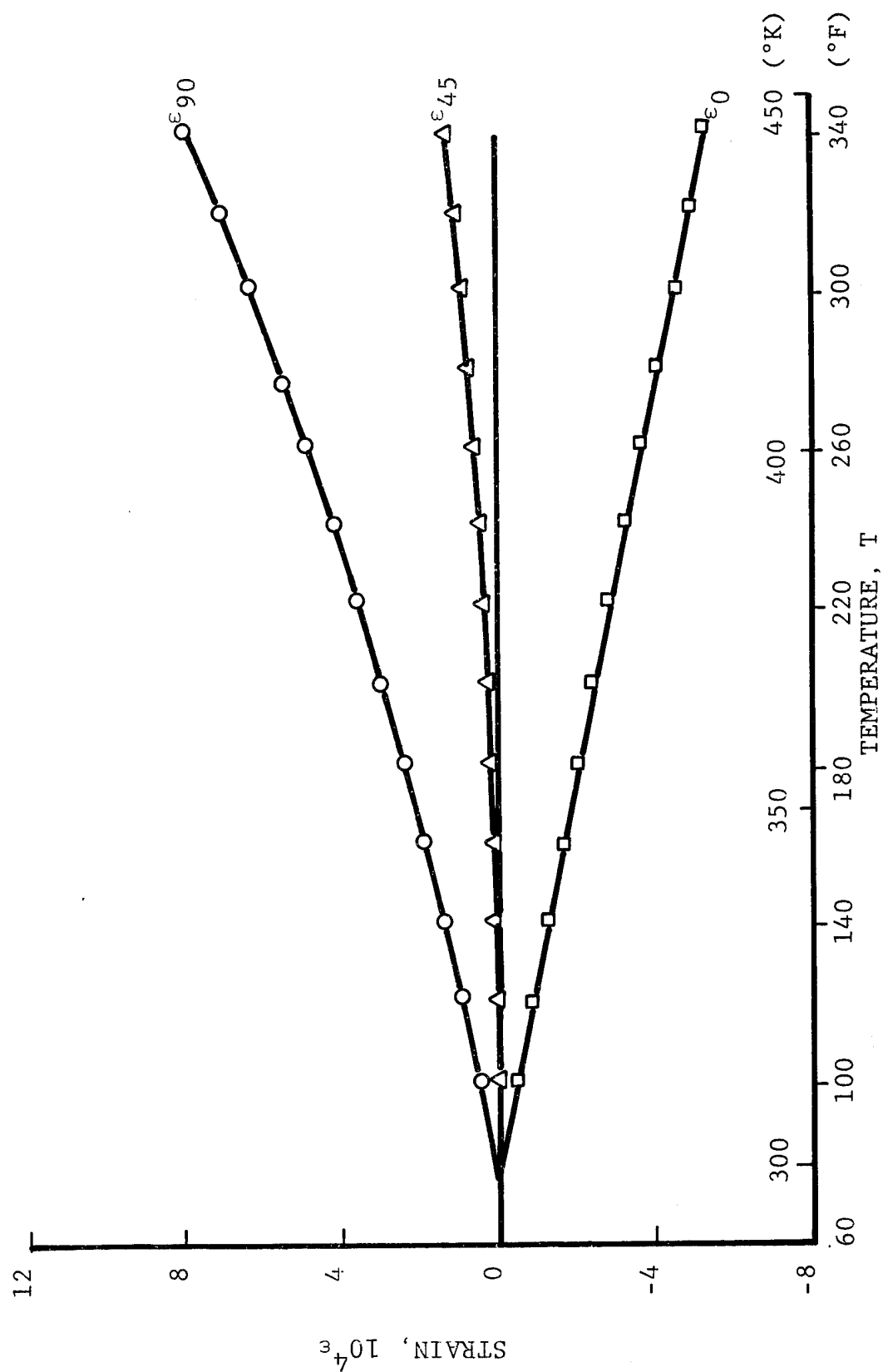


Fig. 35 STRAINS IN $[\pm 45^\circ / 0_2]_s$ GRAPHITE/KEVLAR 49/HIGH MODULUS EPOXY SPECIMEN

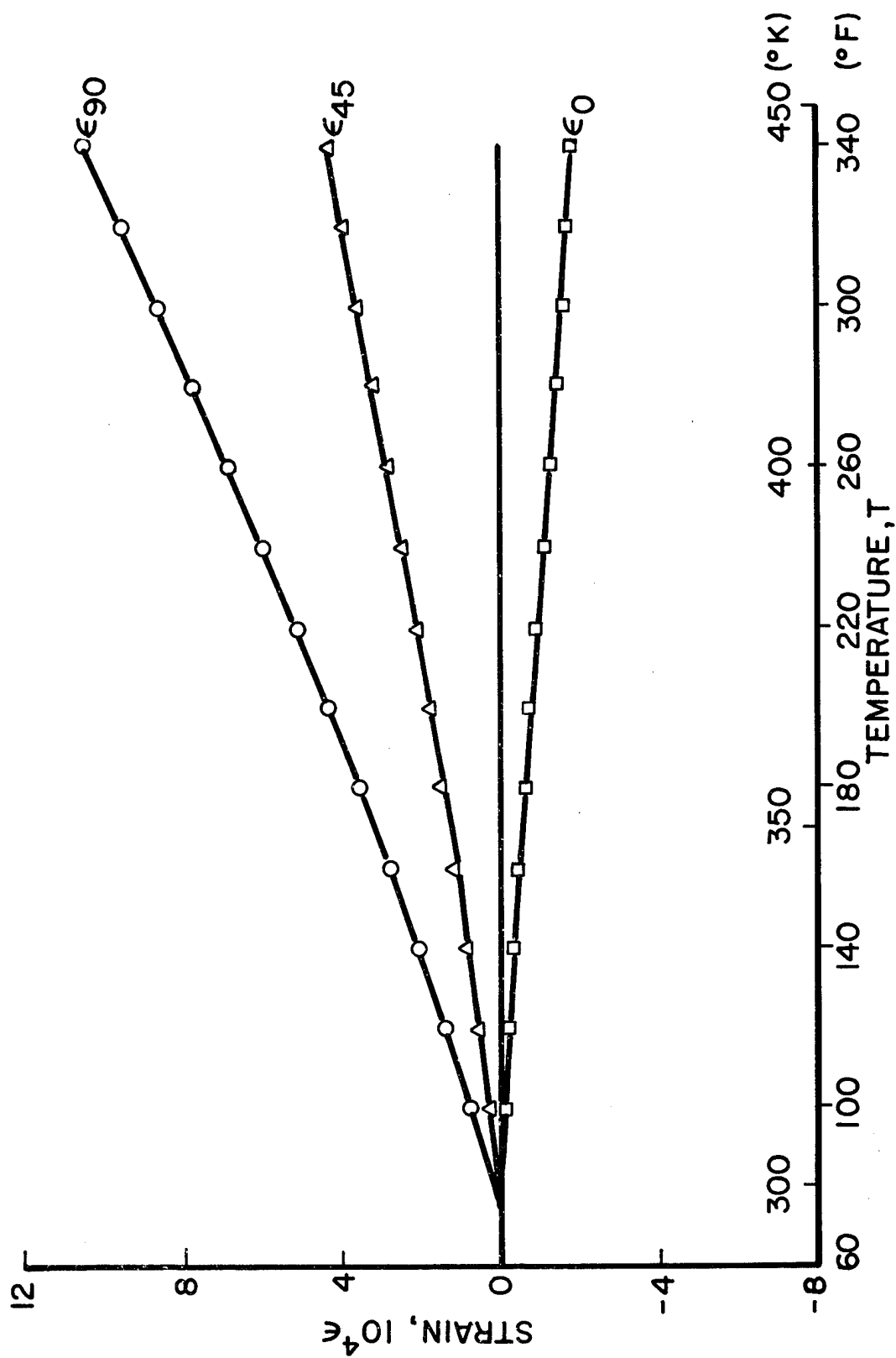


Fig. 36 STRAINS IN $[0^G/+45^C/0^C]_s$ GRAPHITE/S-GLASS/HIGH MODULUS EPOXY SPECIMEN

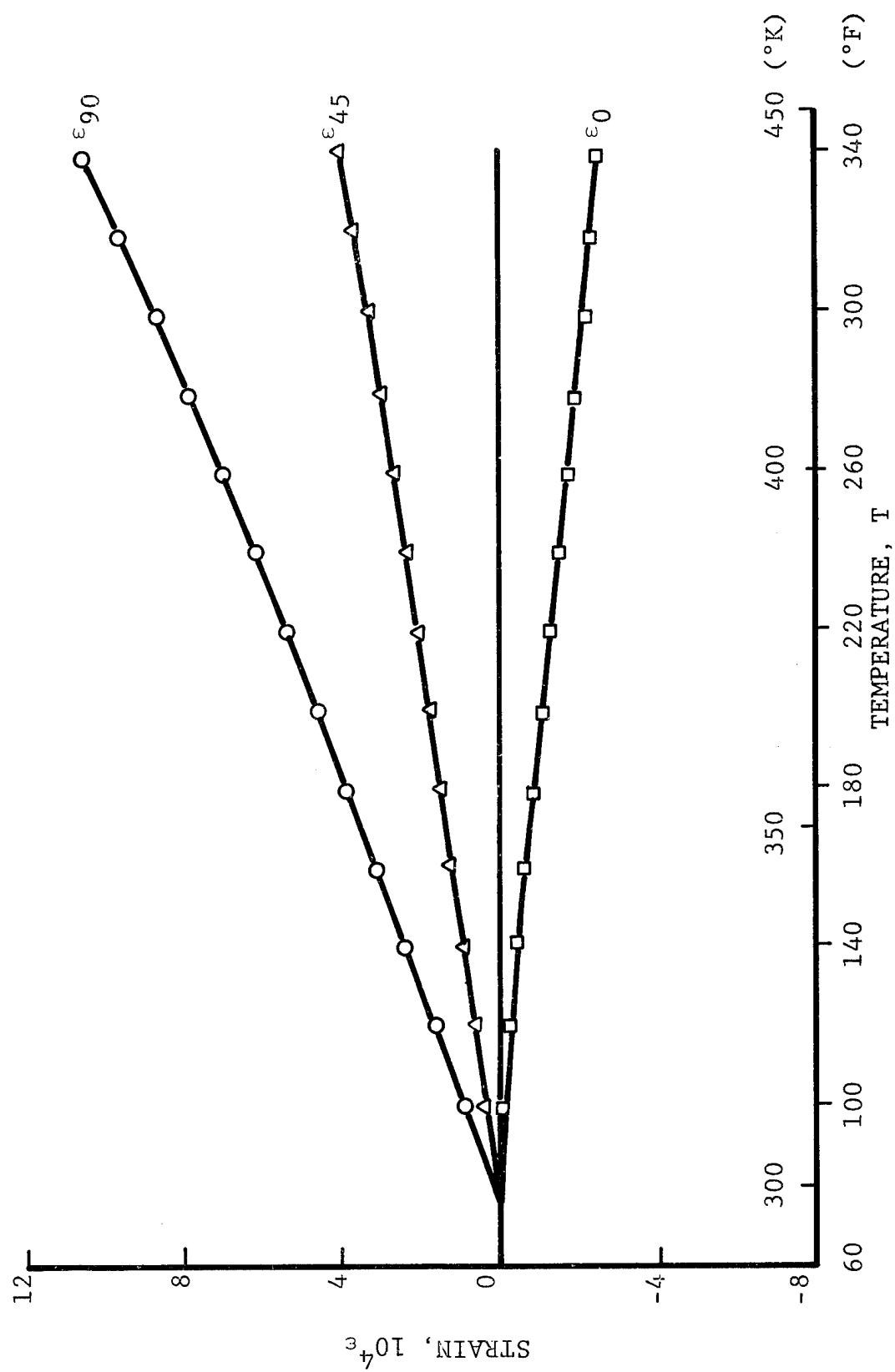


Fig. 37 STRAINS IN $[+45^{\circ}/0^{\circ}/0^{\circ}]_s$ GRAPHITE/S-GLASS/HIGH MODULUS EPOXY SPECIMEN

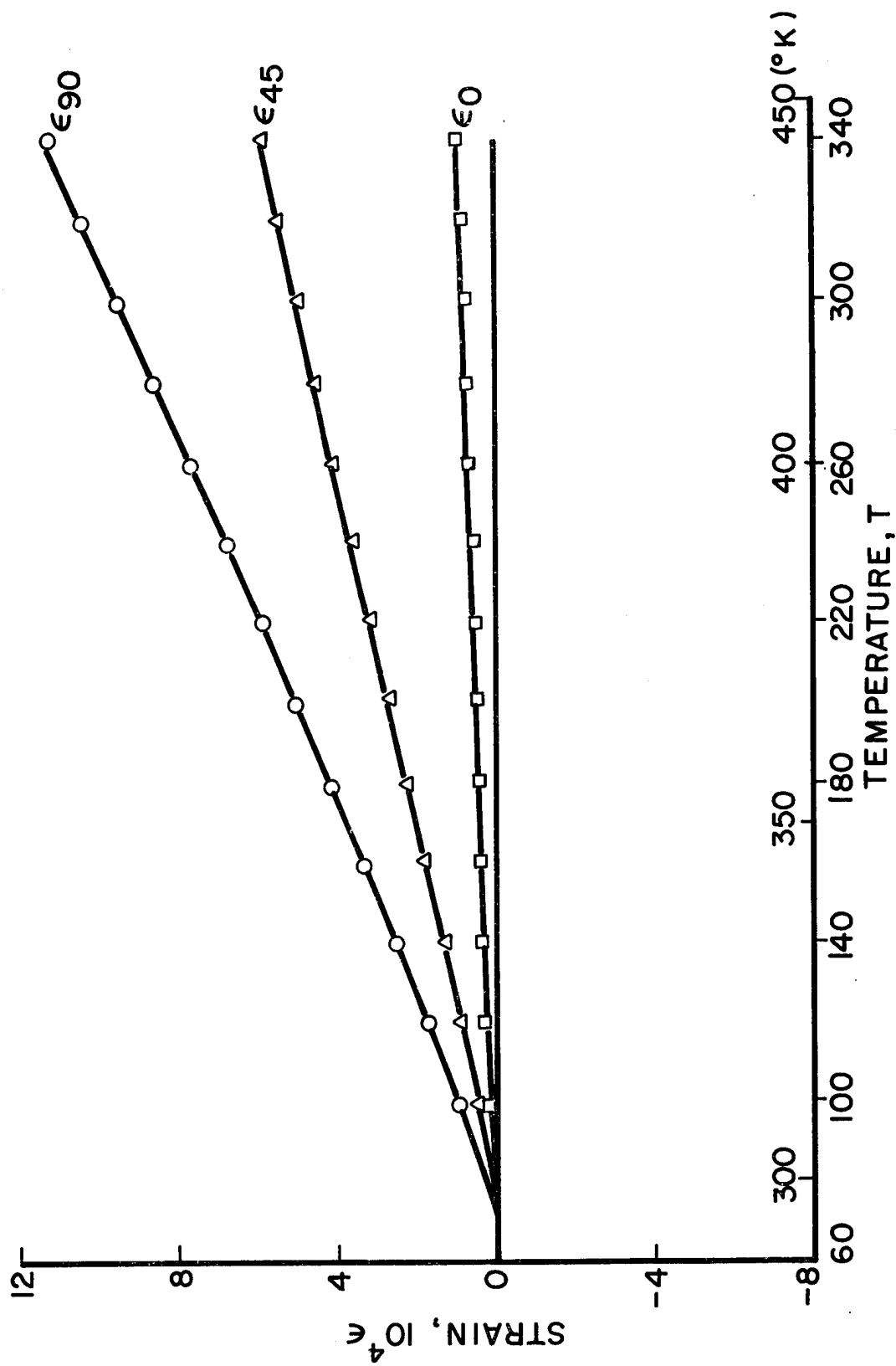


Fig. 38 STRAINS IN $[0^G/+45^G/0^G]_s$ GRAPHITE/S-GLASS/HIGH MODULUS EPOXY SPECIMEN

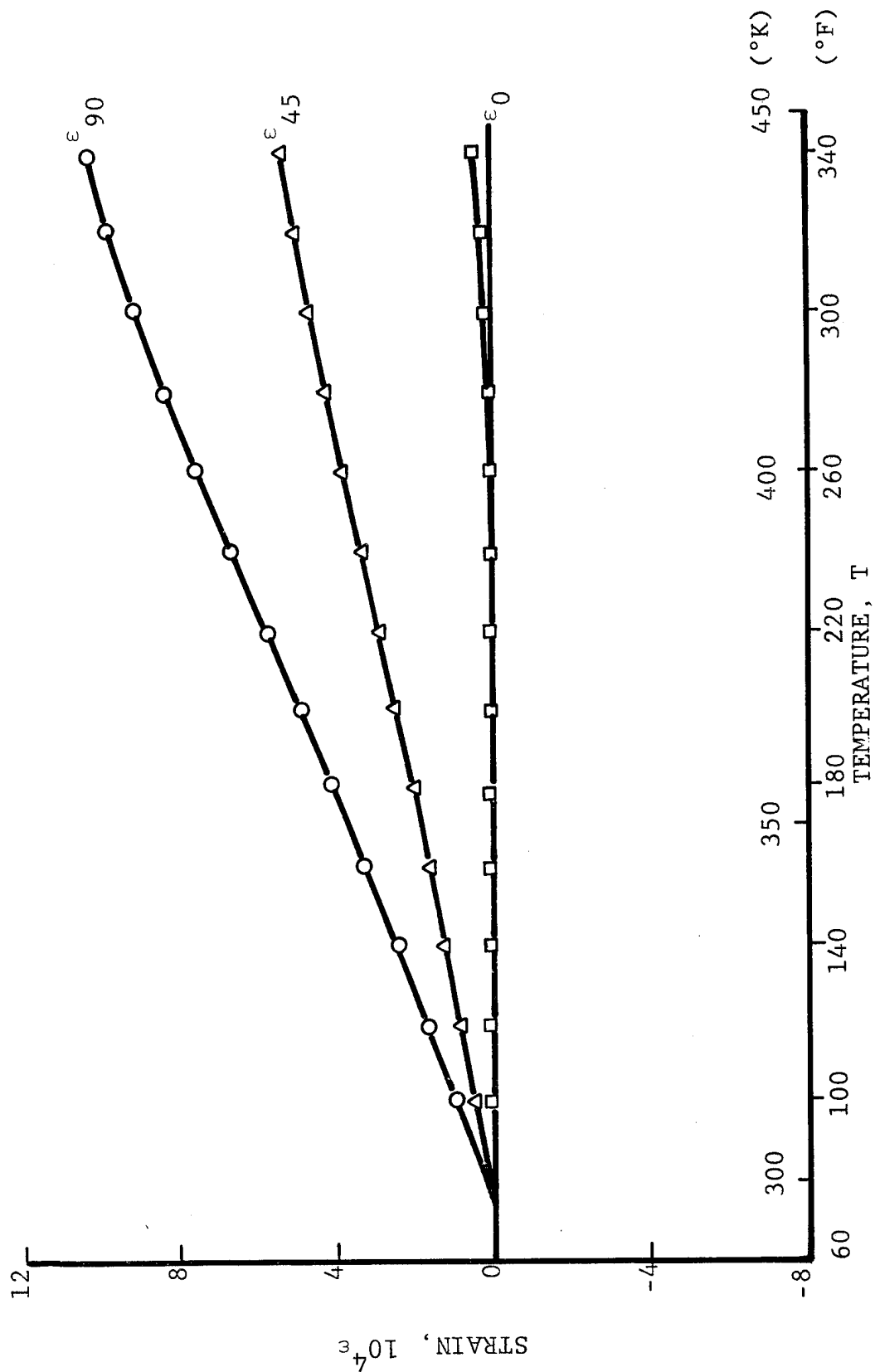


Fig. 39 STRAINS IN $[+45^{\circ}/0_2^G]_s$ GRAPHITE/S-GLASS/HIGH MODULUS EPOXY SPECIMEN

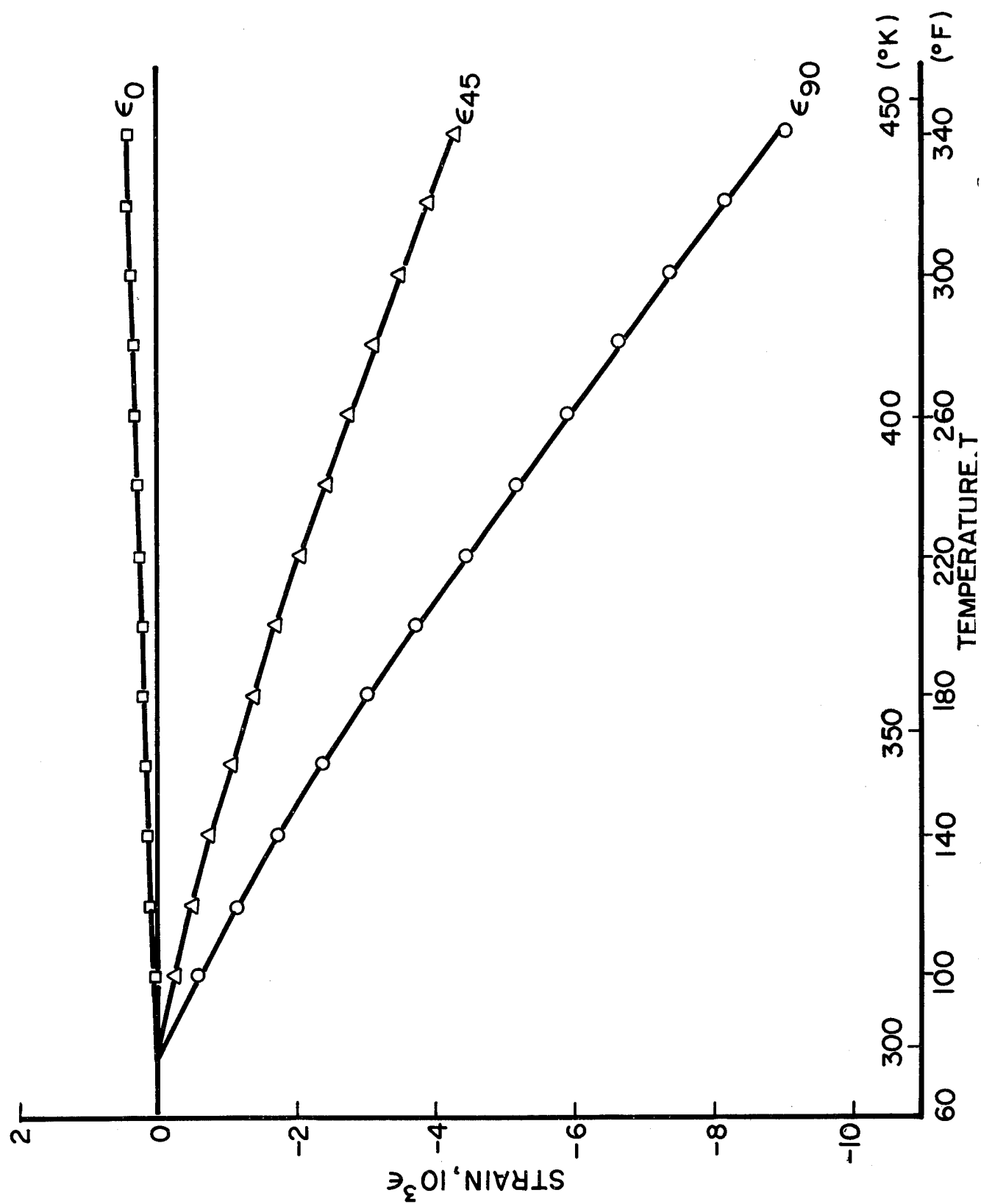


Fig. 40 RESTRAINT STRAINS IN 0-DEG. KEVLAR 49 PLYS OF $[0^{\text{K}}/+45^{\text{C}}/0^{\text{C}}]_s$ GRAPHITE/KEVLAR 49/HIGH MODULUS EPOXY SPECIMEN

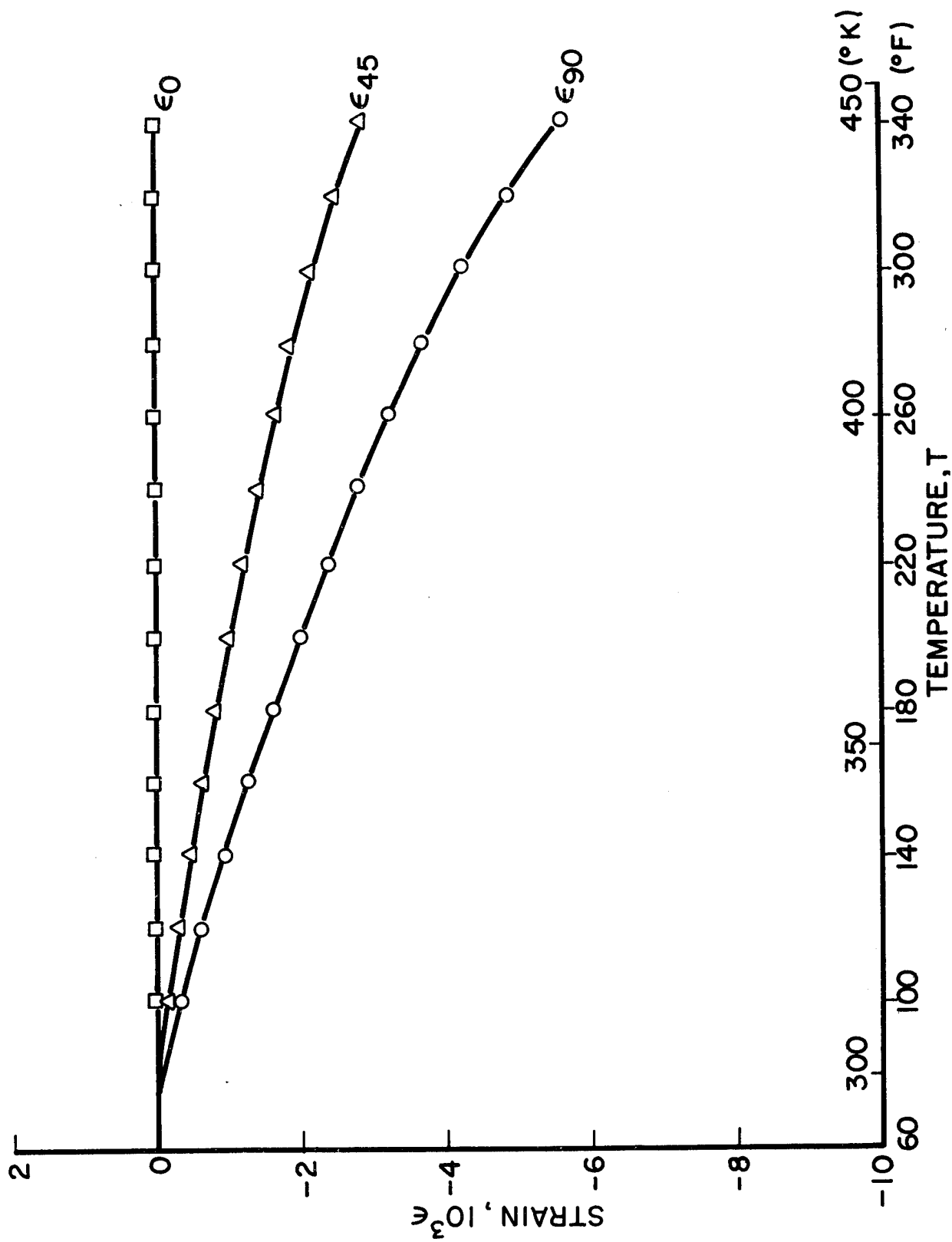


Fig. 41 RESTRAINT STRAINS IN 0-DEG. GRAPHITE PLIES OF $[0^{\text{K}}/_{+45^{\text{C}}}/0^{\text{C}}]_s$
GRAPHITE/KEVLAR 49/HIGH MODULUS EPOXY SPECIMEN

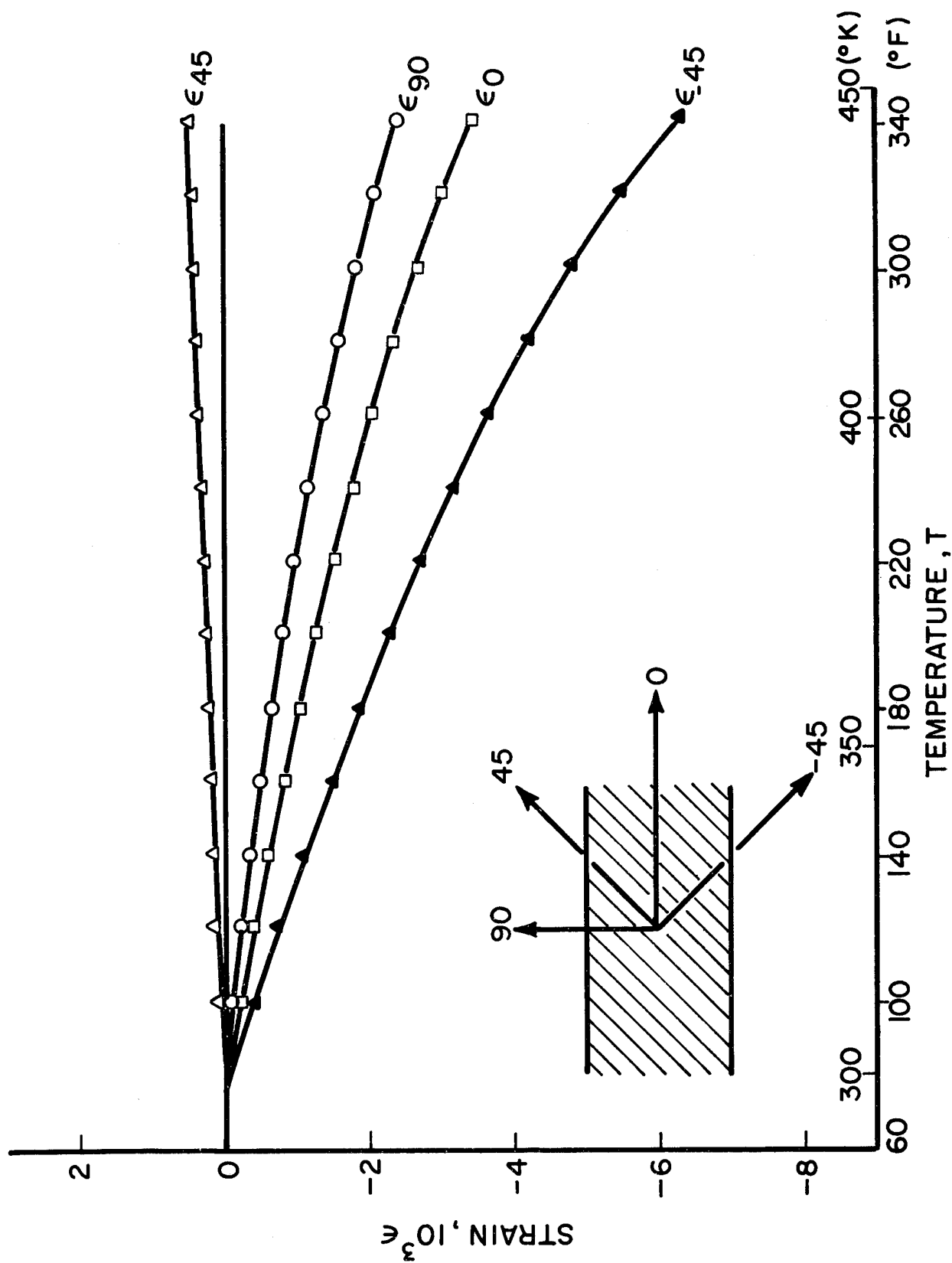


Fig. 4.2 RESTRAINT STRAINS IN 45-DEG. GRAPHITE PLYS OF $[0^K/+45^C/0^C]_s$ GRAPHITE/KEVLAR 49/HIGH MODULUS EPOXY SPECIMEN

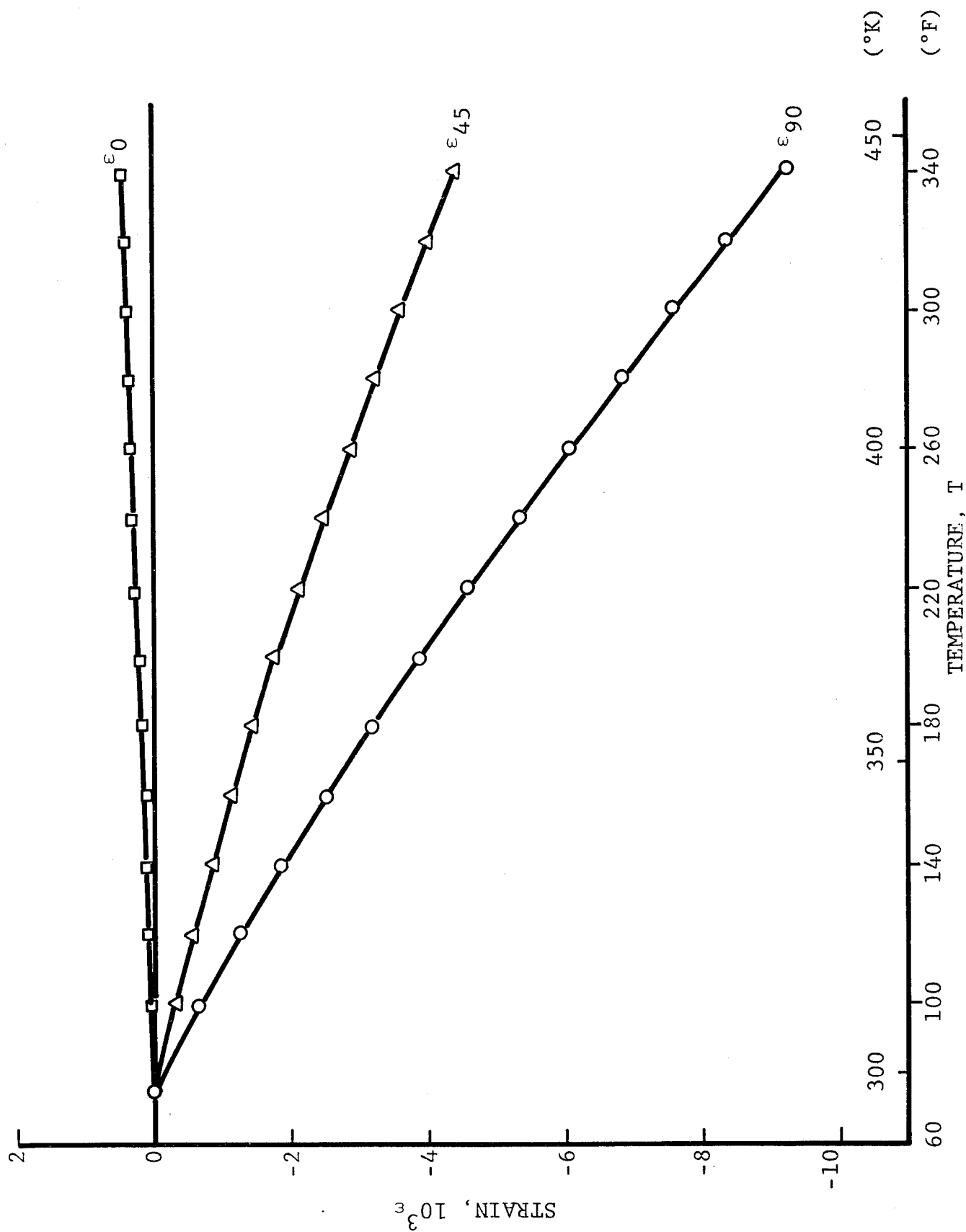


Fig. 43 RESTRAINT STRAINS IN 0-DEG. KEVLAR 49 PLYS OF $[+45^\circ/0^\circ/0^\circ]_s$ GRAPHITE/KEVLAR 49/HIGH MODULUS EPOXY SPECIMEN

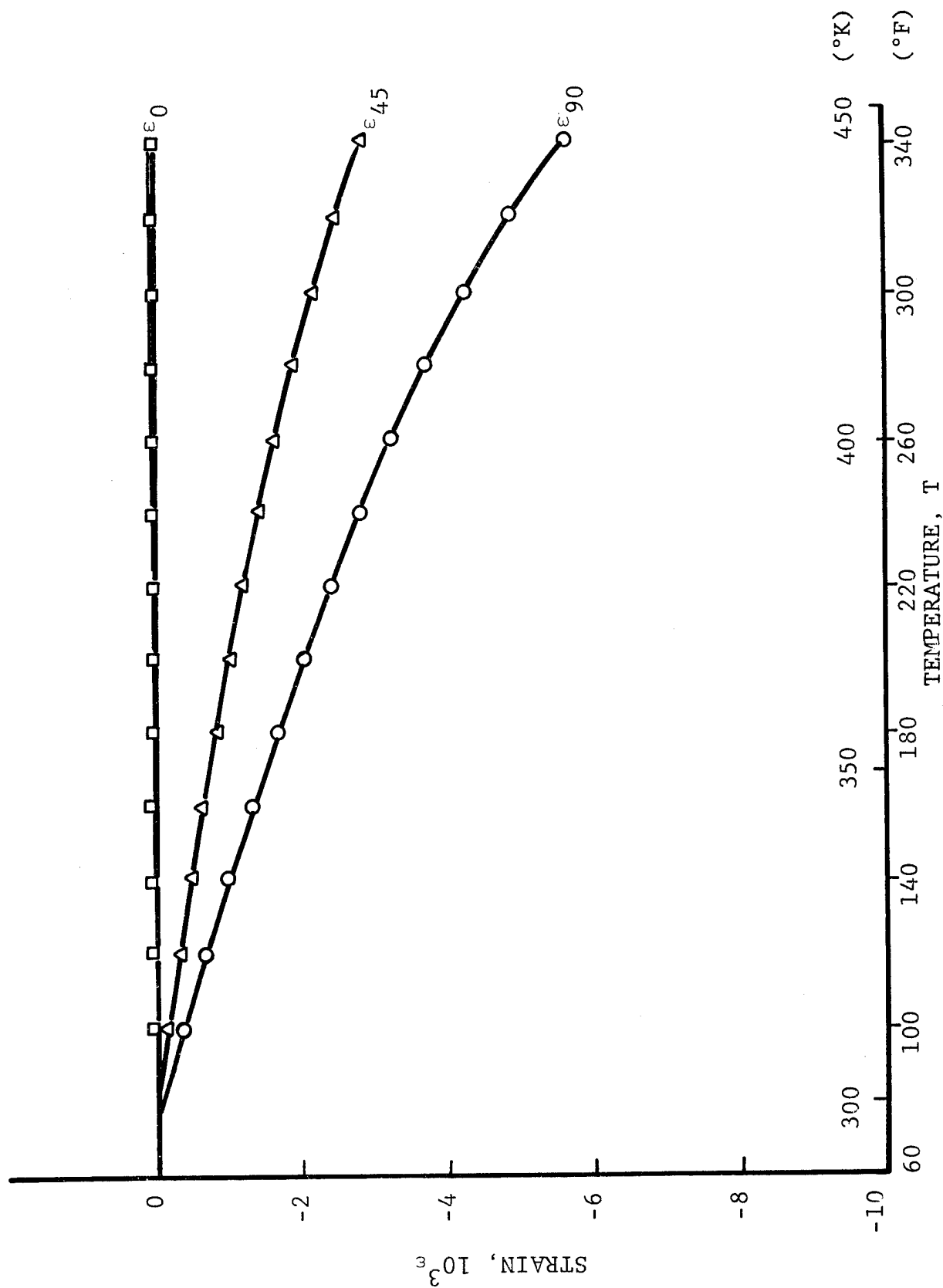
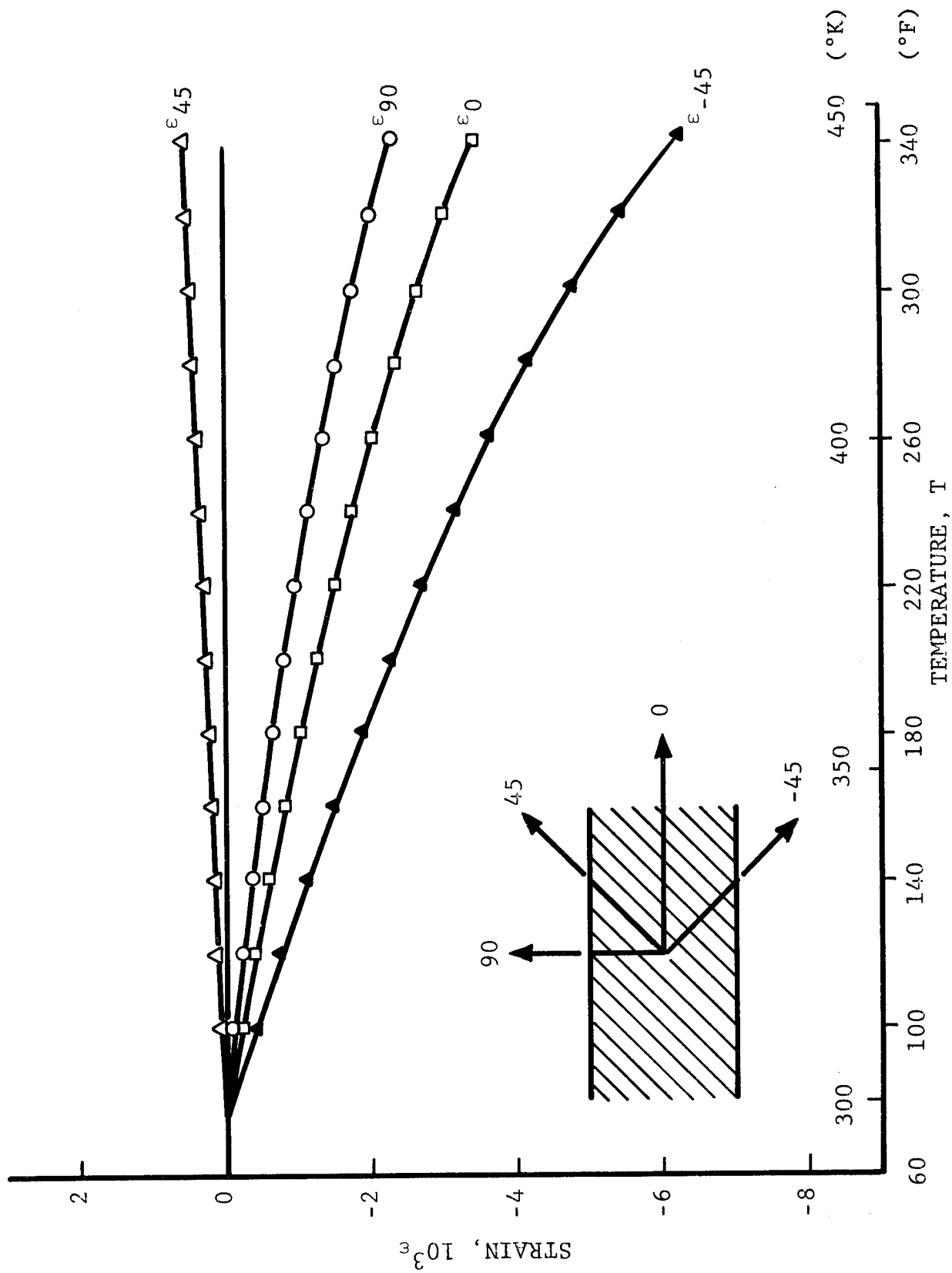


Fig. 44 RESTRAINT STRAINS IN 0-DEG. GRAPHITE PLIES OF $[+45^{\circ}/0^{\circ}/0^{\circ}]_s$ GRAPHITE/KEVLAR 49/HIGH MODULUS EPOXY SPECIMEN



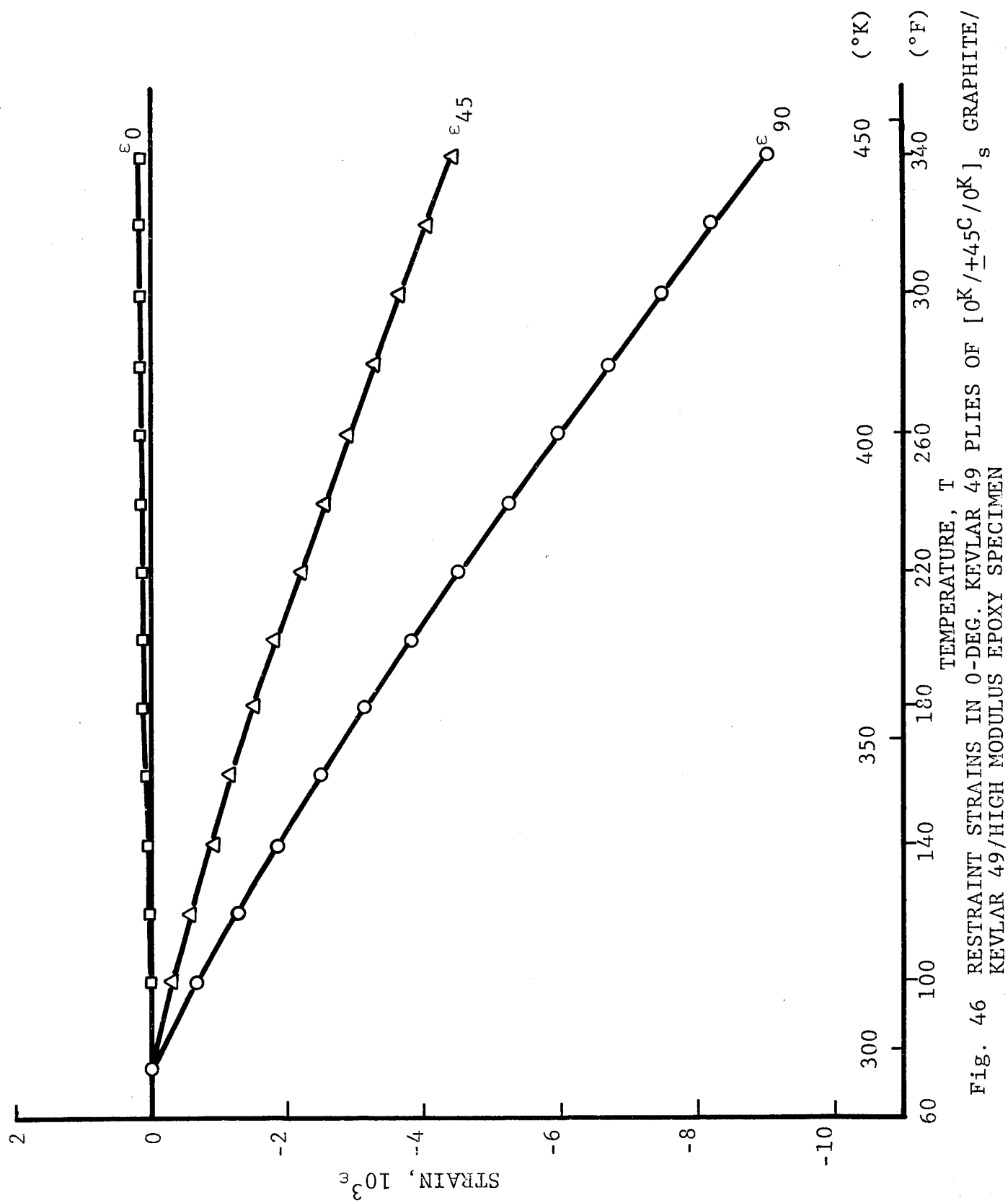


Fig. 46 RESTRAINT STRAINS IN 0-DEG. KEVLAR 49 PLYS OF $[0^k/+45^c/0^k]_s$ GRAPHITE/KEVLAR 49/HIGH MODULUS EPOXY SPECIMEN

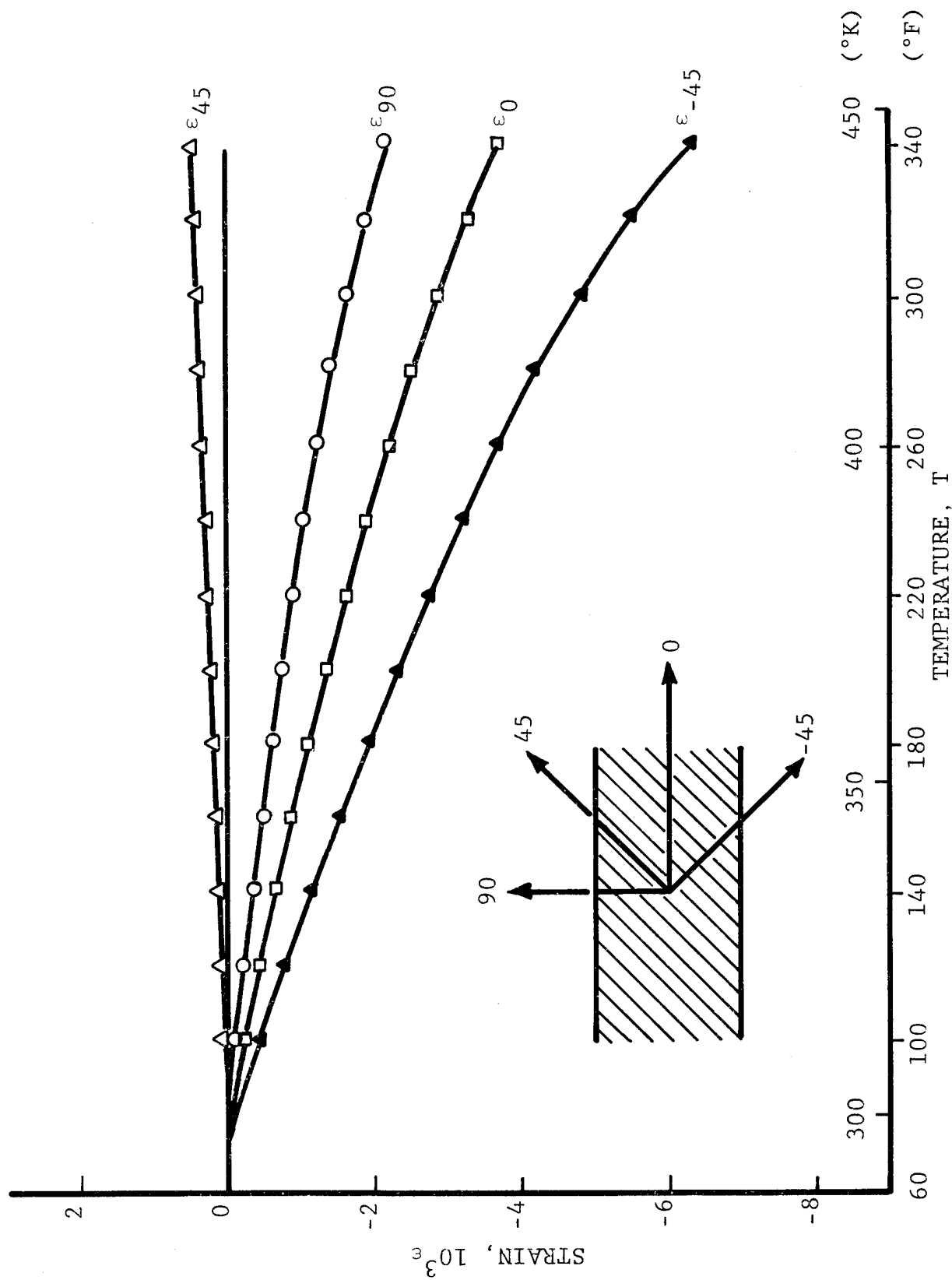


Fig. 47 RESTRAINT STRAINS IN 45-DEGREE GRAPHITE PLYS OF $[0^K/+45^C/0^K]_s$ GRAPHITE/KEVLAR 49/HIGH MODULUS EPOXY SPECIMEN

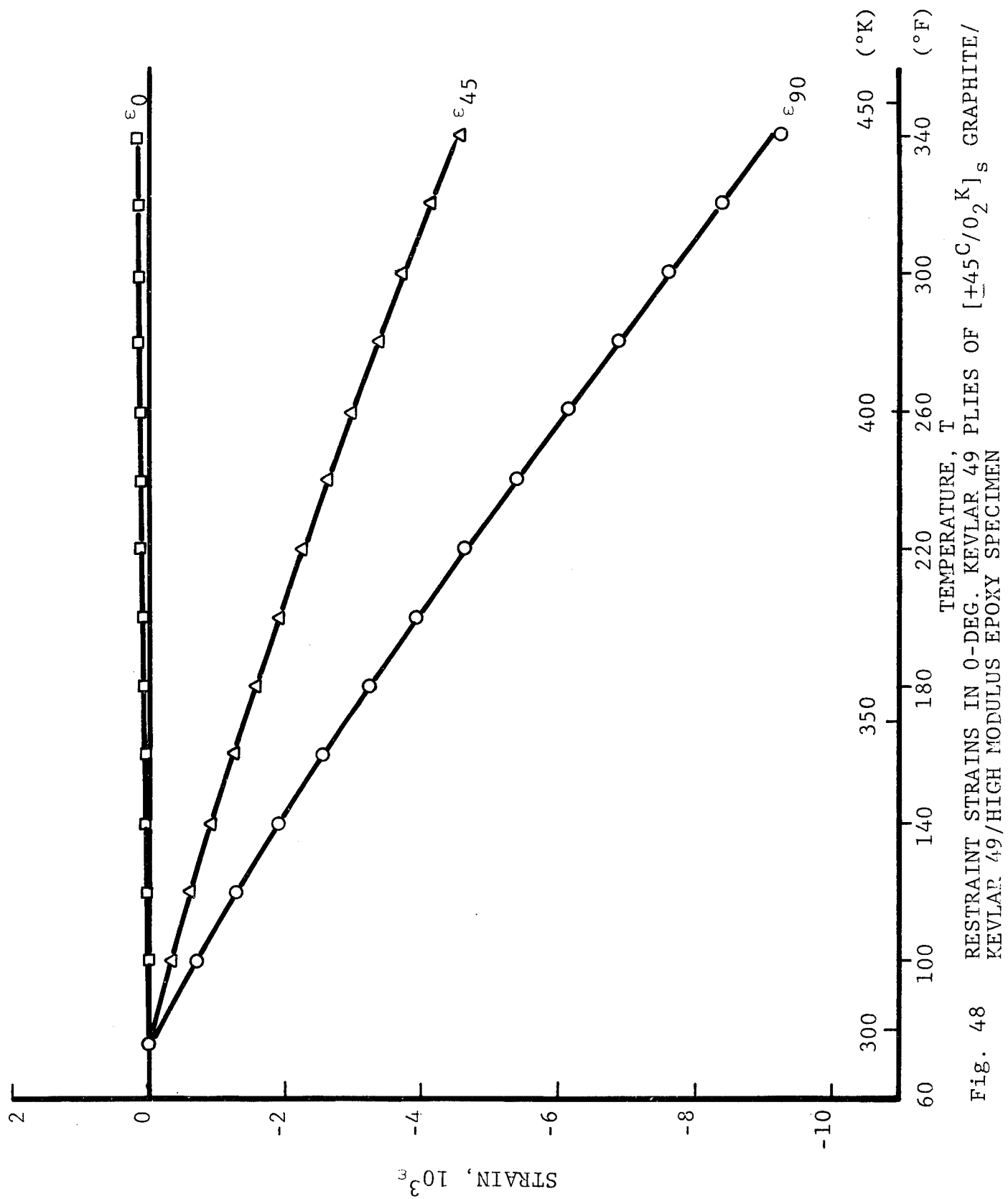


Fig. 48 RESTRAINT STRAINS IN 0-DEG. KEVLAR 49 PLYS OF [+45°/0°K]_s GRAPHITE/KEVLAR 49/HIGH MODULUS EPOXY SPECIMEN

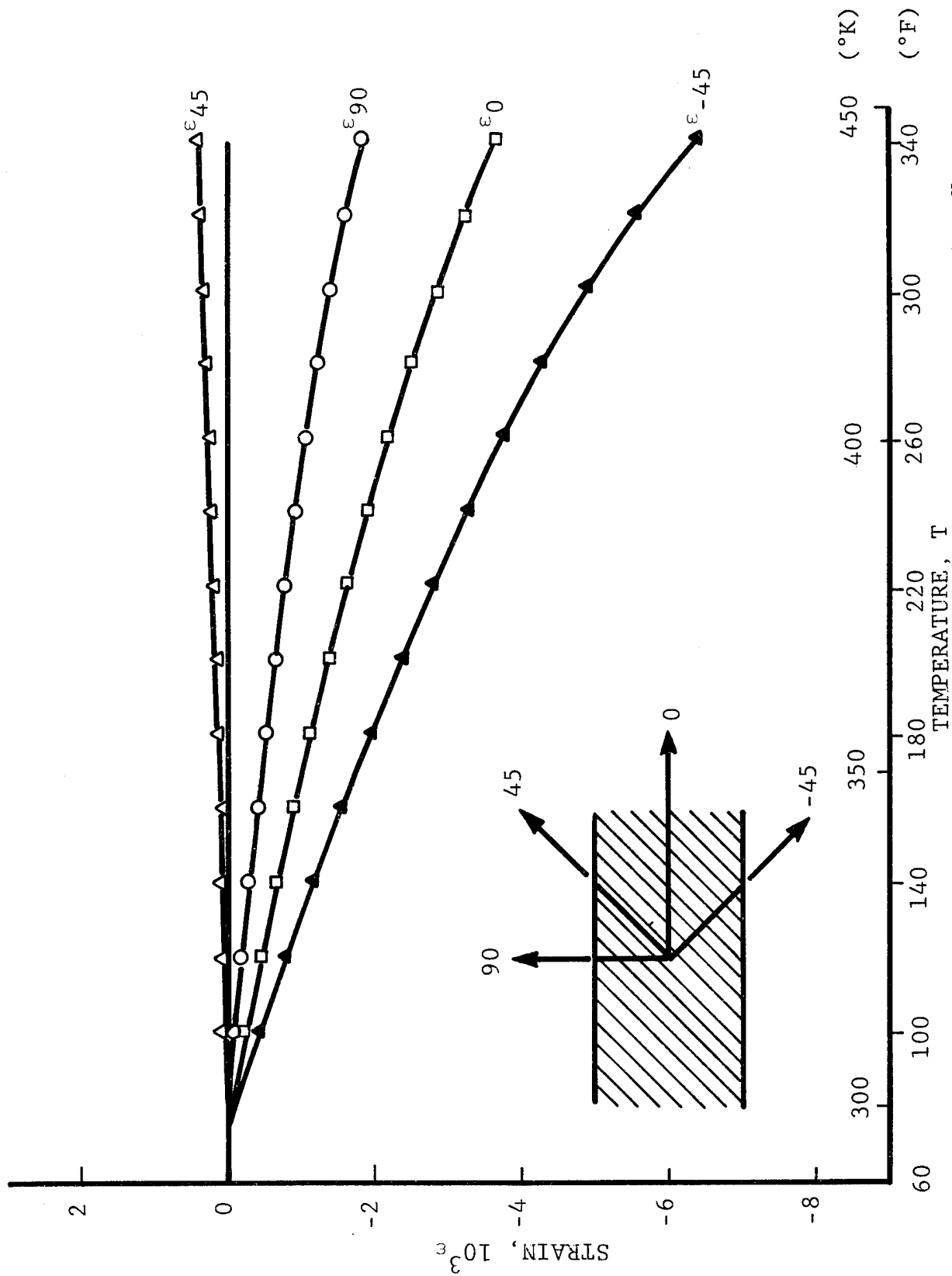


Fig. 49 RESTRAINT STRAINS IN 45-DEG. GRAPHITE PLYS OF $[+45^C/0_2^K]_s$ GRAPHITE/KEVLAR 49/HIGH MODULUS EPOXY SPECIMEN

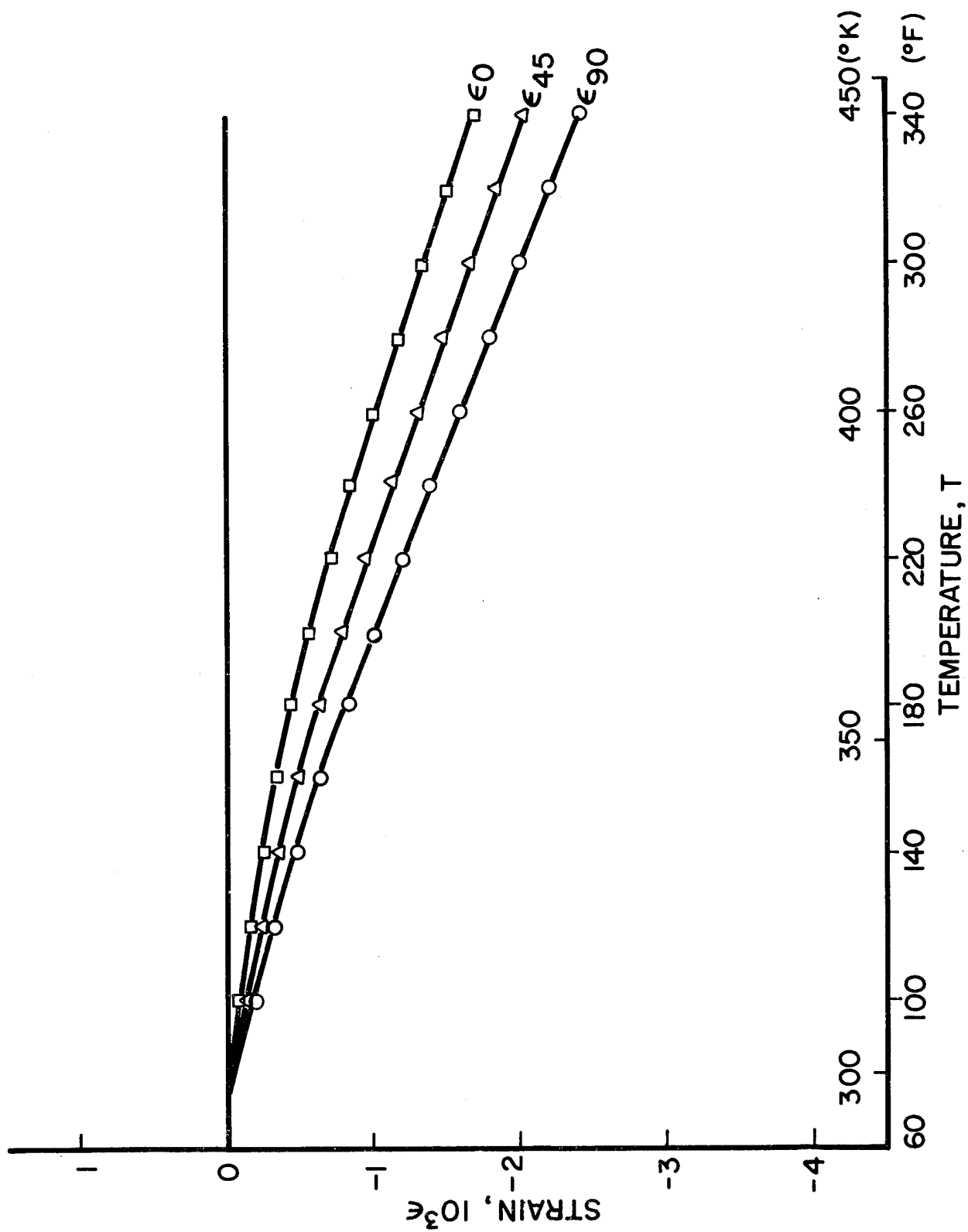


Fig. 50 RESTRAINT STRAINS IN 0-DEG. S-GLASS PLYS OF $[0^G/+45^C/0^C]_s$ GRAPHITE/
S-GLASS/HIGH MODULUS EPOXY SPECIMEN

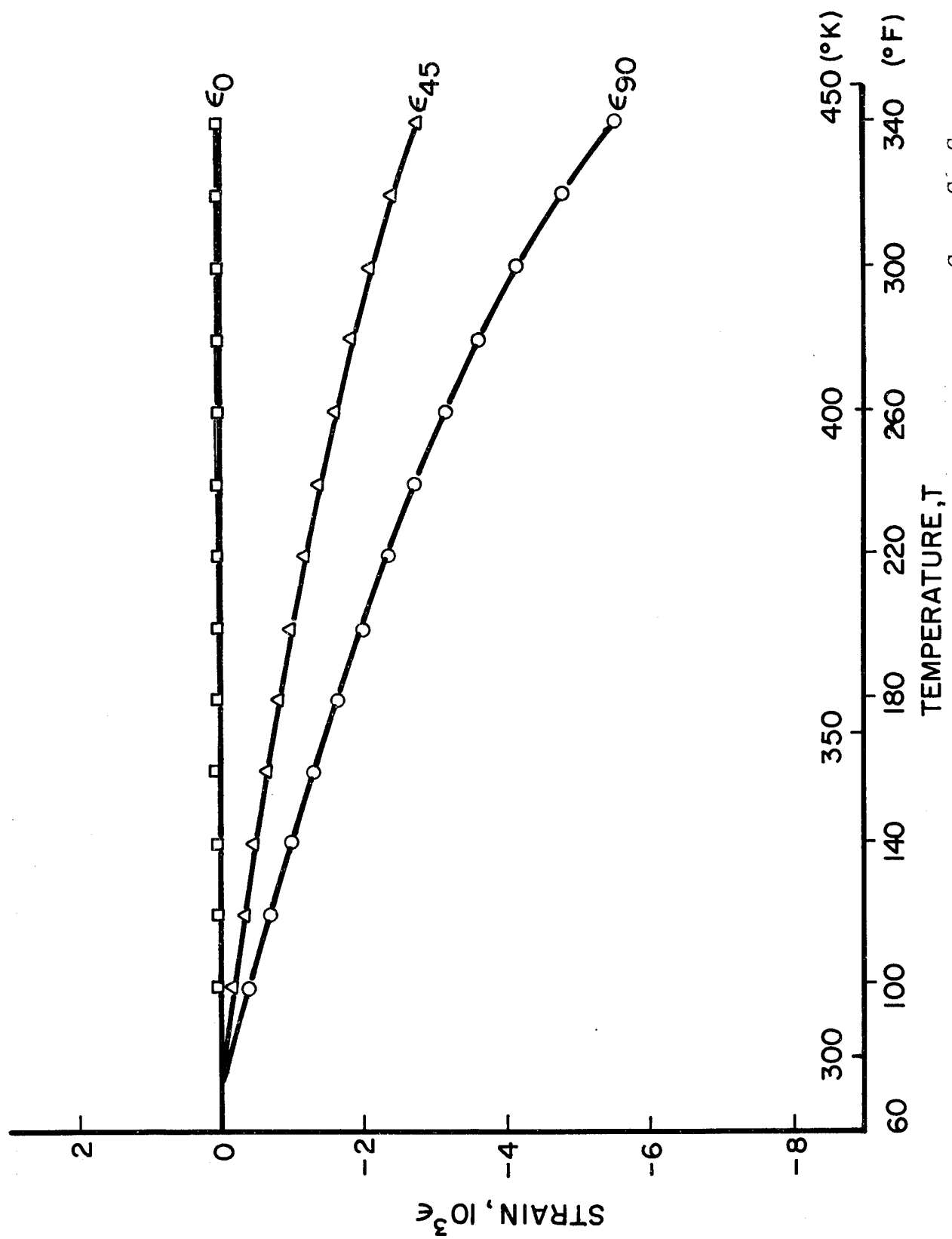


Fig. 51 RESTRAINT STRAINS IN 0-DEG. GRAPHITE PLYS OF $[0^G/+45^C/0^C]_s$ GRAPHITE/S-GLASS/HIGH MODULUS EPOXY SPECIMEN

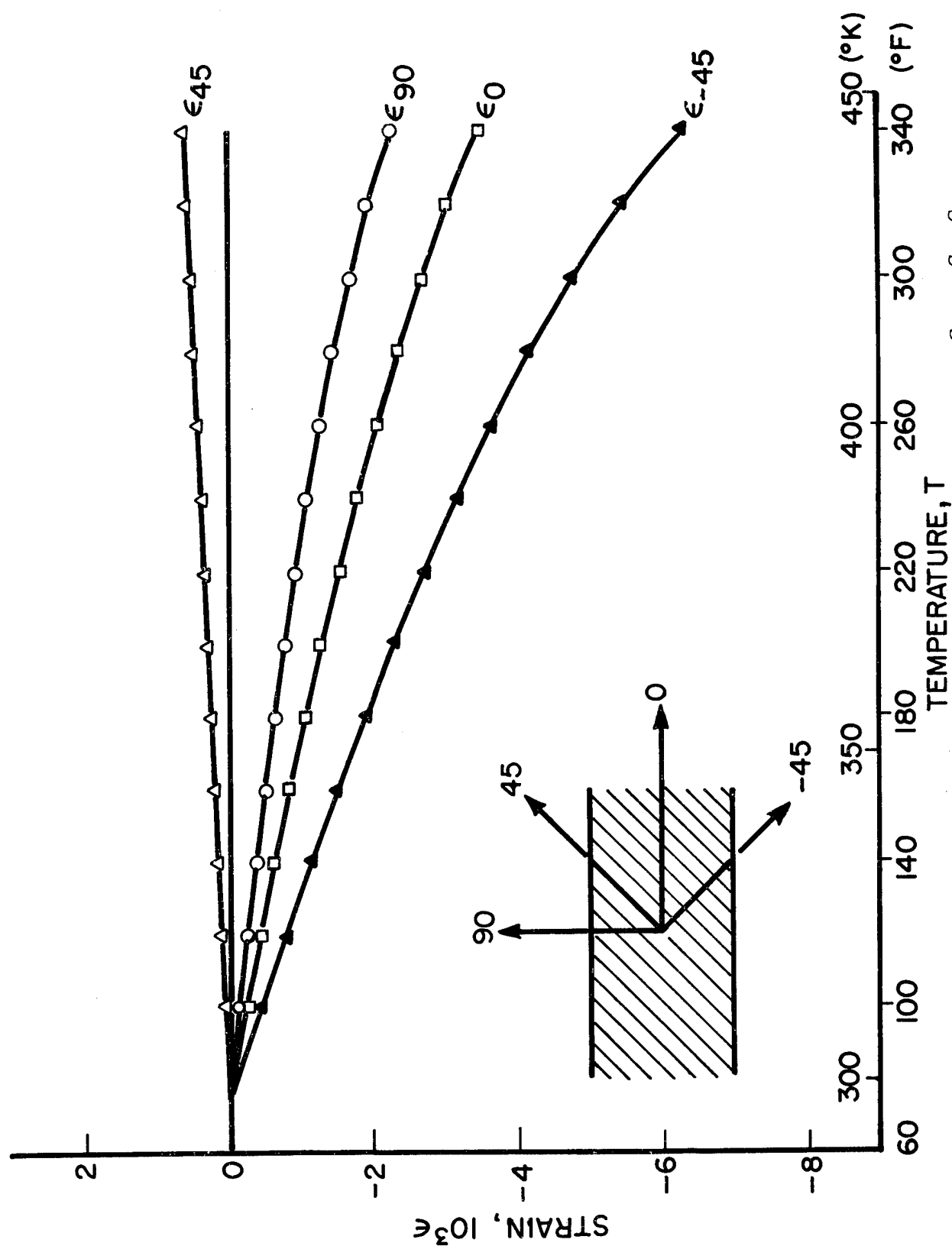


Fig. 52 RESTRAINT STRAINS IN 45-DEG. GRAPHITE PLYS OF $[0^C/+45^C/0^C]_s$ GRAPHITE/S-GLASS/HIGH MODULUS EPOXY SPECIMEN

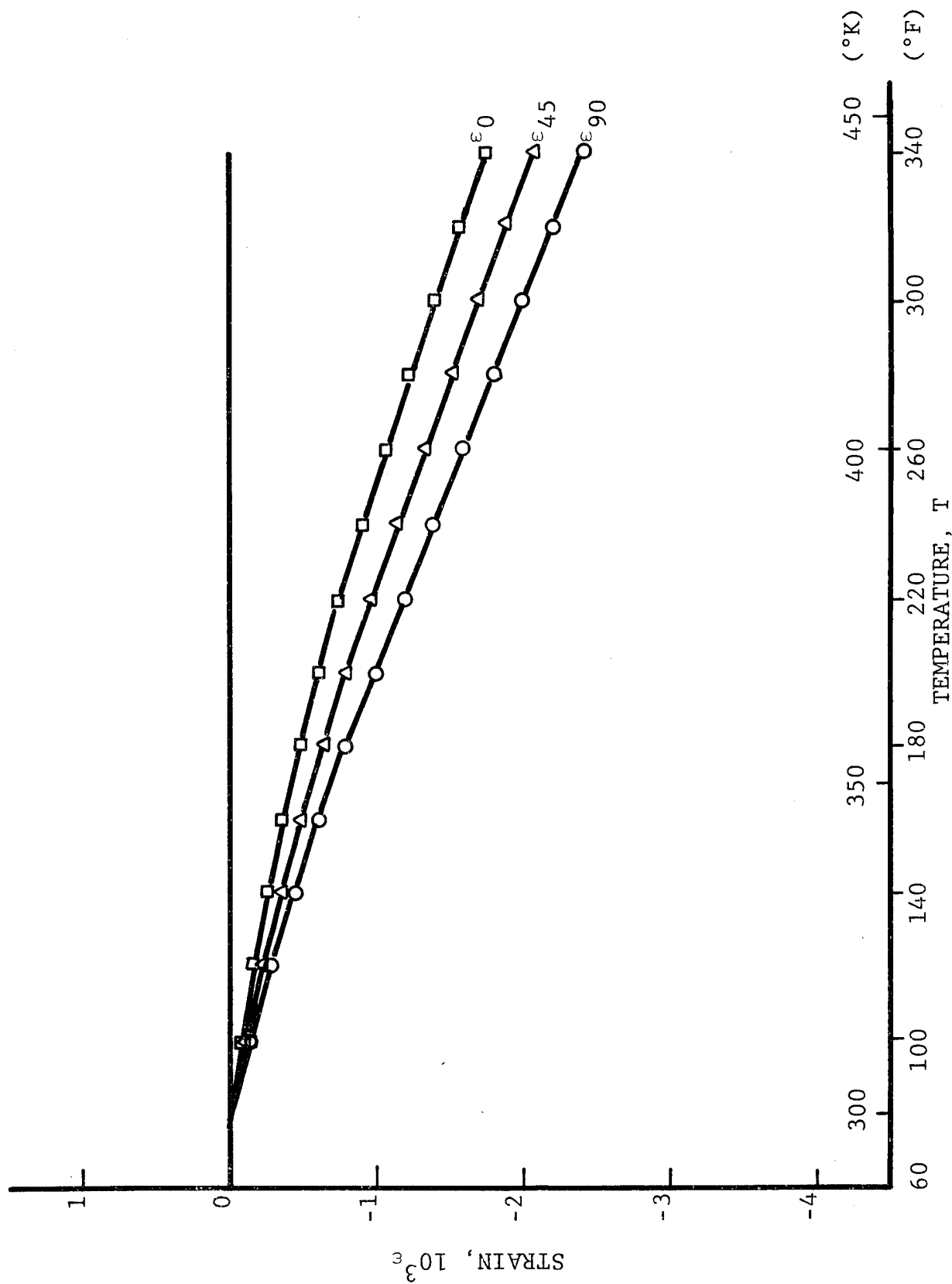


Fig. 53 RESTRAINT STRAINS IN 0-DEG. S-GLASS PLYS OF $[+45^C/0^C]_s$ GRAPHITE/
S-GLASS/HIGH MODULUS EPOXY SPECIMEN

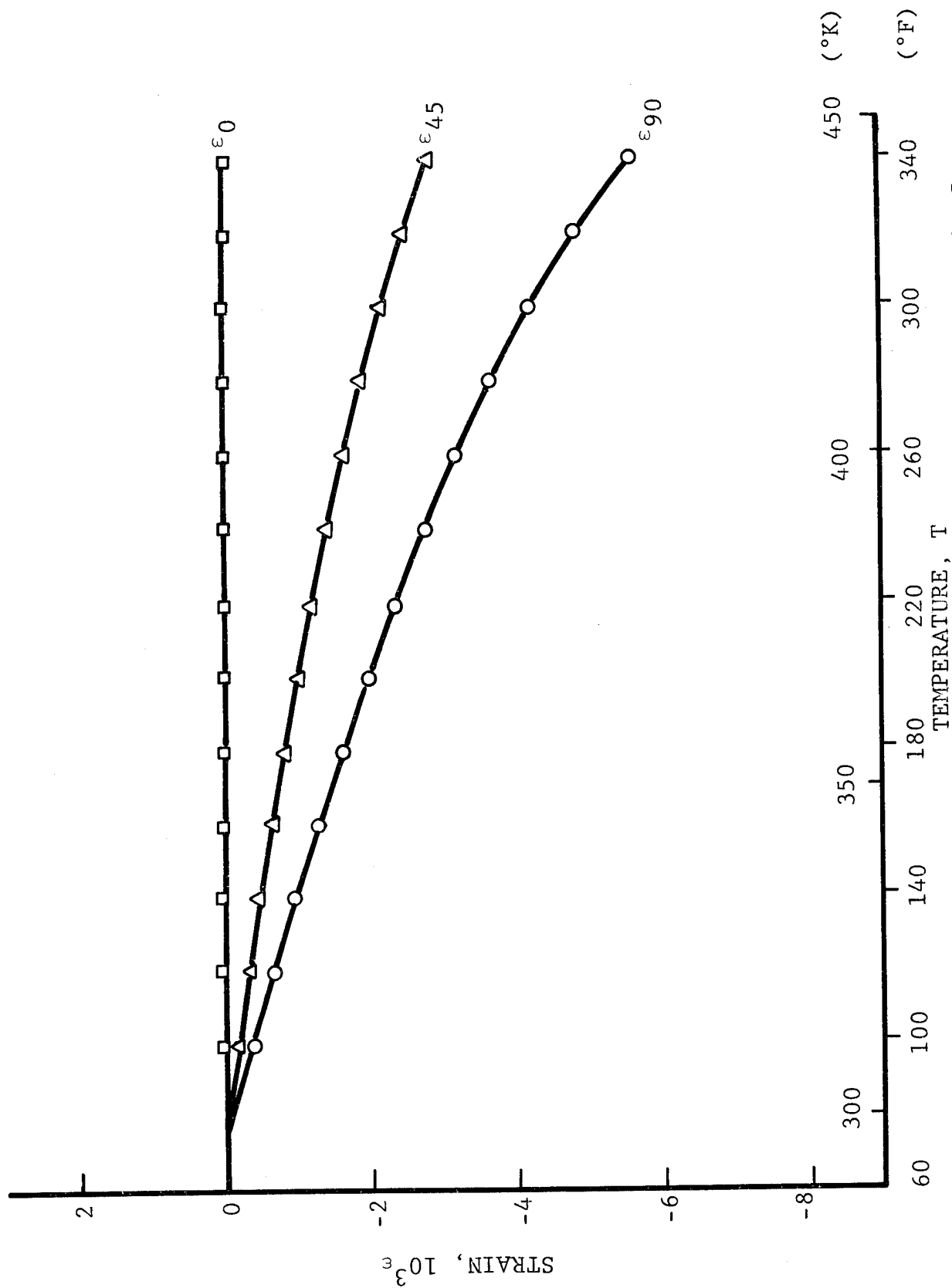


Fig. 54 RESTRAINT STRAINS IN 0-DEG. GRAPHITE PLYS OF $[+45^C/0^G/0^C]_s$ GRAPHITE/
S-GLASS/HIGH MODULUS EPOXY SPECIMEN

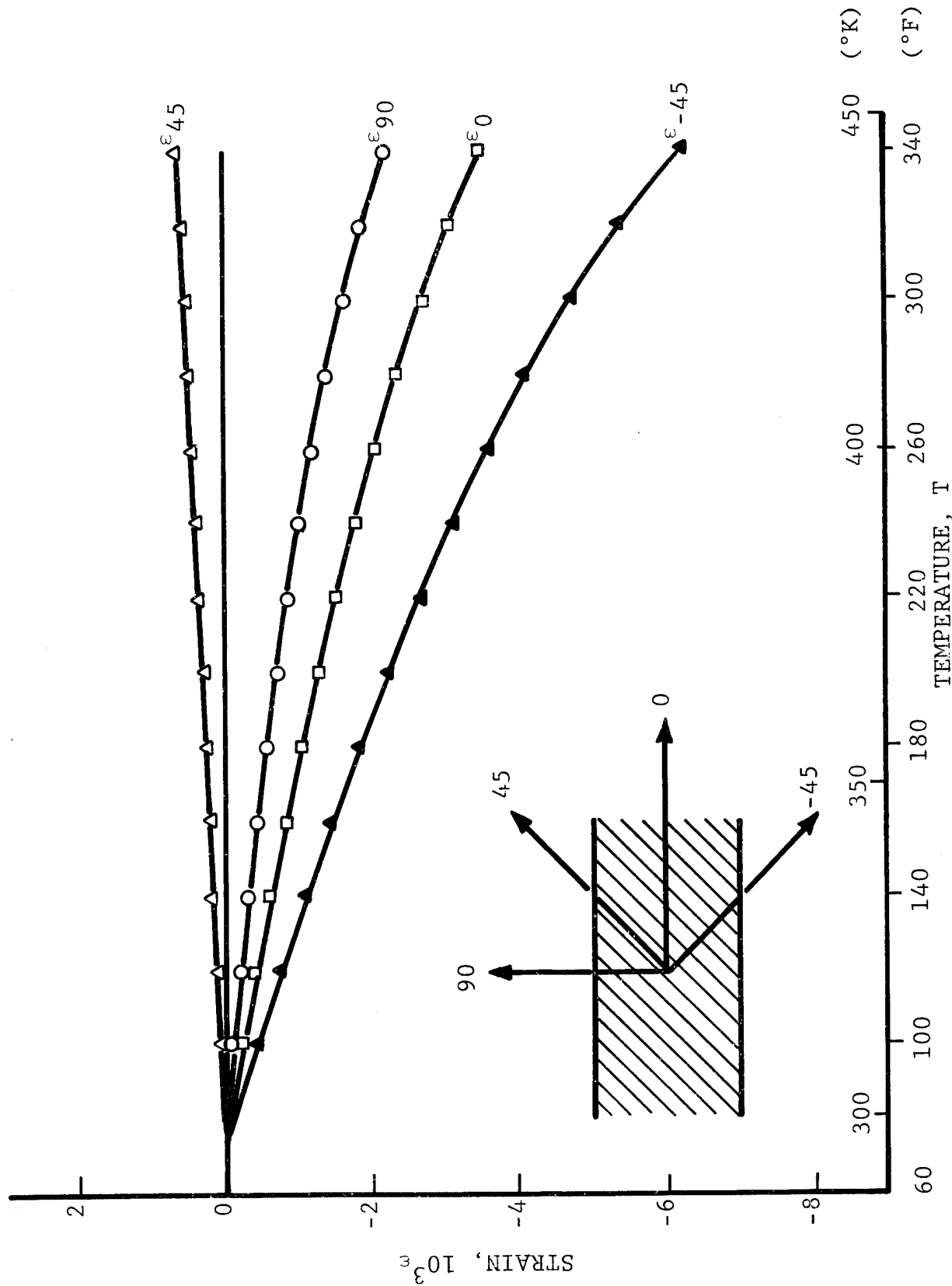


Fig. 55 RESTRAINT STRAINS IN 45-DEG. GRAPHITE PLIES OF $[\pm 45^{\circ}/0^{\circ}/0^{\circ}]_s$ GRAPHITE/S-GLASS/HIGH MODULUS EPOXY SPECIMEN

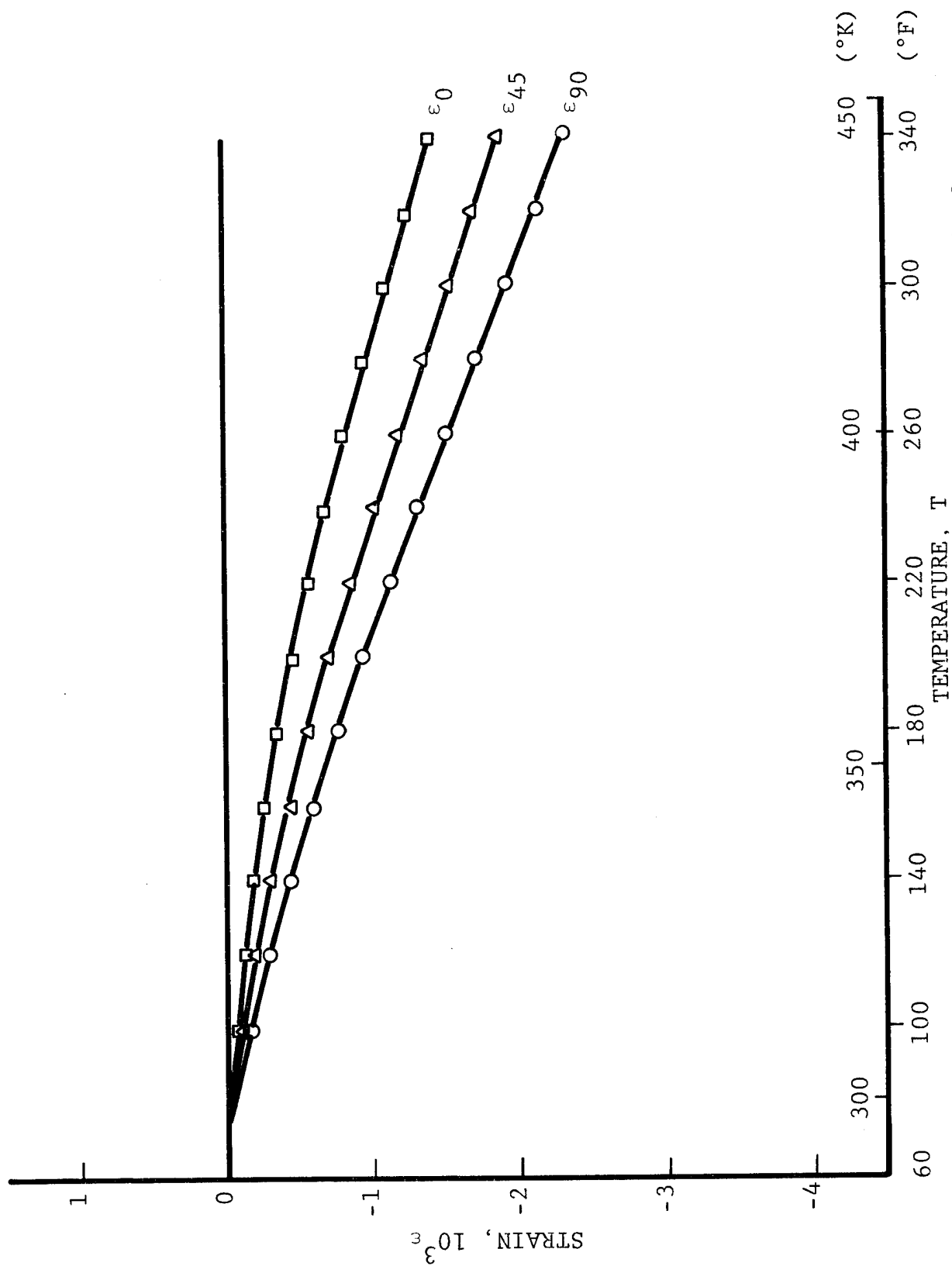


Fig. 56 RESTRAINT STRAINS IN 0-DEG. S-GLASS PLYS OF $[0^G/+45^C/0^G]_s$ GRAPHITE/
S-GLASS/HIGH MODULUS EPOXY SPECIMEN

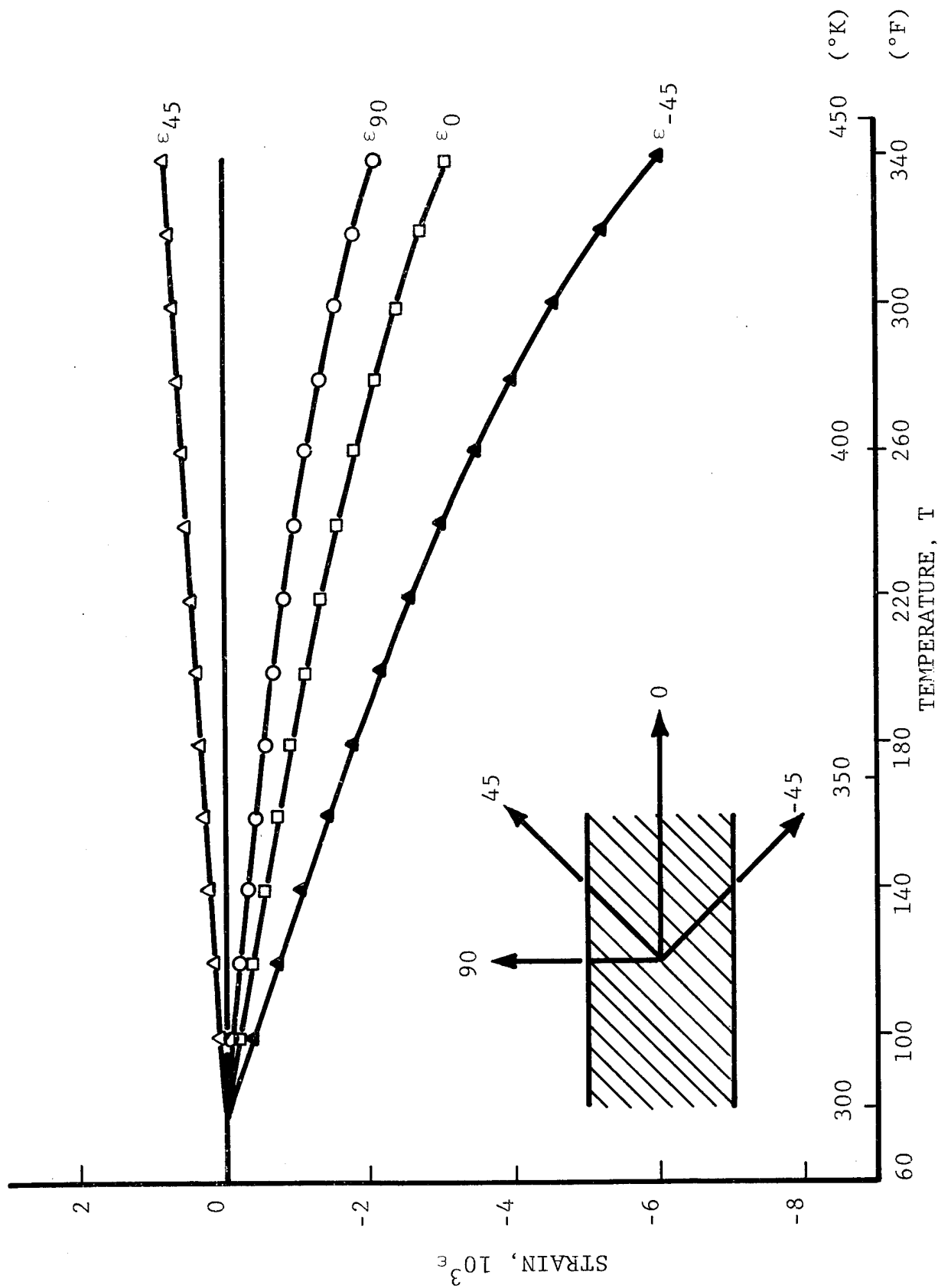


Fig. 57 RESTRAINT STRAINS IN 45-DEG. GRAPHITE PLYS OF $[0^G/+45^C/0^G]_S$ GRAPHITE/S-GLASS/HIGH MODULUS EPOXY SPECIMEN

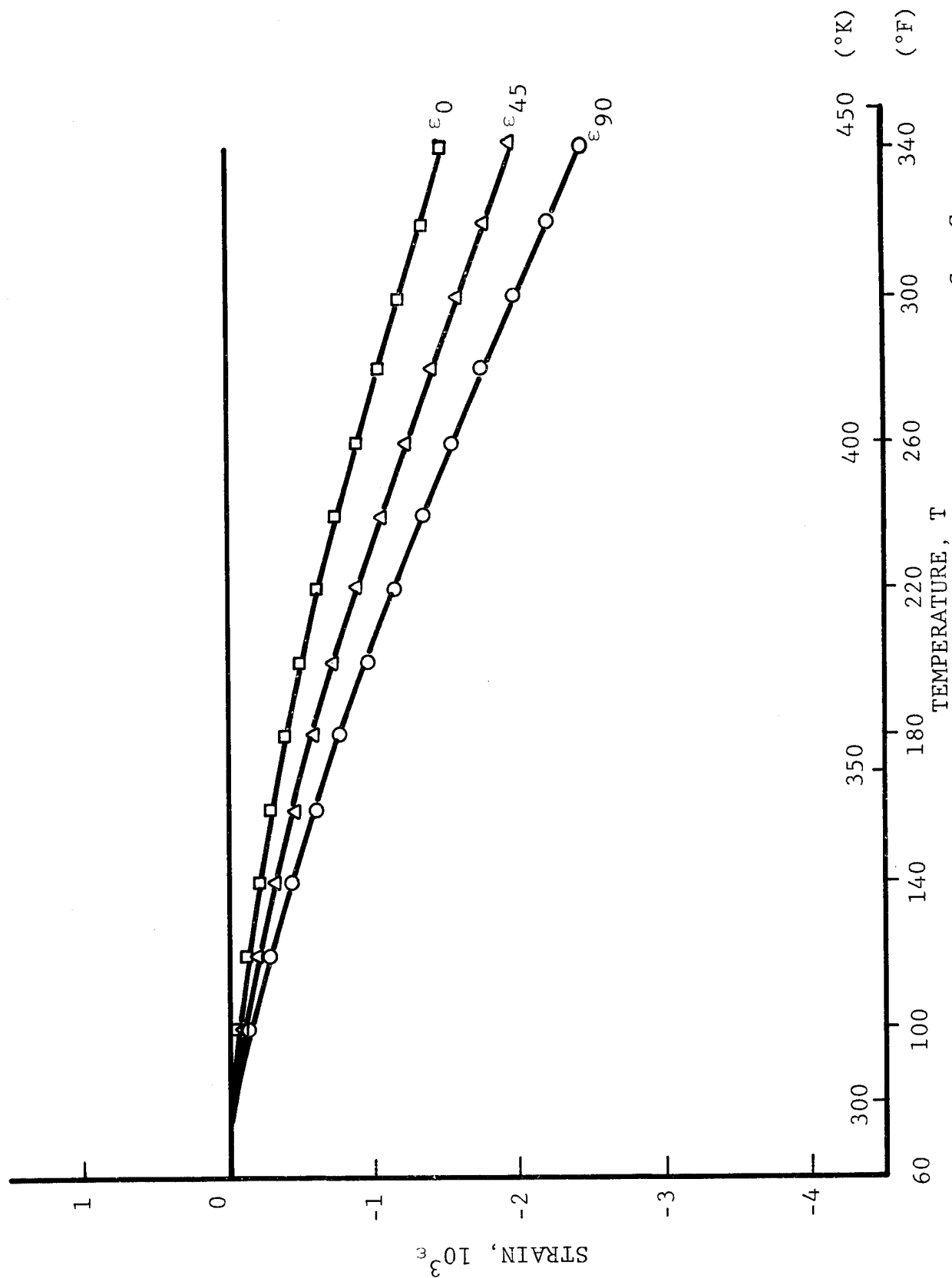


Fig. 58 RESTRAINT STRAINS IN 0-DEG. S-GLASS PLYS OF $[+45^C/0_2^G]_s$
GRAPHITE/S-GLASS/HIGH MODULUS EPOXY SPECIMEN

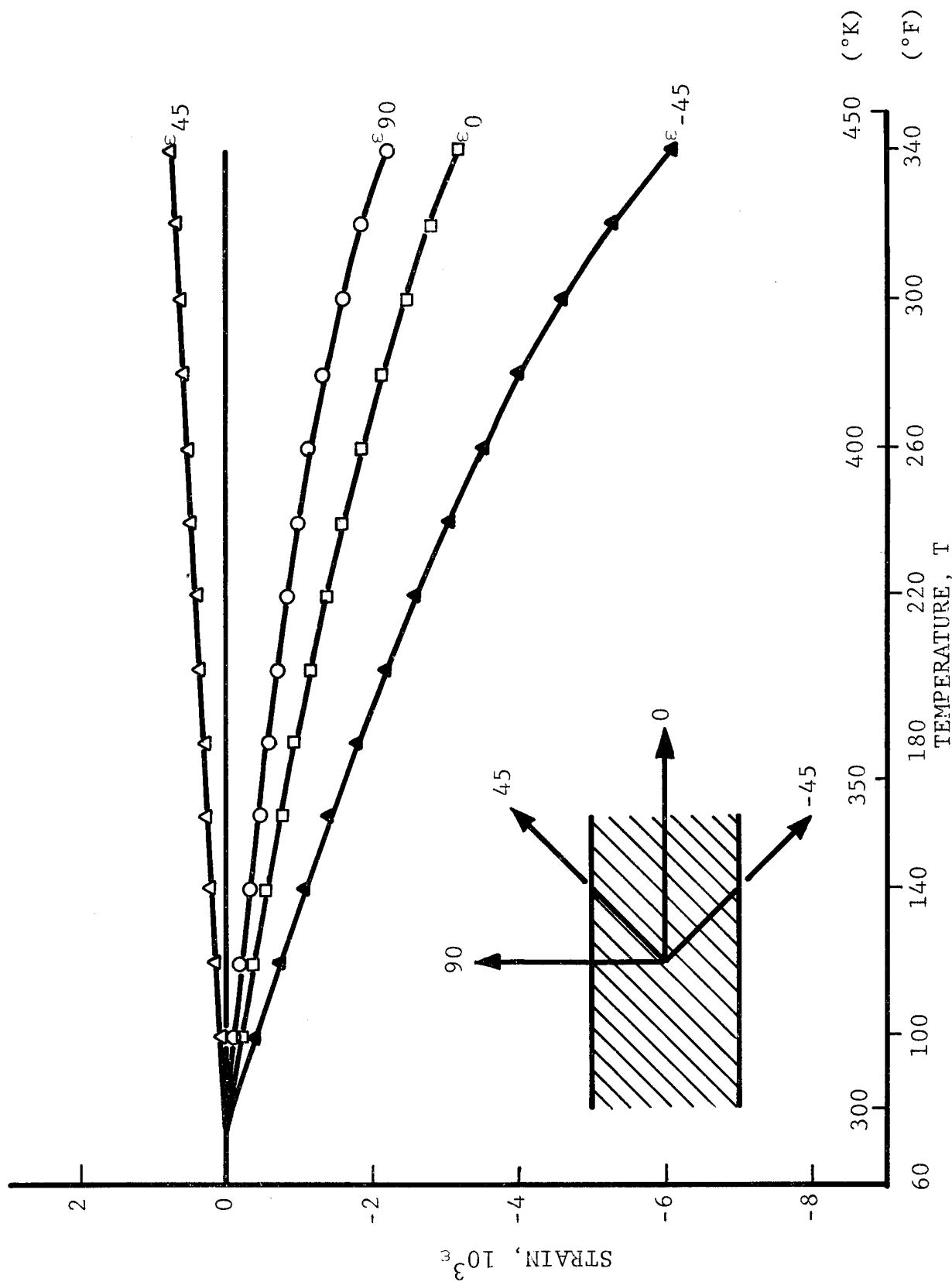


Fig. 59 RESTRAINT STRAINS IN 45-DEG. GRAPHITE PLYS OF $[\pm 45^{\circ}/0_2^G]_s$ GRAPHITE/S-GLASS/HIGH MODULUS EPOXY SPECIMEN

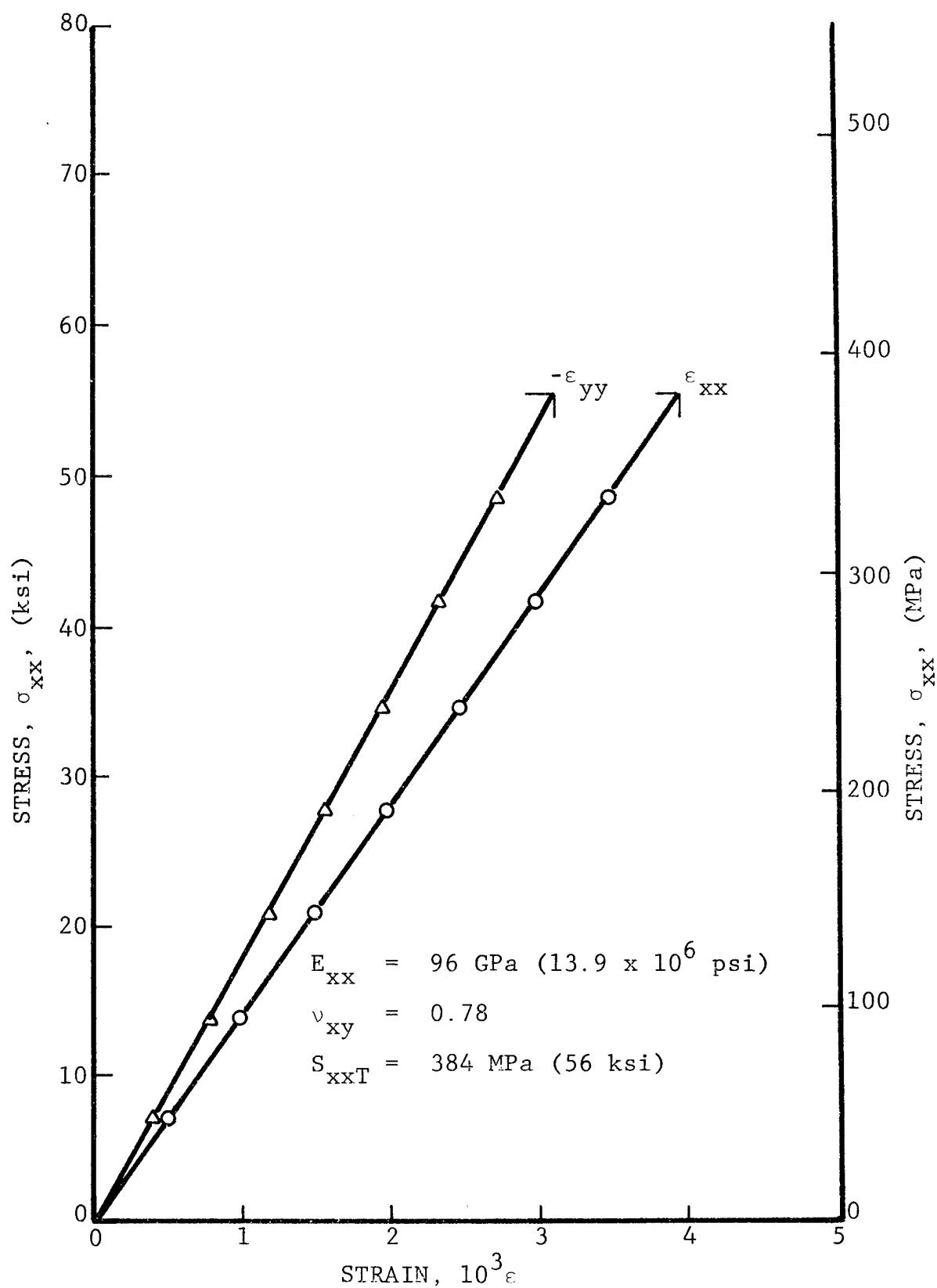


Fig. 60 STRAINS IN $[0^K/\pm 45^C/0^C]_s$ GRAPHITE/KEVLAR 49/
HIGH MODULUS EPOXY SPECIMEN UNDER UNIAXIAL
TENSILE LOADING

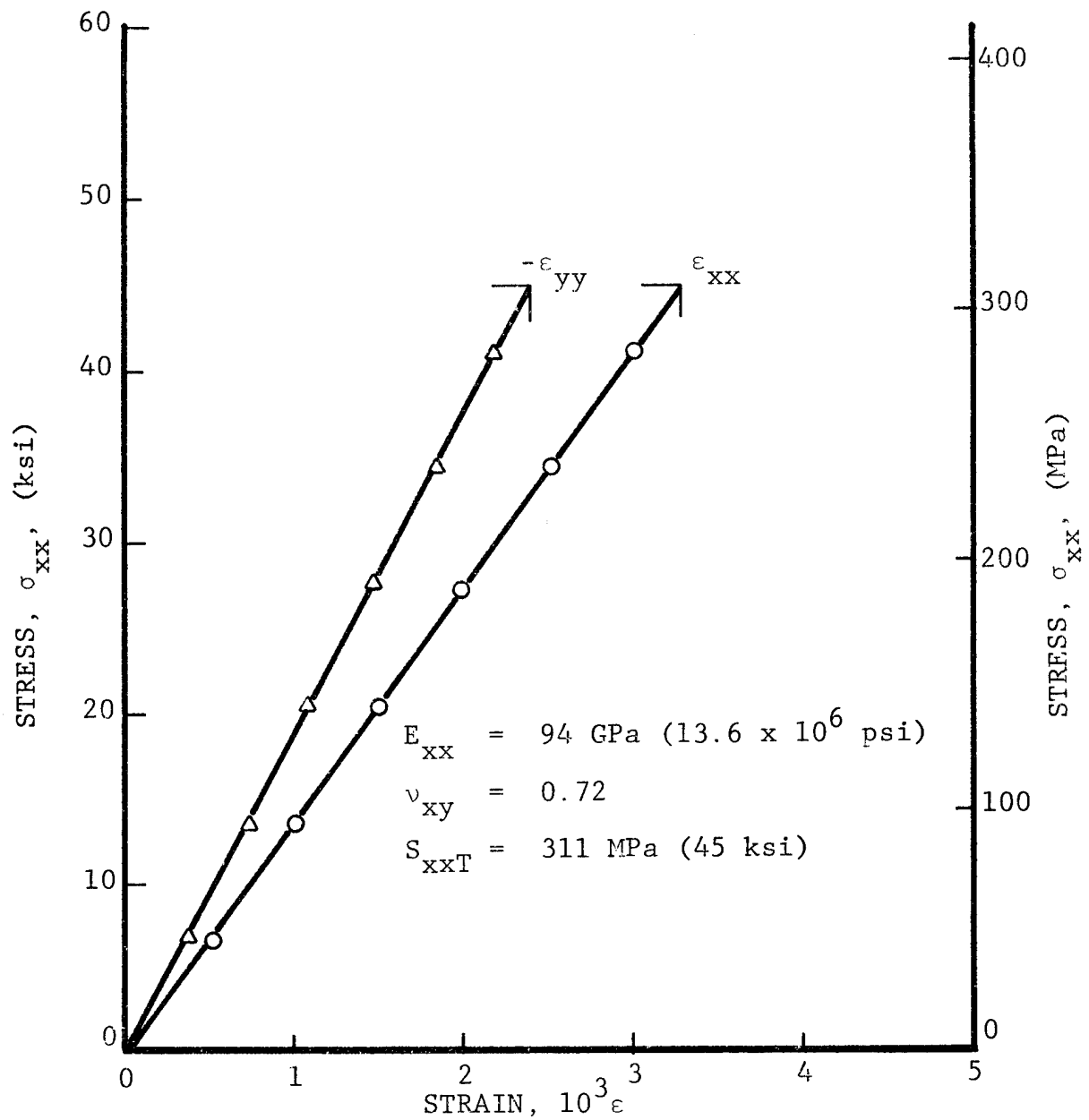


Fig. 61 STRAINS IN $[0^K/\pm 45^C/0^C]_S$ GRAPHITE/KEVLAR 49/
HIGH MODULUS EPOXY SPECIMEN UNDER UNIAXIAL
TENSILE LOADING

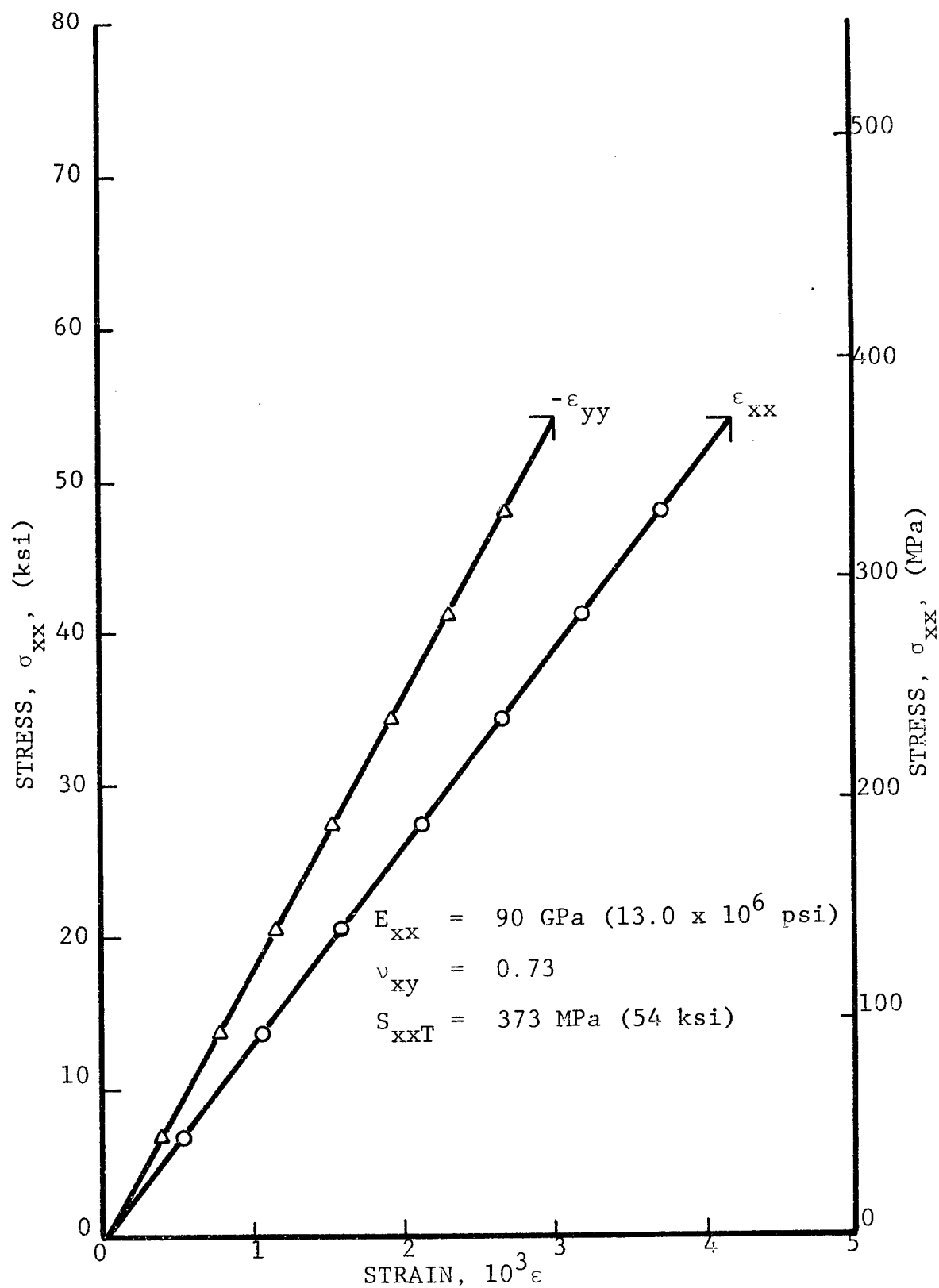


Fig. 62 STRAINS IN $[\pm 45^{\circ} / 0^{\circ} / 0^{\circ}]_s$ GRAPHITE/KEVLAR 49/HIGH MODULUS EPOXY SPECIMEN UNDER UNIAXIAL TENSILE LOADING

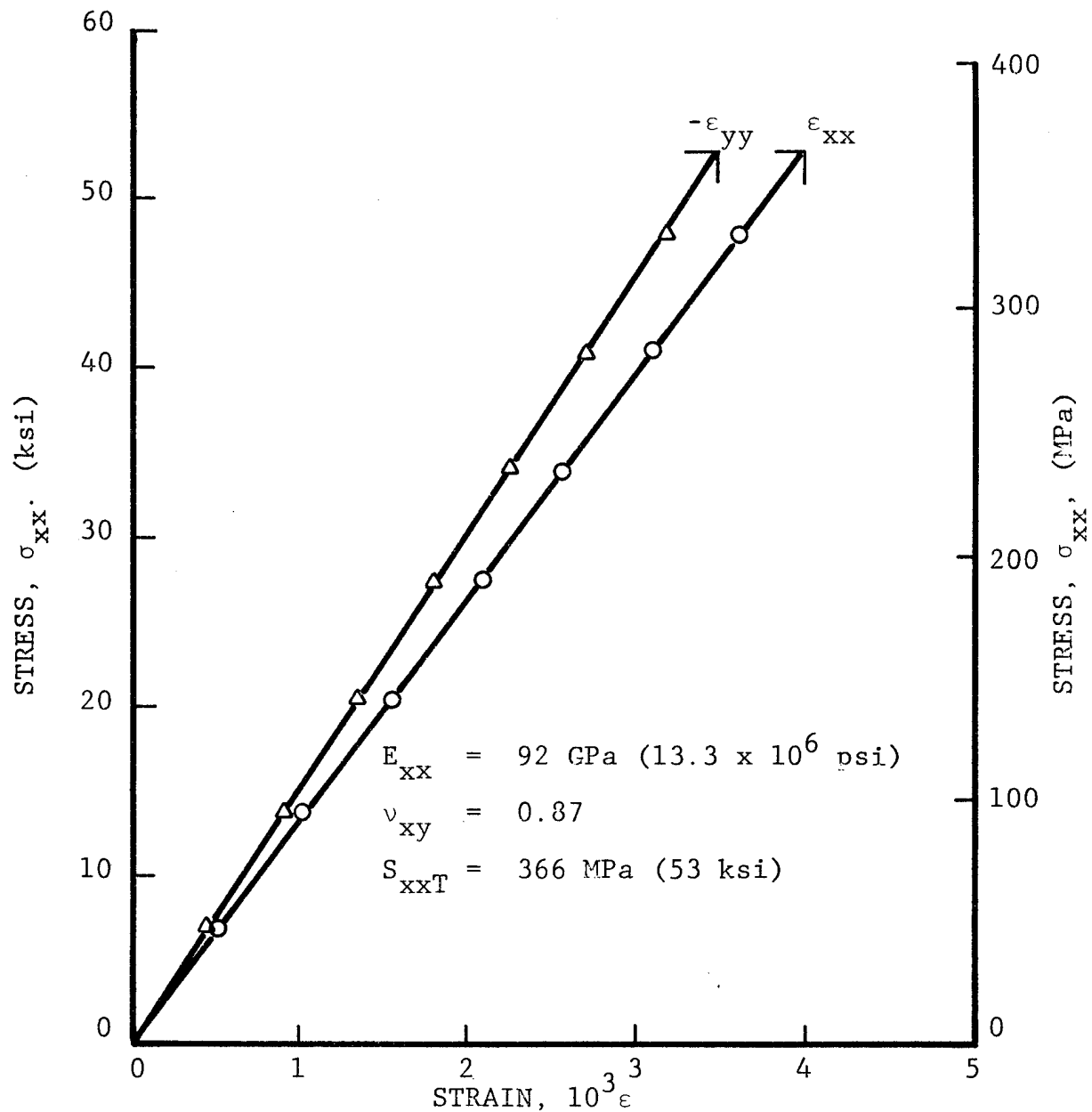


Fig. 63 STRAINS IN $[\pm 45^{\circ}/0^{\circ}/0^{\circ}]_s$ GRAPHITE/
KEVLAR 49/HIGH MODULUS EPOXY SPECIMEN
UNDER UNIAXIAL TENSILE LOADING

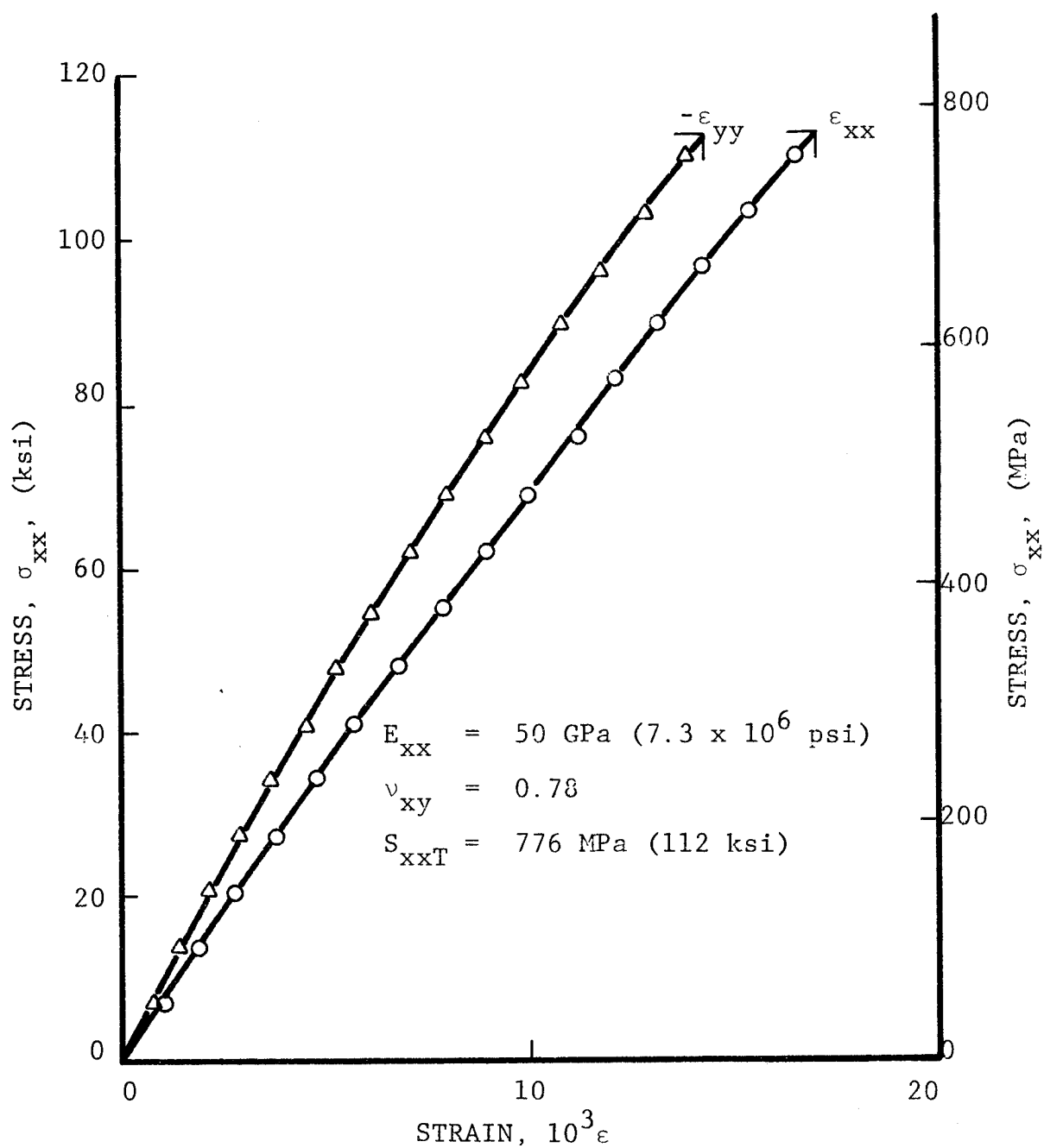


Fig. 64 STRAINS IN $[0^K/\pm 45^C/0^K]_s$ GRAPHITE/KEVLAR 49/HIGH MODULUS EPOXY SPECIMEN UNDER UNIAXIAL TENSILE LOADING

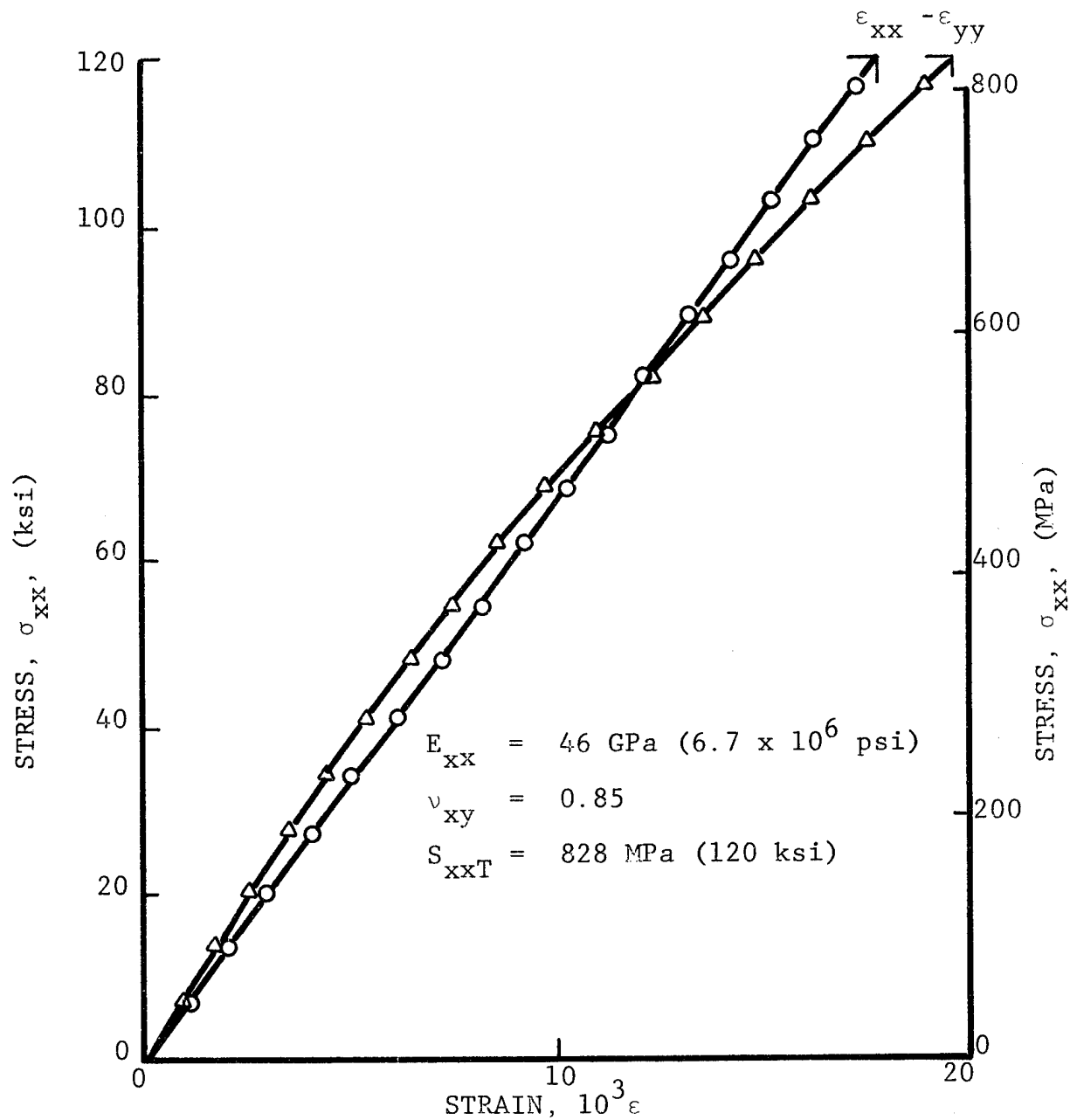


Fig. 65 STRAINS IN $[0^K/\pm 45^C/0^K]_s$ GRAPHITE/
 KEVLAR 49/HIGH MODULUS EPOXY SPECIMEN
 UNDER UNIAXIAL TENSILE LOADING

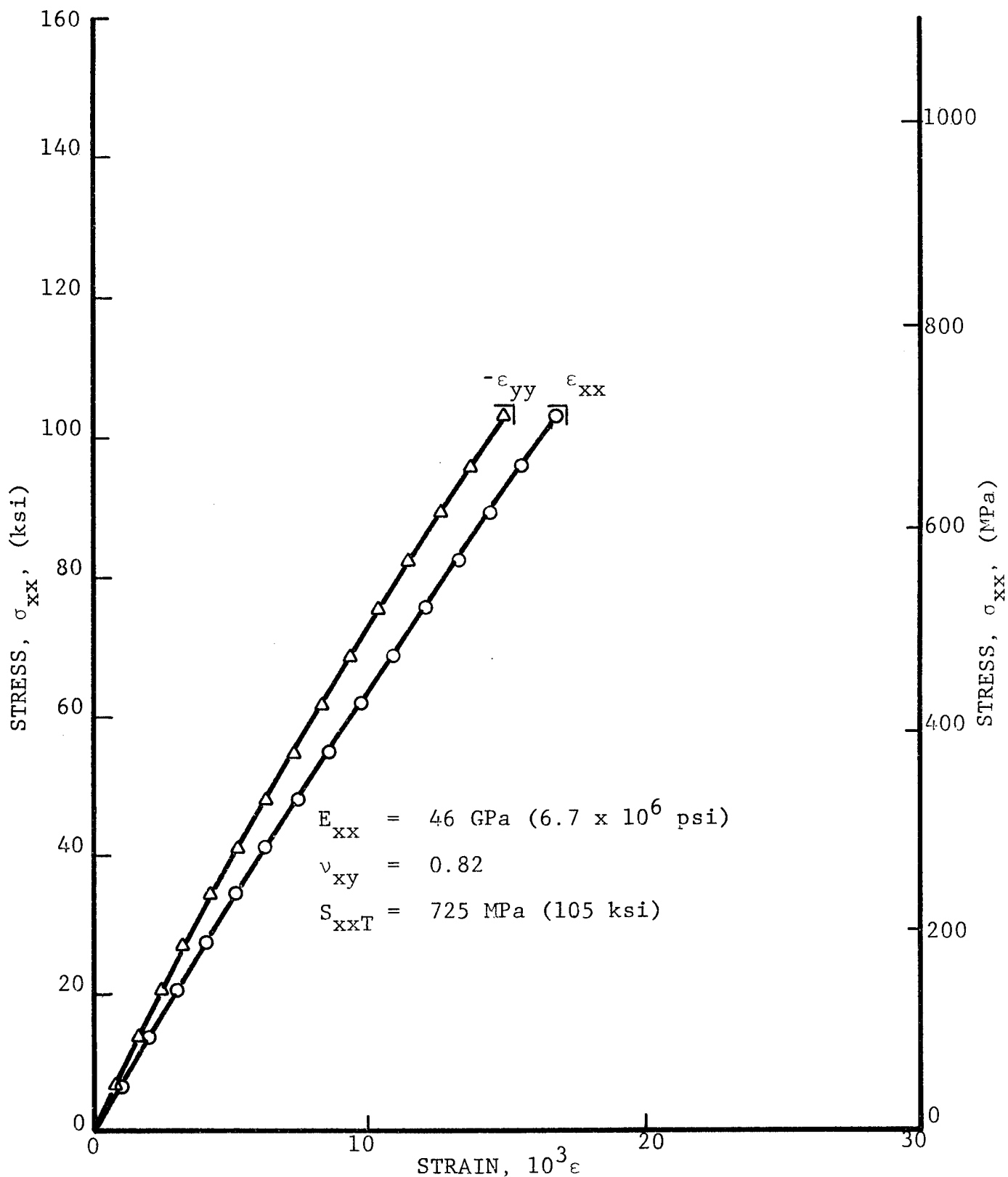


Fig. 66 STRAINS IN $[+45^{\circ}/0_2^k]_s$ GRAPHITE/KEVLAR 49/HIGH MODULUS EPOXY SPECIMEN UNDER UNIAXIAL TENSILE LOADING

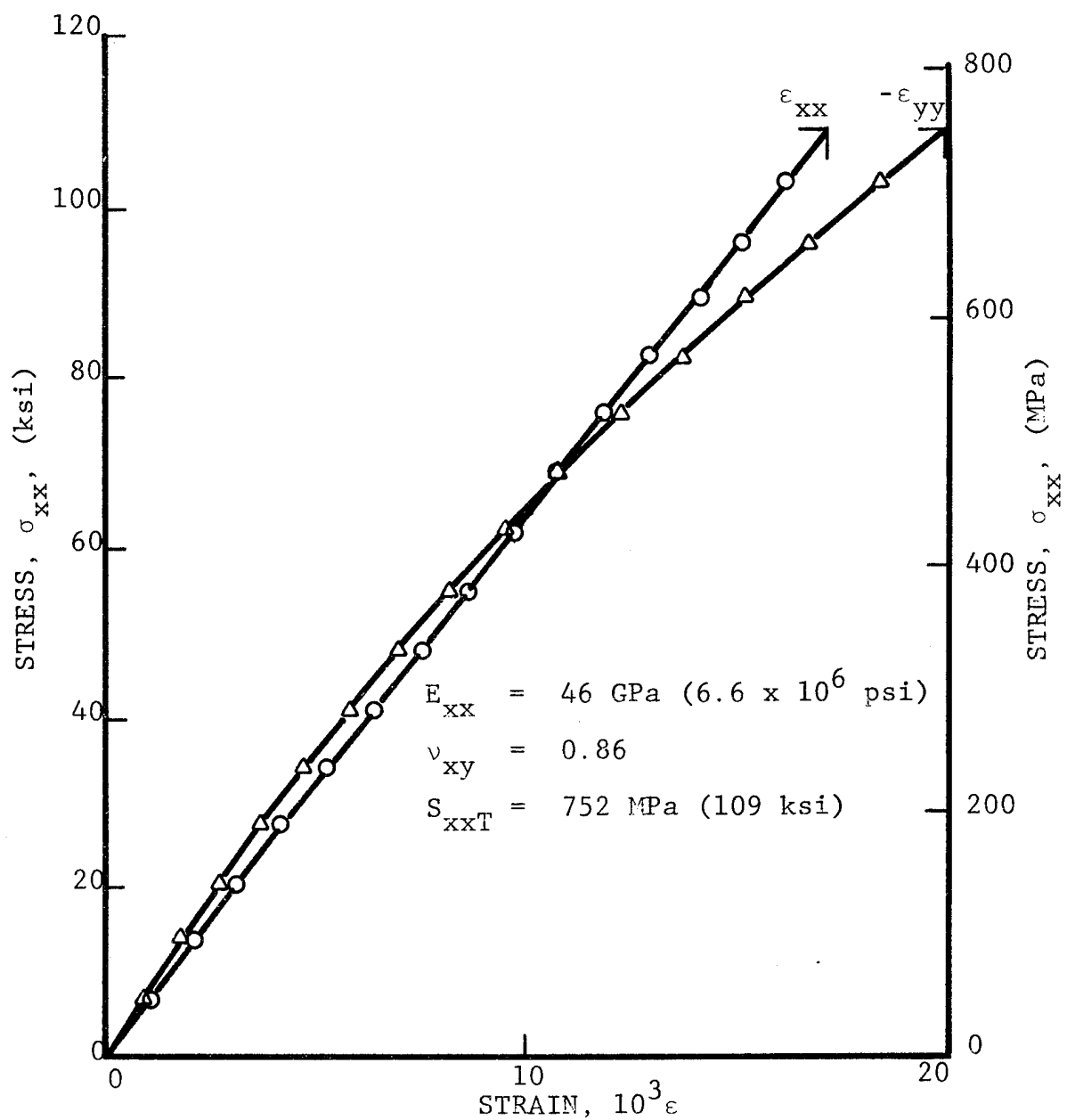


Fig. 67 STRAINS IN $[+45^C/0_2^K]_s$ GRAPHITE/KEVALR 49/
HIGH MODULUS EPOXY SPECIMEN UNDER UNIAXIAL
TENSILE LOADING

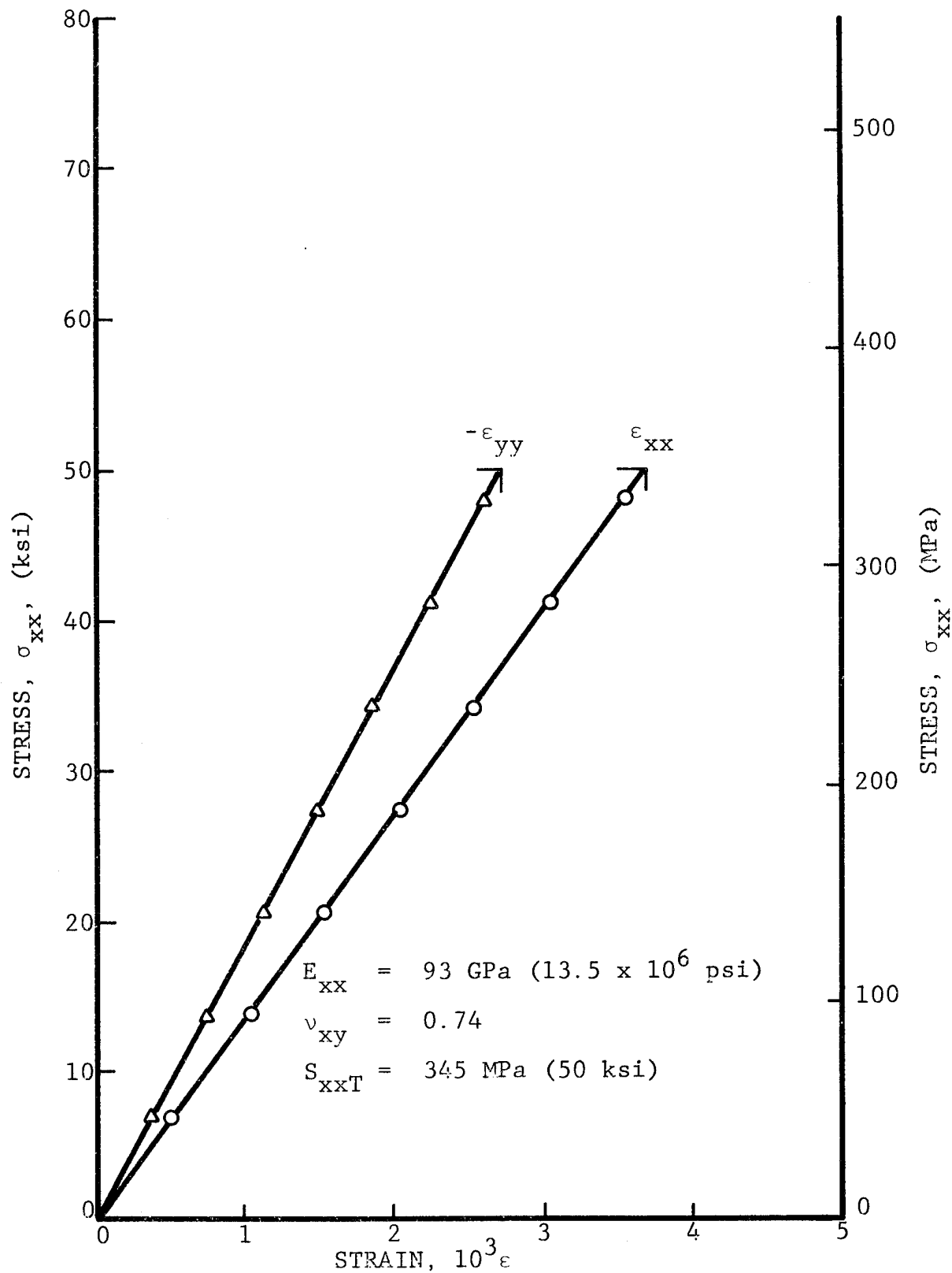


Fig. 68 STRAINS IN $[0^G/+45^C/0^C]_s$ GRAPHITE/S-GLASS/HIGH MODULUS EPOXY SPECIMEN UNDER UNIAXIAL TENSILE LOADING

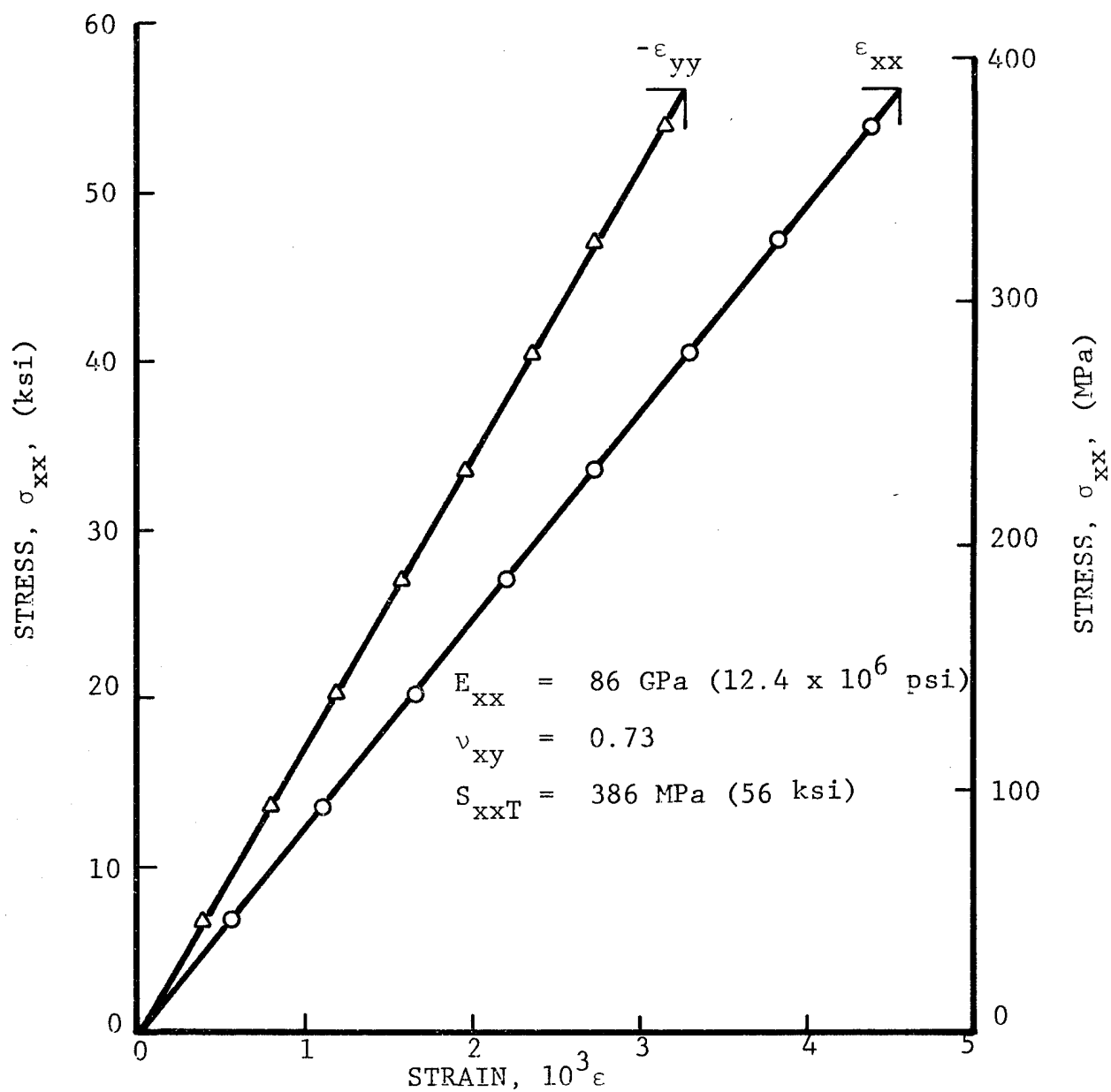


Fig. 69 STRAINS IN $[0^G/\pm 45^C/0^C]_S$ GRAPHITE/S-GLASS/HIGH MODULUS EPOXY SPECIMEN UNDER UNIAXIAL TENSILE LOADING

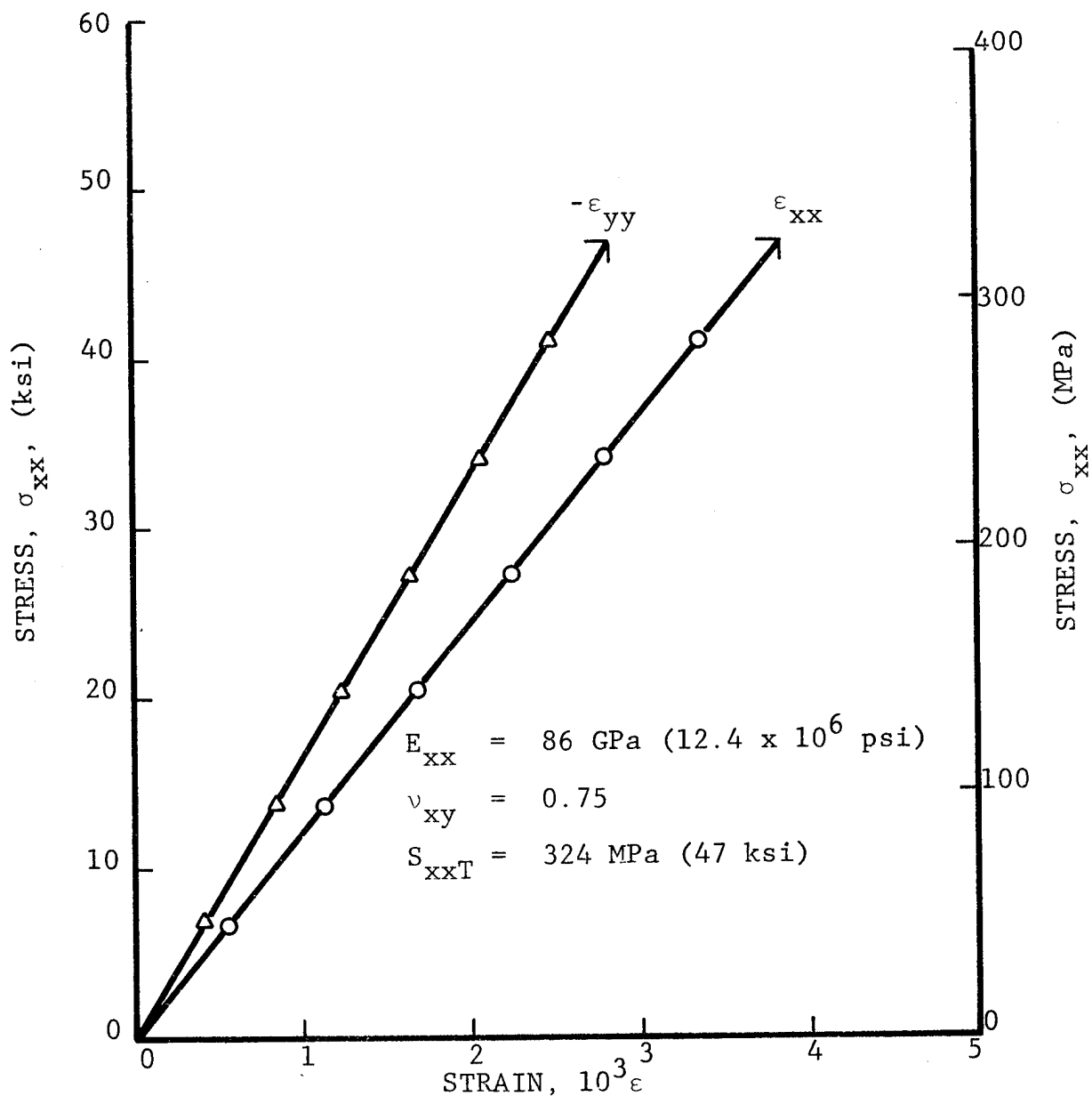


Fig. 70 STRAINS IN $[\pm 45^C/0^G/0^C]_s$ GRAPHITE/S-GLASS/HIGH MODULUS EPOXY SPECIMEN UNDER UNIAXIAL TENSILE LOADING

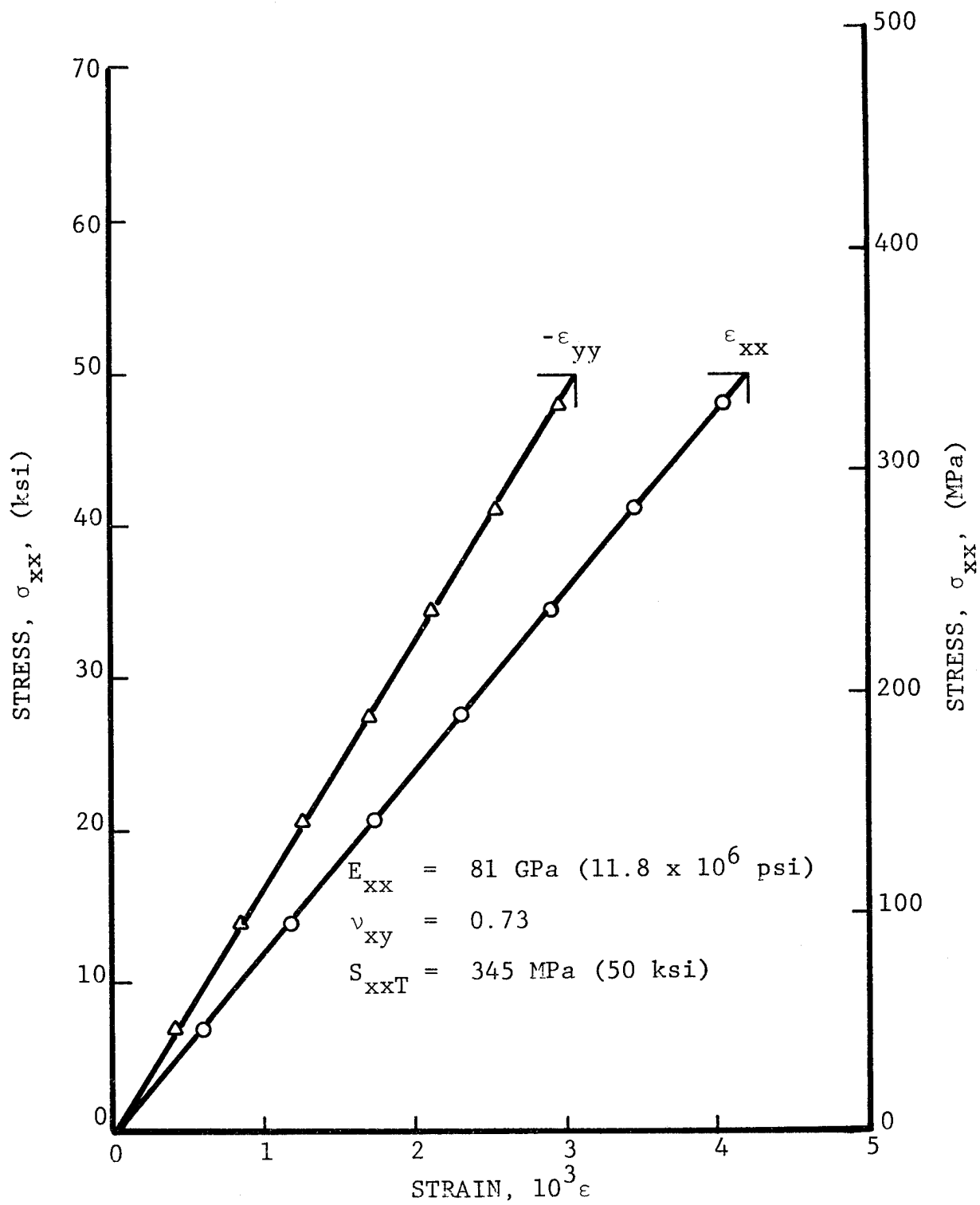


Fig. 71 STRAINS IN $[\pm 45^C/0^G/0^C]_s$ GRAPHITE/S-GLASS/HIGH MODULUS EPOXY SPECIMEN UNDER UNIAXIAL TENSILE LOADING

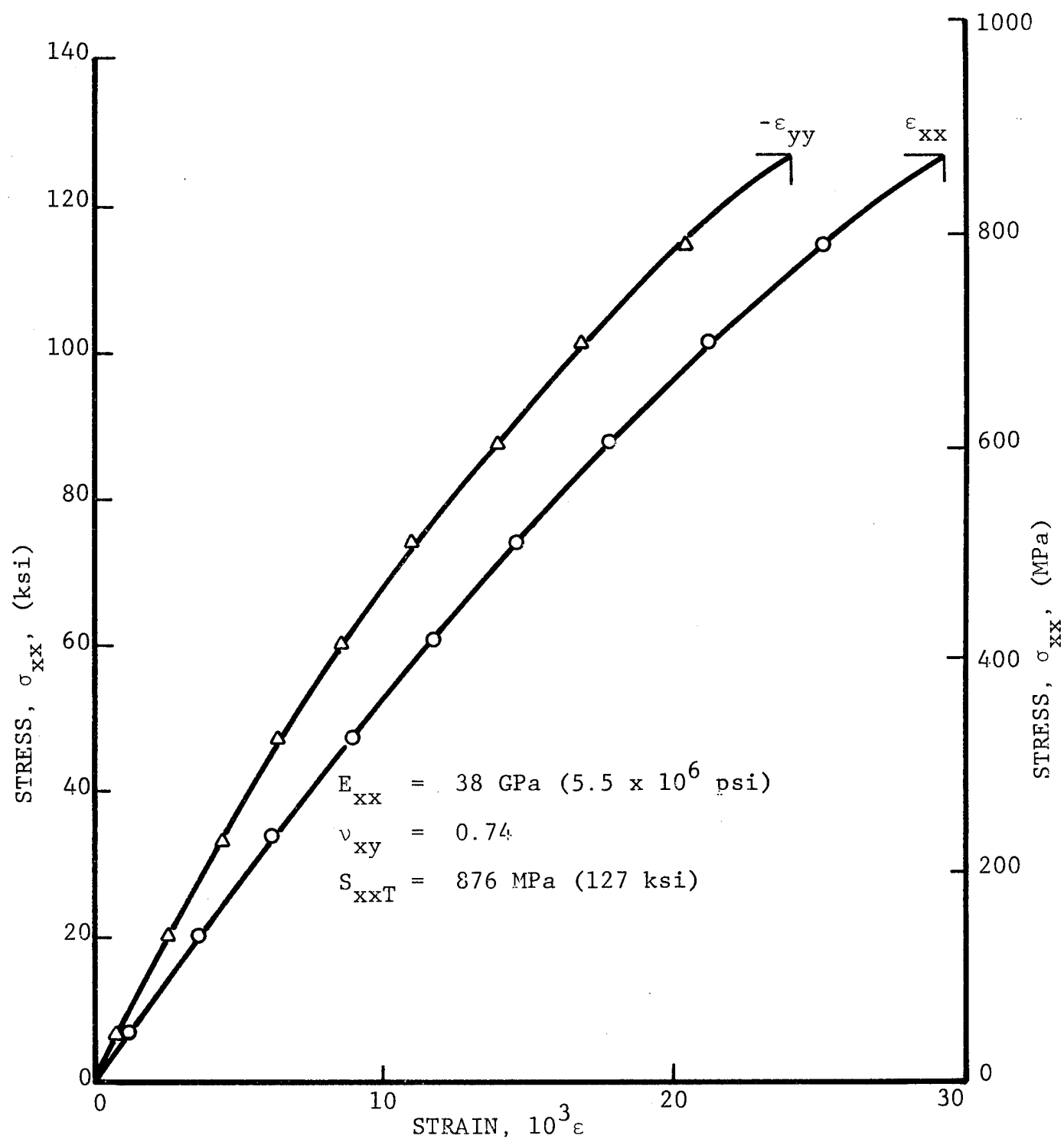


Fig. 72 STRAINS IN $[0^G/\pm 45^C/0^G]_S$ GRAPHITE/S-GLASS/HIGH MODULUS EPOXY SPECIMEN UNDER UNIAXIAL TENSILE LOADING

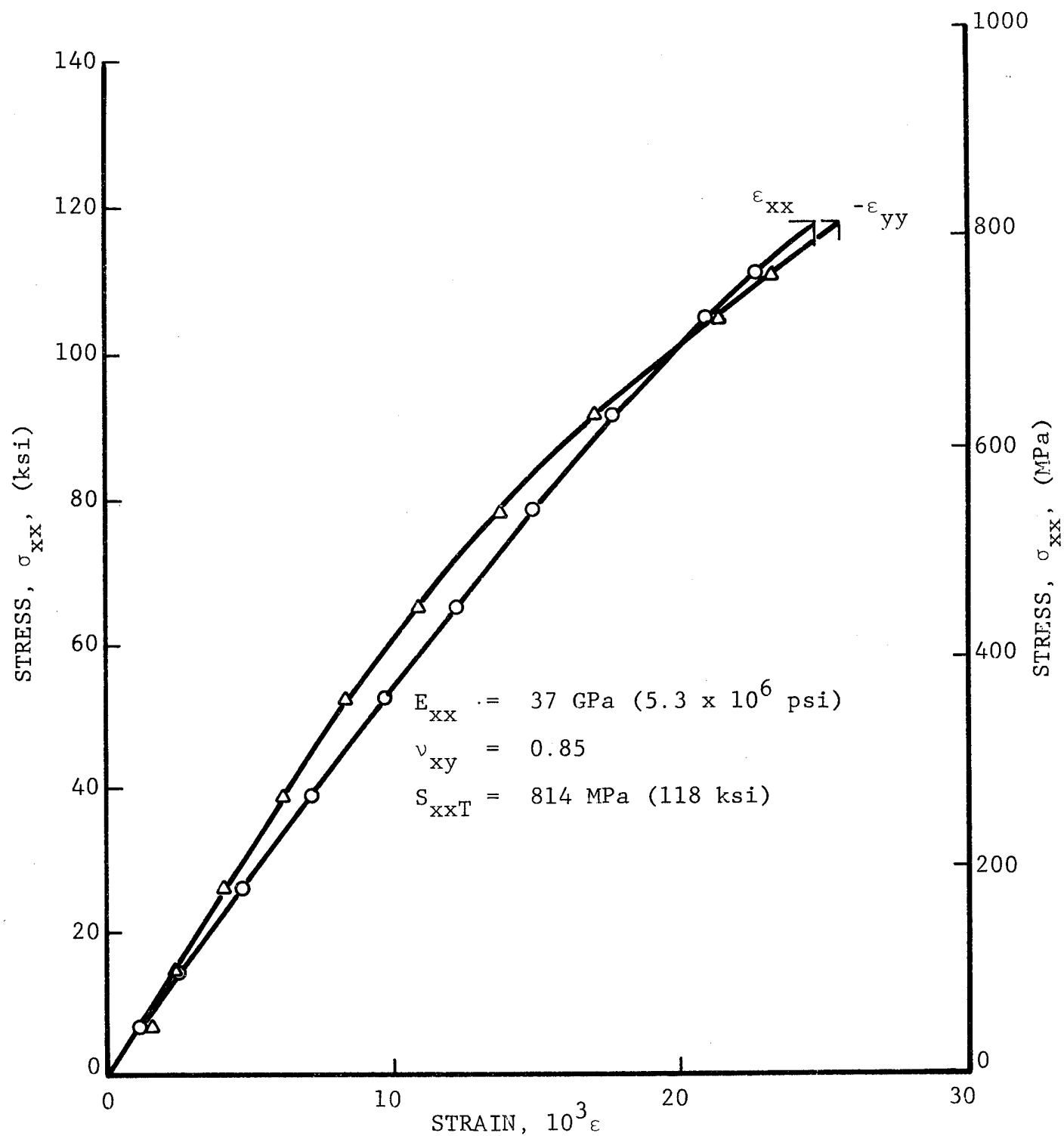


Fig. 73 STRAINS IN $[0^G/\pm 45^C/0^G]_s$ GRAPHITE/S-GLASS/HIGH MODULUS EPOXY SPECIMEN UNDER UNIAXIAL TENSILE LOADING

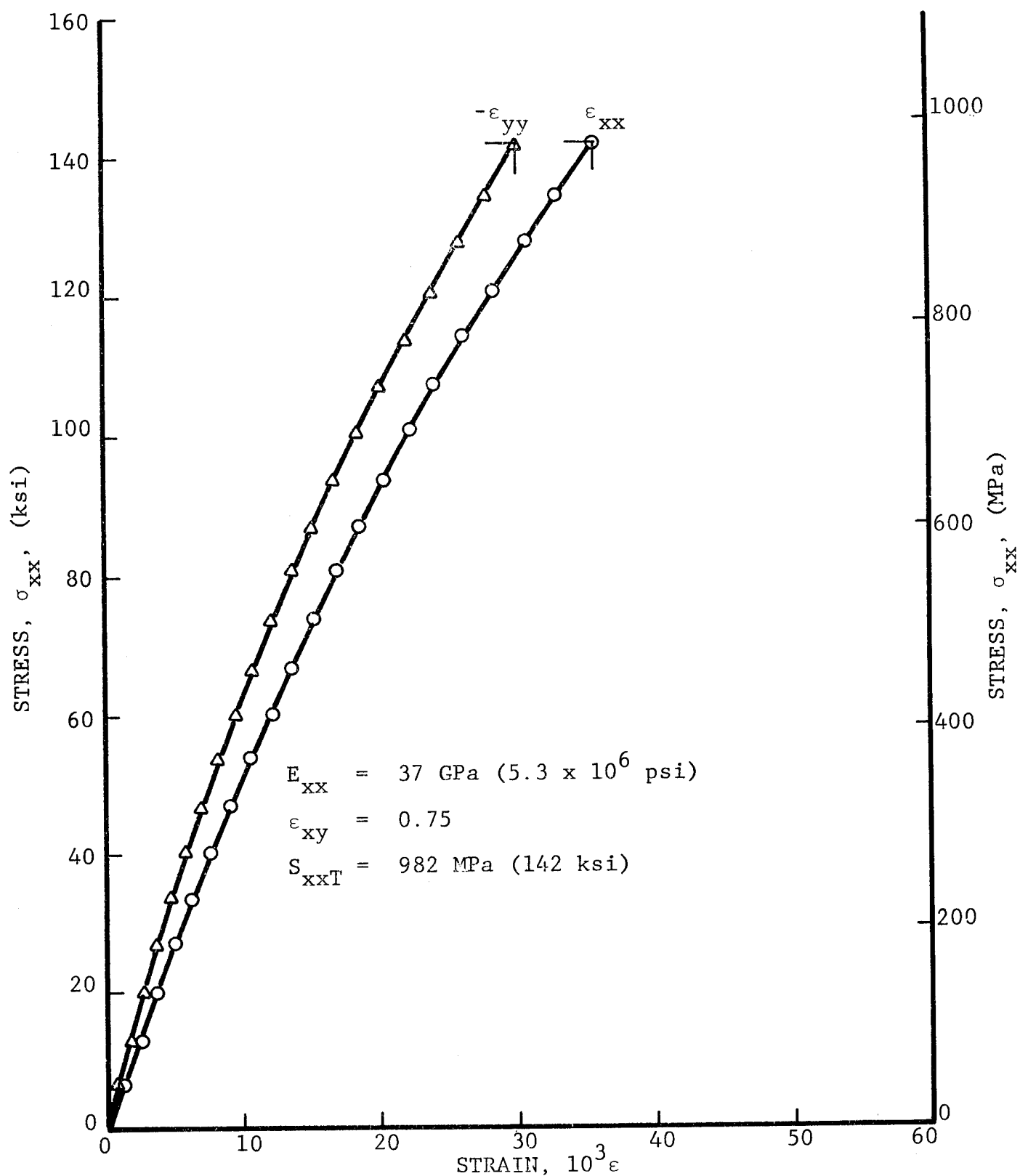


Fig. 74 STRAINS IN $[\pm 45^{\circ}/0_2^G]_s$ GRAPHITE/S-GLASS/HIGH MODULUS EPOXY SPECIMEN UNDER UNIAXIAL TENSILE LOADING

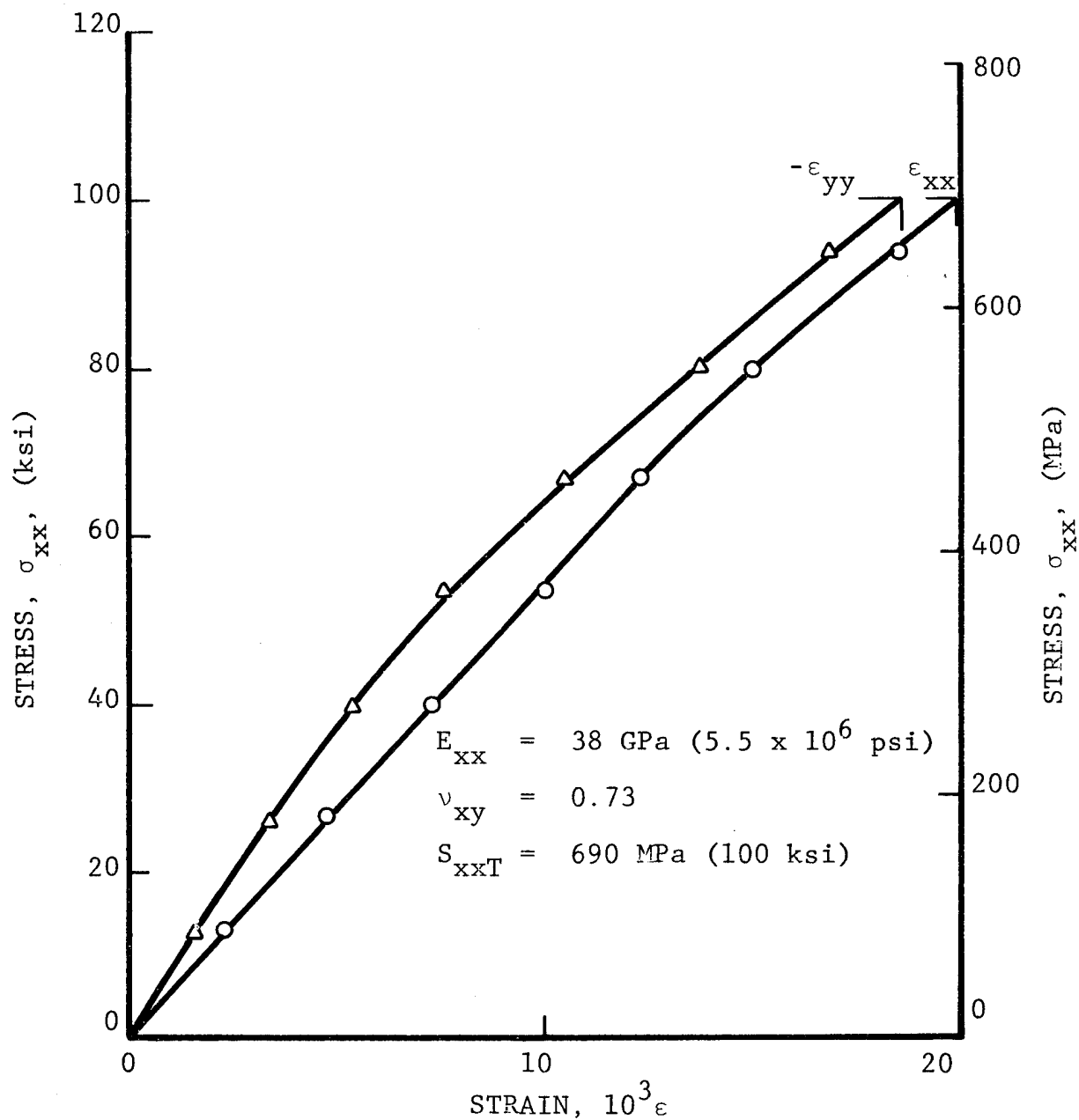


Fig. 75 STRAINS IN $[\pm 45^\circ \text{C}/0_2^G]_s$ GRAPHITE/S-GLASS/
HIGH MODULUS EPOXY SPECIMEN UNDER UNIAXIAL
TENSILE LOADING

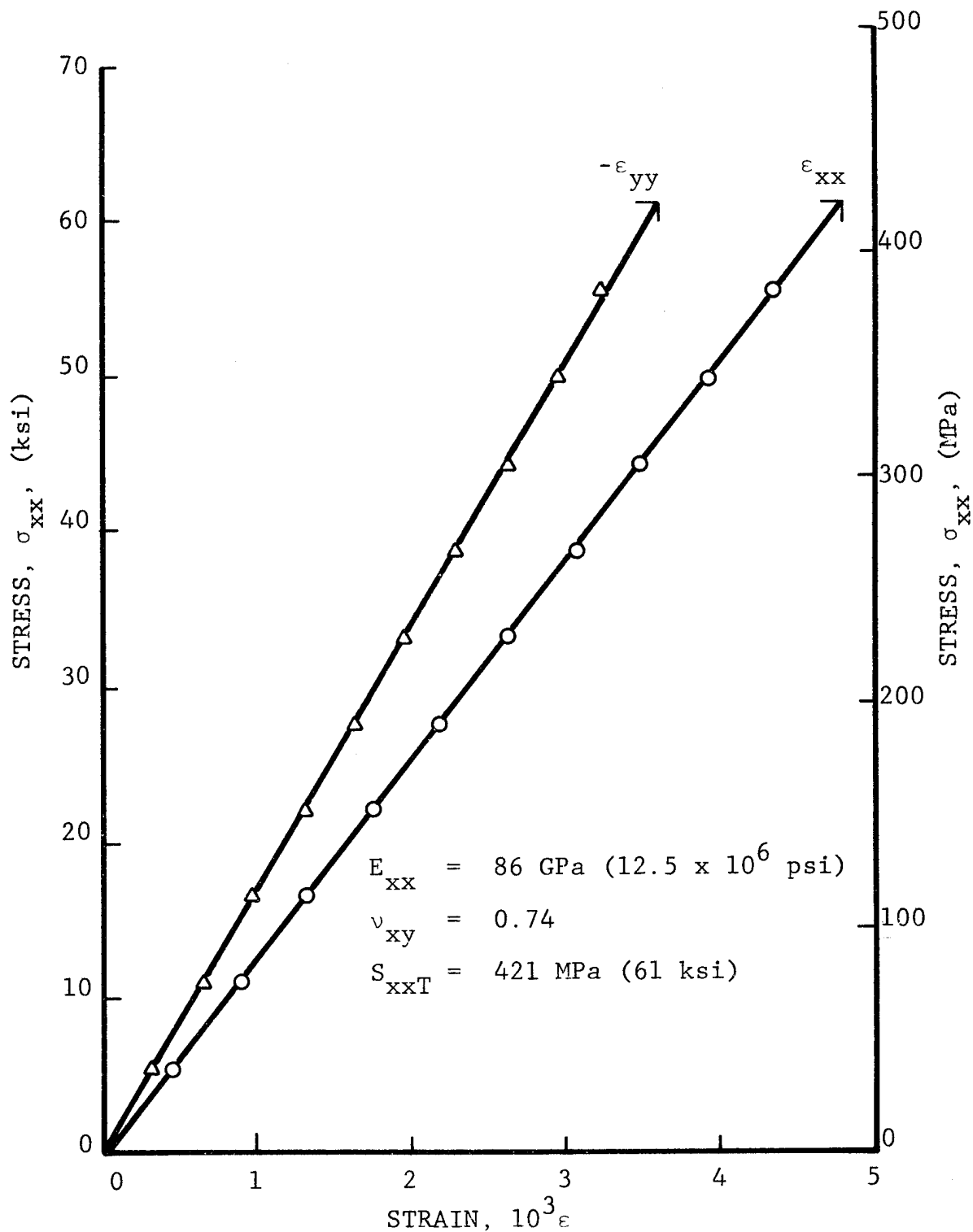


Fig. 76 STRAINS IN $[0^K/+45^C/0^C]_s$ GRAPHITE/KEVLAR 49/HIGH MODULUS EPOXY SPECIMEN UNDER UNIAXIAL TENSILE LOADING AFTER 100 THERMAL CYCLES BETWEEN ROOM TEMPERATURE AND 411 degK (280°F) WITH 244 MPa (35 ksi) TENSILE PRELOAD

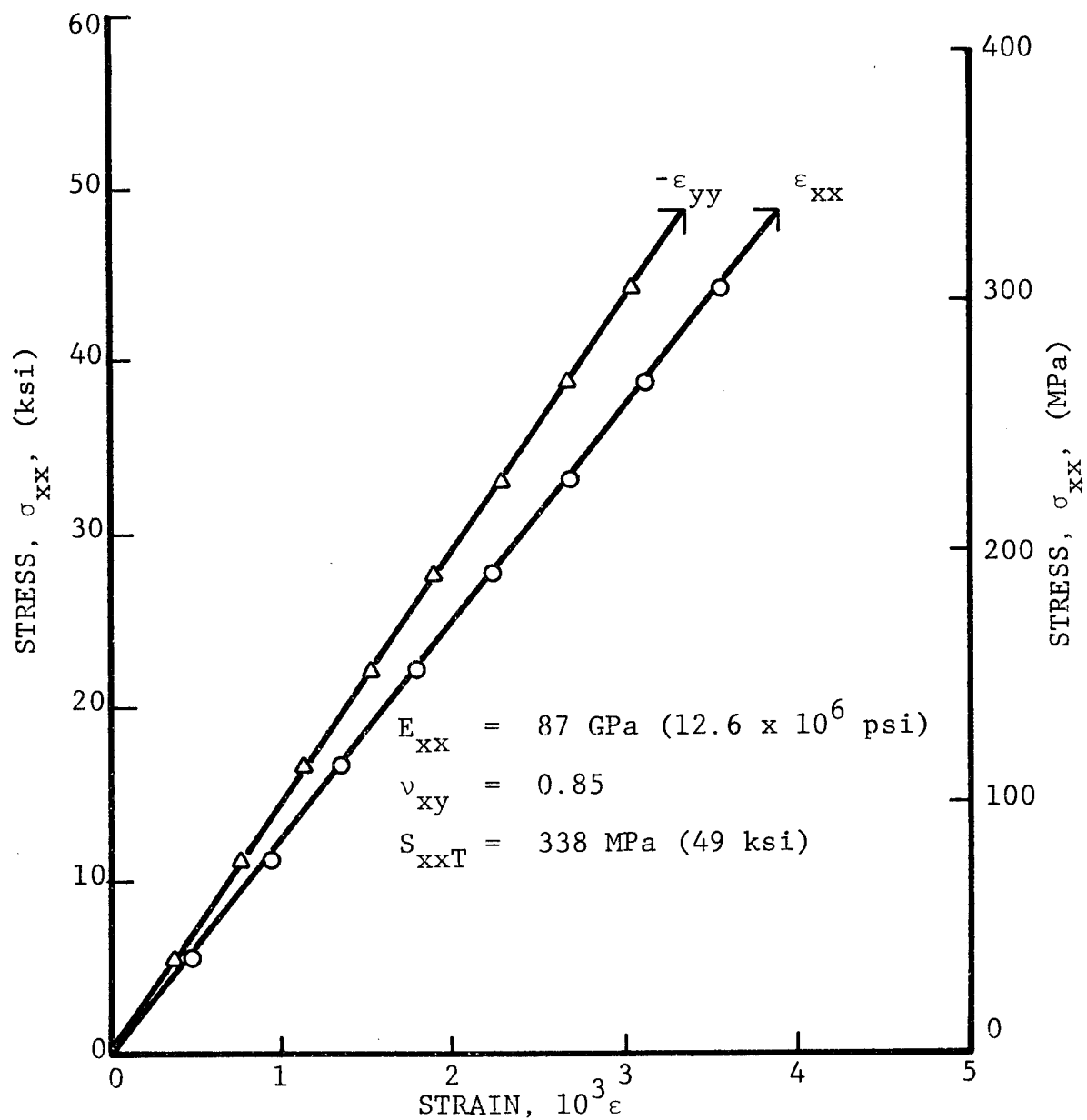


Fig. 77 STRAINS IN $[0^K/+45^C/0^C]_S$ GRAPHITE/KEVLAR 49/HIGH MODULUS EPOXY SPECIMEN UNDER UNIAXIAL TENSILE LOADING AFTER 100 THERMAL CYCLES BETWEEN ROOM TEMPERATURE AND 411 degK (280°F) WITH 244 MPa (35 ksi) TENSILE PRELOAD

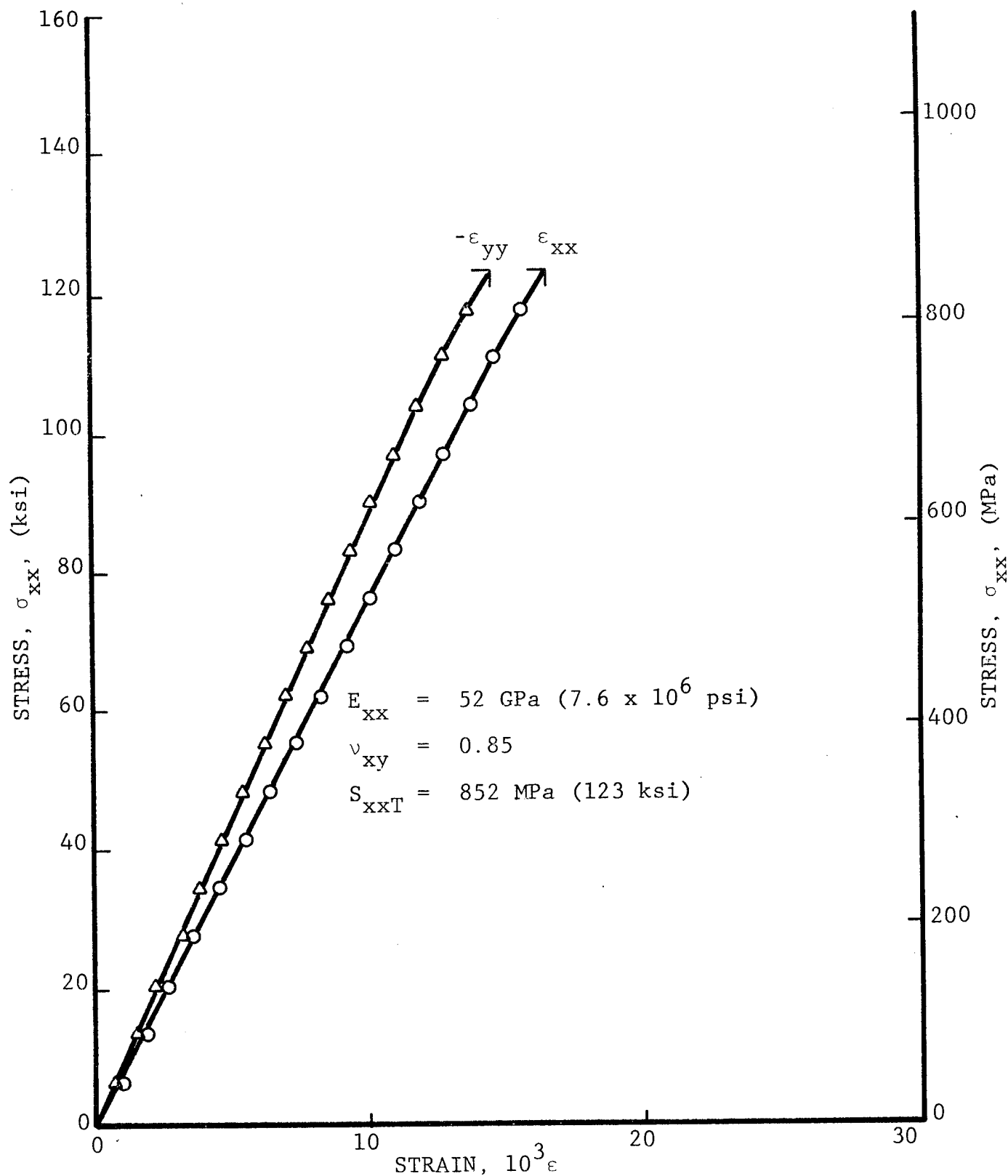


Fig. 78 STRAINS IN $[+45^{\circ}/02^{\circ}]_s$ GRAPHITE/KEVLAR 49/HIGH MODULUS EPOXY SPECIMEN UNDER UNIAXIAL TENSILE LOADING AFTER 100 THERMAL CYCLES BETWEEN ROOM TEMPERATURE AND 411 degK (280°F) WITH 369 MPa (54 ksi) TENSILE PRELOAD

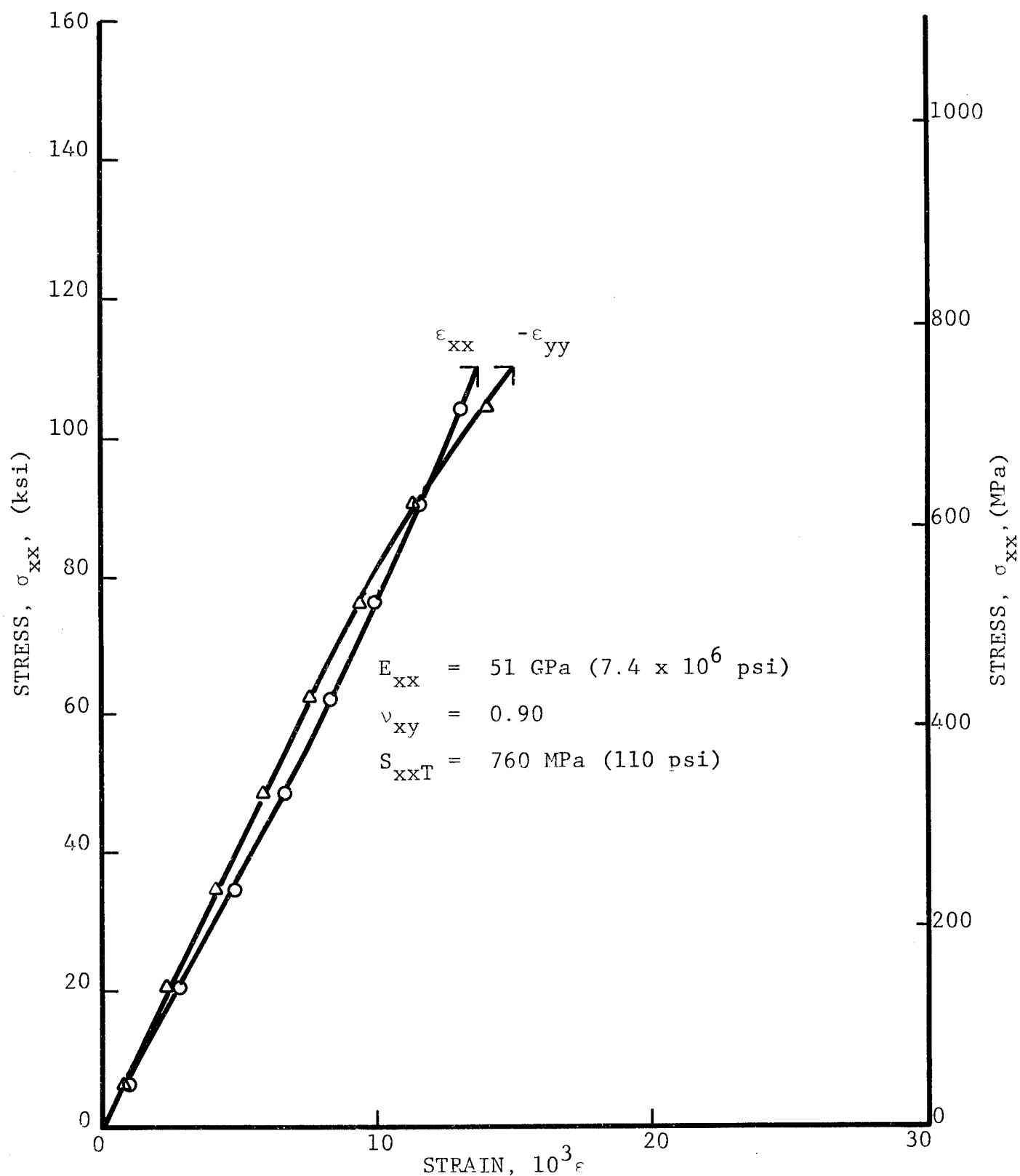


Fig. 79 STRAINS IN $[+45^{\circ}/0^{\circ}]_s$ GRAPHITE/KEVLAR 49/HIGH MODULUS EPOXY SPECIMEN UNDER UNIAXIAL TENSILE LOADING AFTER 100 THERMAL CYCLES BETWEEN ROOM TEMPERATURE AND 411 degK (280°F) WITH 369 MPa (54 ksi) TENSILE PRELOAD

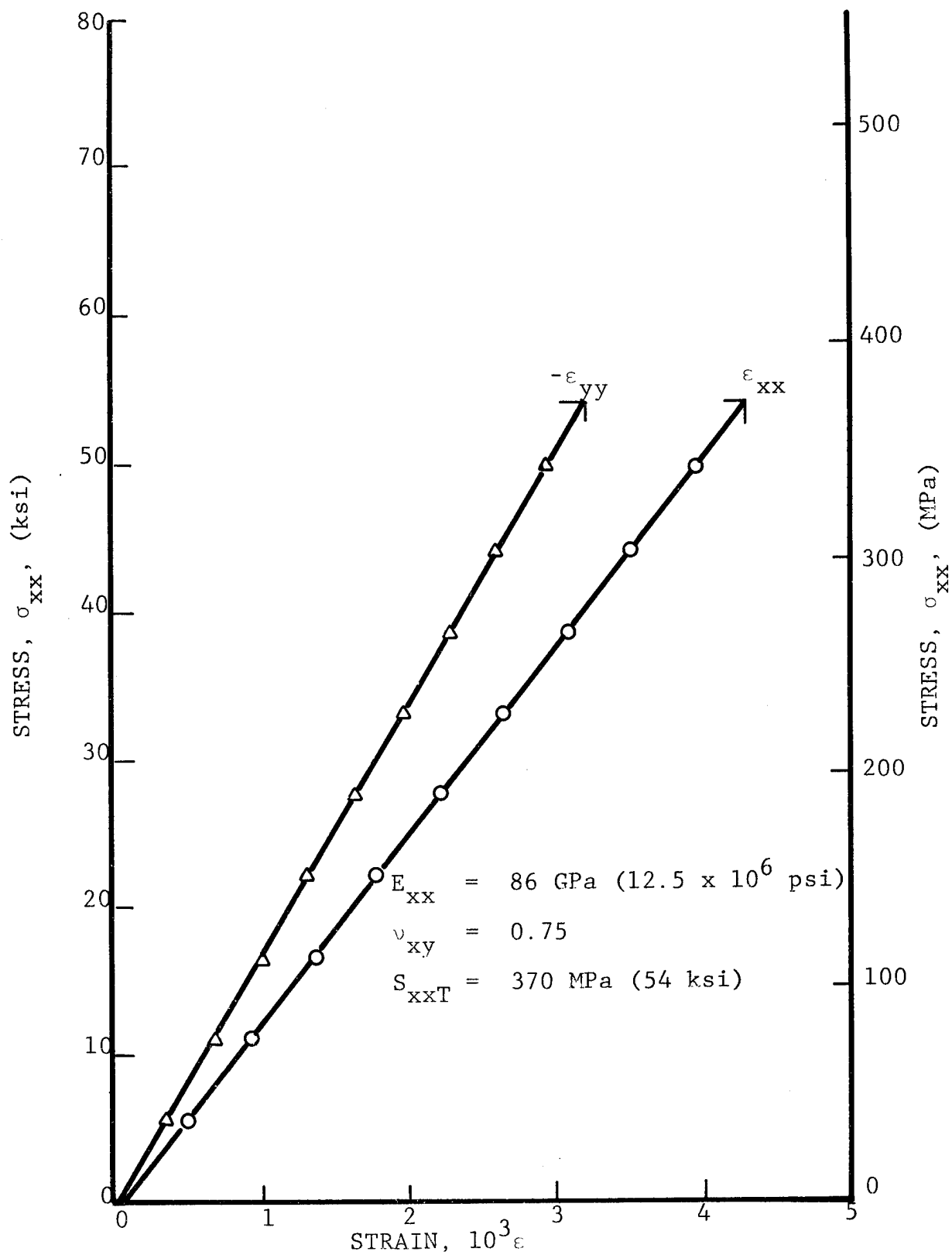


Fig. 80 STRAINS IN $[0^G/+45^C/0^C]_s$ GRAPHITE/S-GLASS/HIGH MODULUS EPOXY SPECIMEN UNDER UNIAXIAL TENSILE LOADING AFTER 100 THERMAL CYCLES BETWEEN ROOM TEMPERATURE AND 411 degK (230°F) WITH 219 MPa (32 ksi) TENSILE PRELOAD

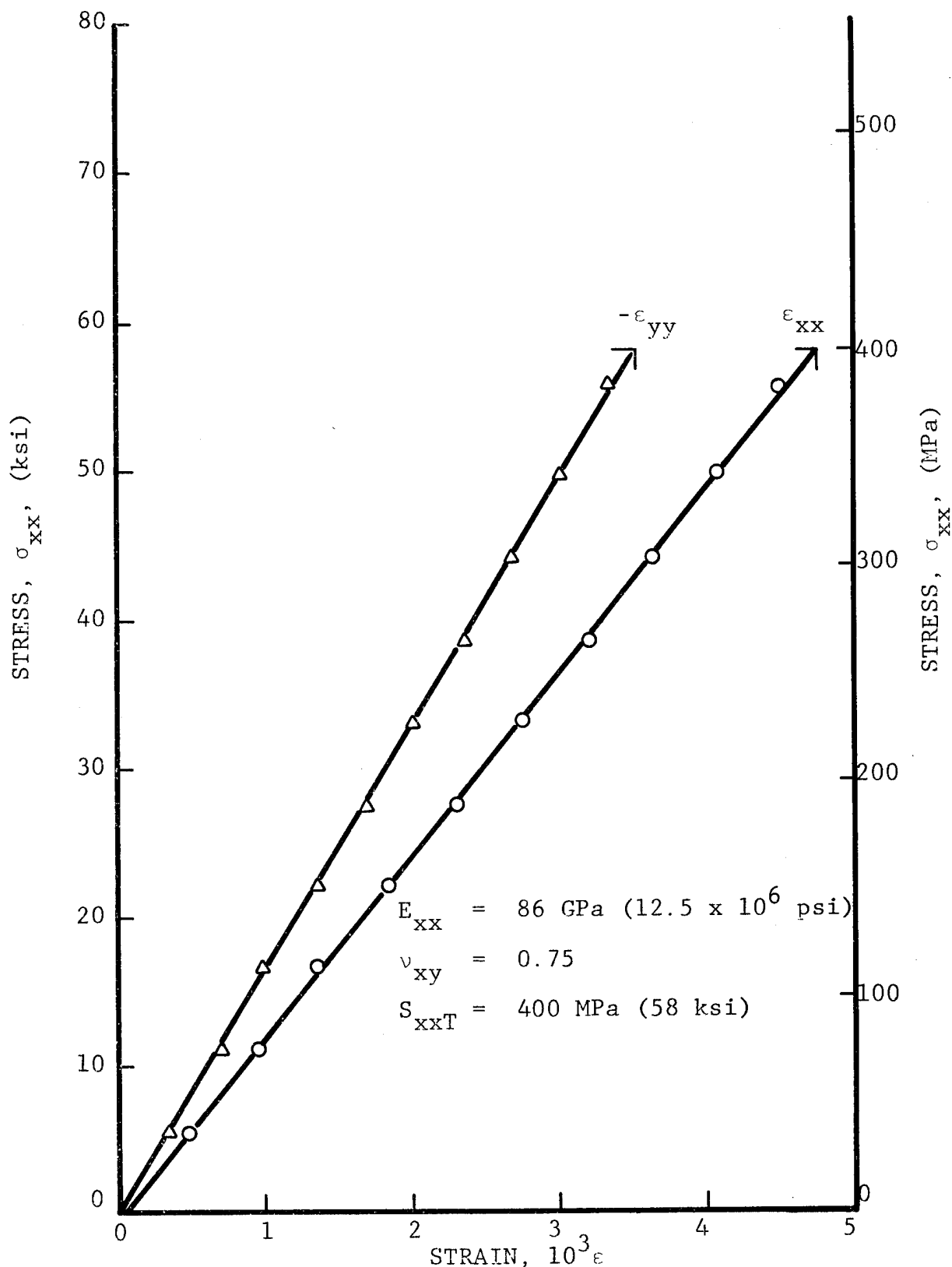


Fig. 81 STRAINS IN $[0^G/+45^C/0^C]_s$ GRAPHITE/S-GLASS/HIGH MODULUS EPOXY SPECIMEN UNDER UNIAXIAL TENSILE LOADING AFTER 100 THERMAL CYCLES BETWEEN ROOM TEMPERATURE AND 411 degK (280°F) WITH 219 MPa (32 ksi) TENSILE PRELOAD

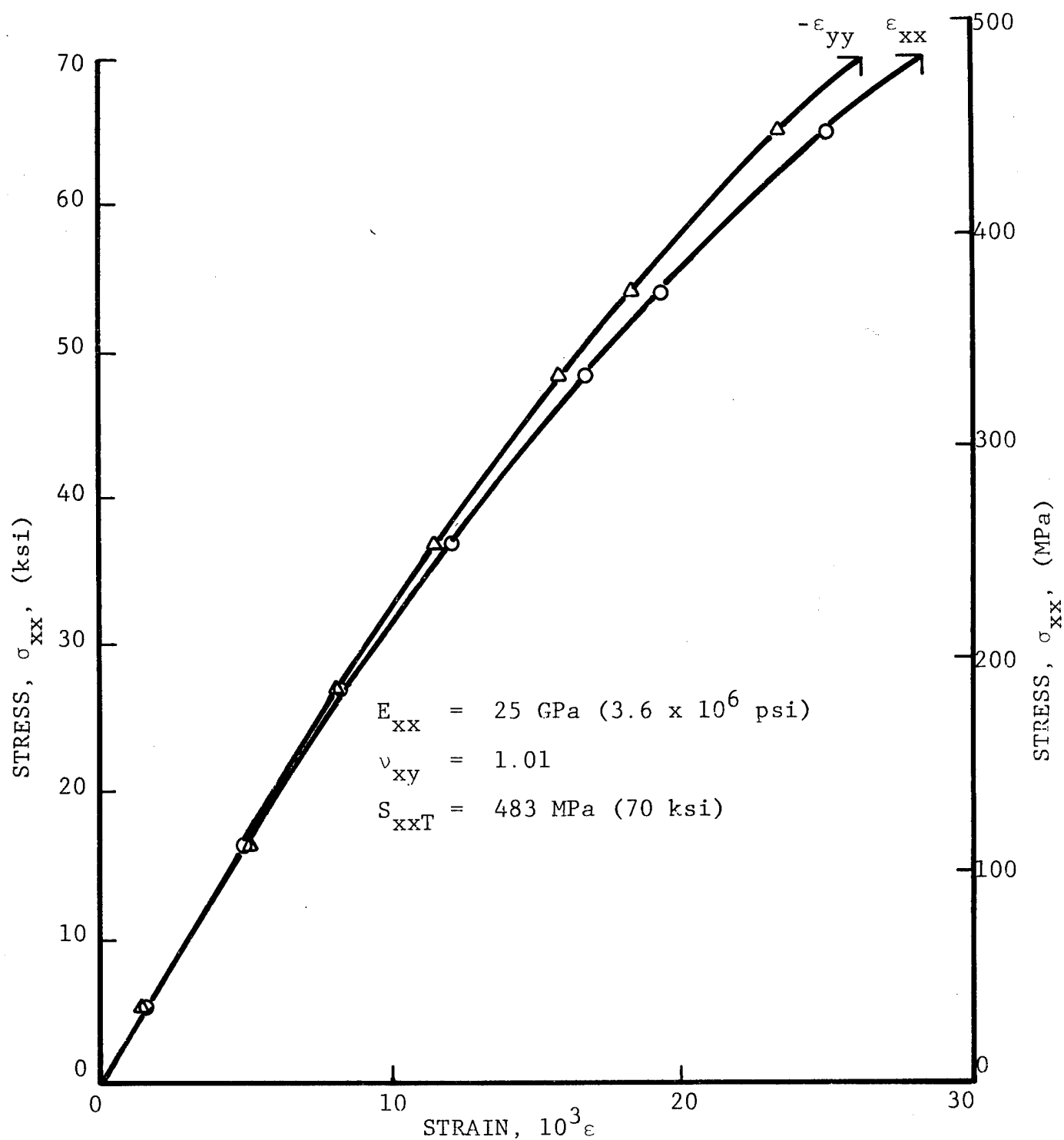


Fig. 82 STRAINS IN $[+45^C/0^G/0^C]_s$ GRAPHITE/S-GLASS/HIGH MODULUS EPOXY SPECIMEN UNDER UNIAXIAL TENSILE LOADING AFTER 100 THERMAL CYCLES BETWEEN ROOM TEMPERATURE AND 411 degK (280°F) WITH 201 MPa (29 ksi) TENSILE PRELOAD (0-DEG. GRAPHITE PLIES FAILED)

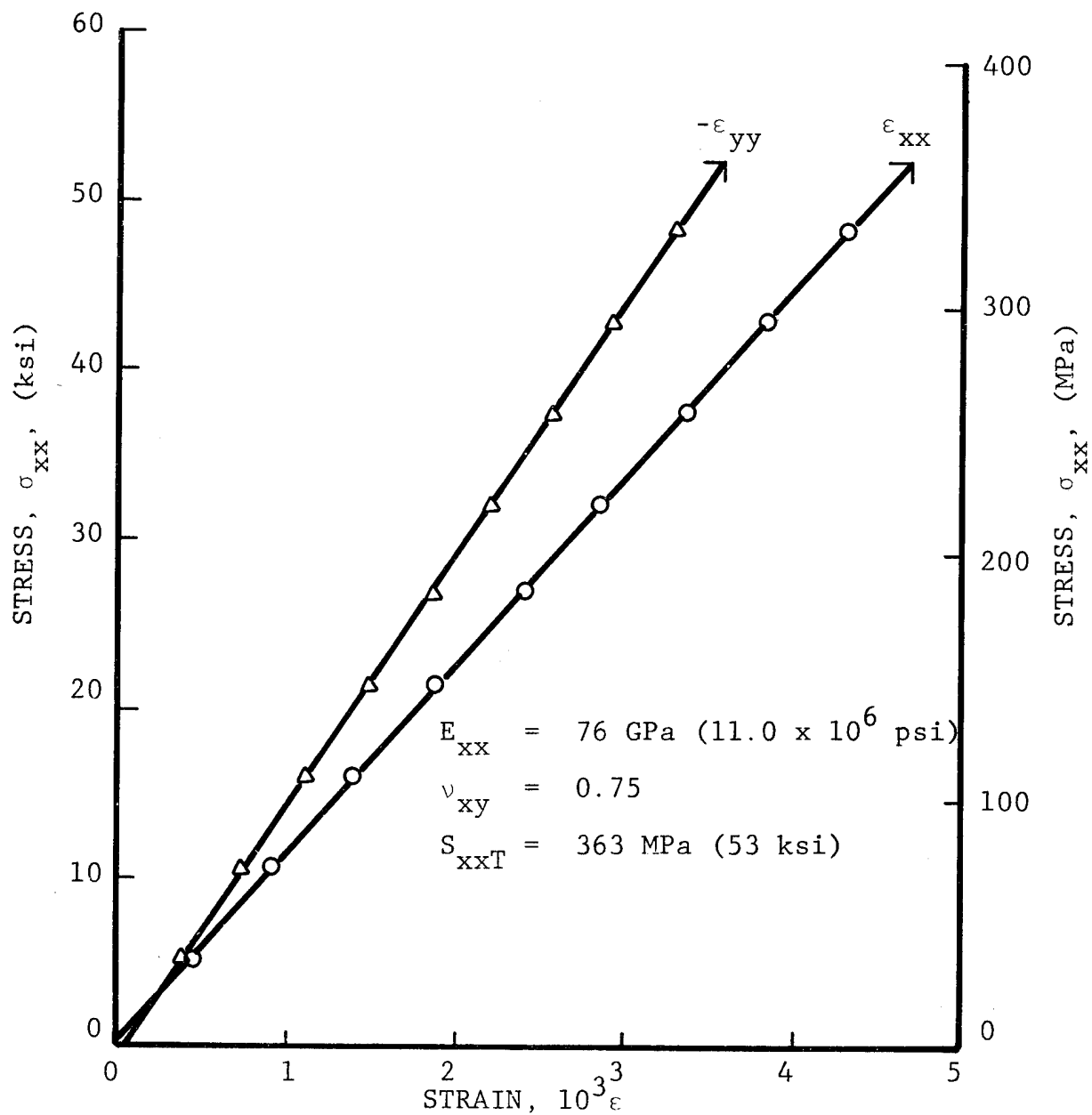


Fig. 83 STRAINS IN $[+45^\circ/0^\circ/0^\circ]_s$ GRAPHITE/S-GLASS/HIGH MODULUS EPOXY SPECIMEN UNDER UNIAXIAL TENSILE LOADING AFTER 100 THERMAL CYCLES BETWEEN ROOM TEMPERATURE AND 411 degK (280°F) WITH 201 MPa (29 ksi) TENSILE PRELOAD

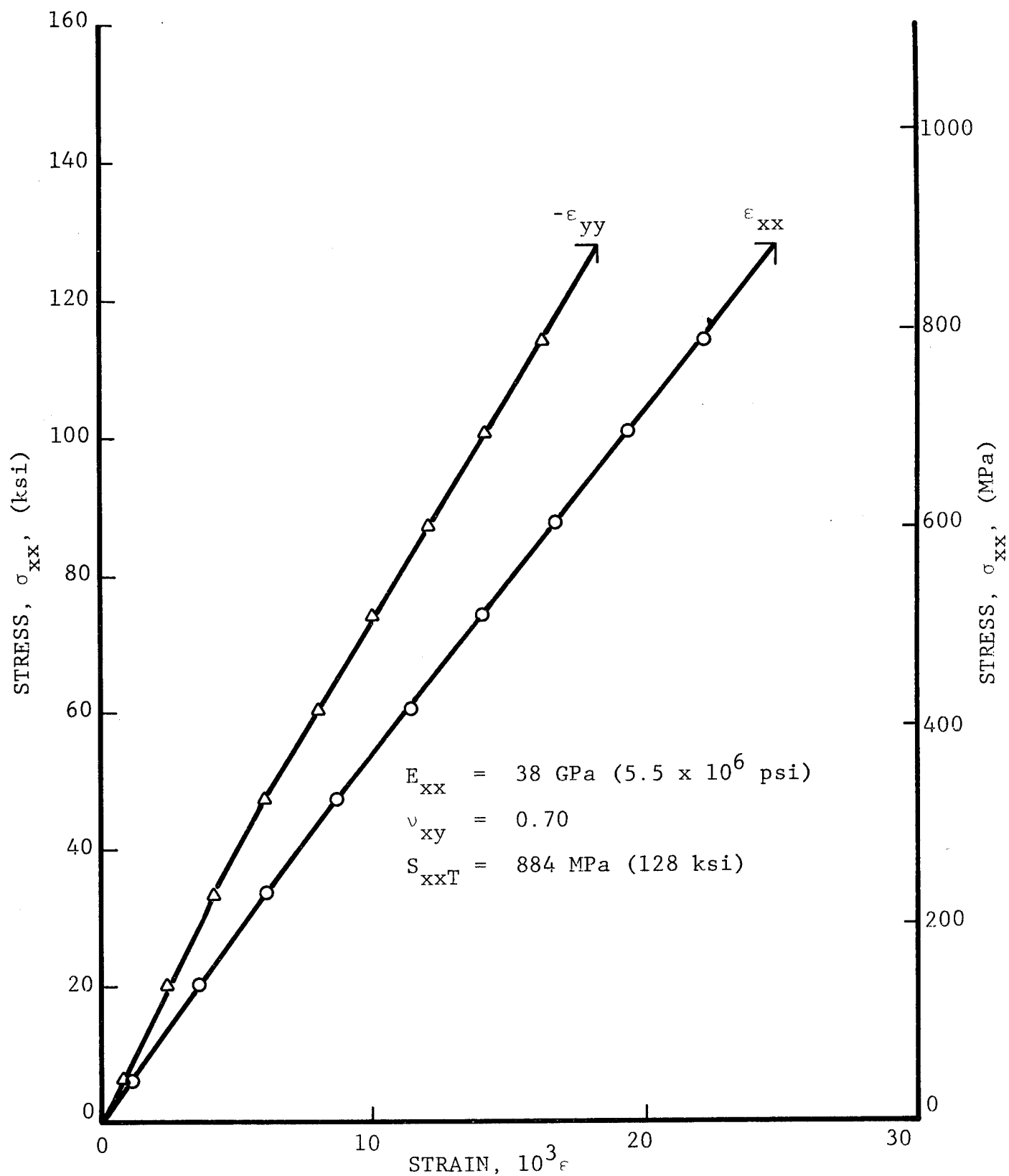


Fig. 84 STRAINS IN $[0^G/+45^C/0^G]_s$ GRAPHITE/S-GLASS/HIGH MODULUS EPOXY SPECIMEN UNDER UNIAXIAL TENSILE LOADING AFTER 100 THERMAL CYCLES BETWEEN ROOM TEMPERATURE AND 411 degK (280°F) WITH 422 MPa (61 ksi) TENSILE PRELOAD

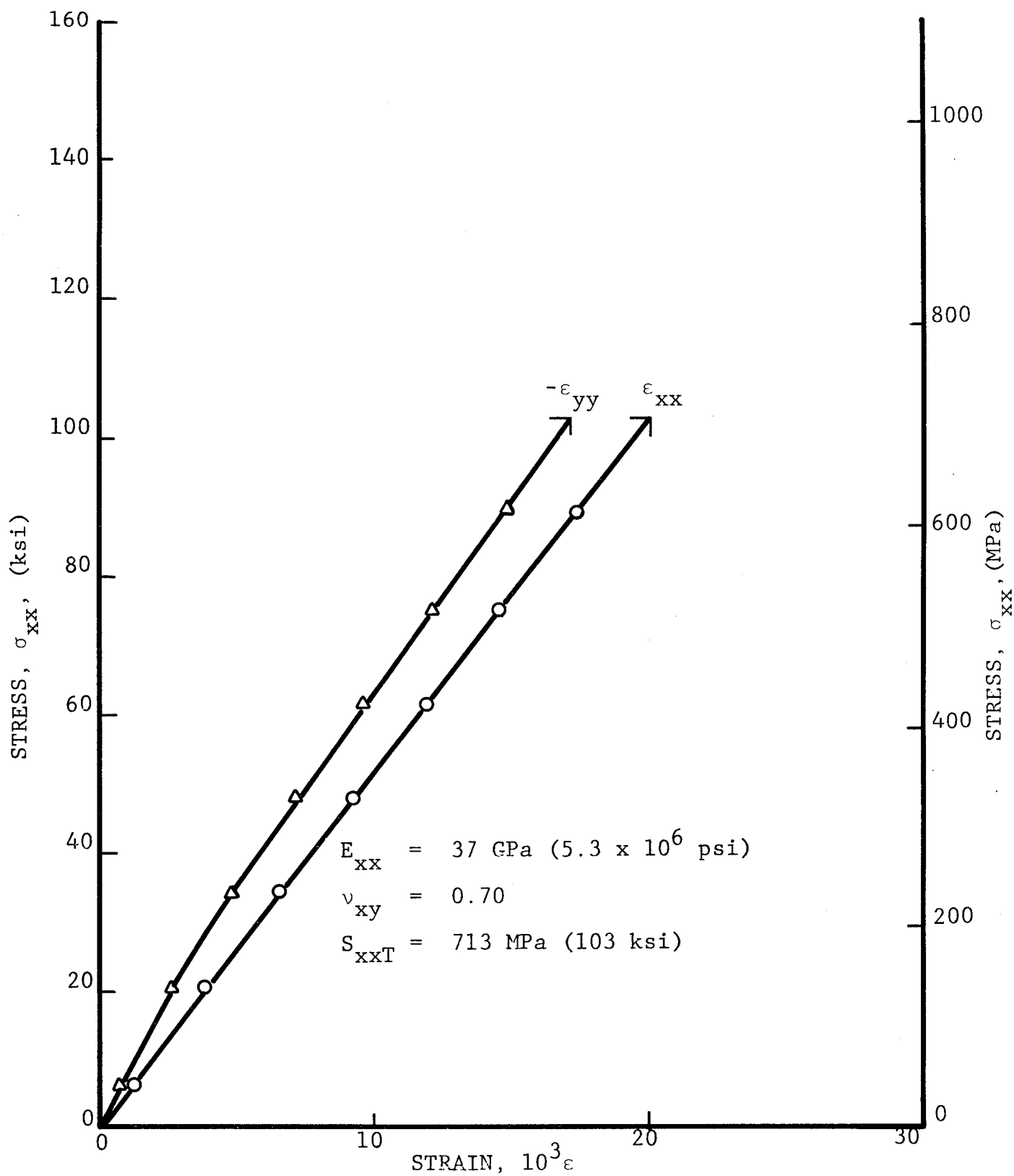


Fig. 85 STRAINS IN $[0^G/+45^C/0^G]_s$ GRAPHITE/S-GLASS/HIGH MODULUS EPOXY SPECIMEN UNDER UNIAXIAL TENSILE LOADING AFTER 100 THERMAL CYCLES BETWEEN ROOM TEMPERATURE AND 400 degK (280°F) WITH 422 MPa (61 ksi) TENSILE PRELOAD

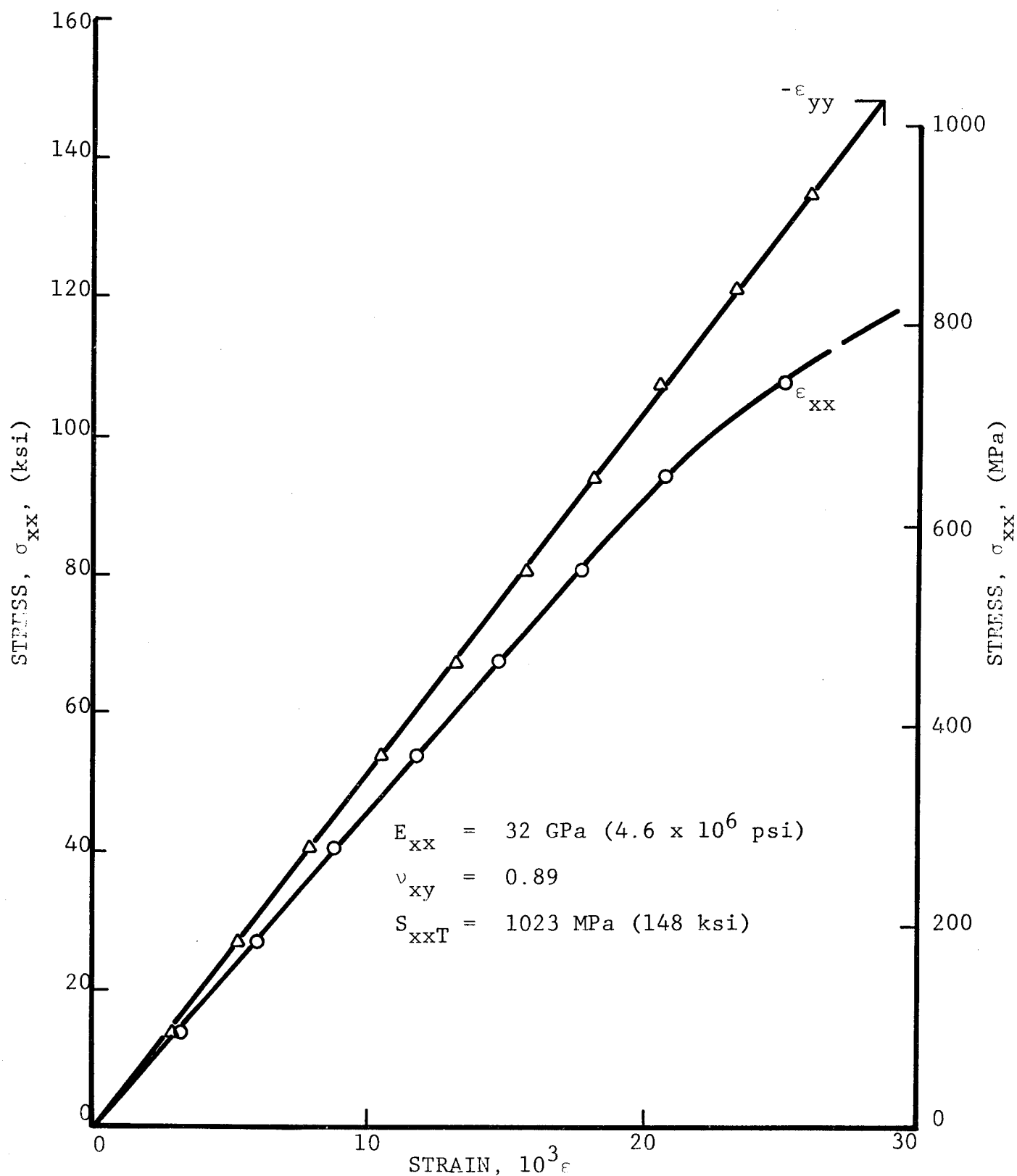


Fig. 86 STRAINS IN $[+45^{\circ}/0_2^G]_s$ GRAPHITE/S-GLASS/HIGH MODULUS EPOXY SPECIMEN UNDER UNIAXIAL TENSILE LOADING AFTER 100 THERMAL CYCLES BETWEEN ROOM TEMPERATURE AND 411 degK (280°F) WITH 422 MPa (61 ksi) TENSILE PRELOAD

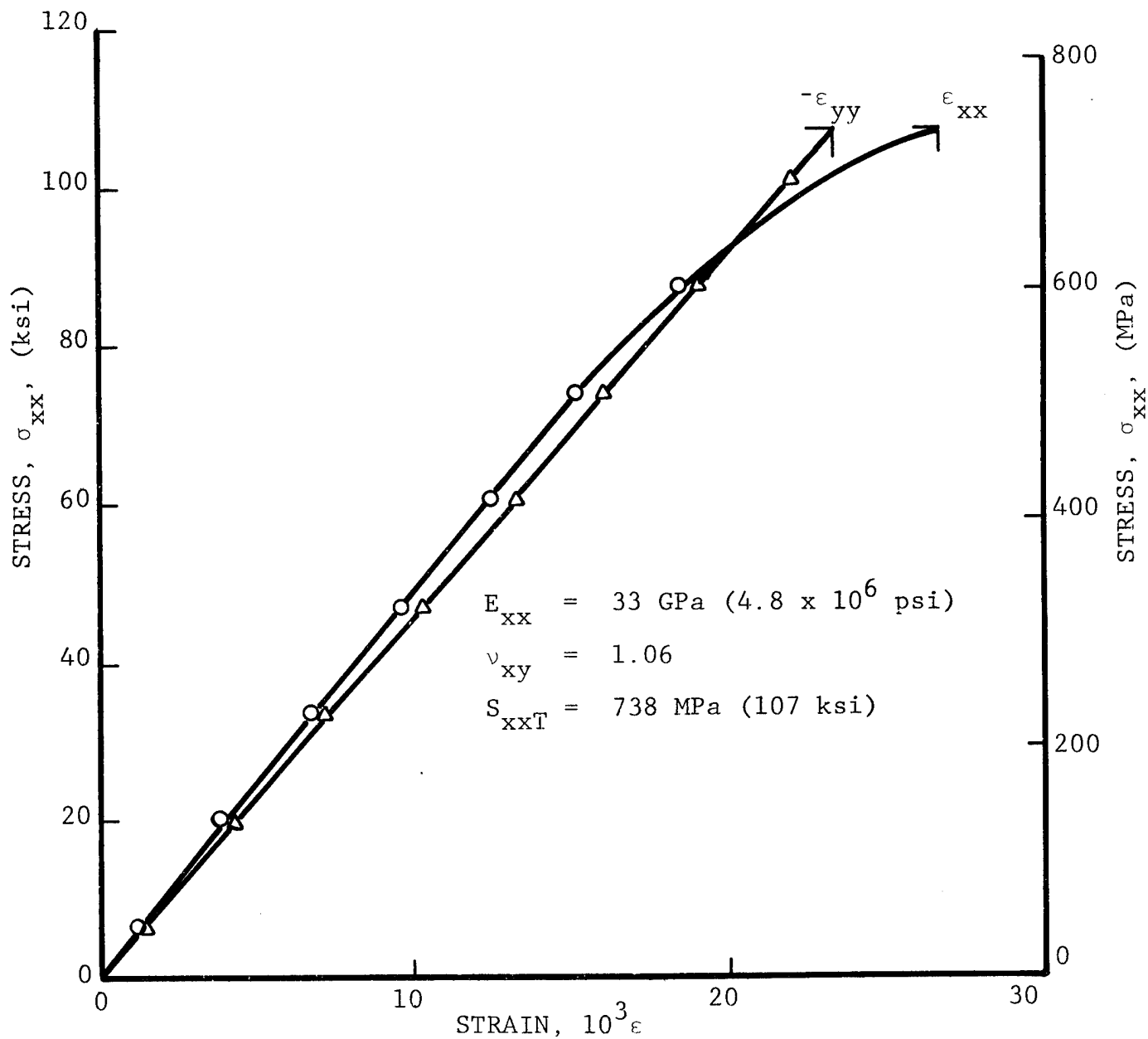


Fig. 37 STRAINS IN $[+45^{\circ}/0_2^G]_s$ GRAPHITE/S-GLASS/HIGH MODULUS EPOXY SPECIMEN UNDER UNIAXIAL TENSILE LOADING AFTER 100 THERMAL CYCLES BETWEEN ROOM TEMPERATURE AND 411 degK (280°F) WITH 422 MPa (61 ksi) TENSILE PRELOAD

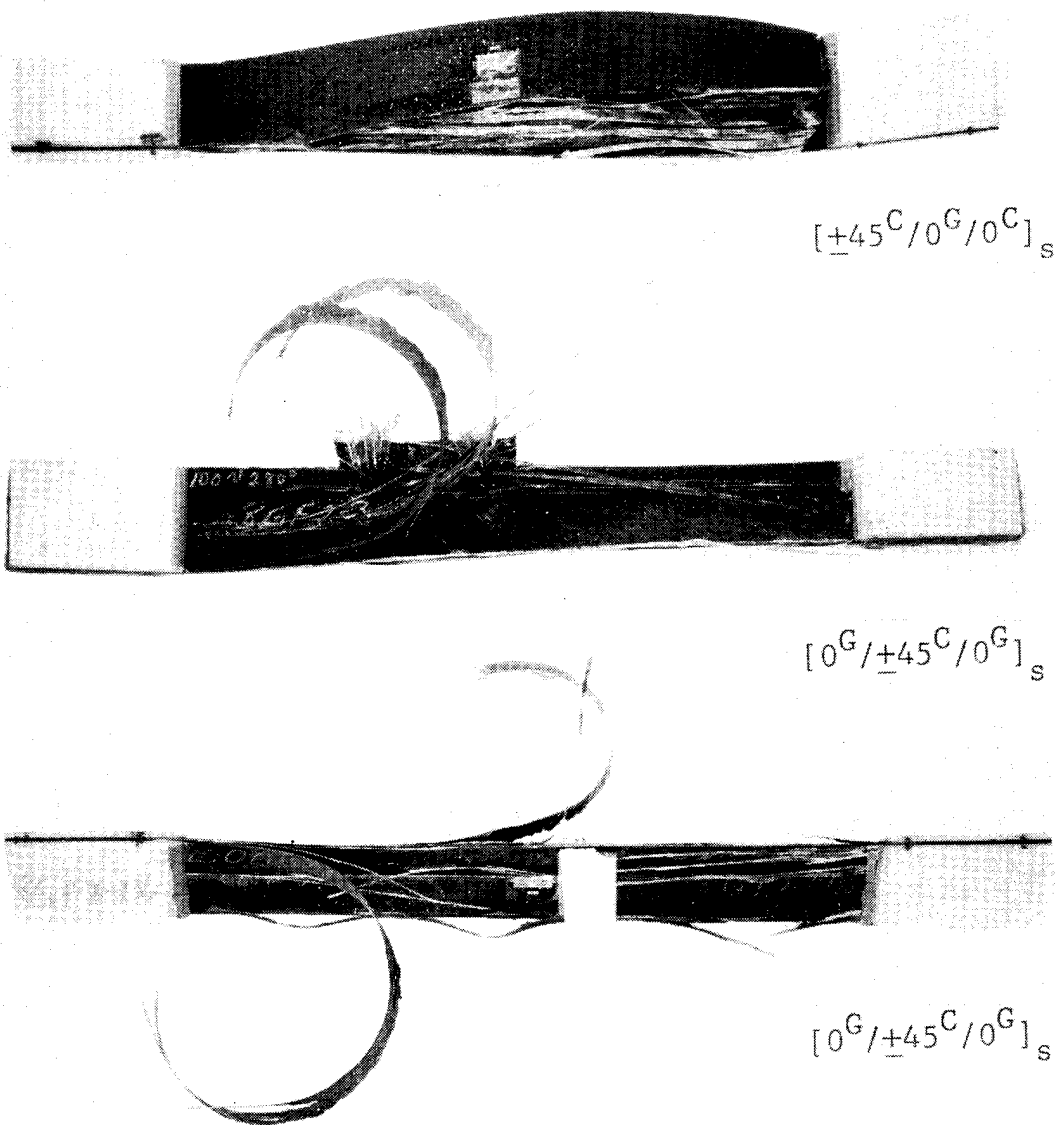


Fig. 88 CHARACTERISTIC FAILURE PATTERNS OF THREE GRAPHITE/S-GLASS/
HIGH MODULUS EPOXY SPECIMENS UNDER UNIAXIAL TENSILE LOADING
AFTER 100 THERMAL CYCLES BETWEEN ROOM TEMPERATURE AND 411
degK (280°F) UNDER TENSILE PRELOAD

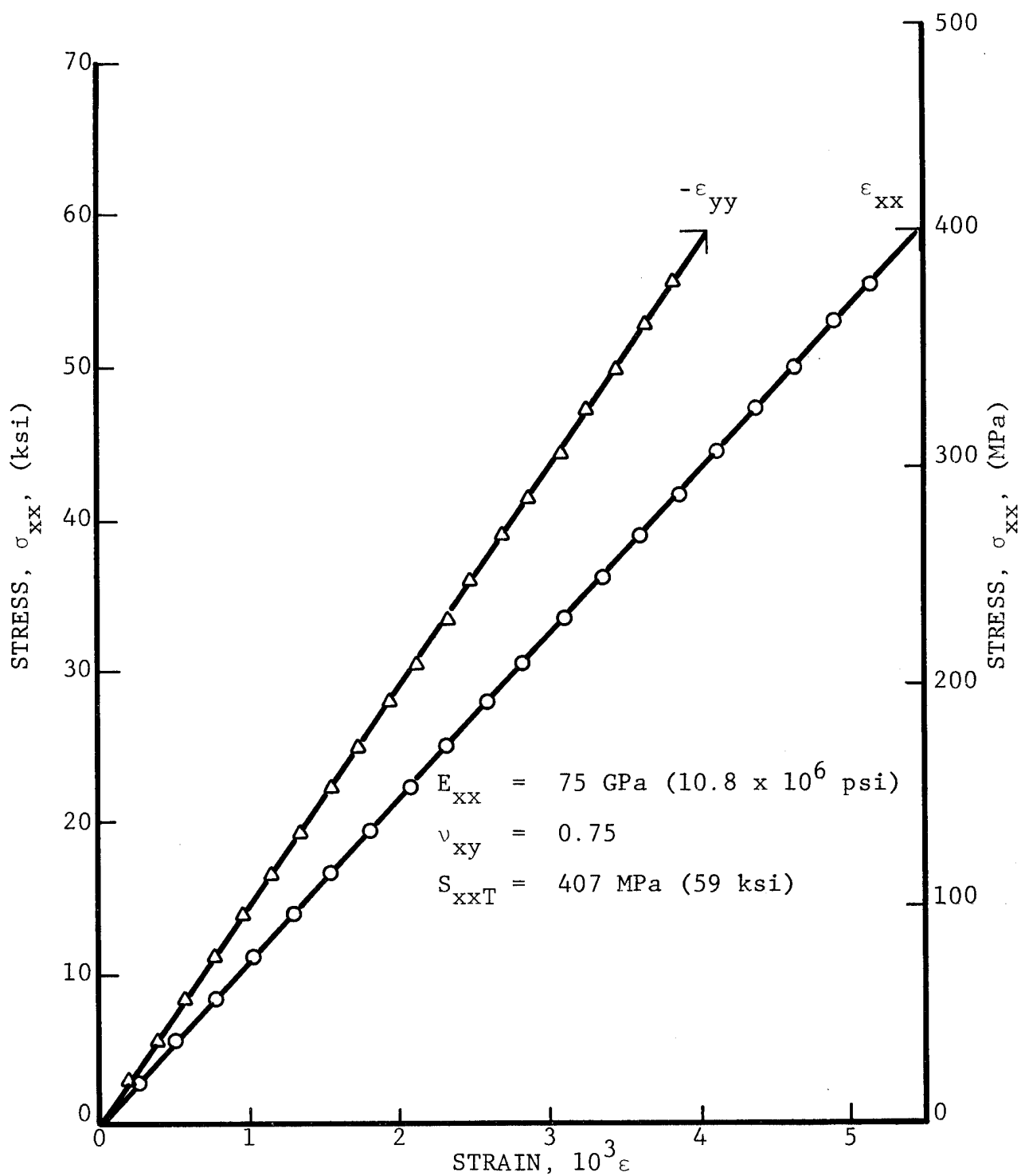


Fig. 89 STRAINS IN $[0^K/+45^C/0^C]_s$ GRAPHITE/KEVLAR 49/
 HIGH MODULUS EPOXY SPECIMEN UNDER UNIAXIAL
 TENSILE LOADING AFTER 100 THERMAL CYCLES BETWEEN
 ROOM TEMPERATURE AND 200 degK (-100°F) WITH
 244 MPa (35 ksi) TENSILE PRELOAD

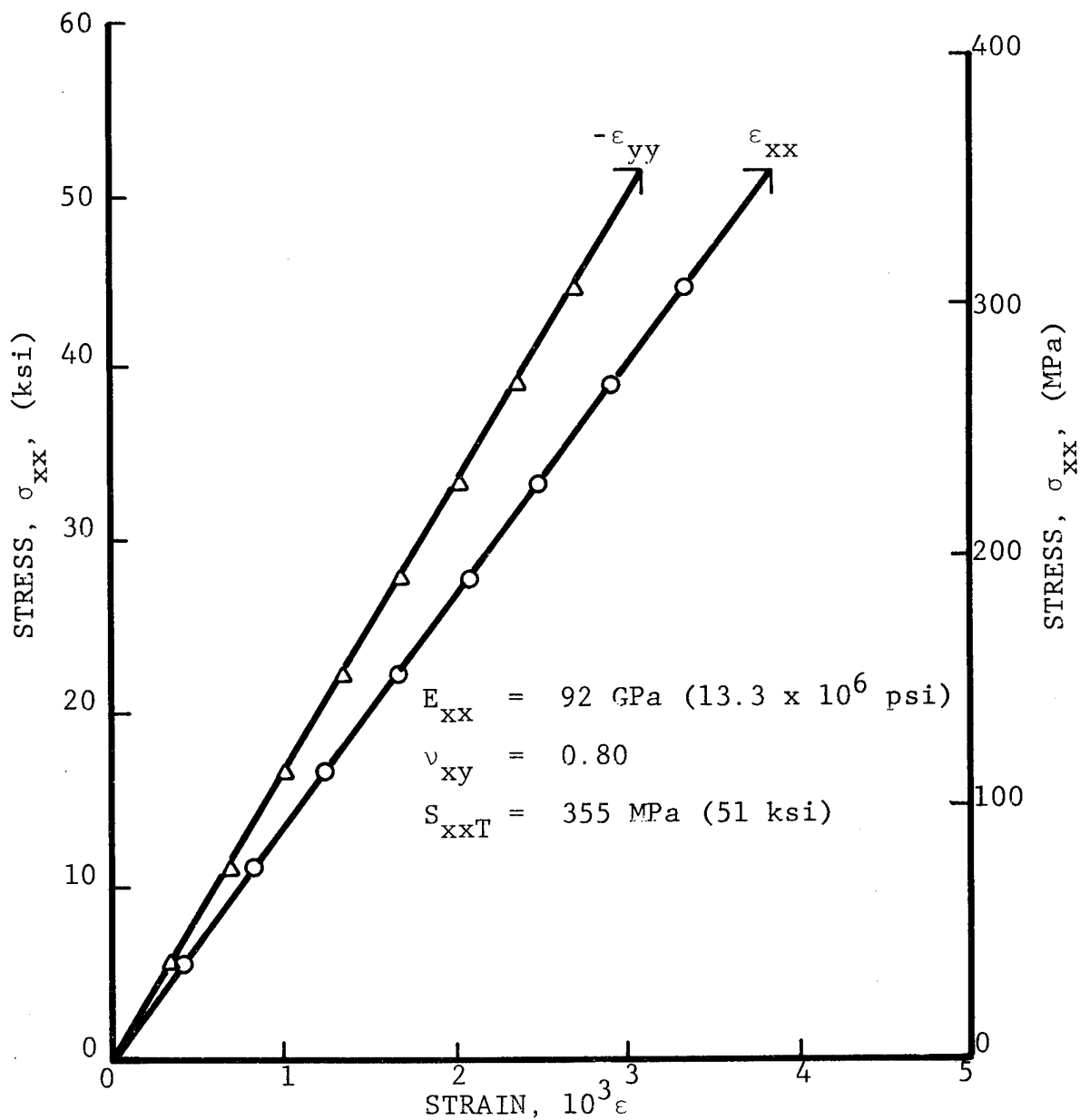


Fig. 90 STRAINS IN $[0^K/+45^C/0^C]_s$ GRAPHITE/KEVLAR 49/
 HIGH MODULUS EPOXY SPECIMEN UNDER UNIAXIAL
 TENSILE LOADING AFTER 100 THERMAL CYCLES
 BETWEEN ROOM TEMPERATURE AND 200 degK (-100°F)
 WITH 244 MPa (35 ksi) TENSILE PRELOAD

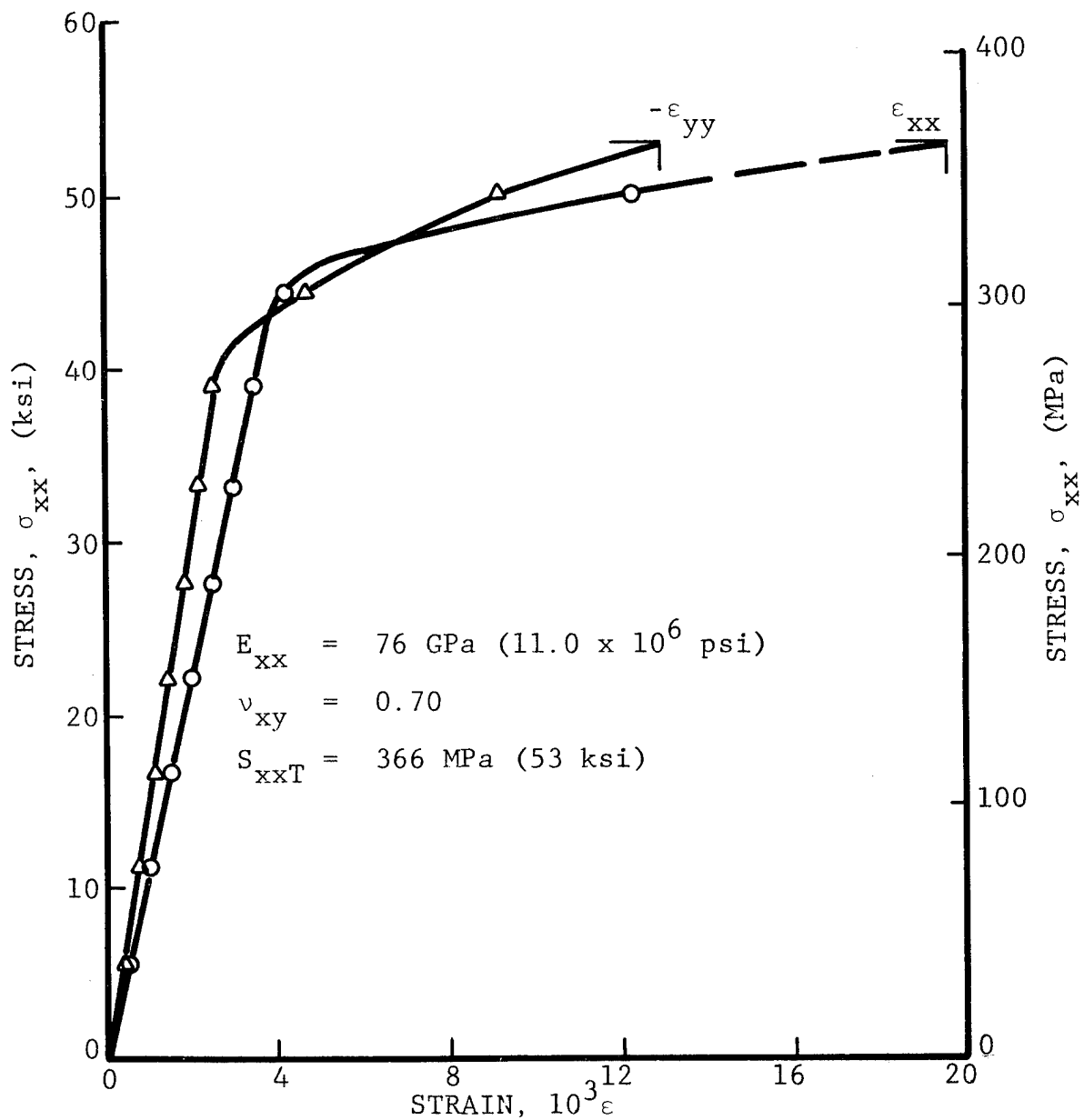


Fig. 91 STRAINS IN $[+45^{\circ}\text{C}/0^{\circ}\text{K}/0^{\circ}\text{C}]_s$ GRAPHITE/KEVLAR 49/
 HIGH MODULUS EPOXY SPECIMEN UNDER UNIAXIAL
 TENSILE LOADING AFTER 100 THERMAL CYCLES BETWEEN
 ROOM TEMPERATURE AND 200 degK (-100°F) WITH
 258 MPa (37 ksi) TENSILE PRELOAD

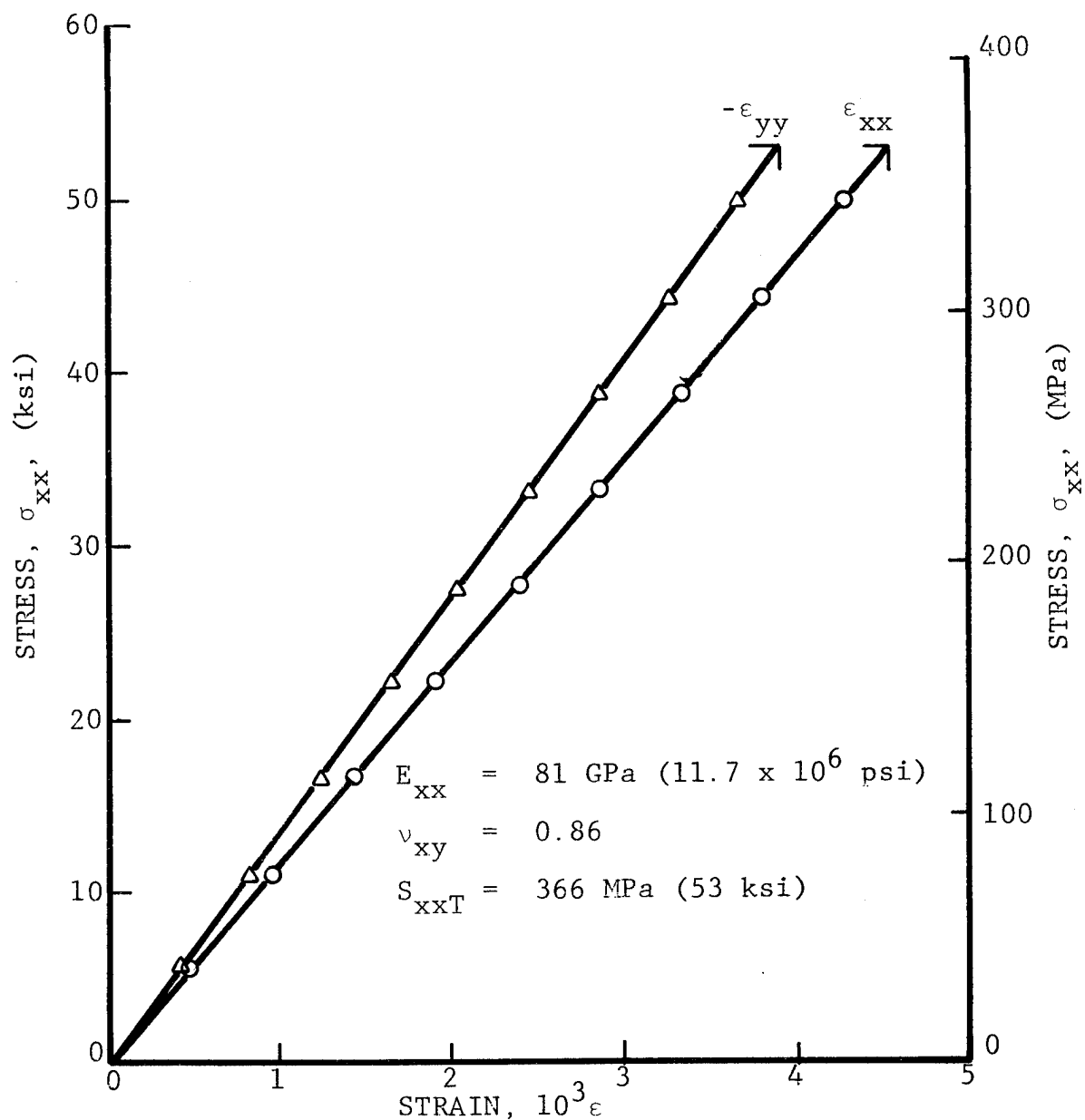


Fig. 92 STRAINS IN $[+45^{\circ}\text{C}/0^{\circ}\text{K}/0^{\circ}\text{C}]_s$ GRAPHITE/KEVLAR 49/
 HIGH MODULUS EPOXY SPECIMEN UNDER UNIAXIAL
 TENSILE LOADING AFTER 100 THERMAL CYCLES
 BETWEEN ROOM TEMPERATURE AND 200 degK (-100°F)
 WITH 258 MPa (37 ksi) TENSILE PRELOAD

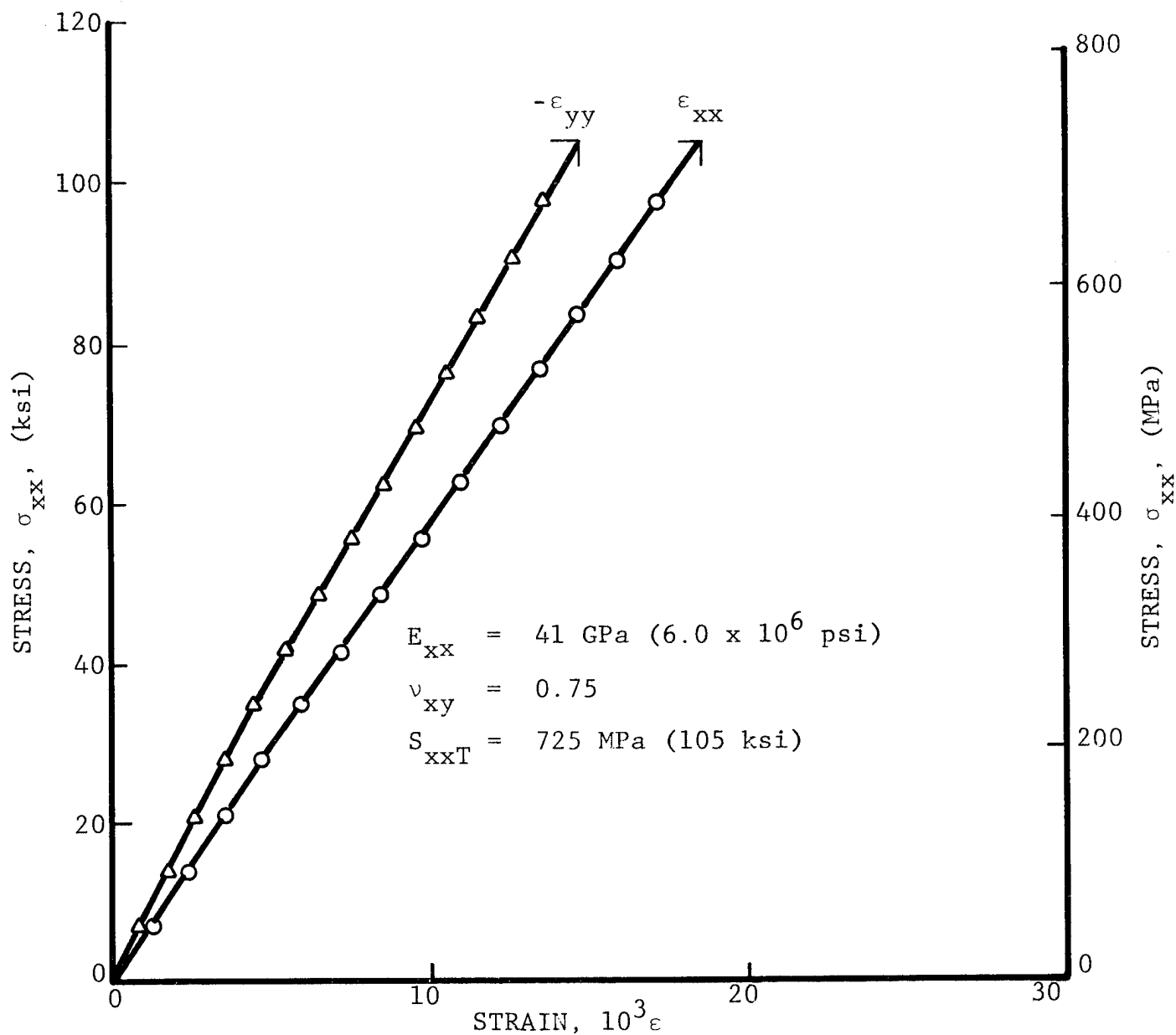


Fig. 93 STRAINS IN $[0^K/+45^C/0^K]_S$ GRAPHITE/KEVLAR 49/HIGH MODULUS EPOXY SPECIMEN UNDER UNIAXIAL TENSILE LOADING AFTER 100 THERMAL CYCLES BETWEEN ROOM TEMPERATURE AND 200 degK (-100°F) WITH 560 MPa (81 ksi) TENSILE PRELOAD

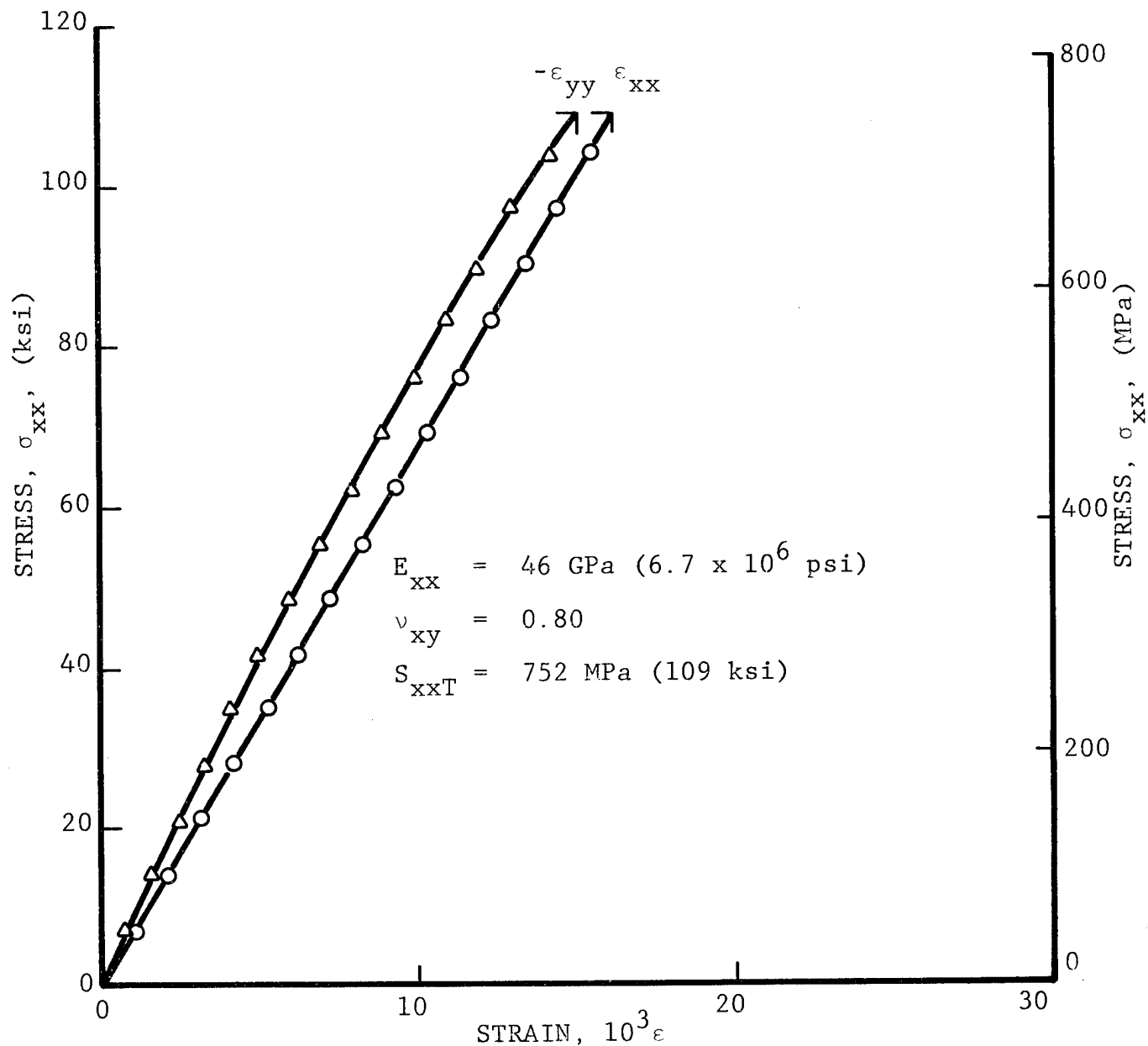


Fig. 94 STRAINS IN $[0^{\text{K}}/+45^{\text{C}}/0^{\text{K}}]_s$ GRAPHITE/KEVLAR 49/HIGH MODULUS EPOXY SPECIMEN UNDER UNIAXIAL TENSILE LOADING AFTER 100 THERMAL CYCLES BETWEEN ROOM TEMPERATURE AND 200 degK (-100°F) WITH 560 MPa (81 ksi) TENSILE PRELOAD

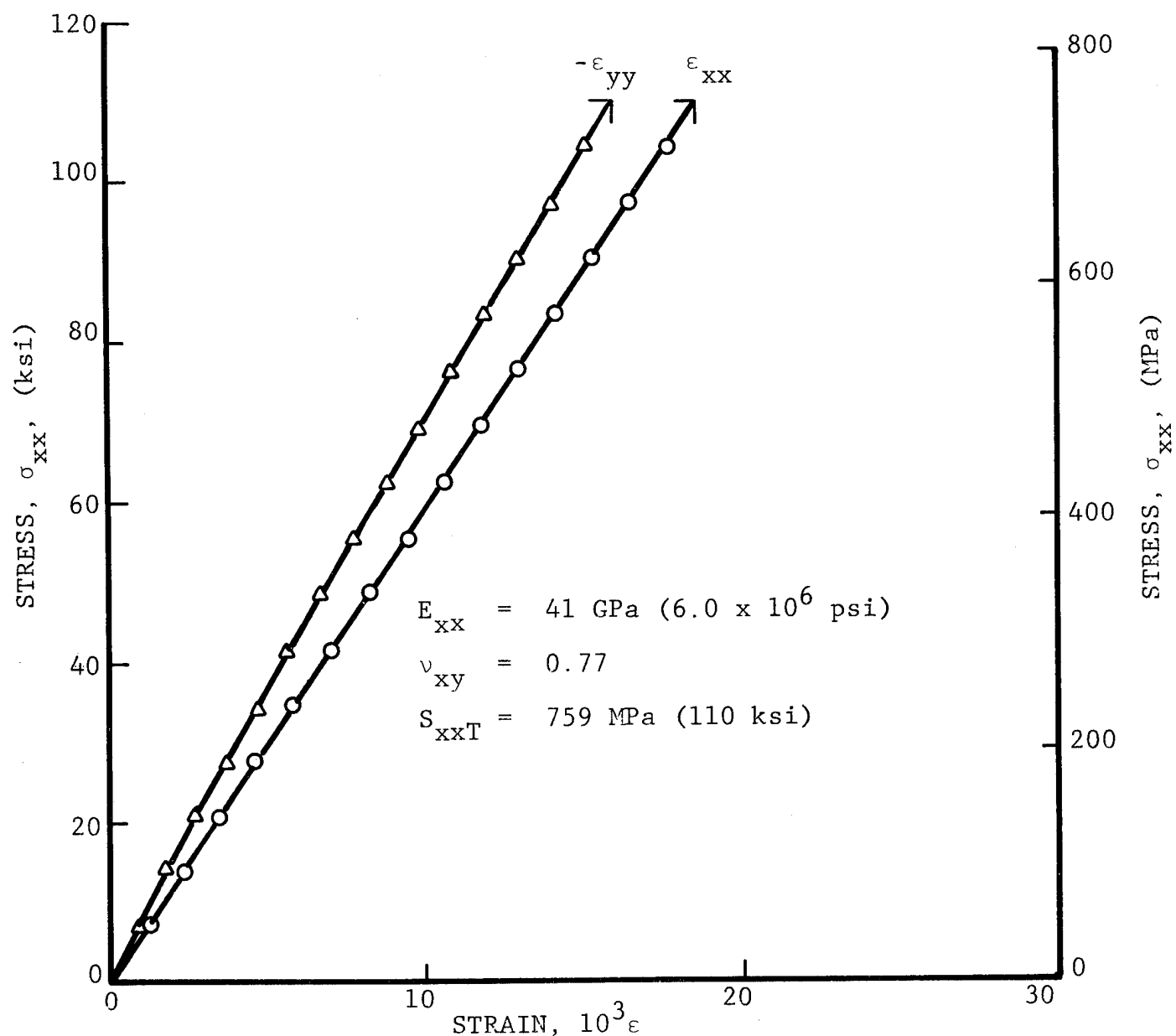


Fig. 95 STRAINS IN $[+45^{\circ}/0^{\circ}]_s$ GRAPHITE/KEVLAR 49/HIGH MODULUS EPOXY SPECIMEN UNDER UNIAXIAL TENSILE LOADING AFTER 100 THERMAL CYCLES BETWEEN ROOM TEMPERATURE AND 200 degK (-100°F) WITH 516 MPa (75 ksi) TENSILE PRELOAD

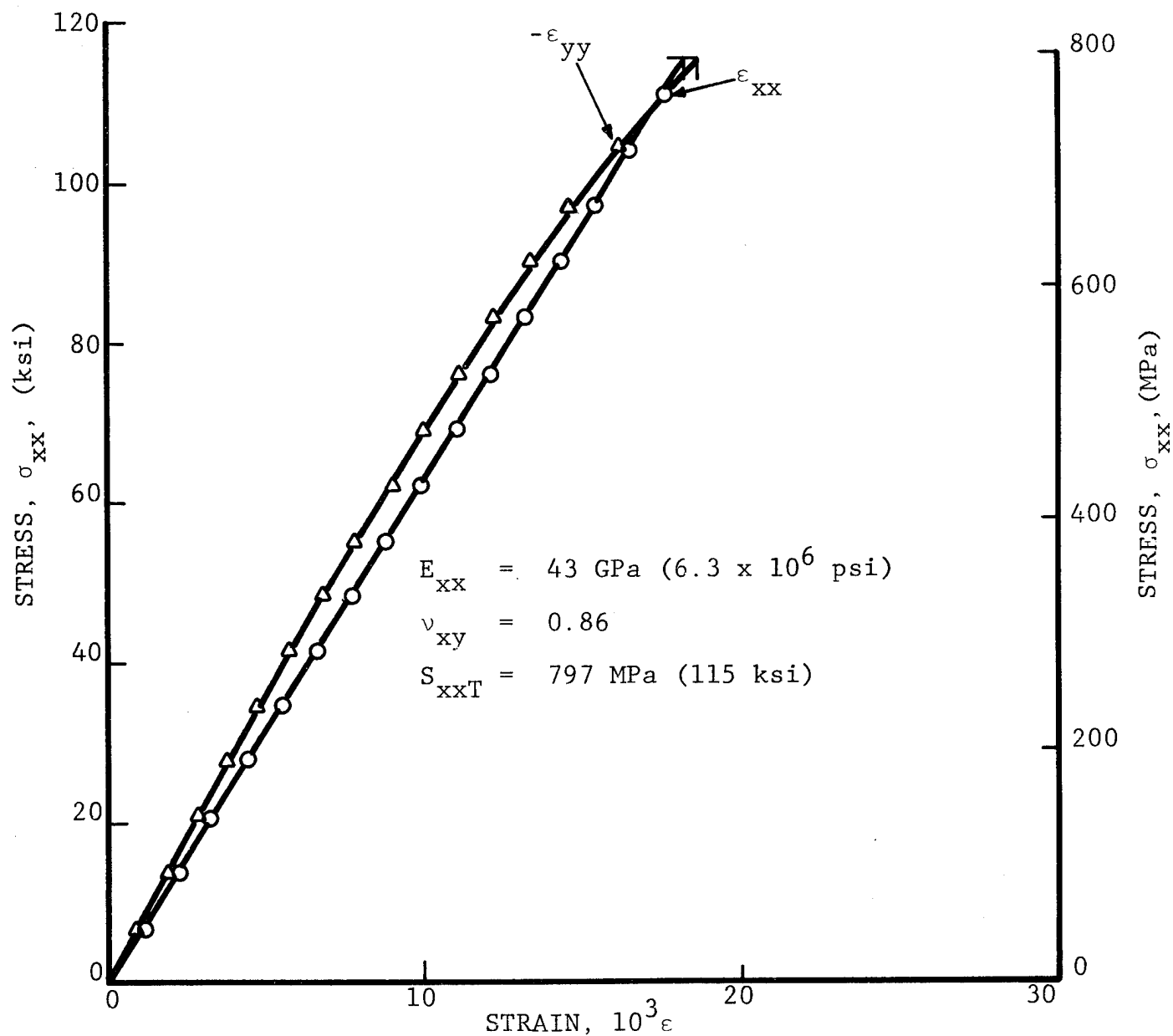


Fig. 96 STRAINS IN $[+45^{\circ}/0_2^{\circ}]_s$ GRAPHITE/KEVLAR 49/HIGH MODULUS EPOXY SPECIMEN UNDER UNIAXIAL TENSILE LOADING AFTER 100 THERMAL CYCLES BETWEEN ROOM TEMPERATURE AND 200 degK (-100°F) WITH 516 MPa (75 ksi) TENSILE PRELOAD

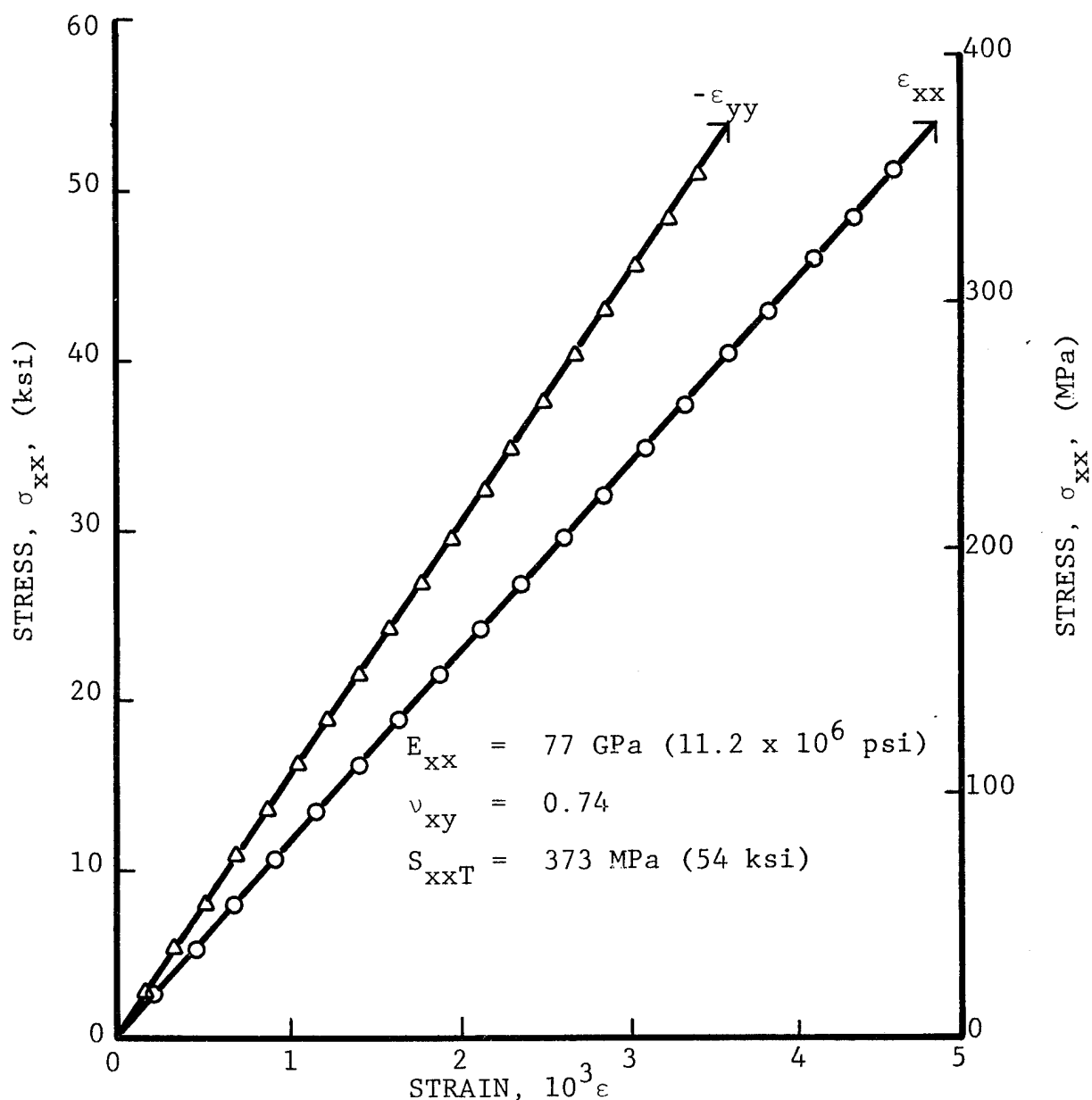


Fig. 97 STRAINS IN $[0^G/+45^C/0^C]_s$ GRAPHITE/S-GLASS/HIGH MODULUS EPOXY SPECIMEN UNDER UNIAXIAL TENSILE LOADING AFTER 100 THERMAL CYCLES BETWEEN ROOM TEMPERATURE AND 200 degK (-100°F) WITH 256 MPa (37 ksi) TENSILE PRELOAD

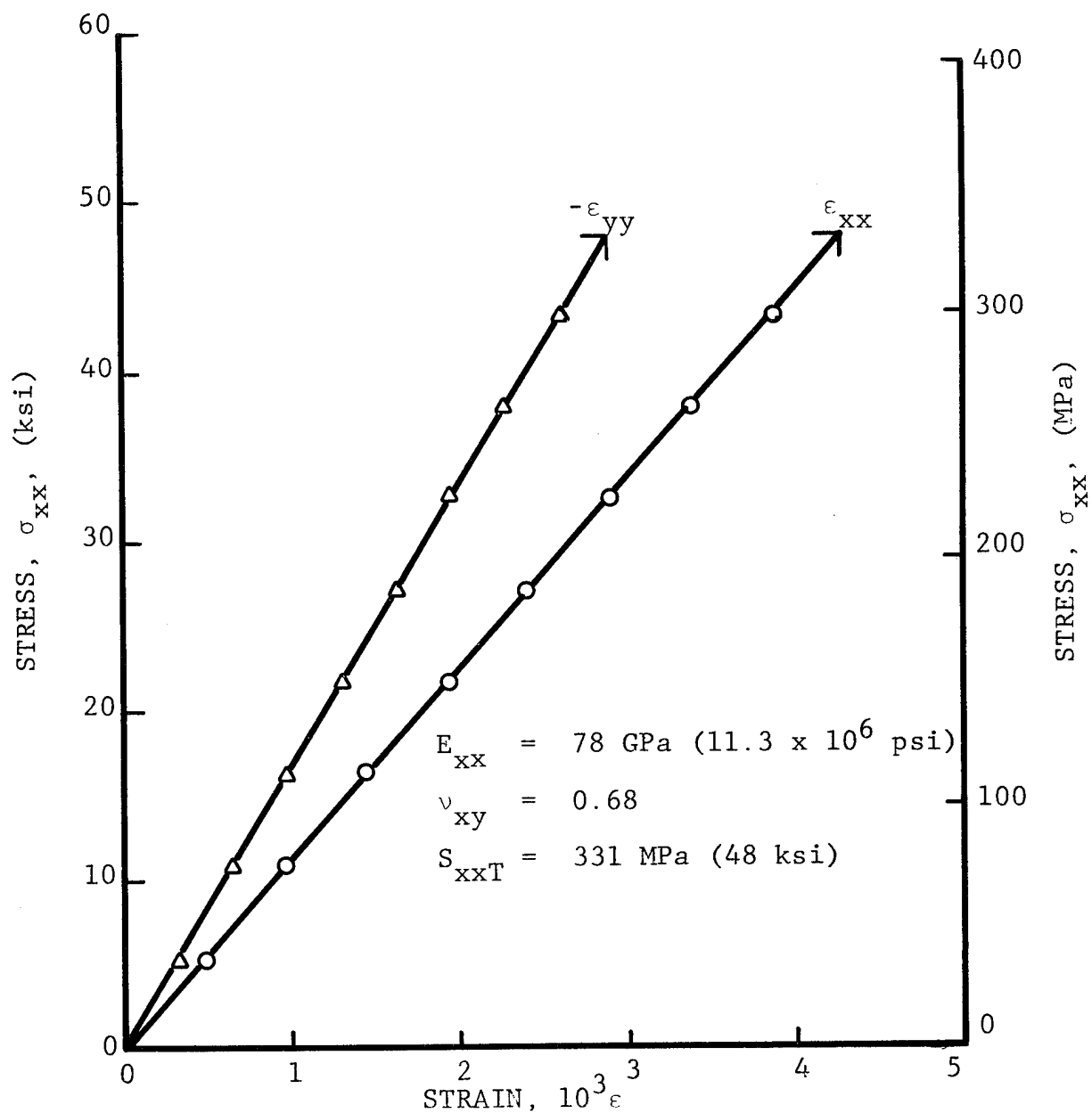


Fig. 98 STRAINS IN $[0^G/+45^C/0^C]_s$ GRAPHITE/S-GLASS/HIGH MODULUS EPÖXY SPECIMEN UNDER UNIAXIAL TENSILE LOADING AFTER 100 THERMAL CYCLES BETWEEN ROOM TEMPERATURE AND 200 degK (-100°F) WITH 256 MPa (37 ksi) TENSILE PRELOAD

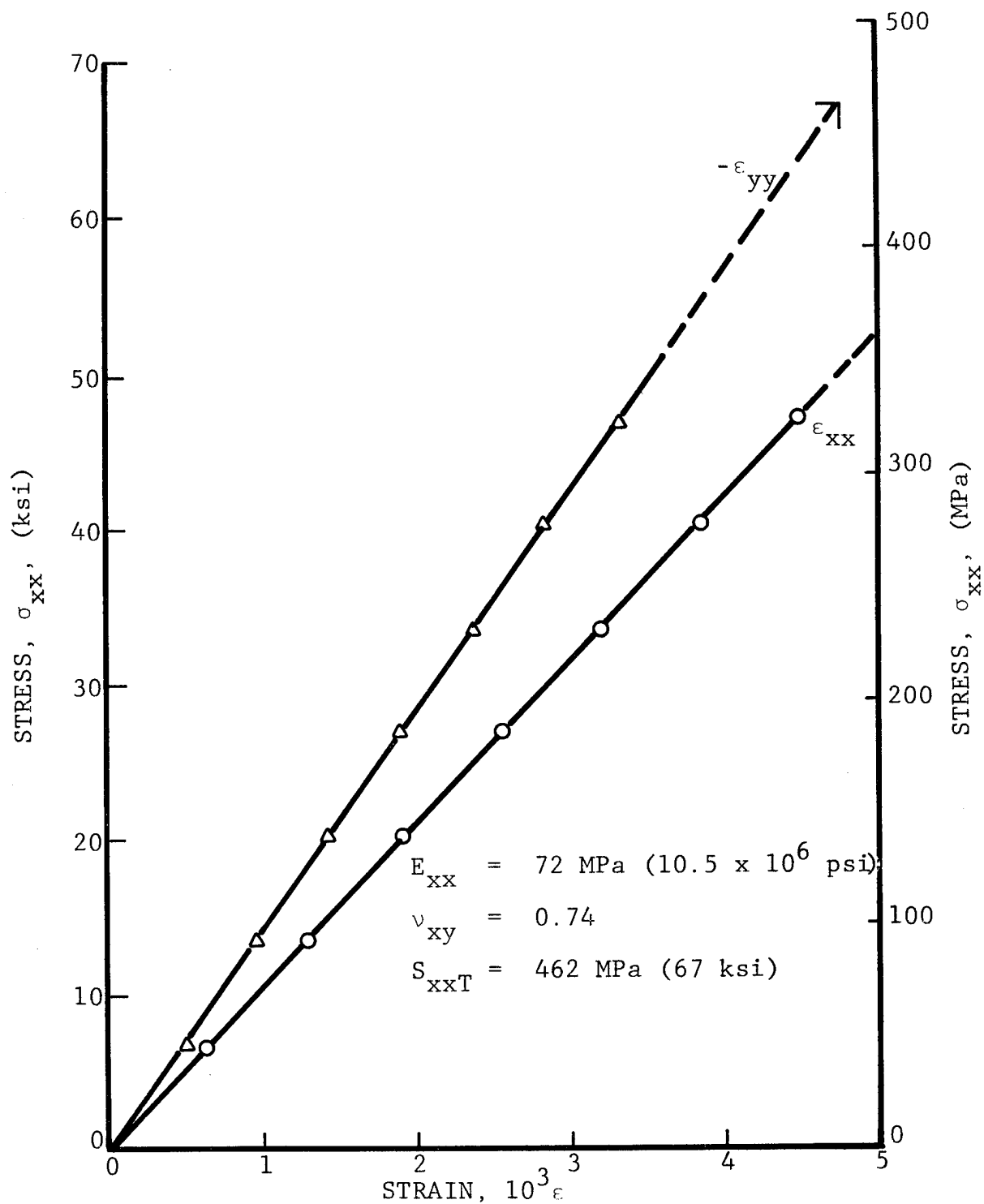


Fig. 99 STRAINS IN $[+45^C/0^G/0^C]_S$ GRAPHITE/S-GLASS/HIGH MODULUS EPOXY SPECIMEN UNDER UNIAXIAL TENSILE LOADING AFTER 100 THERMAL CYCLES BETWEEN ROOM TEMPERATURE AND 200 degK (-100°F) WITH 234 MPa (34 ksi) TENSILE PRELOAD

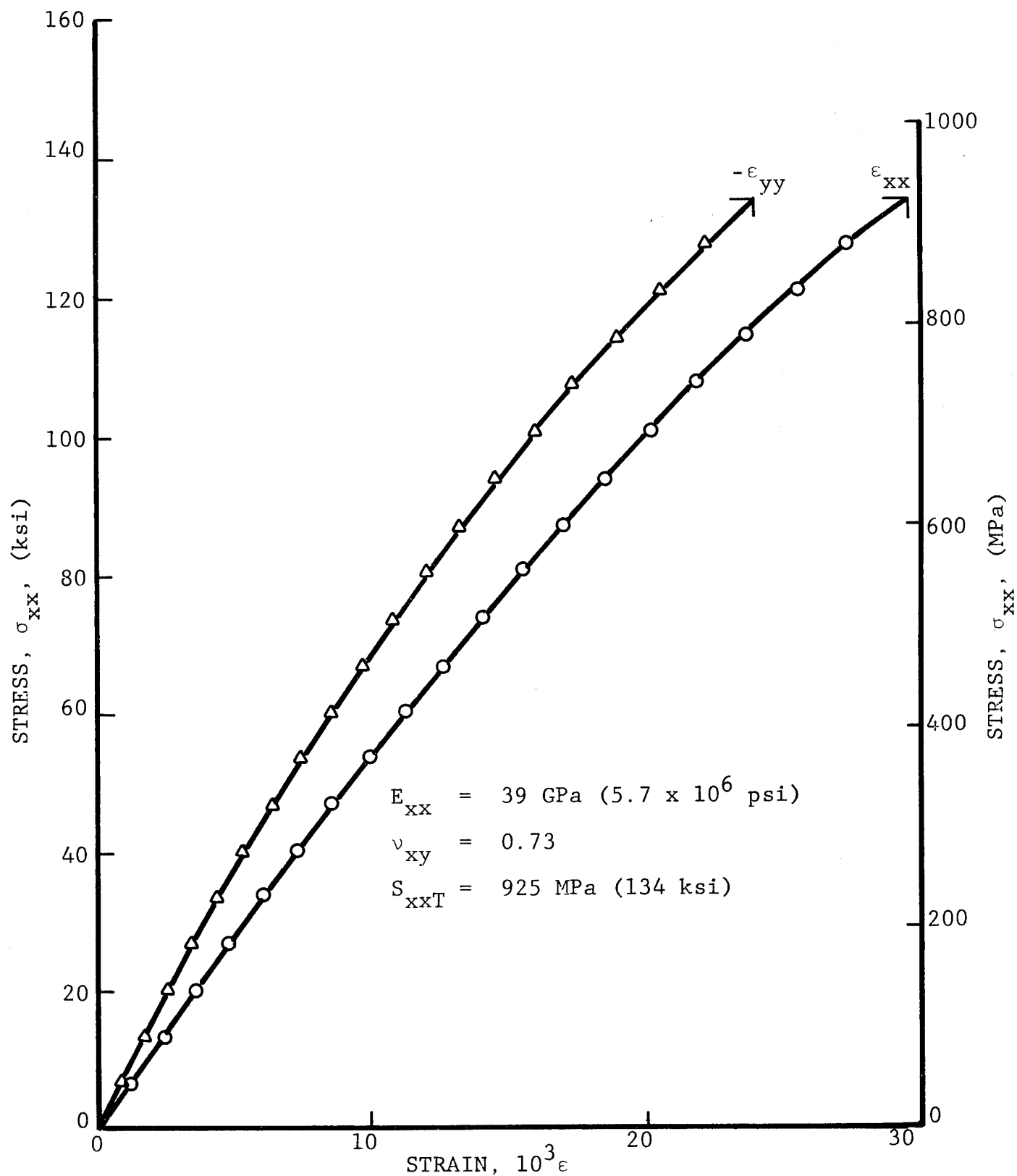


Fig. 100 STRAINS IN $[0^G/+45^C/0^G]_S$ GRAPHITE/S-GLASS/HIGH MODULUS EPOXY SPECIMEN UNDER UNIAXIAL TENSILE LOADING AFTER 100 THERMAL CYCLES BETWEEN ROOM TEMPERATURE AND 200 degK (-100°F) WITH 591 MPa (86 ksi) TENSILE PRELOAD

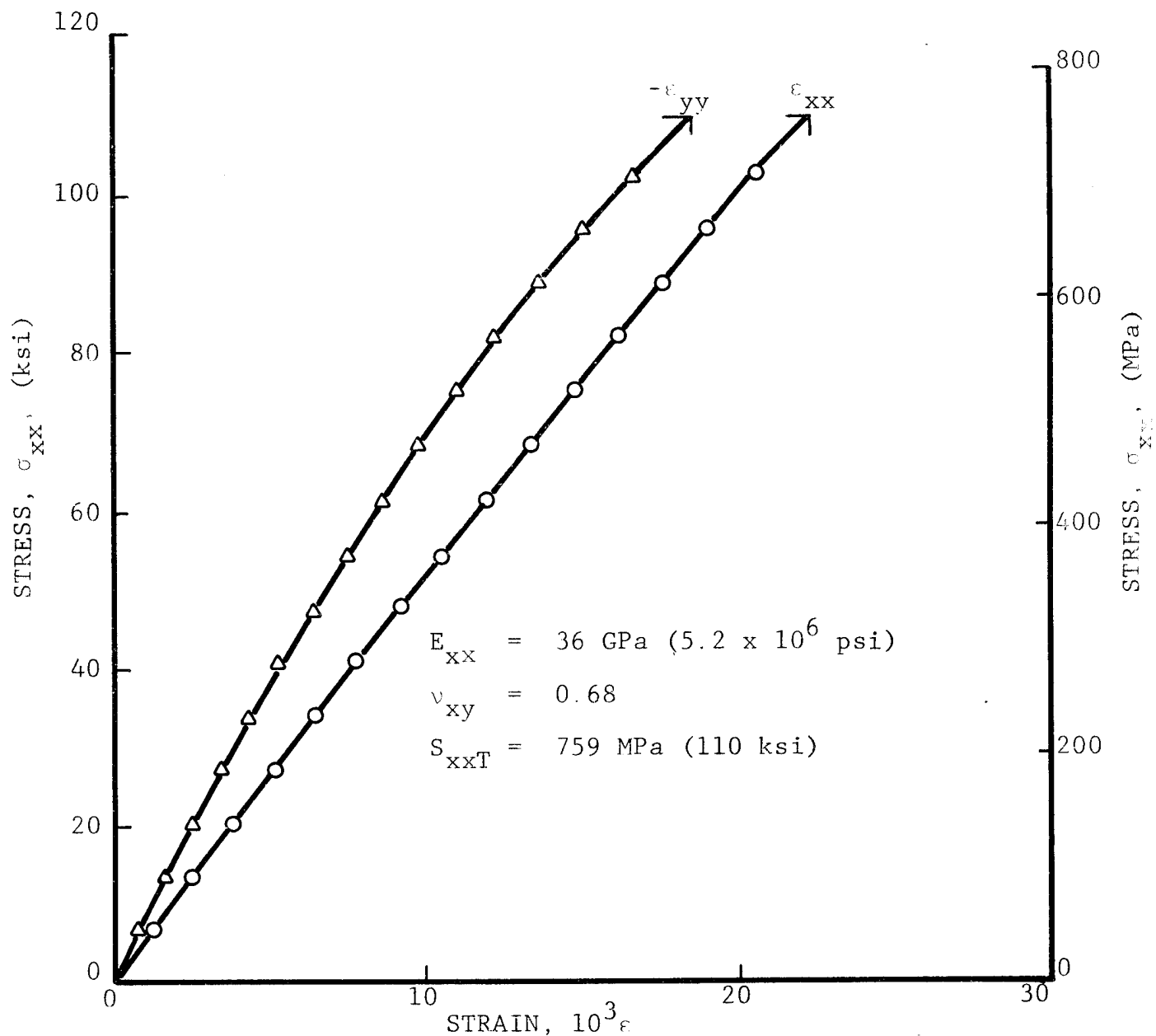


Fig. 101 STRAINS IN $[0^G/+45^C/0^G]_s$ GRAPHITE/S-GLASS/HIGH MODULUS EPOXY SPECIMEN UNDER UNIAXIAL TENSILE LOADING AFTER 100 THERMAL CYCLES BETWEEN ROOM TEMPERATURE AND 200 degK (-100°F) WITH 591 MPa (86 ksi) TENSILE PRELOAD

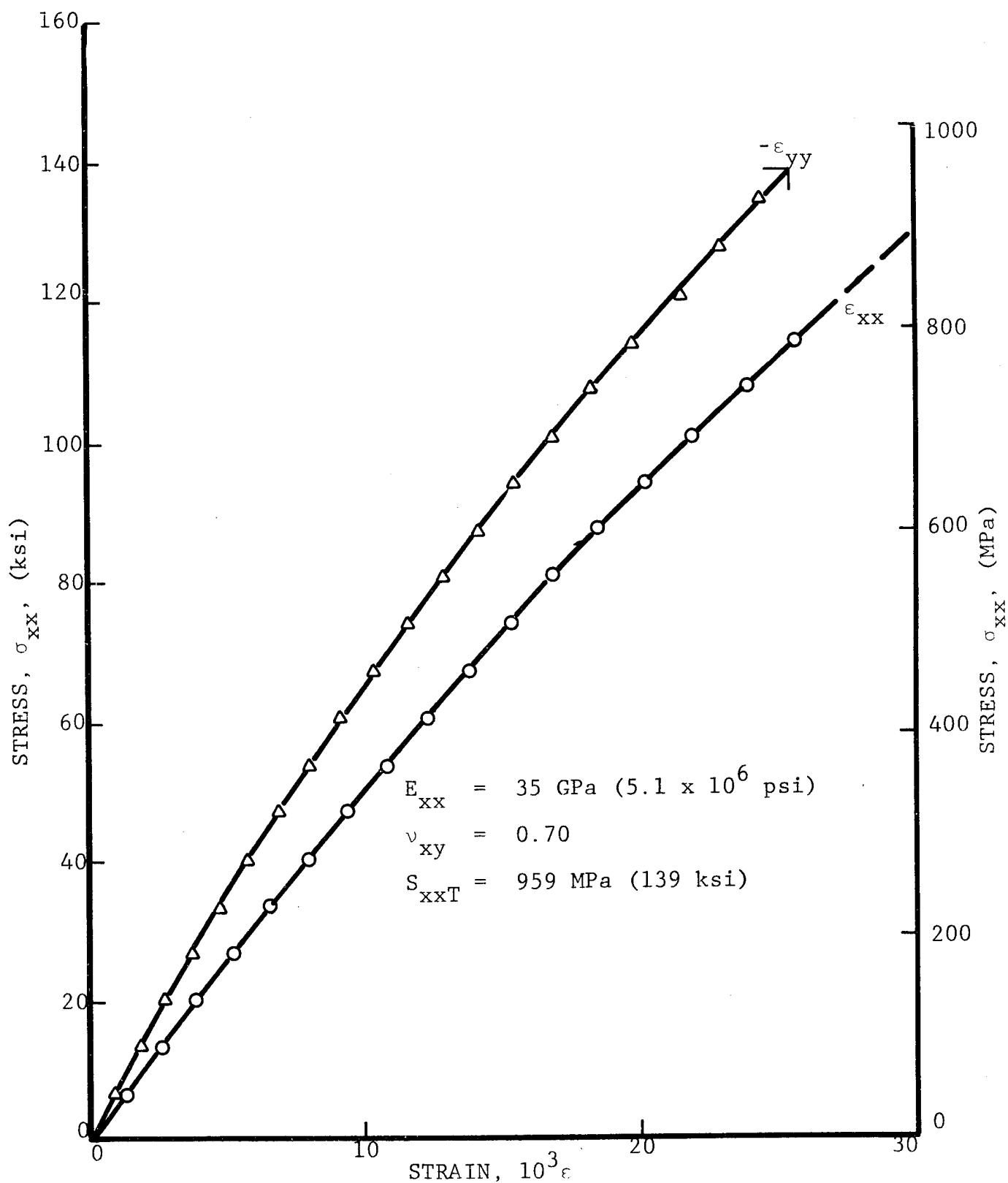


Fig. 102 STRAINS IN $[+45^{\circ}/0_2^{\circ}]_s$ GRAPHITE/S-GLASS/HIGH MODULUS EPOXY SPECIMEN UNDER UNIAXIAL TENSILE LOADING AFTER 100 THERMAL CYCLES BETWEEN ROOM TEMPERATURE AND 200 degK (-100°F) WITH 584 MPa (85 ksi) TENSILE PRELOAD

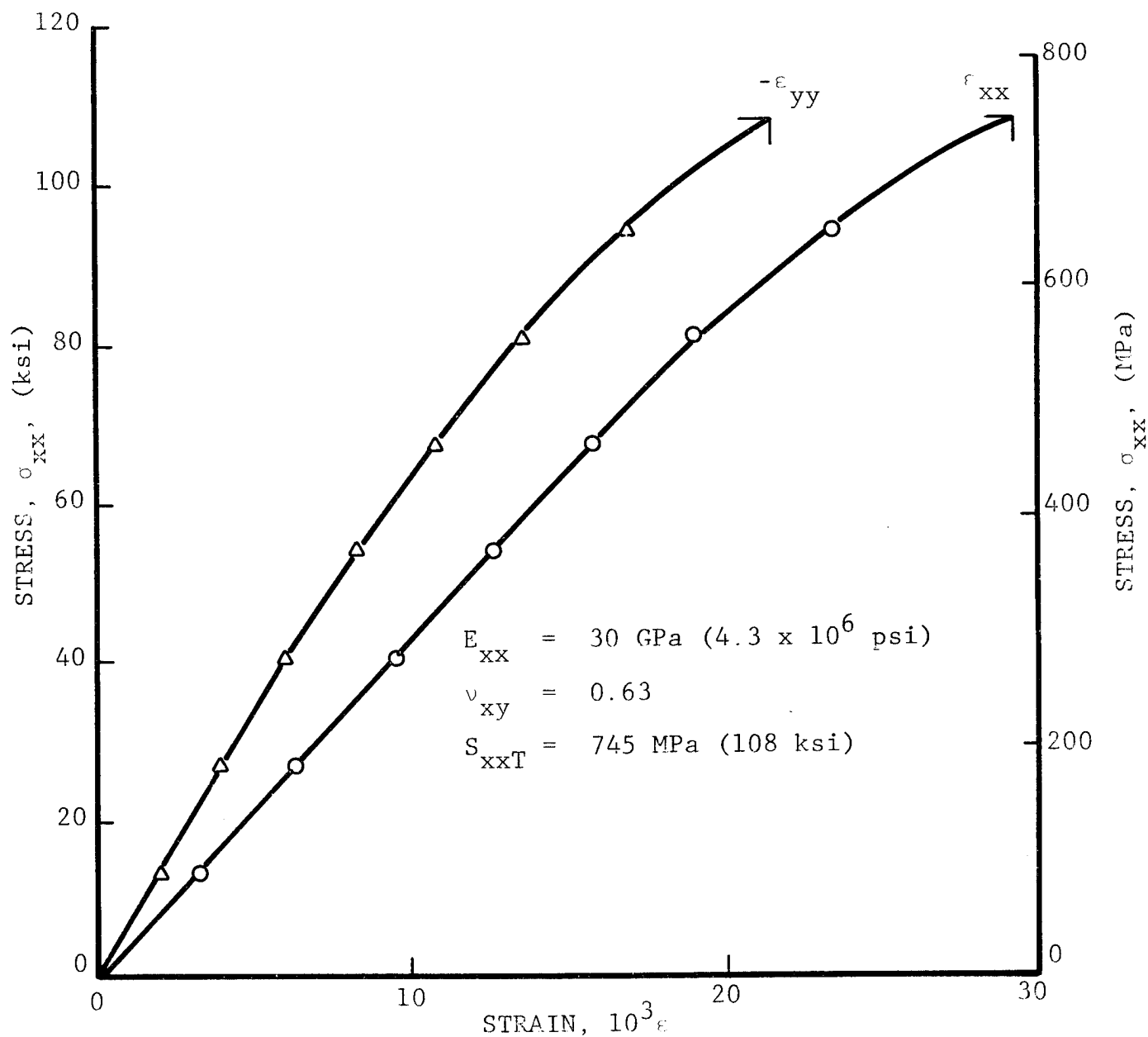


Fig. 103 STRAINS IN $[+45^{\circ}/02^{\circ}]_s$ GRAPHITE/S-GLASS/HIGH MODULUS EPOXY SPECIMEN UNDER UNIAXIAL TENSILE LOADING AFTER 100 THERMAL CYCLES BETWEEN ROOM TEMPERATURE AND 200 degK (-100°F) WITH 584 MPa (85 ksi) TENSILE PRELOAD

REFERENCES

1. Chamis, C.C., "Design and Analysis of Fiber Composite Structural Components," NASA Report SP227, 1970, pp. 217-228.
2. Chamis, C.C., "Lamination Residual Stresses in Cross-Plied Fiber Composites," Proc. of 26th Annual Conference of SPI, Reinforced Plastics/Composites Division, Paper No. 17-D, Feb. 1971.
3. Daniel, I.M., Liber, T. and Chamis, C.C., "Measurement of Residual Strains in Boron/Epoxy and Glass/Epoxy Laminates," Composite Reliability, ASTM STP 580, American Society for Testing and Materials, 1975, pp. 340-351.
4. Chamis, C.C. and Sullivan, T.L., "A Computational Procedure to Analyze Metal Matrix Laminates with Nonlinear Lamination Residual Strains," Composite Reliability, ASTM STP 580, American Society for Testing and Materials, 1975, pp. 327-339.
5. Daniel, I.M. and Liber, T., "Lamination Residual Stresses in Fiber Composites," IITRI Report D6073-I, for NASA-Lewis Research Center; NASA CR-134826, March 1975.
6. Hahn, H.T. and Pagano, N.J., "Curing Stresses in Composite Laminates," J. Composite Materials, Vol. 9, 1975, pp. 91-106.
7. Liber, T., Daniel, I.M. and Chamis, C.C., "The Effects of Thermal Cycling on Advanced Composite Angle-Ply Laminates," Proc. of 30th Annual Conference of SPI, Reinforced Plastics/Composites Division, Paper No. 18-B, Feb. 1975.
8. Liber, T. and Daniel, I.M., "Effects of Tensile Load Cycling on Advanced Composite Angle-Ply Laminates," Proc. of 31st Annual Conference of SPI, Reinforced Plastics/Composites Division, Paper No. 21-E, Feb. 1976.
9. Kevlar 49 Aramid, Data Manual, E.I. DuPont de Nemours and Co., Wilmington, Delaware.
10. Chamis, C.C., private communication.

DISTRIBUTION LIST

Advanced Research Projects Agency
Washington, D.C. 20525
Attn: Library

Advanced Technology Center, Inc.
LTV Aerospace Corporation
P.O. Box 6144
Dallas, Texas 75222
Attn: D.H. Petersen

Air Force Flight Dynamics Laboratory
Wright-Patterson Air Force Base, Ohio 45433
Attn: G.P. Sendeckyj (FBC)
R.S. Sandhu

Air Force Materials Laboratory
Wright-Patterson Air Force Base, Ohio 45433
Attn: J.D. Ray (LTN)
H.S. Schwartz (LN)
T.J. Reinhart (MBC)
G.P. Peterson (LC)
E.J. Morrissey (LAE)
A. Hopkins (LLN)
S.W. Tsai (MBM)
N.J. Pagano
J.M. Whitney (MBM)
J.C. Halpin

Air Force Office of Scientific Research
Washington, D.C. 20333
Attn: J.F. Masi (SREP)

Air Force Office of Scientific Research
1400 Wilson Blvd.
Arlington, VA 22209
Attn: SIGL
W.J. Walker

Air Force Rocket Propulsion Laboratory
Edwards, CA 93523
Attn: Library

Army Mobility Research & Development Laboratory
Langley Research Center, Mail Stop 188A
Hampton, VA 22065
Attn: R.L. Foye

IIT RESEARCH INSTITUTE

DISTRIBUTION LIST (Cont'd)

Bell Helicopter Co.
P.O. Box 482
Ft. Worth, Texas 76101
Attn: H. Zinberg

The Boeing Company
P.O. Box 3999
Seattle, Washington 98124
Attn: J.T. Hoggatt, MS 88-33

The Boeing Company
Vertol Division
Morton, PA 19070
Attn: W.D. Harris
R.A. Pinckney

Battelle Memorial Institute
Columbus Laboratories
505 King Avenue
Columbus, Ohio 43201
Attn: E.F. Rybicki
B. Noton

Brunswick Corporation
Defense Products Division
P.O. Box 4594
43000 Industrial Avenue
Lincoln, Nebraska
Attn: R. Morse

Chemical Propulsion Information Agency
Applied Physics Laboratory
8621 Georgia Avenue
Silver Spring, MD 20910
Attn: Library

Commander
Natick Laboratories
U.S. Army
Natick, MA 01762
Attn: Library

Commander
Naval Air Systems Command
U.S. Navy Department
Washington, D.C. 20360
Attn: M. Stander, AIR-42032D
C. Bersch

IIT RESEARCH INSTITUTE

DISTRIBUTION LIST (Cont'd)

Commander
Naval Ordnance Systems Command
U.S. Navy Department
Washington, D.C. 20360
Attn: B. Drimmer, ORD-033
J. Kinna, ORD-033A

Cornell University
Dept. Theoretical & Applied Mech.
Thurston Hall
Ithaca, New York 14853
Attn: F.C. Moon

Defense Metals Information Center
Battelle Memorial Institute
Columbus Laboratories
505 King Avenue
Columbus, Ohio 43201

Department of the Army
U.S. Army Material Command
Washington, D.C. 20315
Attn: AMCRD-RD

Department of the Army
U.S. Army Aviation Materials Laboratory
Ft. Eustis, Va. 23604
Attn: I.E. Figge, Sr.
R. Berrisford

Department of the Army
U.S. Army Aviation Systems Command
P.O. Box 209
St. Louis, Mo. 63166
Attn: R. Vollmer, AMSAV-A-UE

Department of the Army
Plastics Technical Evaluation Center
Picatinny Arsenal
Dover, New Jersey 07801
Attn: H.E. Pebly, Jr.

Department of the Army
Watervliet Arsenal
Watervliet, New York 12189
Attn: F.W. Schmiedershoff

IIT RESEARCH INSTITUTE

DISTRIBUTION LIST (Cont'd)

Department of the Army
Watertown Arsenal
Watertown, Ma. 02172
Attn: A. Thomas
D.W. Oplinger
E.M. Lenoe

Department of the Army
Redstone Arsenal
Huntsville, Alabama 35809
Attn: R.J. Thompson, AMSMI-RSS

Department of the Navy
Naval Ordnance Laboratory
White Oak
Silver Spring, Maryland 20910
Attn: R. Simon

Department of the Navy
U.S. Naval Ship R&D Laboratory
Annapolis, Maryland 21402
Attn: C. Hersner, Code 2724

Department of the Navy
Air Vehicle Technology Dept.
Naval Air Development Center
Structures Division
Warminster, PA 18974
Attn: E.J. McQuillen

Director
Deep Submergence Systems Project
6900 Wisconsin Avenue
Washington, D.C. 20015
Attn: H. Bernstein, DSSP-221

Director
Naval Research Laboratory
Washington, D.C. 20390
Attn: Code 8430
I. Wolock, Code 8433

E.I. DuPont DeNemours and Co.
DuPont Experimental Station
Wilmington, Delaware 19898
Attn: C.H. Zweben

DISTRIBUTION LIST (Cont'd)

Fiber Science, Inc.
245 East 157th Street
Gardena, California 90248
Attn: L.J. Ashton

General Dynamics
P.O. Box 748
Ft. Worth, Texas 76100
Attn: J.E. Ashley
M.E. Waddoups

General Dynamics/Convair
P.O. Box 1128
San Diego, California 92112
Attn: J.L. Christian

General Electric Co.
Evendale, Ohio 45215
Attn: C. Stotler
R. Ravenhall
C.A. Steinhagen

Goldsworthy Engineering, Inc.
Lomiter Blvd.
Torrance, California 90505
Attn: B.H. Jones

General Motors Corp.
Detroit Diesel-Allison Division
Indianapolis, Indiana
Attn: M. Herman

Grumman Aerospace Corporation
Bethpage, Long Island, N.Y. 11714
Attn: S. Dastin
J.B. Whiteside

Hamilton Standard Division
United Aircraft Corporation
Windsor Locks, Connecticut 06096
Attn: W.A. Percival

Hercules, Inc.
Allegheny Ballistics Laboratory
P.O. Box 210
Cumberland, Maryland 21052
Attn: A.A. Vicario

IIT RESEARCH INSTITUTE

DISTRIBUTION LIST (Cont'd)

Illinois Institute of Technology
10 West 32nd Street
Chicago, Illinois 60616
Attn: L.J. Broutman

Jet Propulsion Laboratory
4800 Oak Grove Drive
Pasadena, California 91103
Attn: A.C. Knoell
W. Jensen

Lawrence Livermore Laboratory
P.O. Box 808, L-421
Livermore, California 94550
Attn: T.T. Chiao
E.M. Wu

Lockheed-Georgia Co.
Advanced Composites Information Center
Dept. 72-14, Zone 402
Marietta, Georgia 30060

Lockheed Missiles and Space Co.
P.O. Box 504
Sunnyvale, California 94087
Attn: R.W. Fenn

McDonnell Douglas Aircraft Corporation
P.O. Box 516
Lambert Field, MS 63166
Attn: J.C. Watson

McDonnell Douglas Aircraft Corporation
3855 Lakewood Blvd.
Long Beach, California 90810
Attn: L. B. Greszczuk

Massachusetts Institute of Technology
Cambridge, MA 02139
Attn: F.J. McGarry
J.F. Mandell

Material Sciences Corporation
1777 Walton Road
Blue Bell, Pa. 19422
Attn: B.W. Rosen

DISTRIBUTION LIST (Cont'd)

NASA-Ames Research Center
Moffett Field, California 94035
Attn: Library
D.P. Williams

NASA-Flight Research Center
P.O. Box 273
Edwards, California 93523
Attn: Library

NASA-George C. Marshall Space Flight Center
Huntsville, Alabama 35812
Attn: D.D. Thompson, S&E, ASTN-PPA
C.E. Cataldo, S&E-ASTN-MX
Library

NASA-Goddard Space Flight Center
Greenbelt, MD 20771
Attn: Library

NASA-Langley Research Center
Hampton, VA 23665
Attn: E.E. Mathauser, MS 188a
R.A. Pride, MS 188a
J.G. Davis, MS 188a
L. Roderic, MS 188e
J.R. Davidson, MS 188e
M.C. Card
Library

NASA-Lewis Research Center
21000 Brookpark Road
Cleveland, Ohio 44135
Attn: Contracting Officer, MS 500-313
Tech. Report Control, MS 5-5
Technical Utilization, MS 3-19
AFSC Liaison, MS 501-3
Rel. and Quality Assur., MS 500-211
R.A. Signorelli, MS 106-1
M.P. Hanson, MS 501-7
R.H. Kemp, MS 49-3
R.F. Lark, MS 49-3
J.C. Freche, MS 49-1
R.H. Johns, MS 49-3
N.T. Saunders, MS 105-1
C.C. Chamis, MS 49-3 (16 copies)
T.T. Serafini, MS 49-1
Library, MS 60-3 (2 copies)
Director, ASRDI, MS 6-2 (2 copies)

IIT RESEARCH INSTITUTE

DISTRIBUTION LIST (Cont'd)

NASA-Lyndon B. Johnson Space Center
Houston, Texas 77001
Attn: R.E. Johnson, SMD-ES5
S. Glorioso, SMD-ES52
Library

NASA Headquarters
Washington, D.C. 20546
Attn: G.C. Deutsch

NASA Scientific and Tech. Information Facility
P.O. Box 33
College Park, MD 20740
Attn: Acquisitions Branch (10 copies)

National Aeronautics and Space Administration
Office of Advanced Research and Technology
Washington, D.C. 20546
Attn: L.A. Harris, Code RWS

National Aeronautics and Space Administration
Office of Technology Utilization
Washington, D.C. 20546

National Bureau of Standards
Eng. Mech. Section
Washington, D.C. 20234
Attn: R. Mitchell

National Technology Information Service
Springfield, VA 22151 (6 copies)

National Science Foundation
Engineering Division
1800 G Street, N.W.
Washington, D.C. 20540
Attn: Library

Northrop Space Laboratories
3401 West Broadway
Hawthorne, CA 90250
Attn: D. Stanbarger

Pratt & Whitney Aircraft
East Hartford, CT
Attn: A.J. Dennis

DISTRIBUTION LIST (Cont'd)

Rockwell International
Los Angeles Division
International Airport
Los Angeles, CA 90009
Attn: L.M. Lackman

Sikorsky Aircraft Division
United Aircraft Corporation
Stratford, CT 06602
Attn: Library

Space and Missile Systems Organization
Air Force Unit Post Office
Los Angeles, CA 90045
Attn: Technical Data Center

Structural Composites Industries, Inc.
6344 N. Irwindale Avenue
Azusa, CA 91702
Attn: E.E. Morris

TRW, Incorporated
23555 Euclid Avenue
Cleveland, Ohio 44117
Attn: W.E. Winters

Union Carbide Corporation
P.O. Box 6116
Cleveland, Ohio 44101
Attn: J.C. Bowman

United Technologies Research Center
East Hartford, CT 06108
Attn: R.C. Novak

University of Dayton Research Institute
Dayton, Ohio 45409
Attn: W.S. Blain

University of Delaware
Dept. of Mechanical and Aerospace Engineering
107 Evans Hall
Newark, DE 19711
Attn: R.B. Pipes

University of Oklahoma
School of Aerospace Mechanical and Nuclear Engineering
Norman, Oklahoma 73069
Attn: C.W. Bert

IIT RESEARCH INSTITUTE

DISTRIBUTION LIST (Cont'd)

University of Wisconsin
Dept. of Engineering Mechanics
Madison, Wisconsin 53706
Attn: R.E. Rowlands

University of Wyoming
Dept. of Mechanical Engineering
Larmie, WY 82070
Attn: D.F. Adams

V.P.I. and S.U.
Dept. of Eng. Mech.
Blacksburg, VA 24061
Attn: R.H. Heller
H.F. Brinson